DOCTORAL THESIS

Submesoscale Variability in the Baltic Sea: Occurrence and Role in the Redistribution of Physical Tracers

Kai Salm

TALLINNA TEHNIKAÜLIKOOL
TALLINN UNIVERSITY OF TECHNOLOGY
TALLINN 2026

TALLINN UNIVERSITY OF TECHNOLOGY
DOCTORAL THESIS
71/2026

Submesoscale Variability in the Baltic Sea: Occurrence and Role in the Redistribution of Physical Tracers

KAI SALM

TAL TECH PRESS

TALLINN UNIVERSITY OF TECHNOLOGY
School of Science
Department of Marine Systems
This dissertation was accepted for the defence of the Doctor of Philosophy (Oceanography and Meteorology) 01/10/2026

Supervisor: Prof Urmas Lips
Department of Marine Systems
School of Science
Tallinn University of Technology
Tallinn, Estonia

Opponents: Dr Aleksi Nummelin
Research Professor
Marine Research Unit
Finnish Meteorological Institute
Helsinki, Finland

Dr Marcel du Plessis
Associate Senior Lecturer
Department of Marine Sciences
University of Gothenburg
Gothenburg, Sweden

Defence of the thesis: 04/11/2026, Tallinn

Declaration:
Hereby I declare that this doctoral thesis, my original investigation and achievement, submitted for the doctoral degree at Tallinn University of Technology has not been submitted for doctoral or equivalent academic degree.

Kai Salm _____

signature

Copyright: Kai Salm, 2026
ISSN 2585-6898 (paperback)
ISBN 978-9916-80-577-0 (paperback)
ISSN 2585-6901 (PDF)
ISBN 978-9916-80-578-7 (PDF)
https://doi.org/10.23658/taltech.71/2026
Printed by Koopia Niini & Rauam

Salm, K. (2026). *Submesoscale Variability in the Baltic Sea: Occurrence and Role in the Redistribution of Physical Tracers* [TalTech Press]. https://doi.org/10.23658/taltech.71/2026

TALLINNA TEHNIKAÜLIKOOL
DOKTORITÖÖ
71/2026

Submesomastaapi muutlikkus Läänemeres: esinemine ja roll vee füüsikaliste omaduste ümberjaotamises

KAI SALM

TAL TECH
KIRJASTUS

Contents

List of Publications 6
Author's Contribution to the Publications 7
1 Introduction 8
1.1 Baltic Sea and Gulf of Finland as a Stratified Coastal System 8
1.2 From Mesoscale to Submesoscale 8
1.3 Observational and Modelling Challenges 10
2 Motivation and Objectives 11
Abbreviations 12
3 Materials and Methods 13
3.1 Glider Observations 13
3.1.1 Quality Control of Glider Data 13
3.1.2 Sensor-Response Corrections 13
3.1.3 Glider Missions 14
3.2 Model Setup 15
3.2.1 Model–Observation Consistency 16
3.3 Derived Quantities and Diagnostics 17
3.3.1 Dynamical Diagnostics 18
3.3.2 Potential Vorticity Diagnostics 18
3.3.3 Tracer Diagnostics 19
3.3.4 Spectral Analysis 20
4 Results and Discussion 21
4.1 Identifying Submesoscale Variability from Gliders 21
4.1.1 Structural Signatures 21
4.1.2 Diagnostic Evidence 22
4.1.2.1 Dynamical Conditions 24
4.1.2.2 Spectral Evidence 25
4.2 Spatial Structure of Submesoscale Variability 28
4.2.1 Horizontal Structure of Submesoscale Indicators 30
4.2.2 Vertical Structure of Spice Variability 31
4.3 Linking Mesoscale Forcing and Tracer Organisation 34
4.4 Pathways for Tracer Redistribution 36
4.5 Implications for the Baltic Sea 37
5 Conclusions 41
References 43
Acknowledgements 52
Abstract 53
Lühikokkuvõte 54
Appendix 55
Curriculum vitae 131
Elulookirjeldus 133

List of Publications

The list of author's publications, on the basis of which the thesis has been prepared:

I Salm, K.; Liblik, T.; Lips, U. (2023). Submesoscale Variability in a Mesoscale Front Captured by a Glider Mission in the Gulf of Finland, Baltic Sea. Frontiers in Marine Science, 10. DOI: 10.3389/fmars.2023.984246.

II Salm, K.; Väli, G.; Liblik, T.; Lips, U. (2025). Forcing-dependent submesoscale variability and subduction in a coastal sea area (Gulf of Finland, Baltic Sea). Ocean Science, 21 (5), 2555−2577. DOI: 10.5194/os-21-2555-2025.

III Lips, U.; Salm, K.; Väli, G.; Liblik, T.; Arneborg, L.; Biddle, L. C.; Bulczak, A. I.; Chrysagi, E.; Falarz, M.; Holtermann, P.; Jakacki, J.; Meier, H. E. M.; Mohrmann, M.; Myrberg, K.; Pemberton, P.; Umlauf, L. (2026). Submesoscale dynamics in the Baltic Sea – a review. Progress in Oceanography, 245, #103746. DOI: 10.1016/j.pocean.2026.103746.

Author's Contribution to the Publications

Contribution to the papers in this thesis are:

I The author contributed to the design and execution of the glider surveys and was responsible for the processing and analysis of the glider data. The manuscript was primarily written by the author, with valuable contributions from the co-authors.

II The author contributed to the design and execution of the glider surveys and was responsible for the processing and analysis of the glider data, as well as for the analysis of the model data. The manuscript was primarily written by the author, with valuable contributions from the co-authors.

III The author contributed to drafting the manuscript, participated in its review and editing, and contributed to the preparation of the figures.

1 Introduction

1.1 Baltic Sea and Gulf of Finland as a Stratified Coastal System

The Baltic Sea is a semi-enclosed, non-tidal marginal sea in northern Europe, characterized by strong horizontal and vertical hydrographic gradients. Its circulation and stratification are shaped by restricted water exchange with the North Sea, substantial freshwater input from rivers, and large-scale atmospheric forcing. Together, these processes maintain an estuarine-like overturning circulation, with a brackish surface layer overlying saltier water of North Sea origin. This vertical salinity structure forms a persistent halocline that restricts vertical mixing and deep-water ventilation across much of the basin (Döös et al., 2004; Leppäranta & Myrberg, 2009; Väli et al., 2013).

The geometry of the Baltic Sea and its wide latitudinal extent produce marked differences between its sub-basins. Narrow basins with strong freshwater input, such as the Gulf of Finland (GoF), are particularly prone to strong lateral density gradients and seasonally varying vertical stratification. Situated at the eastern end of the Baltic Sea, the GoF is a narrow and elongated sub-basin that receives substantial freshwater input from the Neva River. This input maintains a pronounced along-basin salinity contrast in the upper layer, with the freshest waters in the east and progressively increasing salinity toward the Baltic Proper in the west (Ylöstalo et al., 2016).

Circulation in the GoF is strongly controlled by wind forcing and density structure (Lilover et al., 2017; Suhhova et al., 2018). Long-term mean currents have low stability, and the circulation is therefore better described as variable and seasonally modulated rather than as a persistent mean flow (Elken et al., 2011; Westerlund et al., 2019).

Vertical stratification in the GoF is strong, but the structure of the upper water column changes markedly from spring to summer. A shallow thermocline develops in the upper 10–20 m during spring and strengthens through summer. Below the seasonal thermocline, winter-cooled water can remain trapped as a cold intermediate layer. Deeper in the water column, a permanent halocline typically lies between 40 and 80 m, separating the upper layers from more saline deep water of Baltic Proper origin (Leppäranta & Myrberg, 2009; Lips et al., 2017). By winter, surface cooling and wind-driven mixing homogenise the upper water column, often down to 60–80 m, eroding the seasonal thermocline. Waters below the halocline are largely insulated from vertical mixing and respond mainly through wind-driven inflow and outflow events. Under sufficiently strong and persistent up-estuary winds, episodic circulation changes can enhance vertical exchange and temporarily weaken stratification (Liblik et al., 2013; Lips et al., 2017).

Together, these characteristics make the GoF a strongly stratified and wind-sensitive coastal system, creating conditions favourable for the mesoscale circulation features discussed below and for smaller-scale motions that may develop within intensified frontal zones.

1.2 From Mesoscale to Submesoscale

Within this stratified and wind-forced setting, a range of mesoscale features emerges in the GoF. These include eddies (e.g., Zhurbas et al., 2008; Westerlund et al., 2019), meandering coastal currents (e.g., Maljutenko & Raudsepp, 2019; Stipa, 2004), and baroclinic fronts and associated jet currents driven by coastal upwelling (e.g., Lehmann & Myrberg, 2008; Lips et al., 2009). Together, these features organise regional

circulation, regulate exchange between coastal and offshore sea areas, and structure the upper-layer flow over spatial scales of tens of kilometres and timescales from days to weeks.

Frontal structures are particularly prominent in the GoF (Pavelson, 2005). Owing to its elongated geometry and stratified water column, local wind forcing frequently generates coastal upwelling and downwelling events characterised by sharp baroclinic fronts and intensified currents (Lehmann et al., 2012; Lips et al., 2009; Myrberg & Andrejev, 2003). In addition, differential surface warming in shallow areas (Lips et al., 2014), wind-driven cross-shore inclination of pycnoclines (Liblik & Lips, 2017), and the spreading of riverine freshwater (Liblik et al., 2020; Lips et al., 2017; Stipa et al., 1999) create horizontal buoyancy gradients and associated vertical shear.

The mesoscale circulation and frontal structures of the GoF therefore provide favourable conditions for the emergence of smaller-scale, ageostrophic motions. Submesoscale (SMS) processes typically occupy spatial scales from a few hundred metres to O(10 km) in the open ocean (Capet et al., 2008; Taylor & Thompson, 2023), but are expected to occur at somewhat smaller scales in the Baltic Sea (Väli et al., 2017) owing to its relatively high latitude, shallow depth, and layered structure of the water column. SMS activity is commonly enhanced in regions of mesoscale straining and frontogenesis, where lateral density gradients are sharpened and geostrophic balance is locally disrupted (e.g., Adams et al., 2017; Garcia-Jove et al., 2022). This suggests that such processes may play an important role in Baltic Sea circulation and tracer dynamics (Lips et al., 2016).

Dynamically, SMS motions occupy a transitional regime between geostrophic mesoscale flow and smaller-scale three-dimensional turbulence. Whereas mesoscale dynamics are characterised by small Rossby numbers ($Ro \ll 1$) and large Richardson numbers ($Ri \gg 1$), reflecting the dominance of rotational and buoyancy forces, SMS motions exhibit Rossby and Richardson numbers of order one. This indicates a reduced rotational constraint and an increased role of inertial and ageostrophic motions (Taylor & Thompson, 2023; Thomas et al., 2008). As a result, SMS flows can exhibit enhanced vertical vorticity and intensified vertical exchange relative to the mesoscale, providing an efficient pathway for transporting momentum, buoyancy, and tracers between the surface layer and the stratified interior (Callies et al., 2015).

Idealised studies have identified several instability mechanisms through which mesoscale fronts can generate variability at submesoscales (Taylor & Thompson, 2023). A fundamental mechanism acting across both mesoscale and submesoscale ranges is baroclinic instability (Eady, 1949). At submesoscales, this process is commonly expressed as mixed-layer instability, whereby horizontal buoyancy gradients within the weakly stratified surface mixed layer generate SMS eddies that restratify the upper ocean and modify mixed-layer depth (Boccaletti et al., 2007; Fox-Kemper et al., 2008; Mahadevan et al., 2010).

Other instability pathways may also become active in frontal environments. Symmetric instability can develop when baroclinic effects reduce the potential vorticity toward zero or negative values, for example under downfront winds (directed along the frontal jet) or surface cooling (Taylor & Ferrari, 2009; Thomas et al., 2013). It generates ageostrophic overturning circulations that enhance vertical exchange and can promote the subduction of surface waters along sloping isopycnals (Bosse et al., 2021; Pham et al., 2024).

These examples illustrate how mesoscale frontal structures can act as sources of SMS variability and associated vertical and lateral exchange. However, in realistic coastal environments, multiple processes may coexist and evolve rapidly under variable wind forcing and stratification, making it difficult to identify a single instability mechanism from observations alone. These mechanisms therefore provide a useful conceptual framework, while this thesis focuses primarily on how SMS activity is expressed in observed and modelled tracer structure and how it contributes to exchange in the stratified coastal environment of the GoF.

1.3 Observational and Modelling Challenges

Because SMS processes are intermittent, rapidly evolving, and embedded within mesoscale frontal systems, resolving their structure and impacts requires observations and numerical models with sufficiently high spatial and temporal resolution. Conventional ship-based measurements are therefore increasingly complemented by autonomous observing platforms, including gliders, drifters, and profilers, as well as towed vehicles and flow-through systems. These approaches have been used to capture SMS variability in the ocean (Rudnick & Cole, 2011; Swart et al., 2023) and in the Baltic Sea (Carpenter et al., 2020; Lips et al., 2016). However, observations remain limited by trade-offs between spatial coverage, temporal resolution, and sampling duration.

Numerical models provide a widely used tool for investigating SMS dynamics and their broader circulation context. In the Baltic Sea, realistic high-resolution simulations have been used to examine the sensitivity of SMS variability to grid spacing (Gröger et al., 2022), reproduce observed SMS processes and events (Chrysagi et al., 2021; Väli et al., 2017), extend observational findings over larger spatial domains, and characterise the temporal and spatial variability of SMS intensity (Väli et al., 2024). Nevertheless, the limited availability of observations with sufficient resolution and coverage hinders robust validation and introduces uncertainty in the interpretation of modelled SMS features.

Models operating at SMS-permitting resolutions have revealed a rich spectrum of variability and dynamical features at kilometre scales (Capet et al., 2008; Väli et al., 2017). By explicitly representing part of the SMS range, such models can capture fine-scale dynamics that are absent or parameterised in coarser simulations. This may affect not only the representation of local frontal processes, but also the simulated mesoscale and larger-scale circulation (Andrejev et al., 2004; Maljutenko & Raudsepp, 2019; Westerlund et al., 2019). Robust validation of SMS-permitting simulations is therefore essential, both for interpreting high-resolution model results and for improving parameterisations in coarser Baltic Sea models used for long-term and operational applications.

Taken together, these challenges show that neither observations nor models alone are sufficient to fully characterise SMS variability in realistic coastal environments. A combined approach is needed to link basin-scale hydrographic conditions, mesoscale frontal environments, and fine-scale tracer variability under contrasting forcing conditions. Such a perspective is necessary to clarify how larger-scale atmospheric and hydrographic drivers shape the emergence of SMS motions, and how these motions contribute to the redistribution of thermohaline and biogeochemical tracers in the stratified coastal water column.

2 Motivation and Objectives

Growing evidence shows that SMS processes are a widespread component of stratified marine environments, including the Baltic Sea (e.g., Carpenter et al., 2020; Gurova & Chubarenko, 2012; Lips et al., 2016). In the Baltic Sea, their effects may be especially important because of the system's compressed dynamical range: shallow depth, presence of strong pycnoclines, and relatively small deformation scales reduce the separation between surface forcing, frontal adjustment, and the interior water column. As a result, comparatively small SMS motions may influence a large fraction of the water column. The GoF is particularly well suited for examining these processes, as rapidly varying winds act on a strongly stratified, freshwater-influenced basin where fronts form and are repeatedly redistributed by changing forcing.

The aim of this thesis is to investigate the conditions under which SMS variability emerges, including the roles of mesoscale dynamics, atmospheric forcing, and stratification, and to assess how SMS processes contribute to tracer redistribution and exchange.

This thesis relies primarily on high-resolution observations collected with an autonomous underwater glider in the GoF, complemented by numerical modelling that places the measurements in a broader dynamical context. Such a combined approach is essential, as observations are limited in spatial and temporal coverage, whereas models remain sensitive to resolution and parameterization choices.

The specific objectives are as follows:

- to demonstrate that high-resolution autonomous glider observations can reliably detect SMS variability through consistent physical tracer signatures (Paper I);

- to characterize the horizontal and vertical organization of SMS variability in a shallow, stratified coastal sea (Paper II);

- to examine how SMS activity is related to mesoscale density structure, including mesoscale fronts and coastal currents (Papers I, II);

- to investigate how SMS processes drive tracer redistribution, including signatures consistent with subduction along sloping isopycnals (Paper II);

- to assess the role of SMS processes in the Baltic Sea, with emphasis on their contribution to vertical and lateral tracer redistribution and energy transfer (Paper III).

Abbreviations

CTD	Senor measuring conductivity, temperature, and pressure
GoF	Gulf of Finland
GPS	Global Positioning System
PV	Potential vorticity
RMS	Root mean square
SMS	Submesoscale
UML	Upper mixed layer

3 Materials and Methods

3.1 Glider Observations

Observations were collected using a Slocum G2 autonomous underwater glider (MIA), a buoyancy-driven platform designed for operation to 200 m depth. In the Baltic Sea, a single set of alkaline batteries typically supports missions of up to one month, with energy consumption dominated by the buoyancy pump because of the shallow water depths. The glider was equipped with a pumped CTD (Sea-Bird), chlorophyll-a fluorescence and turbidity sensors (Wet Labs), and a dissolved oxygen sensor (Aanderaa). The sensors typically sample during both ascent and descent, operating at 0.5 Hz.

The glider navigated between predefined waypoints and performed repeated dive–climb cycles to prescribed inflection depths. Typical horizontal and vertical speeds for the glider are 0.35 and 0.10 m s^{-1}, respectively. Periodic surfacing provided GPS position fixes, and the glider used the offset between the estimated underwater position and the GPS position at surfacing to estimate drift and adjust its subsequent path toward the target waypoint. Surfacing also enabled two-way satellite communication for data transmission and mission updates. All deployments were assisted in piloting by the author, including regular monitoring of vehicle health, position, and current estimates, and adjustment of waypoints when required to maintain effective sampling, particularly under strong current conditions or near shipping lanes.

Glider data were retrieved from onboard memory and processed by merging flight and science data streams and converting raw binary files using manufacturer-provided tools. A subset of variables relevant for scientific processing was extracted from the full dataset and combined into mission-level NetCDF files.

3.1.1 Quality Control of Glider Data

Raw glider data were quality controlled following procedures adapted from Argo quality-control protocols (Wong et al., 2019), with standard quality-control flags applied to all science variables. Automated checks included range tests for time, position, pressure, and all measured variables (temperature, conductivity, turbidity, chlorophyll, and dissolved oxygen) based on sensor specifications, as well as surface-zeroing and stuck-value tests for CTD data and air-bubble detection for conductivity. Spike detection for temperature and salinity followed the Argo protocol (Wong et al., 2019), while chlorophyll, turbidity, and dissolved oxygen were screened using a threshold-based spike test from D'Ortenzio et al. (2010). Surface chlorophyll measurements were additionally screened for isolated near-zero outliers that were inconsistent with adjacent observations and likely reflected measurement artefacts during surface intervals. Manual interventions were kept to a minimum. Profiles that appeared clearly questionable relative to adjacent profiles during subsequent processing were excluded from bin-averaged analyses.

3.1.2 Sensor-Response Corrections

Temperature and conductivity sensors exhibit finite response times, which can lead to misalignment with pressure when the glider transits strong vertical gradients. The resulting lag differs between ascents and descents due to the reversal of temperature and salinity gradients. In addition, heat storage within the conductivity cell introduces

small errors in inferred salinity (thermal lag), as temperature is measured at the cell exterior while conductivity is measured internally.

Response-time and thermal-lag corrections were applied to minimise differences between consecutive profiles, following the approach introduced in Paper I by the author and further developed since. Response times shorter than the sampling interval were explored over 0–2 s at 0.1 s resolution. Rather than applying a simple linear time shift, response-time effects were corrected using a three-point least-squares lag filter after Fofonoff et al. (1974), with lag incorporated through regression-derived weighting. For the thermal-lag correction, response-time adjustments were first applied to temperature and conductivity. Combinations of the thermal-lag parameters α_{tl} (0.01–0.1, step 0.01) and τ_{tl} (5–20 s, step 0.5 s) were then tested prior to salinity calculation.

For each parameter configuration, pairs of consecutive profiles were compared by computing the area between profiles using the trapezoidal method around the depth of strongest vertical gradients. The median area across the dataset and its percentage change relative to the uncorrected case were used to assess performance. Optimal parameters were selected based on visual inspection, favouring configurations where further parameter changes yielded diminishing improvements.

3.1.3 Glider Missions

The glider missions presented here were conducted in the coastal GoF, where typical water depths range from approximately 40 to 100 m. During each dive–climb cycle, the glider reversed direction approximately 4 m below the surface and 5–6 m above the seafloor to avoid surface interference and bottom contact. Each sampling cycle typically comprised four individual dives, yielding repeated, high-resolution vertical sections along the transect. Mission details are summarised in Table 1, and sampling locations are shown in Figure 1.

Table 1. Overview of glider missions presented in this thesis.

Mission name	*Mission start*	*Mission end*	*Average transect length, km*	*Sampled transects*	*Profiles gathered*	*Dive-climb recorded*	*Used in Paper(s)*
Mia20160504	*4 May 2016*	*16 May 2016*	*26*	*8*	*837*	*dives only*	
Mia20180507	*9 May 2018*	*6 June 2018*	*18*	*28*	*4368*	*both*	*I, II, III*
Mia20190521	*21 May 2019*	*19 June 2019*	*4.5*	*96*	*3872*	*both*	*II, III*
Mia20190719	*21 July 2019*	*10 August 2019*	*5.5*	*90*	*4140*	*both*	*II, III*

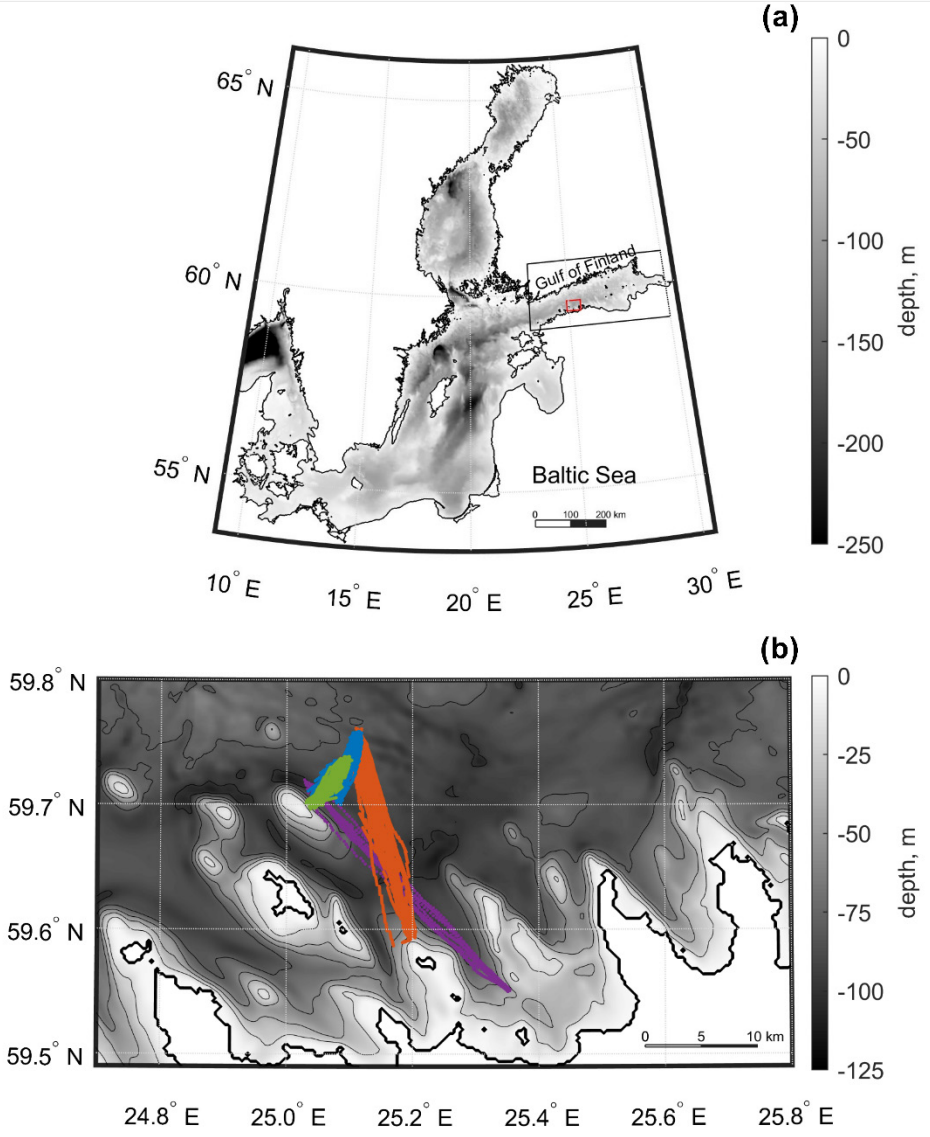


Figure 1. Map of the Baltic Sea (a), with the red rectangle marking the location of the study area shown in panel (b). The colormap indicates the bathymetry used in the model, while depth isolines in panel (b) are shown at 20 m intervals. Glider mission tracks from May 2016, May–June 2018, May–June 2019, and July–August 2019 are shown in purple, orange, blue, and green, respectively. Modified from Paper II.

3.2 Model Setup

Numerical simulations were performed using a three-dimensional nested setup of the General Estuarine Transport Model (GETM; Burchard & Bolding, 2002) to simulate circulation and temperature–salinity structure in the GoF. GETM is a hydrostatic, free-

surface primitive-equation model employing vertically adaptive coordinates, which enhance resolution near boundaries and in strongly stratified layers (Gräwe et al., 2015; Hofmeister et al., 2010; Klingbeil et al., 2018). Vertical mixing was calculated using the General Ocean Turbulence Model (GOTM; Umlauf & Burchard, 2005) with a two-equation k–ε turbulence model (Burchard & Bolding, 2001; Canuto et al., 2001).

The high-resolution model domain covered the entire GoF with a uniform horizontal grid spacing of 0.125 nautical miles (approximately 232 m) and 60 adaptive vertical layers. Bathymetry was obtained from the EMODnet database and interpolated to the model grid. The model domain was connected to the Baltic Proper through an open western boundary, where temperature, salinity, velocity, and sea surface height were specified from coarser-resolution simulations (for details see Paper II).

Atmospheric forcing was derived from the European Centre for Medium-Range Weather Forecasts atmospheric reanalysis dataset (ERA5, Hersbach et al., 2020) using bulk formulae Kondo (1975), and riverine freshwater input was prescribed from the Baltic Model Intercomparison Project (BMIP; Gröger et al., 2022) dataset, based on E-HYPE (Lindström et al., 2010) hindcast and forecast products (Väli et al., 2019).

3.2.1 Model–Observation Consistency

To assess whether the numerical model provides a physically consistent representation of the hydrographic structure, modelled temperature, salinity, and Brunt–Väisälä frequency fields were compared with glider observations (see Figs. 3–5 in Paper II). Overall, the model reproduces the observed patterns of variability in temperature and salinity and captures the characteristic vertical density structure of the GoF, including the development of the seasonal thermocline and the general structure of the cold intermediate layer. Although some biases are present, including an underestimation of salinity by about 0.4 g kg^{-1} and an overestimation of cold intermediate layer temperature by 1.5–2 °C, the main stratification features relevant to SMS dynamics are reproduced reasonably well.

Comparison of the vertical stratification structure shows generally good agreement in average UML depth across the missions, while the model tends to place the strongest stratification slightly shallower than observed, with the depth of maximum N^2 underestimated by about 2–5 m. The model does not always reproduce the full vertical complexity seen in the glider data, such as the occasional presence of multiple stratification maxima in the upper water column (Fig. 2), pointing to a simplified representation of fine-scale stratification. Nevertheless, the agreement in the dominant stratification features indicates that the model provides a suitable dynamical framework for interpreting the observed SMS variability.

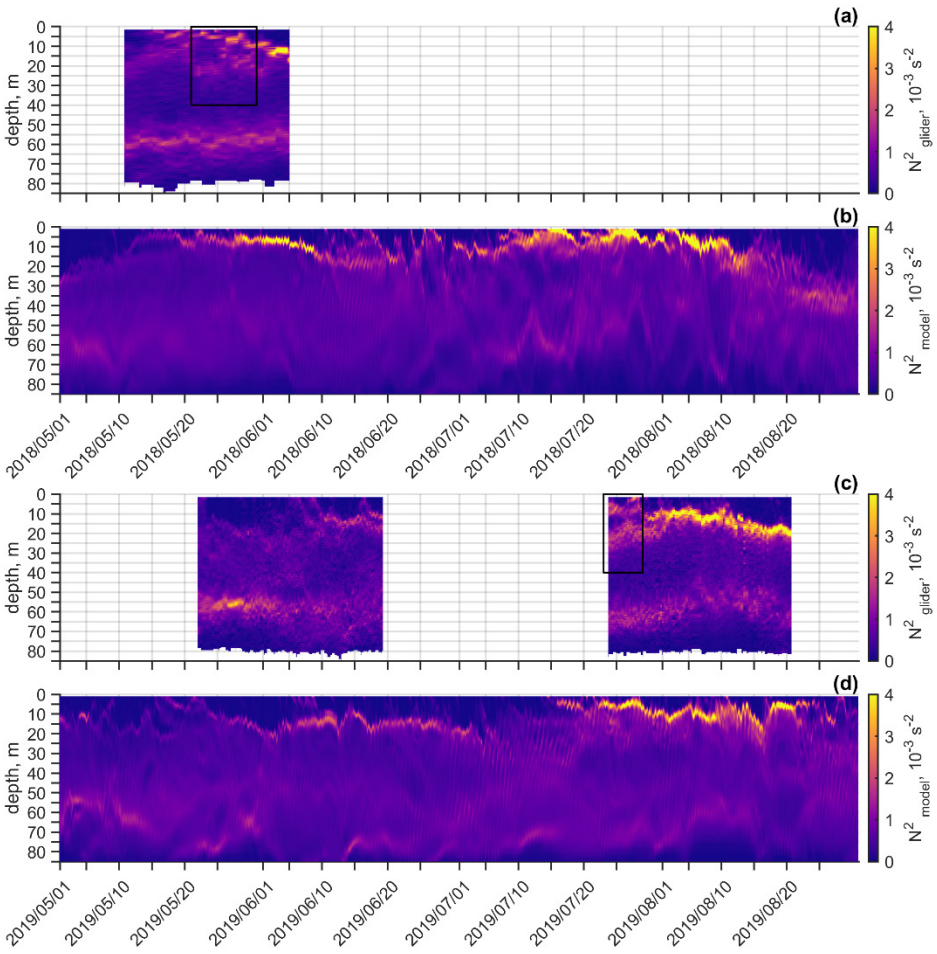


Figure 2. Vertical stratification variability expressed as the squared Brunt–Väisälä frequency (N^2) derived from glider observations (a, c) and model output (b, d) for May–August 2018 (a, b) and 2019 (c, d). The glider data represent average profiles for each section within the selected area, based on observations collected along approximately 1 km of glider track, and thus form a composite vertical structure. The model data show average profiles within a 1×1 km window at each model output time. Black boxes indicate periods of two local maxima in N^2: 21–30 May 2018 (a) and 23–28 July 2019 (c). Modified from Paper II.

3.3 Derived Quantities and Diagnostics

A set of derived quantities and diagnostic measures was calculated to characterise stratification, frontal structure, and SMS variability. Buoyancy was calculated to provide a compact measure of density variability relevant for stratification and frontal dynamics. Buoyancy was defined as

$$b = -\frac{g}{\rho_0}(\rho - \rho_0), \quad (1)$$

where ρ is density and ρ_0 a reference density of 1000 kg m^{-3}. From buoyancy, the Brunt–Väisälä frequency was computed to identify regions of enhanced stratification. The squared Brunt-Väisälä frequency was expressed over 2 m vertical intervals as

$$N^2 = b_z, \tag{2}$$

subscript indicating partial derivative.

Horizontal buoyancy gradients were calculated from the buoyancy field to characterise the strength of lateral density contrasts. From the glider observations, along-transect buoyancy gradients were calculated as $b_s = \frac{\partial b}{\partial s}$, using a horizontal step of 5 km. For the model output, the horizontal buoyancy gradient magnitude was computed as

$$|\nabla_h b| = \sqrt{b_x^2 + b_y^2}, \tag{3}$$

where b_x and b_y denote the zonal and meridional buoyancy gradients, estimated using a centred finite-difference scheme with a horizontal spacing of 5 km.

Isopycnal slopes were calculated from the depth variations of selected density surfaces along the section using a horizontal spacing of 5 km, with density surfaces defined on a σ-grid at 0.1 kg m^{-3} intervals. A linear regression was applied to the depth–distance relationship of each isopycnal surface, and the slope was obtained from the fitted coefficient. This diagnostic was introduced to quantitatively characterize the frontal structure described in Paper I.

The relative geostrophic velocity component was estimated from glider-derived hydrographic observations using the dynamic height method at a lateral scale of 5 km. The component normal to the glider transect was obtained from the geopotential slope of an isobaric surface as

$$u_g = -\frac{1}{f}\frac{\partial \Phi}{\partial s}, \tag{4}$$

where f is the Coriolis parameter and Φ is geopotential, related to dynamic height by $\Phi = gD$. Dynamic height was calculated from the measured temperature and salinity profiles using a reference level of 80 dbar (IOC et al., 2010; McDougall & Barker, 2011).

3.3.1 Dynamical Diagnostics

The Rossby number was used to identify regions where ageostrophic motions become important. It was estimated from the model output as

$$Ro = \frac{\zeta}{f}, \tag{5}$$

where the relative vorticity is

$$\zeta = v_x - u_y \tag{6}$$

Spatial derivatives of u and v, denoting the zonal and meridional velocity components, respectively, were computed using a centred finite-difference scheme with a horizontal grid spacing of 500 m.

3.3.2 Potential Vorticity Diagnostics

Potential vorticity (PV) provides a useful diagnostic for assessing the susceptibility of the flow to instabilities (Hoskins, 1974). In this thesis, PV was estimated using a simplified balanced form, appropriate away from the equator and under the thermal-wind approximation. In this form, PV is expressed as the balance between a stratification–vorticity term and a baroclinic term associated with horizontal buoyancy gradients (e.g., Thompson et al., 2016; Buckingham et al., 2019; Johnson et al., 2020), yielding

$$q = (f + \zeta)N^2 - \frac{1}{f}|\nabla_h b|^2. \tag{7}$$

Following Thompson et al. (2016), the along-transect buoyancy gradient is used as a proxy for the horizontal buoyancy gradient, and the relative vorticity is approximated from the along-transect derivative of the cross-transect geostrophic velocity as

$$\zeta_g \approx \frac{\partial u_g}{\partial s}, \tag{8}$$

evaluated using a horizontal step of 5 km. The observational estimate of PV then becomes

$$q_{obs} = \left(f + \zeta_g\right)N^2 - \frac{b_s^2}{f}. \tag{9}$$

This formulation assumes that the glider transect is approximately perpendicular to the frontal structure, so that the along-transect buoyancy gradient represents the cross-front gradient and the cross-transect velocity captures the dominant shear. The hydrographic PV estimate therefore identifies potential locations of PV reduction under balanced-flow assumptions.

To highlight departures from the leading-order background PV, q_{obs} was expressed in nondimensional form using fN^2 as the reference scale. This scale represents the PV expected for a stably stratified flow dominated by planetary vorticity, before the effects of relative vorticity and lateral buoyancy gradients (Pedlosky, 1996; Haine & Marshall, 1998; Buckingham et al., 2019). The nondimensional PV was therefore calculated as

$$q_{nd} = \frac{q_{obs}}{fN^2} = 1 + \frac{\zeta_g}{f} - \frac{b_s^2}{f^2N^2}. \tag{10}$$

The second term represents an observational estimate of the Rossby number, while the third term represents the reduction of PV by horizontal buoyancy gradients. Because the Rossby-number term is generally small, low or negative q_{nd} values mainly occur where horizontal buoyancy gradients are strong enough to offset the positive background PV. Since the nondimensionalisation uses positive scaling factors ($N^2 > 0$ and $f \neq 0$), the sign of PV is preserved, and negative values continue to indicate conditions favourable for frontal instabilities.

Given the assumptions in the observational estimate and the uncertainty associated with glider sampling, the 10th percentile of q_{nd} in the upper 0–30 m layer was used as a summary metric. This lower-tail measure highlights periods when low-q_{nd} conditions were most pronounced, while reducing the influence of isolated noisy extrema.

3.3.3 Tracer Diagnostics

Spice was calculated to isolate along-isopycnal thermohaline variability and to provide a tracer-based measure of water-mass deformation associated with SMS stirring. Following the formulation introduced in Paper II by the author, spice was treated as a density-compensated tracer of lateral thermohaline variability and defined as the projection of temperature–salinity anomalies along isopycnals,

$$spice = \alpha\Delta T + \beta\Delta S, \tag{11}$$

where α and β are the thermal expansion and haline contraction coefficients, respectively. The anomalies ΔT and ΔS were defined relative to the mean Conservative Temperature and Absolute Salinity along the same isopycnal within a surrounding 4 km window. For the observations, this was implemented as a moving window along the glider trajectory, whereas for the model it was calculated within a 4 × 4 km square around each grid point. Spice anomalies were scaled by a reference density to express them in density units, enabling direct comparison with buoyancy-related diagnostics. To characterise the intensity of lateral water-mass variability, root mean square (RMS) spice was calculated over density layers spanning the surface to the depth of the temperature

minimum. This combined temperature–salinity measure allows fine-scale thermohaline variability to be compared across both spring and summer missions, which is particularly relevant in the GoF where the relative roles of temperature and salinity vary seasonally.

The magnitude of the vertical advective tendency of spice was calculated from the model fields and is defined as

$$A_z(spice) = \left| w \frac{\partial spice}{\partial z} \right|, \tag{12}$$

where w is vertical velocity. This quantity represents the effect of vertical velocity acting on the vertical spice gradient (e.g., Meng et al., 2020; Zhu et al., 2024). It is used here as a measure of the intensity of vertical tracer redistribution associated with the subduction event suggested in Paper II.

3.3.4 Spectral Analysis

Wavenumber spectra of isopycnal temperature were computed to assess whether tracer variability exhibits scaling consistent with SMS dynamics. In addition to the spectra reported in Paper I, an analogous analysis was applied to the 2016 mission to include a second frontal case and to evaluate whether similar spectral structure was observed under comparable conditions.

Because glider sampling is irregular in space and time, isopycnal tracer fields were mapped to uniform along-track spacing prior to spectral analysis. Temperature profiles were first averaged within density bins of 0.1 kg m^{-3} and then interpolated to a constant time step of 10 min for the 2018 mission and 20 min for the 2016 mission. These intervals corresponded to approximate horizontal spacings of 145 m and 270 m on average, respectively. For the 2018 mission, the analysed period was restricted to approximately two weeks to better isolate the frontal regime.

Wavenumber spectra were computed using a Fast Fourier Transform and smoothed by averaging over 11 elementary frequency bands. The analysis focused on density layers whose median depths were within the upper 40 m, including the UML and thermocline. Spectral slopes were estimated over 10–1 km and, additionally, over 5–1 km, because the frontal-period spectra showed increased variability at 10–5 km, where mesoscale frontal structure and SMS-related tracer variability may overlap.

4 Results and Discussion

4.1 Identifying Submesoscale Variability from Gliders

SMS dynamics in the ocean are commonly associated with order one Rossby numbers (McWilliams, 2016; Taylor & Thompson, 2023) and are therefore frequently characterized using velocity-based diagnostics (e.g., Adams et al., 2017; Ramachandran et al., 2018). In glider observations, however, direct measurements of full velocity gradients or vertical velocity are not always available, depending on the sensor package. Nevertheless, observational studies have shown that glider data can provide robust signatures of SMS dynamics through hydrographic structure and derived diagnostics (e.g., Cole & Rudnick, 2012; Shang et al., 2023; Thompson et al., 2016). This section examines SMS variability identified from glider observations by analysing thermohaline structure, revealing filamentary tracer intrusions, and SMS-relevant diagnostics, with emphasis on their co-evolution.

4.1.1 Structural Signatures

The presence of SMS signatures in glider observations is demonstrated using repeated transects across a mesoscale frontal system in the GoF (Paper I). The observations reveal persistent fine-scale thermohaline variability, filamentary tracer intrusions, and spectral signatures consistent with active SMS dynamics.

Figure 3 shows a representative glider section across a frontal structure, illustrating the characteristic thermohaline and spice signatures associated with SMS activity. Strongly tilted isopycnals indicate a sharp horizontal buoyancy gradient and an active frontal zone. Within this environment, coherent spice anomalies appear as adjacent positive and negative patches, revealing fine-scale thermohaline variability within the mesoscale front (Fig. 3a). These features reflect lateral contrasts between distinct water masses. In the present spring example, the pattern is clearly seen in temperature (Fig. 3b, c), whereas in summer it is often more evident in salinity, depending on which variable contributes more to the vertical density structure.

The intrusions exhibit an apparent vertical extent of at least 5 m and are horizontally confined to scales of about 2 km, consistent with expected SMS spatial scales in the Baltic Sea (e.g., Lips et al., 2016; Zhurbas et al., 2022). In rotating, stratified flows close to geostrophic balance, mesoscale strain and shear stretch passive tracers into elongated filaments whose vertical-to-horizontal aspect ratio is expected to approach f/N (Smith & Ferrari, 2009). Similar aspect ratio relationships have been reported in observational studies of fine-scale tracer structure, where filament slopes are broadly consistent with this theoretical scaling (e.g., Cole & Rudnick, 2012; Kolodziejczyk et al., 2018). Using the observed scales $H \approx 5\ m$ and $L \approx 2\ km$ gives $H/L \approx 0.003$, while typical values near the pycnocline where the intrusion occurs ($f \approx 1.26 \cdot 10^{-4}\ s^{-1}$, $N \approx 0.03 - 0.04\ s^{-1}$) give $f/N \approx 0.003 - 0.004$. For this example, the close agreement in aspect ratio supports the interpretation that the observed intrusion has the geometry expected for frontal tracer structures. Because SMS motions are expected to emerge within such frontal zones, the intrusion is consistent with SMS activity and represents an identifiable signature in glider-measured thermohaline fields.

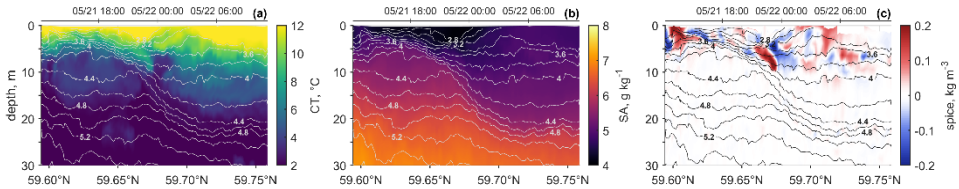


Figure 3. Representative example of SMS-related thermohaline deformation observed by a glider crossing a mesoscale front. Panels showing (a) temperature, (b) salinity, and (c) spice, with density contours overlaid at 0.2 kg m^{-3} intervals, based on glider data from 21–22 May 2018. The area between ticks presenting latitude is approximately 5.5 km. Modified from Paper I.

4.1.2 Diagnostic Evidence

Individual SMS features are inherently transient and difficult to observe directly (e.g., Lévy et al., 2018), motivating the use of broader diagnostics that capture their integrated occurrence and evolution. Section 4.1.1 illustrated the structural signatures through which SMS presence can be identified in individual glider sections. In Paper I, these signatures were diagnosed using glider observations of thermohaline structure, buoyancy gradients, and associated temperature anomalies within an evolving mesoscale frontal system under weak atmospheric forcing.

The mesoscale frontal system was identified from the pronounced tilt of the density field across the glider transect and the enhanced along-transect buoyancy gradient at 15 m depth (Fig. 4d–f, 5d in Paper I). Sustained positive gradients after 21 May indicate that the frontal density contrast persisted throughout the study period, providing a stable background for smaller-scale variability. The front developed under persistent NE–E winds that drove surface waters offshore along the southern coast of the GoF and induced coastal upwelling. At the same time, a westward flow exceeding 20 cm s^{-1} developed along the sloping density surfaces (Fig. 4d–f in Paper I), consistent with a geostrophic frontal jet associated with upwelling event (e.g., Lehmann & Myrberg, 2008).

The emergence of the front on 21–22 May coincided with an asymmetric development of stratification across the section. On the denser side, stratification intensified through the combined effects of surface heating and mesoscale vertical motions associated with the frontal circulation (Fig. 5b in Paper I). On the lighter side, two stratification maxima developed (Fig. 5a in Paper I): an upper maximum associated with progressive surface heating and a deeper one likely linked to pre-existing haline stratification. Consistent with this shallow structure, the along-transect buoyancy gradient at 3 m depth differs from the deeper frontal gradient (Fig. 5c–d in Paper I).

Smaller-scale variability embedded within the mesoscale front was examined using temperature deviations along isopycnals, calculated relative to the surrounding 4-km mean (Fig. 4g–i in Paper I). In spring conditions in the GoF, density variability is primarily controlled by salinity (e.g., Lips et al., 2014), so temperature anomalies along isopycnals provide an effective tracer of small-scale stirring. Adjacent positive and negative anomalies indicate counter-directed motions along the sloping isopycnals, consistent with downward displacement of warmer surface-influenced water and upward displacement of colder water from below. These anomalies emerged together with the frontal structure and, on 21–22 May, were co-located with the steepest isopycnal slope,

reaching peak deviations of 1.2 °C and −1.4 °C (Fig. 4h in Paper I). Their kilometre-scale organisation supports the interpretation of localized vertical exchange and ageostrophic motions within the frontal zone (e.g., Garcia-Jove et al., 2022; McWilliams, 2016).

To examine the co-evolution of multiple SMS-relevant indicators in a consistent way, the diagnostics used in Paper I are reformulated in this thesis as quantitative time series. This does not change their physical interpretation but allows their temporal evolution to be compared more directly.

The frontal structure is represented by the mean isopycnal slope in the upper water column. Enhanced positive slopes during the last third of May indicate the persistence and strengthening of the front, while the marked decrease at the beginning of June signals reorganisation of the water column (Fig. 4a). The along-transect buoyancy gradient is represented by its average value in the 0–30 m layer. Its increase during the late-May frontal period complements the isopycnal-slope evolution and confirms the strengthening of the frontal density contrast (Fig. 4b).

Fine-scale thermohaline variability is here summarized by RMS spice. RMS spice rises as the frontal structure becomes established in the glider sections and remains elevated through a series of recurrent peaks toward the end of May and beginning of June, during a period of changing wind forcing (Fig. 4a). The temporal correspondence between isopycnal slope, buoyancy gradient, and RMS spice indicates that enhanced fine-scale variability is linked to periods when the front is established and the background forcing is changing.

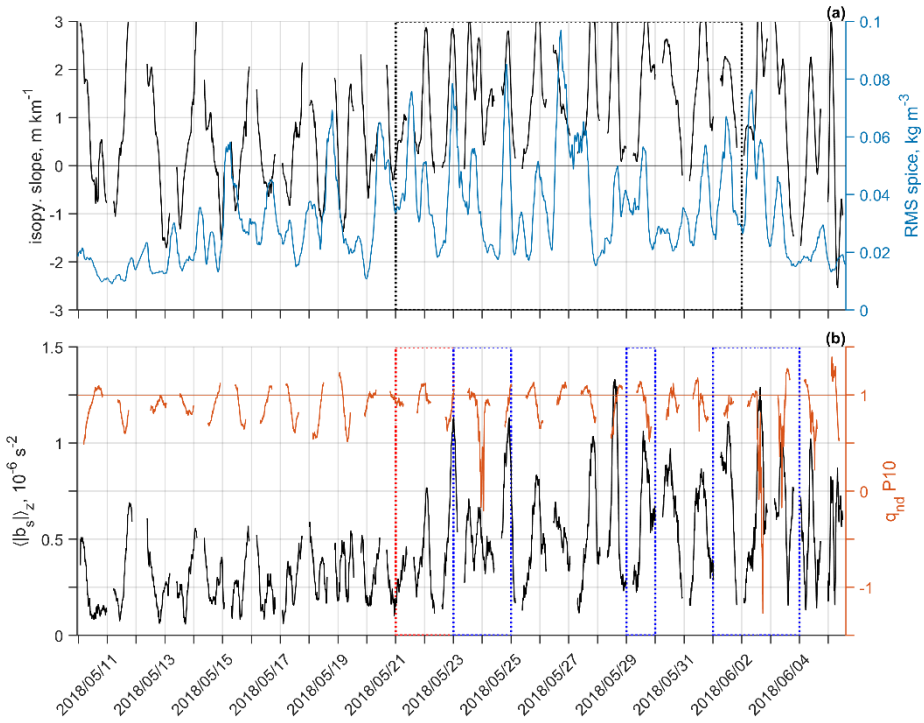


Figure 4. Time series of diagnostics indicative of SMS activity derived from glider observations during the May–June 2018 mission. (a) Isopycnal slope (black; m km^{-1}), computed over a 5 km

horizontal scale, and RMS spice (blue; kg m $^{-3}$), filtered with a 5 km moving window. Both variables were averaged over density layers spanning the surface to the depth of minimum temperature (~0–30 m). A positive slope indicates that the isopycnal layer is elevated on the southern side of the section. (b) Along-transect buoyancy gradient computed over a 5 km horizontal scale (black; 10 $^{-6}$ s $^{-2}$), and the 10th percentile of non-dimensional potential vorticity (orange), both evaluated over the upper 0–30 m layer. The black box in panel (a) marks the period when the glider-observed hydrographic structure indicated a front. Red and blue rectangles in panel (b) denote periods of enhanced equivalent heat flux associated with baroclinic and wind-driven processes, respectively.

4.1.2.1 Dynamical Conditions

In Paper I, several diagnostics were used to assess whether the observed frontal conditions were favourable for SMS processes. These included equivalent heat fluxes associated with wind-driven and baroclinic processes (Fox-Kemper et al., 2008; Thomas, 2005; Thompson et al., 2016), PV, and estimates of the Obukhov length (Figs. 6–7 in Paper I). Although the observations did not allow unambiguous identification of specific instability mechanisms, the diagnostics identified two dynamically active periods.

The first occurred during the initial appearance of the front around 22 May, when the strongest structural SMS signatures coincided with elevated equivalent heat fluxes associated with baroclinic restratification. Such restratification is consistent with the effects of baroclinic instability in frontal regions (e.g., Mahadevan et al., 2010).

The second period occurred around 29 May and the beginning of June, when enhanced wind-driven equivalent heat fluxes coincided with reductions in PV. While this combination is broadly consistent with conditions that may favour SI, the Obukhov length estimates indicated that the direct influence of surface forcing remained shallow. Because the frontal structure extended below the UML, the overlap between the wind-affected layer and the deeper baroclinic structure appears limited. Thus, the observations do not consistently support the combination of reduced PV and sufficiently strong surface forcing required for symmetric instability to develop at density fronts (Taylor & Ferrari, 2010; Thomas et al., 2013).

In this thesis, these two periods are summarised using q_{nd}, which highlights PV reductions associated with horizontal buoyancy gradients relative to the local background stratification. The q_{nd} time series shows reductions during the well-defined frontal period on 23–24 May and again at the beginning of June.

The first reduction follows the baroclinic restratification peak identified in Paper I and coincides with enhanced wind-driven contributions (Fig. 6b in Paper I). This timing may suggest dynamical intermittency within the frontal zone, consistent with the view that frontal systems can reflect the combined influence of multiple mechanisms (e.g., Mahadevan et al., 2010).

The early-June reduction occurs during a period of stronger surface-layer variability, when smaller-scale along-transect buoyancy gradients often differed from the deeper mesoscale frontal structure. In contrast to the earlier event, the buoyancy field was therefore less vertically coherent and more variable in the surface layer. This suggests a more surface-related adjustment of the frontal system, likely influenced by wind forcing (Thomas, 2005; Thomas & Ferrari, 2008).

As a complementary diagnostic, the observational Rossby-number proxy, Ro_{obs}, was then used to examine whether the dynamically active periods were also expressed in the geostrophic velocity structure sampled by the glider. Following Thompson et al. (2016), Ro_{obs} was derived from the section-based approximation of relative vorticity (Eqs. 5 and 8). Because this formulation represents only the geostrophic component of the flow,

Ro_{obs} is not expected to reach order one values. Enhanced Ro_{obs}, or increased moving-window variance of $|Ro_{obs}|$, therefore indicates stronger section-resolved variability of the geostrophic flow.

Figure 5 compares Ro_{obs} averaged over 0–10 m and 0–30 m to assess the vertical extent of this variability. During 22–23 May, the signal remains comparable across both depth ranges, suggesting variability extending through much of the upper water column. In contrast, the 28–29 May signal weakens markedly in the 0–30 m average, indicating a more surface-confined response. This supports the interpretation made from the q_{nd} analysis: the earlier event was more vertically coherent, whereas the later event was more surface intensified. Together with the equivalent heat flux diagnostics, this contrast suggests that the two events may reflect different dominant adjustment pathways (e.g., Boccaletti et al., 2007; Fox-Kemper et al., 2008; Thomas & Lee, 2005).

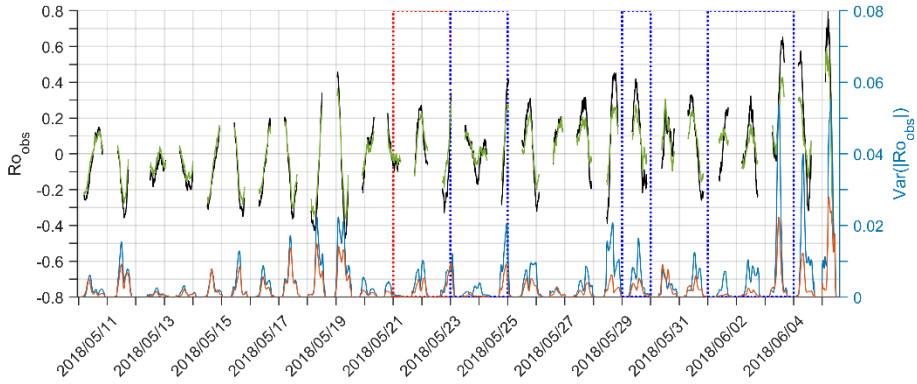


Figure 5. Observational Rossby number proxy (Ro_{obs}) estimated from glider observations and its moving-window variance. The Rossby number proxy is shown for vertical averaging over 0–10 m (black) and 0–30 m (green), while the corresponding moving-window variance is shown in blue (0–10 m) and orange (0–30 m). Red and blue rectangles denote periods of enhanced equivalent heat flux associated with baroclinic and wind-driven processes, respectively.

4.1.2.2 Spectral Evidence

Spectral slopes are commonly used to distinguish dynamical regimes because different turbulence theories predict different rates at which variance decreases toward smaller scales. For kinetic energy, predictions with k^{-3} are expected for interior quasi-geostrophic turbulence (Charney, 1971) and a $k^{-5/3}$ for surface quasi-geostrophic dynamics (Blumen, 1978). Tracer-variance spectra are often used as a complementary diagnostic to energy spectra. For tracers that behave passively on isopycnal surfaces, near-k^{-2} spectra are commonly interpreted as evidence of lateral stirring by frontal and SMS-related motions (Balwada et al., 2024; Callies & Ferrari, 2013; Cole & Rudnick, 2012). This differs from the flatter k^{-1} slope expected for passive tracer variance in the ocean interior under dominant quasi-geostrophic turbulence (Erickson et al., 2020).

To assess whether the dynamically active frontal states identified from the time-series diagnostics were consistent with SMS-related tracer stirring, wavenumber spectra of along-isopycnal temperature were examined. Because internal waves mainly displace density surfaces rather than modify tracer structure along them, variance on isopycnals is expected to reflect horizontal stirring processes (Callies & Ferrari, 2013; Ferrari &

Rudnick, 2000). In Paper I, isopycnal-temperature spectra showed slopes close to -2 in both the surface layer and thermocline over spatial scales of 10–1 km. In this thesis, the analysis was restricted to the frontal period and extended to the 2016 mission as a second frontal case. During the frontal periods, the spectra showed increased variability at wavelengths of approximately 10–5 km, where mesoscale frontal structure and smaller-scale tracer stirring may overlap (Fig. 6a, d). The 5–1 km slopes therefore provide a more focused estimate of the smaller-scale part of the spectrum (transition from mesoscale to submesoscale).

For the 2018 mission, the clearest correspondence with SMS-related stirring occurred in the density range 4.3–5.2 kg m^{-3}, located at depths of approximately 10–25 m. In this layer, the isopycnals were strongly inclined and the averaged spectrum had a slope of -1.9 (Fig. 6a, c). The upper density range showed a slightly steeper slope of -2.2, while below 25 m the spectra became slightly shallower in the 5.3–5.7 kg m^{-3} layer, with an averaged slope of -1.8. This suggests that the 2018 frontal signal was strongest in the upper stratified layer and weakened with depth. The 10–25 m layer also shows intrusion-like features in both temperature and chlorophyll (Fig. 6b, c). Chlorophyll distribution shows a layer of slightly higher concentrations near the maximum density gradient, suggesting a connection to the near-surface front.

A similar frontal setting was observed during the 2016 mission, but the vertical expression of the variability extended deeper (Fig. 6f). The upper density range had a flatter averaged slope of -1.8, whereas within the density ranges of 4.3–4.7 and 4.8–5.2 kg m^{-3}, corresponding approximately to depths of 15–25 m and 25–40 m, respectively, spectra showed slopes of -2.0 and -2.1 (Fig. 6d). These steeper slopes coincide with the inclined pycnocline and pronounced lateral buoyancy gradients, and with temperature and chlorophyll variability extending into and below the pycnocline (Fig. 6e, f).

Thus, both frontal cases show spectral signatures consistent with SMS-related along-isopycnal tracer stirring in subsurface layers, particularly where the pycnocline, horizontal buoyancy gradients, and tracer variability coincide. However, the vertical extent of this active layer differed between missions. In 2018, the variability was concentrated around the strong upper pycnocline, whereas in 2016 the frontal structure and associated tracer variability extended deeper under slightly weaker stratification.

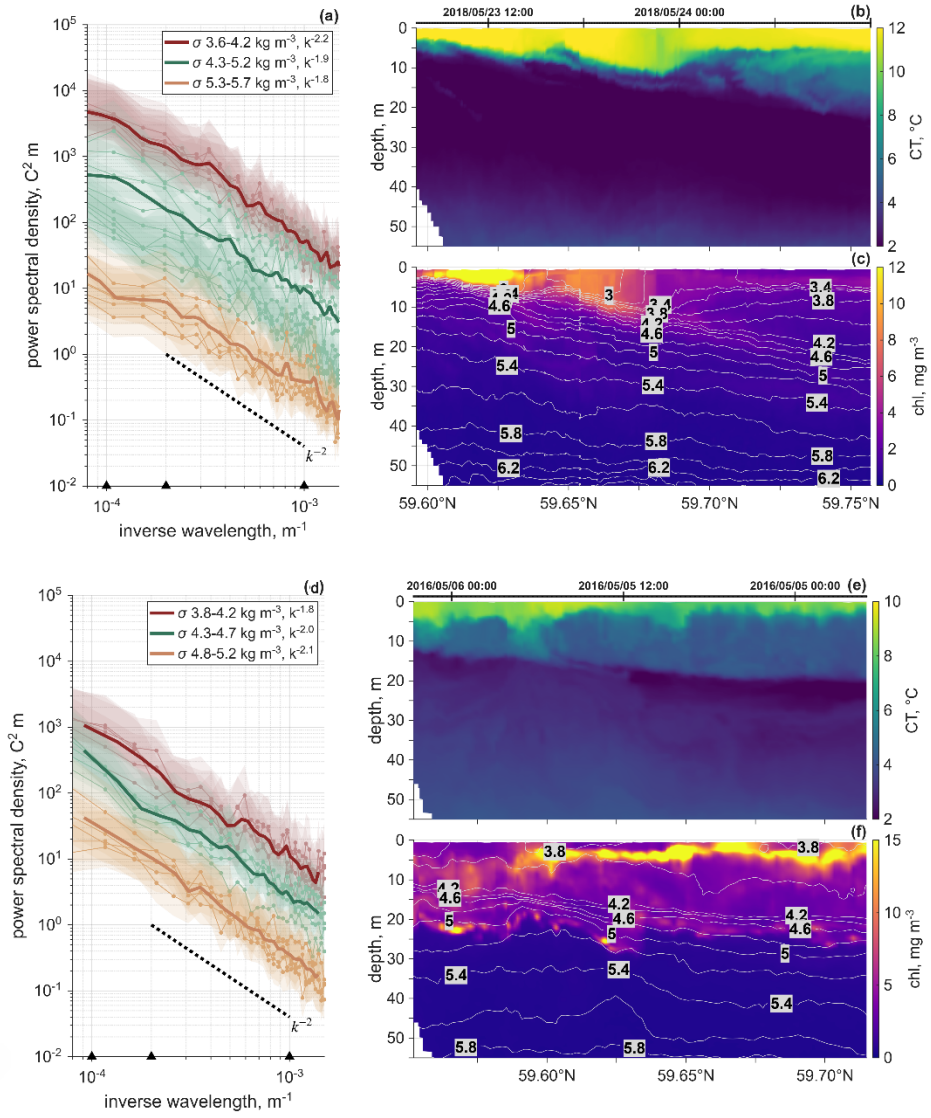


Figure 6. Wavenumber spectra and hydrographic structure during frontal missions in 2018 and 2016. Panels (a, d) show along-isopycnal temperature spectra for the 2018 and 2016 missions, respectively, grouped into three σ-ranges shown in red, green, and orange. The red range corresponds to the upper density layer, extending to approximately 10 m in 2018 and 15 m in 2016. The green range extends from the base of this upper layer to approximately 25 m, and the orange range corresponds to approximately 25–40 m. Thin lines show individual spectra, thick lines show mean spectra, and shaded envelopes indicate 95% confidence intervals. The dashed black line indicates a k^{-2} reference slope, and triangles mark wavelengths of 10, 5, and 1 km. Panels (b, c) and (e, f) show example temperature and chlorophyll distributions overlaid with σ-contours at 0.2 kg m^{-3} intervals from 2018 and 2016, respectively.

4.2 Spatial Structure of Submesoscale Variability

After identifying SMS signatures in the glider observations, the analysis was extended to the surrounding mesoscale density field to examine the dynamical setting in which SMS-permissive conditions developed. Paper II presented characteristic events from May to August, with similar wind-forcing patterns identified in both analysed years, 2018 and 2019 (Fig. 7 in Paper II). These forcing regimes produced upwelling, downwelling, and mesoscale advection events that were repeatedly associated with order one Rossby numbers and intensified horizontal buoyancy gradients, indicating the formation of SMS-permissive fronts and filaments. Upwelling-favourable northeasterly–easterly winds led to coastal upwelling along the southern coast, where strong lateral density gradients coincided with regions of order one Rossby number (Fig. 7a, c, e). During strong downwelling-favourable southwesterly to westerly wind events, regions with order one Rossby numbers extended across much of the gulf rather than remaining confined to narrow frontal zones, indicating more widespread SMS-permissive conditions (Fig. 7b). During periods with southerly to southwesterly winds, mesoscale eddy activity and westward intrusion of low-salinity water were associated with strengthened lateral density contrasts and regions of elevated Rossby number (Fig. 7d, f).

The association between forcing-driven mesoscale structures and SMS diagnostics suggests that atmospheric forcing helps organise the density field in which SMS activity can develop in the GoF. The wind regimes identified here are characteristic of the Baltic Sea and help sustain pronounced mesoscale variability in the region (e.g., Kikas & Lips, 2016; Liblik et al., 2022). This regional context is consistent with previous Baltic Sea observations showing that SMS processes may be important during changing wind-forcing conditions, particularly during the development and relaxation of coastal upwelling and downwelling events (Lips et al., 2016). More broadly, ocean observations show that mesoscale fronts and eddy edges can host complex thermohaline structures and instability-prone SMS conditions (Adams et al., 2017).

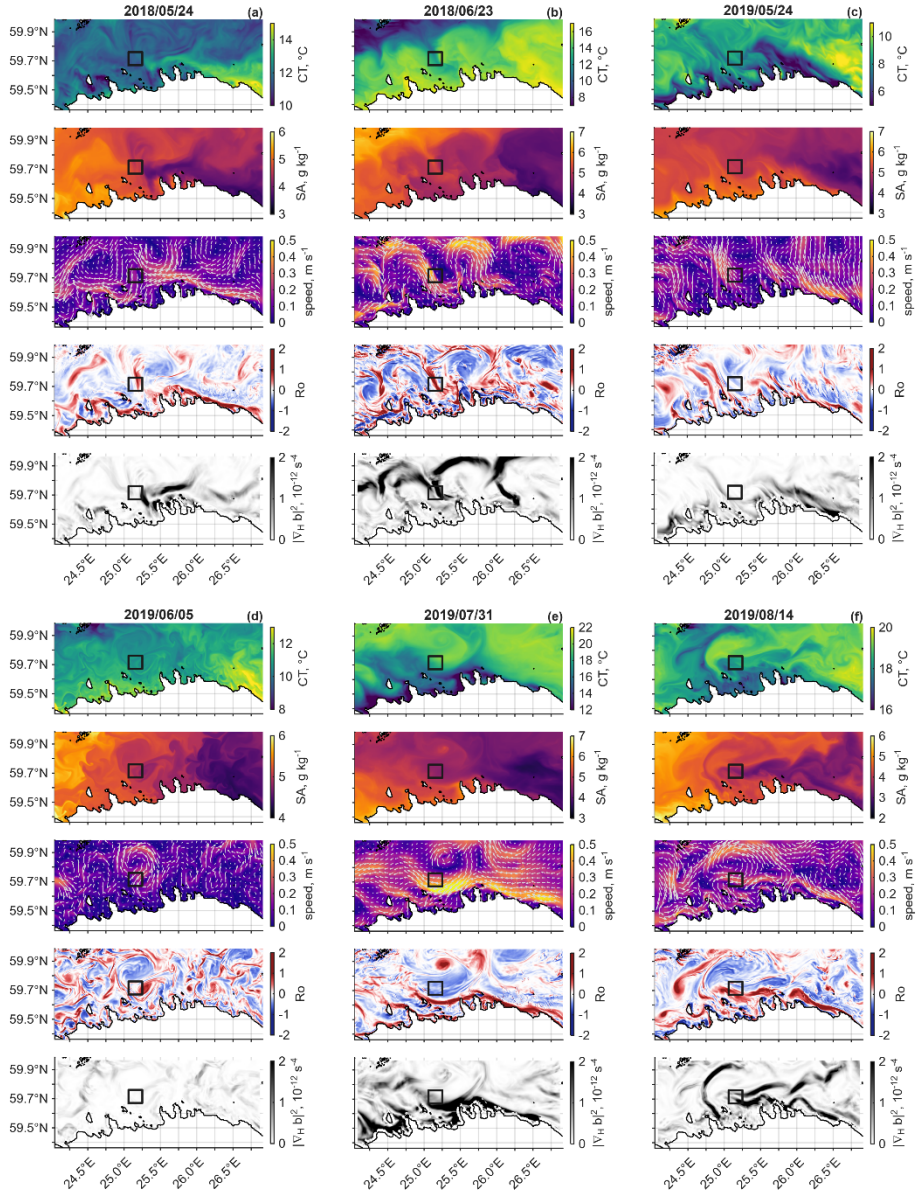


Figure 7. Overview of surface hydrographic and dynamical conditions in the GoF during spring–summer 2018–2019, illustrating the variability of SMS-relevant fields. Example dates characterizing the evolving dynamical background are shown in (a–c) first row: 24 May 2018, 23 June 2018, and 24 May 2019, and in (d–f) second row: 5 June, 31 July, and 14 August 2019. For each date, panels from top to bottom display surface (0–3 m) Conservative Temperature (°C), Absolute Salinity (g kg^{-1}), velocity (m s^{-1}), Rossby number, and squared horizontal buoyancy gradient modulus (s^{-4}). The black box marks the 10×10 km study window. Modified from Paper II.

4.2.1 Horizontal Structure of Submesoscale Indicators

The forcing-driven fronts and filaments identified in the model provide the mesoscale context for the glider observations. In Paper II, this connection was examined using three glider missions spanning different spring–summer forcing conditions. Spice was used as the main tracer-based measure of SMS variability, while model-derived Rossby number, Richardson number, and horizontal buoyancy gradients described the surrounding dynamical field.

Because the glider sampled only a narrow section through the mesoscale density field, RMS spice was compared with surface Rossby number to assess whether tracer variability coincided with nearby dynamically active regions. RMS spice derived from glider observations and model output showed good qualitative agreement. Elevated values tended to occur during periods of enhanced surface Rossby number (Fig. 8). However, the correspondence was not one-to-one, suggesting that tracer signal can persist or be advected away from regions of instantaneous dynamical activity (Lévy et al., 2018). During the spring–early summer transition, when surface buoyancy flux was positive and the seasonal thermocline was developing, the glider missions showed predominantly coupled behaviour between elevated RMS spice and surface Rossby number (Fig. 8). Examples in Figure 10 of Paper II illustrate elevated RMS spice in regions of low Richardson number associated with elongated frontal structures and the periphery of an eddy, suggesting that the tracer signal was closely linked to active frontal dynamics.

In contrast, the summer mission, when stratification was well established and surface forcing was more variable, illustrates partial decoupling between tracer-based and dynamical indicators (Fig. 8c, d). Enhanced RMS spice and patches of low Richardson number appeared within the study area (Fig. 10 in Paper II), whereas the regions of order one Rossby number and intensified horizontal buoyancy gradients occurred south of the study area, within the coastal current region formed during the upwelling event (Fig. 7e). Thus, the glider sampled enhanced tracer variability adjacent to the dynamically active region. This spatial arrangement is consistent with the tracer signal remaining linked to nearby frontal dynamics, even when dynamical indicators peak outside the sampled region, because SMS motions can redistribute tracer anomalies within frontal systems (e.g., Archer et al., 2020; Hosegood et al., 2017). This case is discussed further in Section 4.3.

Taken together, these examples show that the horizontal expression of SMS variability is not uniform but depends on the surrounding mesoscale setting and the seasonal state of the water column. The spring and summer cases suggest that tracer-based signatures can either coincide with or become offset from the strongest dynamical indicators, implying that the observed spice patterns reflect both the instantaneous dynamical setting and the history of tracer redistribution within the mesoscale flow. The role of vertical stratification in shaping these different expressions is considered further in the following section.

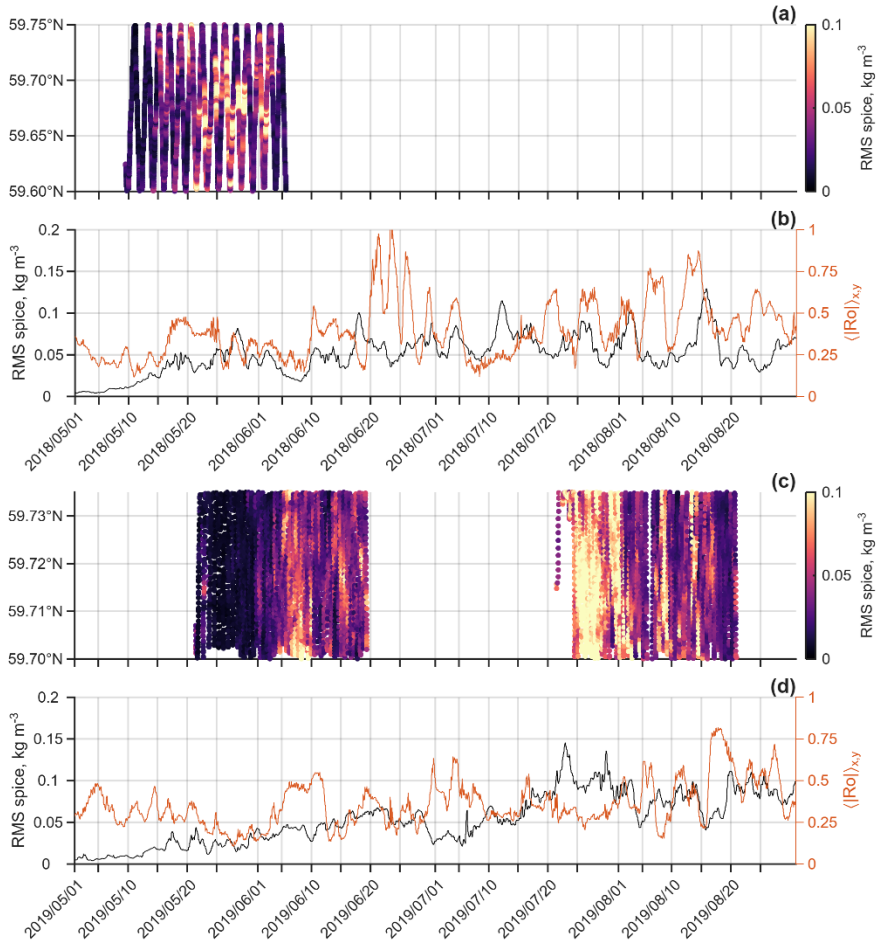


Figure 8. RMS spice in spring–summer 2018–2019, calculated over the density range extending from the surface to the depth of minimum temperature (approximately the upper 0–30 m). Panels (a, c) show the latitude–time distribution of RMS spice from the glider missions. Panels (b, d) show the corresponding model diagnostics within a 10×10 km study window: RMS spice in black and RMS surface Rossby number in orange. Modified from Paper II.

4.2.2 Vertical Structure of Spice Variability

Paper II reveals a pronounced seasonal contrast in the vertical distribution of spice variability. During the spring–early summer missions, spice maxima are located near the base of the UML, at densities shallower than the maximum vertical density gradient (Fig. 9a, b). By summer, the spice maximum shifts below the UML to densities immediately beneath the strongest density gradient, within the seasonal thermocline (Fig. 9c). This apparent shift is interpreted as part of the seasonal evolution of stratification and forcing.

The strengthening and deepening of stratification from May to August are illustrated by the evolution of the Brunt–Väisälä frequency (Fig. 2). Although the timing differs between years, the development of seasonal stratification coincides with enhanced spice

variability (Figs. 2a, c and 8a, c). This co-occurrence may indicate that, as the water column becomes increasingly layered, redistributed temperature and salinity contrasts leave a clearer spice signal. It may also reflect the development of horizontal gradients, driven in spring partly by differential warming of shallow coastal and offshore areas (Lips et al., 2014) and influenced by persistent riverine freshwater advection (Lips et al., 2017; Stipa et al., 1999). Such gradients can create favourable conditions for SMS activity.

The spring–early summer missions were both characterized by positive surface heat flux during the seasonal development of stratification. Under these conditions, horizontal buoyancy gradients can develop while intermittent weakening of wind forcing prevents continuous erosion of variability near the base of the UML. The spice maximum near the UML base may therefore indicate a transition layer that is less exposed to wind-driven mixing, allowing SMS activity to develop there (Johnston & Rudnick, 2009). This interpretation is also supported by Fig. 3 in Paper III, where scanfish sections show intrusions of water with different temperature and salinity properties above inclined pycnoclines.

In summer, the relevant background state is different. The seasonal thermocline is already established, and the water column is strongly layered. Upwelling- and downwelling-favourable winds are frequent in the GoF during summer (Kikas & Lips, 2016), tilting and displacing the thermocline and thereby creating strong horizontal buoyancy gradients. More generally, wind-dependent pycnocline inclination is a common feature across the GoF (Liblik & Lips, 2017), even when surface temperature and salinity gradients are weak.

Horizontal buoyancy gradients are exposed to variable forcing, with surface heat flux no longer persistently positive and airflow over the GoF becoming more persistent than in May–June (Keevallik & Soomere, 2014). This may allow the existing gradient field to be repeatedly modified, helping to sustain conditions favourable for SMS activity. Sloping isopycnals provide pathways for tracer redistribution (e.g., Erickson & Thompson, 2018; Freilich & Mahadevan, 2021), consistent with the summer spice maximum being located within the pycnocline. This interpretation is also supported by Paper III, where scanfish sections show intrusions of water with different temperature and salinity properties along inclined pycnoclines.

The vertical organisation of spice variability inferred from the glider observations is broadly reproduced by the model results (Fig. 9a–c). The contrasting vertical structure suggests that SMS variability is shaped by different seasonal settings. In a broader seasonal context, the modelled monthly evolution of spice shows a systematic transition from spring to summer conditions (Fig. 9d–g). From May to August, the strengthening and deepening of stratification are accompanied by a progressive shift of spice maxima toward higher densities, indicating that tracer variability follows the seasonal development of the pycnocline. During summer, elevated spice intensities also span a broader density range, reflecting the thickening and intensification of the stratified layer.

Selected months, such as June 2018 and August 2019, exhibit secondary near-surface spice maxima in addition to the deeper dominant signal. This feature may be related to vertically layered stratification. The May 2018 and July 2019 observations illustrate such layering, with several local maxima in Brunt–Väisälä frequency indicating multiple stratified interfaces (Fig. 2a, c) during periods of elevated spice variability (Fig. 8a, c). In this setting, the deeper seasonal pycnocline can host the main spice maximum, while additional near-surface gradients, generated for example by surface heating or freshwater advection, may support secondary spice maxima in the upper layer.

This suggests that the vertical expression of SMS variability is shaped by the interaction between horizontal buoyancy gradients, vertical stratification, and forcing within the evolving seasonal water column. Similar vertical spice structures between missions may indicate comparable redistribution pathways. However, differences in spice magnitude should be interpreted cautiously across spring and summer conditions, because the available temperature–salinity contrasts and density gradients differ seasonally. Weaker spice variability in spring therefore does not necessarily imply weaker SMS-related redistribution.

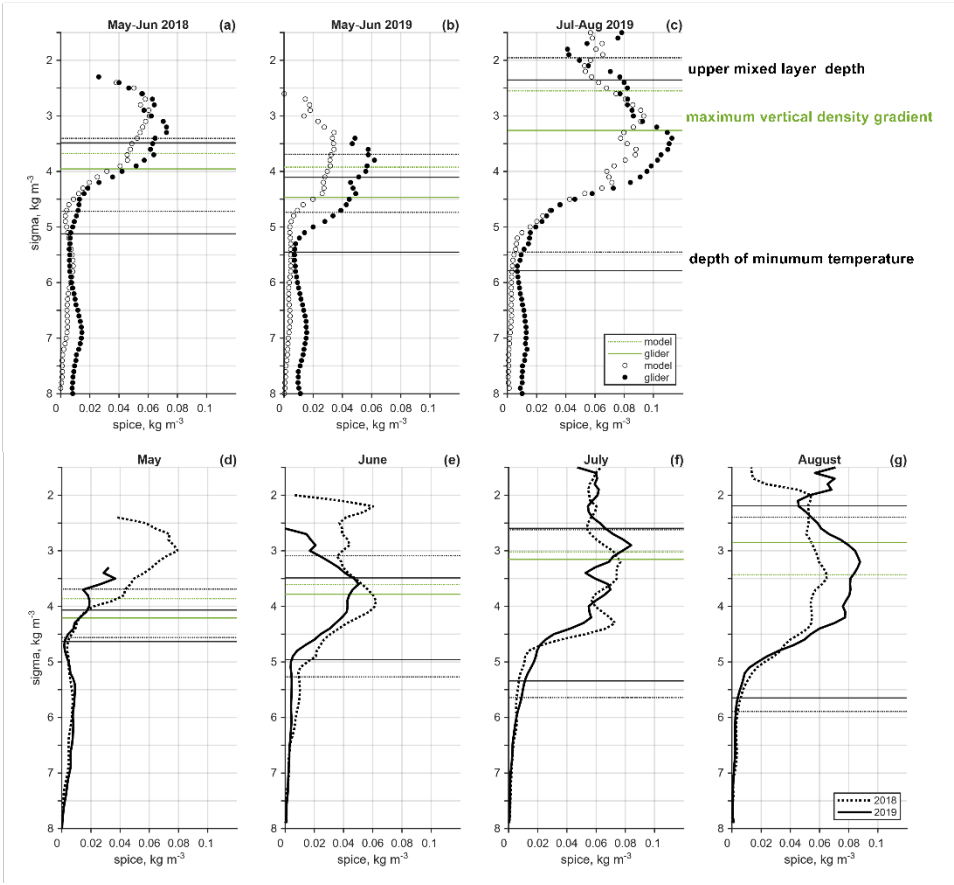


Figure 9. Vertical distribution of spice variability expressed as the standard deviation of spice. Panels (a–c) show spice variability from glider observations (black dots) and model output (white circles) for each glider mission period. Solid and dashed black lines indicate the average depth of the UML and the depth of minimum temperature derived from observations and model output, respectively. Green lines denote the average depth of the maximum Brunt–Väisälä frequency. Panels (d–g) show the monthly standard deviation of modelled spice from May to August for 2018 (dashed lines) and 2019 (solid lines). The same reference depths shown in panels (a–c) are indicated by black and green horizontal lines. From Paper II.

4.3 Linking Mesoscale Forcing and Tracer Organisation

Building on the analysis of the timing and spatial expression of SMS variability, the focus now shifts to the physical pathways through which mesoscale forcing generates fine-scale tracer structure. To address this, Paper II analysed the modelled late-summer upwelling period of 23–31 July 2019 as a case study of mesoscale-to-submesoscale coupling.

By 31 July, extensive coastal upwelling had developed, as seen in the surface temperature and salinity fields (Fig. 7e). The resulting horizontal buoyancy gradients were accompanied by a strong westward coastal current and order one surface Rossby numbers near the coast, indicating a mesoscale environment favourable for SMS activity.

Daily vertical transects resolved the evolving hydrographic structure during this period (Figs. S1–S9 in Paper II). Following the strengthening of easterly winds after 25 July, a coherent coastal current developed by 26 July, accompanied by enhanced subsurface variability in temperature and salinity. By 29 July, the upwelling signal was clearly expressed in the transects as marked surface cooling and strongly tilted isopycnals indicative of frontal sharpening, while order one Rossby numbers remained largely confined to the coastal current and were comparatively weak offshore (Fig. 11 in Paper II).

During 27–28 July, the subsurface spice field broadly mirrored the pattern of elevated Rossby number, although spice variability extended across a wider part of the section (Figs. S5–S6 in Paper II). Thereafter, the spatial correspondence between Rossby number and spice weakened, suggesting a transition from active SMS generation toward tracer redistribution, with anomalies advected and subducted along sloping isopycnals within the established mesoscale frontal framework (e.g., Freilich & Mahadevan, 2021; Hosegood et al., 2017; Spall, 1995).

To complement the daily-transect analysis, I present period-mean fields for 26–31 July, representing the phase after establishment of the coherent coastal current and frontal structure (Fig. 10). This reformulation does not alter the interpretation but expresses multiple SMS-relevant diagnostics consistently across the analysed period and highlights persistent co-evolving patterns.

The period-mean Rossby number identifies a vertically coherent core near 59.625° N, extending to about 30 m depth, coincident with the strongest isopycnal tilt (Fig. 10a, c). Such alignment of elevated Rossby numbers with strongly sloping isopycnals is typical of frontal zones where ageostrophic circulations intensify (e.g., Garcia-Jove et al., 2022; McWilliams, 2019).

To link this dynamical setting to tracer redistribution and to illustrate the role of vertical motions expected to be enhanced at fronts (e.g., Tarry et al., 2022; Taylor & Thompson, 2023), I additionally examine the period-mean magnitude of the vertical advective tendency of spice that highlights persistent zones where vertical motions act on strong vertical spice gradients. A near-surface maximum appears between 59.625 and 59.65° N, coinciding with elevated Rossby number, while a broader maximum occurs farther offshore around 59.67–59.675° N at 10–15 m depth, reaching about 1.2×10^{-5} kg m^{-3} s^{-1} (Fig. 10b).

The full period mean reflects an evolving redistribution pattern. More specifically, the event appears to evolve from an earlier surface-intensified phase, when the near-surface maximum is strongest and spice remains more closely aligned with elevated Rossby number, toward a later phase in which the subsurface tracer-restructuring signal strengthens and becomes more prominent within the established frontal circulation.

Along-transect RMS spice is consistent with this, showing that the strongest fine-scale tracer variability is confined to the same frontal/current structure, with lower values on both the coastal and offshore sides (Fig. 10c).

The associated vertical velocities are of order 10 m d^{-1}. Although this lies toward the lower range of reported SMS vertical velocities, it is still consistent with energetic SMS motions and with indirect estimates from other stratified environments (e.g., Capet et al., 2008; Zhang et al., 2021). In the Baltic Sea, higher instantaneous velocities occur in high-resolution simulations (Chrysagi et al., 2021), but the estimates presented here are period means based on one snapshot per day and therefore miss instantaneous peak velocities. Smaller vertical velocities are also realistic in stratified coastal environments, as SMS dynamics depend on mixed-layer depth (Callies et al., 2015; Erickson & Thompson, 2018). Deep mixed layers contain large reservoirs of potential energy available for SMS instabilities (e.g., Fox-Kemper et al., 2008), whereas the shallow summer mixed layer in the GoF (~13 m; Liblik & Lips, 2011) limits the vertical extent of frontal circulations and thus the associated vertical velocities (Erickson & Thompson, 2018).

The spatially non-uniform pattern of the vertical advective tendency of spice reflects an evolving event and suggests that vertical tracer restructuring is concentrated within specific parts of the frontal/current system. As the event progresses, the increasingly prominent subsurface signal remains associated with the observed region of elevated spice variability, consistent with tracer transport within the frontal circulation (e.g., Archer et al., 2020; Freilich & Mahadevan, 2021; Yoshikawa et al., 2012). Because frontal tracer transport can be localized and follow sloping isopycnals that outcrop in the mixed layer, this pattern supports subduction as a likely three-dimensional pathway for transferring tracers into the pycnocline, with its efficiency influenced by atmospheric forcing (Mahadevan et al., 2020; Pham et al., 2024; Yoshikawa et al., 2012). Overall, the composite analysis reinforces the interpretation from Paper II that the observed tracer variability and the dynamical indicators are linked through the same frontal/current system along the transect.

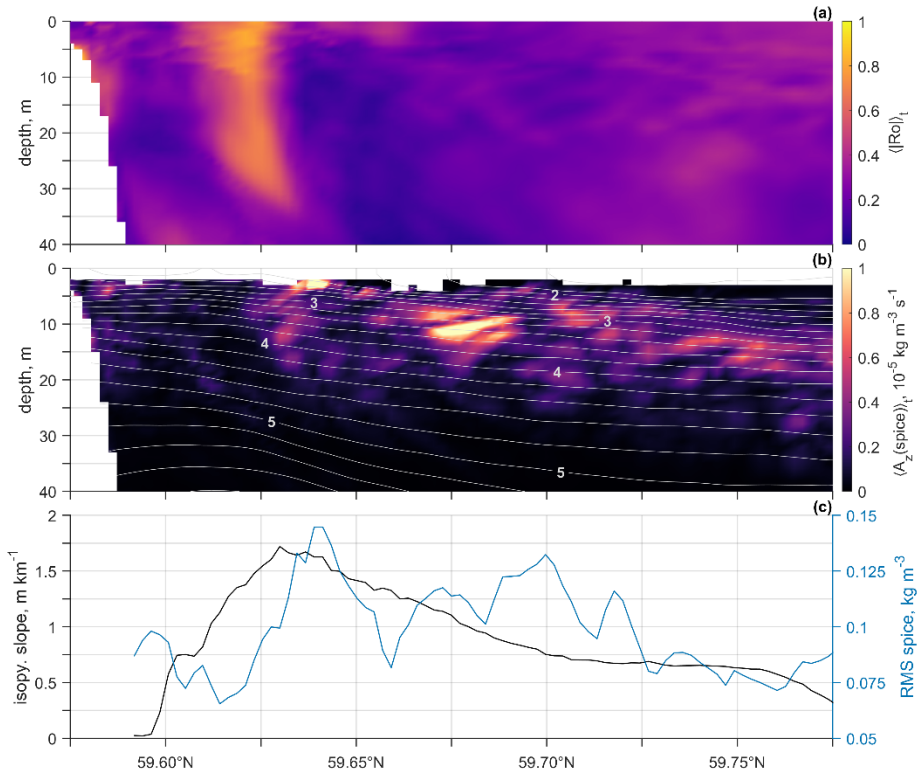


Figure 10. Period-mean dynamical and tracer diagnostics for the upwelling period of 26–31 July 2019 along the meridional transect at 25.25° E. Panels show (a) the magnitude of the Rossby number, and (b) the magnitude of the vertical advective tendency of spice. Panel (c) shows along-transect isopycnal slope and RMS spice, averaged from the surface down to the depth of minimum temperature.

4.4 Pathways for Tracer Redistribution

In this thesis, SMS variability in the GoF is interpreted as a manifestation of processes that redistribute tracers both laterally and vertically within an evolving mesoscale buoyancy field. Horizontal buoyancy gradients provide the frontal setting for such processes (Taylor & Thompson, 2023). Mesoscale frontal flows are approximately in geostrophic and hydrostatic balance, so horizontal buoyancy gradients are linked to vertical shear through thermal-wind balance. As frontogenesis sharpens the front, horizontal buoyancy gradients intensify, the frontal zone narrows, vertical shear in the along-front jet strengthens, and relative vorticity increases. When this sharpening proceeds faster than the balanced flow can adjust, ageostrophic circulations emerge, identified, e.g., by the Rossby number approaching order one (Hoskins, 1982; Hoskins & Bretherton, 1972; McWilliams, 2016).

This behaviour is reflected throughout the thesis by the repeated association of order one Rossby number, enhanced buoyancy gradients, sloping density surfaces, and subsurface tracer variability at submesoscales. Together, these features indicate frontal

environments where ageostrophic motions become dynamically relevant and can modify tracer distributions across and along density surfaces. In such settings, along-isopycnal stirring of tracers is a recurring pathway for tracer redistribution, associated, e.g., with restratification near the UML base and with local subduction or intrusion of tracer anomalies into the stratified interior.

For passive tracers along isopycnals, spectra approaching k^{-2} are commonly interpreted as evidence of SMS-related lateral stirring (Balwada et al., 2024; Callies & Ferrari, 2013). In this thesis, such redistribution appears most evident where sloping density surfaces, horizontal buoyancy gradients, and larger-scale lateral tracer gradients coincide. Within fronts, inclined density surfaces provide pathways along which temperature, salinity, spice, or chlorophyll anomalies can be stretched and redistributed (e.g., Erickson et al., 2016; Freilich & Mahadevan, 2021). The expression of this along-isopycnal stirring depends on the vertical structure of the front, as suggested by the contrasting 2018 and 2016 frontal cases (see Section 4.1.2.2).

Under strong positive surface heat flux and weak or intermittent wind forcing, typical of the spring and early summer period, wind-driven mixing is reduced, and horizontal buoyancy gradients can persist near the lower part of the UML. Under these conditions, SMS-related restratification may contribute to tracer reorganisation near the UML base during the development of the seasonal thermocline. This is consistent with studies showing how lateral buoyancy gradients can shape vertical tracer structure (e.g., Mahadevan et al., 2010).

Wind forcing provides an important control on these redistribution pathways by modifying the frontal buoyancy field and determining where SMS-favourable conditions develop in the GoF (Kikas & Lips, 2016; Liblik & Lips, 2017; Lilover et al., 2017). In the late-summer upwelling case, this thesis suggests SMS subduction as one possible pathway through which tracer anomalies are transferred into the pycnocline and stratified interior along sloping isopycnals. The persistence of wind forcing may be important in this context because it can keep the frontal buoyancy field dynamically active while tracer anomalies are redistributed horizontally and vertically.

Overall, the results indicate that tracer redistribution in the GoF depends on how horizontal buoyancy gradients, sloping density surfaces, and wind forcing interact within the seasonally stratified water column.

4.5 Implications for the Baltic Sea

Figure 11 synthesizes the frontal geometry of the southern GoF, illustrating how oppositely sloping thermocline and halocline layers (Liblik & Lips, 2017), together with the coastal current and frontal circulation, can provide pathways for restratification near the UML base and tracer transfer into the pycnocline. In this setting, mesoscale frontal structure provides the background within which SMS processes redistribute tracers between the surface layer and the stratified interior. Paper III places this GoF-based interpretation in a broader Baltic Sea context, identifying SMS dynamics as a basin-relevant component of circulation that contributes to both tracer redistribution and energy transfer across scales.

From a tracer perspective, the results suggest that SMS dynamics can couple lateral and vertical redistribution in stratified coastal conditions, linking surface–interior exchange (e.g., Su et al., 2018; Yu et al., 2019) with coastal–offshore transport (e.g., Fadida et al., 2026; Kubryakov et al., 2023). Because strong horizontal buoyancy gradients are common in the Baltic Sea, SMS processes can develop within mesoscale

frontal and coastal-current systems. In this setting, Paper II suggests subduction, associated with persistent frontal tilting and vertical shear, as one possible frontal pathway for tracer exchange. The broader relevance of this mechanism is supported by other Baltic Sea observations, which show that intrusions of water with contrasting temperature and salinity properties frequently occur along inclined pycnoclines (Lips et al., 2016; Paper III).

Such pathways are relevant not only for physical tracers, but also for biogeochemical structure, as SMS-related lateral and vertical fluxes may influence nutriclines, redoxcline, and subsurface chlorophyll-a maxima (Paper III). In the GoF, where nutrients are often depleted after the spring bloom as the seasonal thermocline develops (Lips et al., 2011), this may affect biological variability (Lips & Lips, 2010), including through subduction of chlorophyll-rich surface waters into the lower seasonal thermocline (e.g., Erickson et al., 2016; Lips & Lips, 2010; Lips et al., 2010; Lips & Lips, 2014).

SMS dynamics in the Baltic Sea appear to exhibit a seasonal cycle in which both vertical and lateral tracer redistribution depend on stratification and mixed-layer depth (e.g., Erickson & Thompson, 2018; Yu et al., 2019). The vertical distribution of spice variability likewise followed the evolving stratification of the water column from spring to summer (Paper II). Joint probability density functions of relative vorticity and strain rate presented in Paper III show that SMS processes occur more frequently in the GoF and the Northern Baltic Proper, and that intense SMS activity is more common in winter than in summer. However, Väli et al. (2024) identify the southern GoF as a region where surface kinetic energy can remain elevated during summer, emphasizing the role of wind-driven coastal currents and upwelling fronts in maintaining surface-intensified dynamics under strongly stratified conditions (Väli et al., 2017, 2024).

Recognizing SMS dynamics as a basin-relevant component of circulation extends the classical view of energy transfer across scales by emphasizing feedbacks and instabilities within the SMS range. In the Baltic Sea, compressed dynamical scales may enhance the relative importance of these processes: in a shallow basin, upper- and bottom boundary layer dynamics can affect a comparatively large fraction of the water column, especially along sloping topography where flow–bottom interactions generate additional buoyancy gradients and instability pathways (e.g., Capó et al., 2023; Gula et al., 2015; Wenegrat & Thomas, 2020).

Paper III proposes that, in addition to internal waves, SMS processes form a distinct pathway for energy transfer across scales (Fig. 12). Their presence is associated with flatter wavenumber spectra of potential energy (slope −2 rather than −3), indicating enhanced retention of buoyancy variance at submesoscales, and with steeper tracer variance spectra (slope −2 rather than −1), reflecting active tracer redistribution. This interpretation is consistent with independent results from the GoF (Paper I; Paper III; Lilover et al., 2025; Lips et al., 2016). Together, these findings imply that energy transfer in stratified coastal seas cannot be described solely as a downscale cascade mediated by internal waves.

The results presented here highlight density-gradient-driven pathways such as restratification and subduction, illustrating how SMS motions redistribute both energy and tracers across the stratified water column. Their existence and role are emphasized here without attributing them to specific instability mechanisms, which lie beyond the scope of this thesis. A defining feature of these pathways is that energy transfer does not necessarily follow a single irreversible route toward dissipation but can be redistributed across scales in ways that vary seasonally (Balwada et al., 2022; Canuto et al., 2018;

Naveira Garabato et al., 2022; Yang et al., 2021). Neglecting them may therefore alter the predicted distributions of temperature, salinity, density, and tracers, influencing both mixing rates and the large-scale organisation of water masses in stratified coastal seas (Fox-Kemper et al., 2008; Mahadevan, 2016; Su et al., 2018; Taylor & Thompson, 2023).

These findings highlight the relevance of sub-grid parameterisations in coarse-resolution ocean and climate models, where SMS dynamics are not explicitly resolved. Because SMS processes couple horizontal density gradients with vertical stratification, parameterisations should account for this coupling rather than treating lateral and vertical mixing independently. This coupling drives tracer and energy redistribution along sloping isopycnals, a pathway not represented in schemes based solely on a classical one-way cascade.

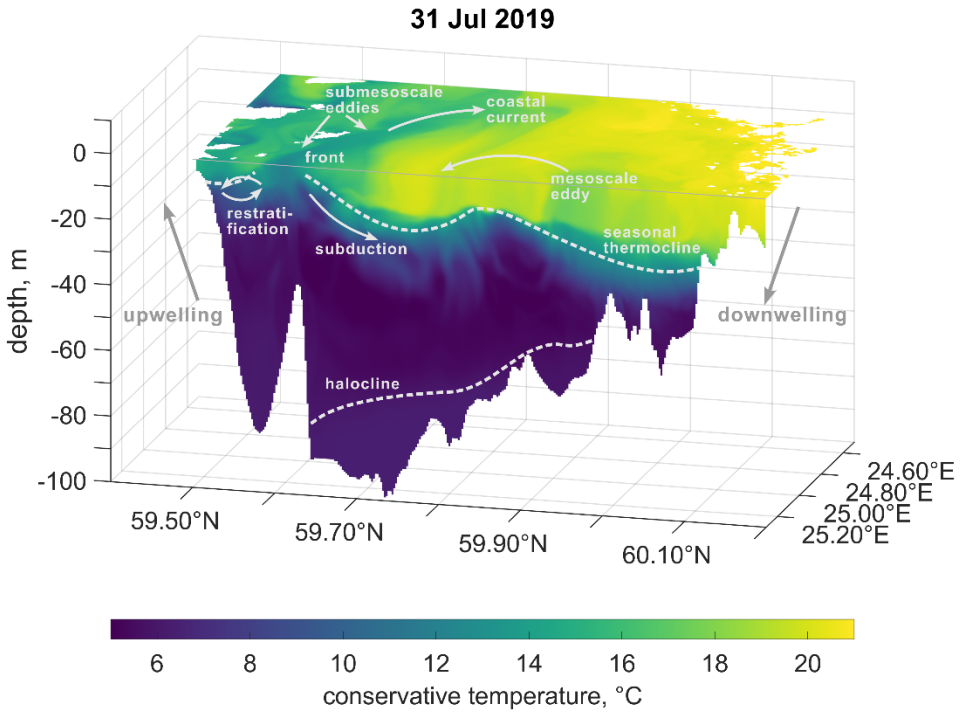


Figure 11. Conceptual three-dimensional view of water-column temperature across the Gulf of Finland on 31 July 2019. The horizontal view spans 59.50–60.20°N and 24.50–25.30°E, while the vertical section follows a meridional transect along 25.30°E. The stratified structure reveals oppositely sloping thermocline and halocline layers and a pronounced frontal zone along the southern coast. Hypothetical contours schematically indicate key features, including the coastal current, mesoscale and submesoscale eddies, frontal zone, subduction, and restratification near the base of the upper mixed layer.

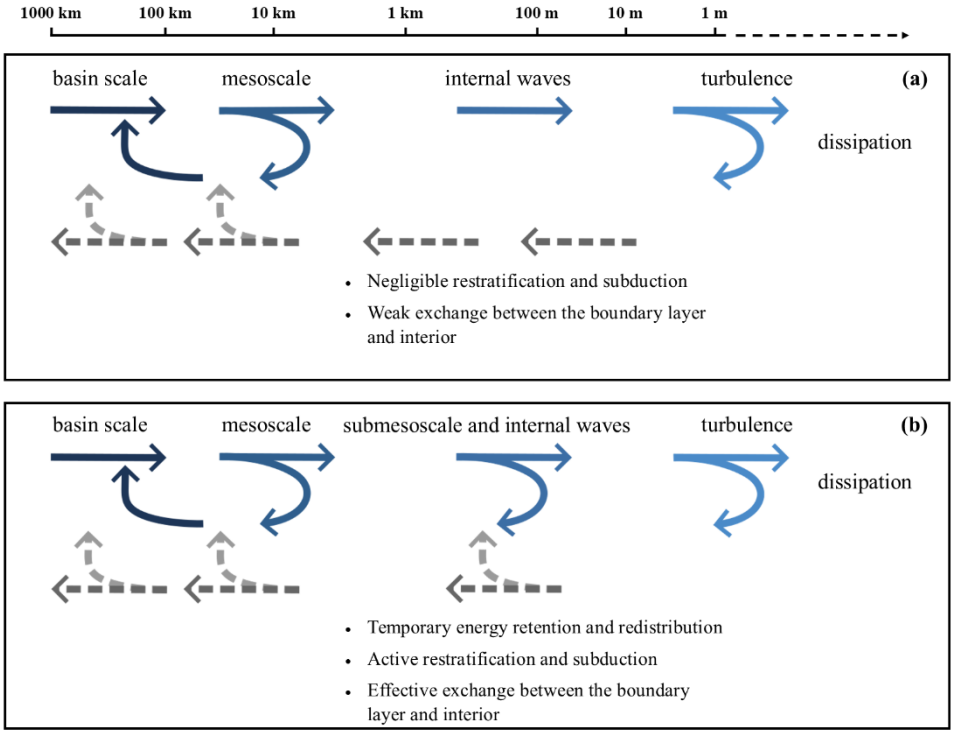


Figure 12. Schematic illustration of energy-transfer pathways across spatial scales. (a) Classical view in which mesoscale energy is transferred toward dissipation primarily via internal gravity waves. (b) Expanded framework including submesoscale processes, which introduce additional, dynamically active pathways for energy redistribution. In this view, energy extracted from mesoscale density gradients is temporarily retained, converted, and redistributed within the SMS range before contributing to dissipation. The schematic emphasises pathways rather than specific instability mechanisms. Modified from Paper III.

5 Conclusions

This thesis provides a characterisation of SMS variability in a shallow, stratified coastal sea, with emphasis on its links to mesoscale dynamics and atmospheric forcing. By combining high-resolution glider observations, spectral analysis, and model-derived dynamical diagnostics, it relates observed tracer structure to its dynamical context and shows how SMS variability in the Baltic Sea can be interpreted in terms of physical pathways of tracer redistribution.

The principal conclusions of this thesis are as follows:

- High-resolution autonomous glider observations provided indirect evidence for SMS activity, as they resolved both mesoscale frontal structures and kilometre-scale tracer features consistent with SMS-related redistribution. This shows that standard glider sensor packages can identify SMS imprints in tracer variability and background density structure, even when the full velocity field is not observed.

- For the mesoscale frontal structure observed in late spring 2018, equivalent heat flux estimates suggested that wind-driven Ekman transport across the front made the strongest diagnosed contribution to frontal imbalance, while baroclinic effects were likely also present during front formation. Rossby number analysis based on glider data supported this interpretation by distinguishing surface-confined variability from variability extending through much of the upper water column.

- Larger-scale atmospheric forcing shaped when and where SMS-permissive conditions developed by modifying mesoscale density structure. Upwelling, downwelling, and mesoscale advection were repeatedly associated with intensified buoyancy gradients and regions of order one Rossby number, indicating that wind-driven regimes characteristic of the Baltic Sea can sustain mesoscale conditions favourable for SMS development.

- The vertical distribution of spice variability changed with the evolving water-column structure, indicating that the layer where lateral thermohaline anomalies were retained shifted seasonally. In spring, the spice maximum occurred near the base of the UML, above the maximum vertical density gradient, whereas in summer it shifted toward the maximum vertical density gradient and occupied a broader density range within the thermocline.

- Spice variability and surface Rossby number were closely coupled during the spring-early summer glider missions, suggesting active frontal dynamics within the study area. During the late-summer upwelling event, however, elevated spice variability was spatially offset from the region with pronounced order one Rossby number. This offset was consistent with SMS-related subduction within the mesoscale frontal system, where sloping density surfaces provided potential pathways for along-isopycnal tracer redistribution. Modelled vertical advection

of spice supported this interpretation by identifying persistent zones where vertical motion acted on subsurface spice gradients.

- The SMS signatures identified in this thesis suggest several connected forms of frontal tracer redistribution in the GoF, whose expression depends on the interaction among horizontal buoyancy gradients, stratification, and wind forcing. Along-isopycnal stirring within sloping frontal surfaces was the most likely pathway, supported by both the tracer spectra and fine-scale thermohaline features resolved by the glider. Indirectly, the results suggest SMS-related vertical reorganisation near the UML base and subduction into the pycnocline.

- The occurrence of k^{-2} spectral slopes of isopycnal temperature in both the surface layer and thermocline suggests that SMS-related along-isopycnal stirring extended into subsurface layers. This supports the interpretation that SMS-related redistribution is relevant within the stratified GoF water column.

- More broadly, the results suggest that SMS processes may provide a pathway through which mesoscale frontal circulation contributes to vertical and lateral tracer redistribution in the Baltic Sea.

In conclusion, the thesis suggests that SMS processes can link frontal adjustment with tracer redistribution in the stratified Baltic Sea water column.

References

Adams, K. A., Hosegood, P., Taylor, J. R., Sallée, J.-B., Bachman, S., Torres, R., & Stamper, M. (2017). Frontal Circulation and Submesoscale Variability during the Formation of a Southern Ocean Mesoscale Eddy. *Journal of Physical Oceanography*, *47*(7), 1737–1753. https://doi.org/10.1175/JPO-D-16-0266.1

Andrejev, O., Myrberg, K., Alenius, P., & Lundberg, P. A. (2004). Mean circulation and water exchange in the Gulf of Finland – a study based on three-dimensional modelling. *Boreal Environment Research*, *9*, 1–16.

Archer, M., Schaeffer, A., Keating, S., Roughan, M., Holmes, R., & Siegelman, L. (2020). Observations of Submesoscale Variability and Frontal Subduction within the Mesoscale Eddy Field of the Tasman Sea. *Journal of Physical Oceanography*, *50*(5), 1509–1529. https://doi.org/10.1175/JPO-D-19-0131.1

Balwada, D., Xie, J.-H., Marino, R., & Feraco, F. (2022). Direct observational evidence of an oceanic dual kinetic energy cascade and its seasonality. *Science Advances*, *8*(41), eabq2566. https://doi.org/10.1126/sciadv.abq2566

Blumen, W. (1978). Uniform Potential Vorticity Flow: Part I. Theory of Wave Interactions and Two-Dimensional Turbulence. *Journal of the Atmospheric Sciences*, *35*(5), 774–783. https://doi.org/10.1175/1520-0469(1978)035<0774:UPVFPI>2.0.CO;2

Boccaletti, G., Ferrari, R., & Fox-Kemper, B. (2007). Mixed Layer Instabilities and Restratification. *Journal of Physical Oceanography*, *37*(9), 2228–2250. https://doi.org/10.1175/JPO3101.1

Bosse, A., Testor, P., Damien, P., Estournel, C., Marsaleix, P., Mortier, L., Prieur, L., & Taillandier, V. (2021). Wind-Forced Submesoscale Symmetric Instability around Deep Convection in the Northwestern Mediterranean Sea. *Fluids*, *6*(3), 123. https://doi.org/10.3390/fluids6030123

Buckingham, C. E., Lucas, N. S., Belcher, S. E., Rippeth, T. P., Grant, A. L. M., Le Sommer, J., Ajayi, A. O., & Naveira Garabato, A. C. (2019). The Contribution of Surface and Submesoscale Processes to Turbulence in the Open Ocean Surface Boundary Layer. *Journal of Advances in Modeling Earth Systems*, *11*(12), 4066–4094. https://doi.org/10.1029/2019MS001801

Burchard, H., & Bolding, K. (2001). Comparative Analysis of Four Second-Moment Turbulence Closure Models for the Oceanic Mixed Layer. *Journal of Physical Oceanography*, *31*(8), 1943–1968. https://doi.org/10.1175/1520-0485(2001)031<1943:CAOFSM>2.0.CO;2

Burchard, H., & Bolding, K. (2002). GETM – a general estuarine transport model, Scientific Documentation. *Tech. Rep. EUR 20253 EN, European Commission*.

Callies, J., & Ferrari, R. (2013). Interpreting Energy and Tracer Spectra of Upper-Ocean Turbulence in the Submesoscale Range (1–200 km). *Journal of Physical Oceanography*, *43*(11), 2456–2474. https://doi.org/10.1175/JPO-D-13-063.1

Callies, J., Ferrari, R., Klymak, J. M., & Gula, J. (2015). Seasonality in submesoscale turbulence. *Nature Communications*, *6*(1), 6862. https://doi.org/10.1038/ncomms7862

Canuto, V. M., Cheng, Y., & Howard, A. M. (2018). Subduction by Submesoscales. *Journal of Geophysical Research: Oceans*, *123*(12), 8688–8700. https://doi.org/10.1029/2018JC014142

Canuto, V. M., Howard, A., Cheng, Y., & Dubovikov, M. S. (2001). Ocean turbulence. Part I: One-point closure model-momentum and heat vertical diffusivities. *Journal of*

Physical Oceanography, *31*(6), 1413–1426. https://doi.org/10.1175/1520-0485(2001)031<1413:OTPIOP>2.0.CO;2

Capet, X., McWilliams, J. C., Molemaker, M. J., & Shchepetkin, A. F. (2008). Mesoscale to submesoscale transition in the California Current system. Part III: Energy balance and flux. *Journal of Physical Oceanography*, *38*(10), 2256–2269. https://doi.org/10.1175/2008JPO3810.1

Capó, E., McWilliams, J. C., & Jagannathan, A. (2023). Flow-Topography Interaction Along the Spanish Slope in the Alboran Sea: Vorticity Generation and Connection to Interior Fronts. *Journal of Geophysical Research: Oceans*, *128*(4). https://doi.org/10.1029/2022JC019480

Carpenter, J. R., Rodrigues, A., Schultze, L. K. P., Merckelbach, L. M., Suzuki, N., Baschek, B., & Umlauf, L. (2020). Shear Instability and Turbulence Within a Submesoscale Front Following a Storm. *Geophysical Research Letters*, *47*(23). https://doi.org/10.1029/2020GL090365

Charney, J. G. (1971). Geostrophic Turbulence. *Journal of the Atmospheric Sciences*, *28*(6), 1087–1095. https://doi.org/10.1175/1520-0469(1971)028<1087:GT>2.0.CO;2

Chrysagi, E., Umlauf, L., Holtermann, P., Klingbeil, K., & Burchard, H. (2021). High-Resolution Simulations of Submesoscale Processes in the Baltic Sea: The Role of Storm Events. *Journal of Geophysical Research: Oceans*, *126*(3). https://doi.org/10.1029/2020JC016411

Cole, S. T., & Rudnick, D. L. (2012). The spatial distribution and annual cycle of upper ocean thermohaline structure. *Journal of Geophysical Research: Oceans*, *117*(C2). https://doi.org/10.1029/2011JC007033

Döös, K., Meier, H. E. M., & Döscher, R. (2004). The Baltic Haline Conveyor Belt or The Overturning Circulation and Mixing in the Baltic. *AMBIO: A Journal of the Human Environment*, *33*(4), 261–266. https://doi.org/10.1579/0044-7447-33.4.261

D'Ortenzio, F., Thierry, V., Eldin, G., Claustre, H., Testor, P., Coatanoan, C., Tedetti, M., Guinet, C., Poteau, A., Prieur, L., Lefevre, D., Bourrin, F., Carval, T., Goutx, M., Garçon, V., Thouron, D., Lacombe, M., Lherminier, P., Loisiel, H., … Antoine, D. (2010). *White Book on Oceanic Autonomous Platforms for Biogeochemical Studies: Instrumentation and Measure (PABIM)*. https://doi.org/10.13140/RG.2.1.3706.5763

Eady, E. T. (1949). Long Waves and Cyclone Waves. *Tellus*, *1*(3), 33–52. https://doi.org/10.1111/j.2153-3490.1949.tb01265.x

Elken, J., Nõmm, M., & Lagemaa, P. (2011). Circulation patterns in the Gulf of Finland derived from the EOF analysis of model results. *Boreal Environment Research*, *16*, 84–102.

Erickson, Z. K., & Thompson, A. F. (2018). The Seasonality of Physically Driven Export at Submesoscales in the Northeast Atlantic Ocean. *Global Biogeochemical Cycles*, *32*(8), 1144–1162. https://doi.org/10.1029/2018GB005927

Erickson, Z. K., Thompson, A. F., Callies, J., Yu, X., Garabato, A. N., & Klein, P. (2020). The Vertical Structure of Open-Ocean Submesoscale Variability during a Full Seasonal Cycle. *Journal of Physical Oceanography*, *50*(1), 145–160. https://doi.org/10.1175/JPO-D-19-0030.1

Erickson, Z. K., Thompson, A. F., Cassar, N., Sprintall, J., & Mazloff, M. R. (2016). An advective mechanism for deep chlorophyll maxima formation in southern Drake

Passage. *Geophysical Research Letters*, *43*(20). https://doi.org/10.1002/2016GL070565

Fadida, Y., Verma, V., Barkan, R., Biton, E., Solodoch, A., & Lehahn, Y. (2026). Coastal-to-offshore submesoscale horizontal stirring enhances wintertime phytoplankton blooms in the ultra-oligotrophic Eastern Mediterranean Sea. *Ocean Science*, *22*(1), 329–343. https://doi.org/10.5194/os-22-329-2026

Ferrari, R., & Rudnick, D. L. (2000). Thermohaline variability in the upper ocean. *Journal of Geophysical Research: Oceans*, *105*(C7), 16857–16883. https://doi.org/10.1029/2000JC900057

Fofonoff, N. P., Hayes, S. P., & Millard Jr, R. C. (1974). *W. H. O. I./Brown CTD microprofiler: Methods of calibration and data handling (No. WHOI-74-89)*.

Fox-Kemper, B., Ferrari, R., & Hallberg, R. (2008). Parameterization of Mixed Layer Eddies. Part I: Theory and Diagnosis. *Journal of Physical Oceanography*, *38*(6), 1145–1165. https://doi.org/10.1175/2007JPO3792.1

Freilich, M., & Mahadevan, A. (2021). Coherent Pathways for Subduction From the Surface Mixed Layer at Ocean Fronts. *Journal of Geophysical Research: Oceans*, *126*(5). https://doi.org/10.1029/2020JC017042

Garcia-Jove, M., Mourre, B., Zarokanellos, N. D., Lermusiaux, P. F. J., Rudnick, D. L., & Tintoré, J. (2022). Frontal Dynamics in the Alboran Sea: 2. Processes for Vertical Velocities Development. *Journal of Geophysical Research: Oceans*, *127*(3). https://doi.org/10.1029/2021JC017428

Gräwe, U., Holtermann, P., Klingbeil, K., & Burchard, H. (2015). Advantages of vertically adaptive coordinates in numerical models of stratified shelf seas. *Ocean Modelling*, *92*, 56–68. https://doi.org/10.1016/j.ocemod.2015.05.008

Gröger, M., Placke, M., Meier, H. E. M., Börgel, F., Brunnabend, S. E., Dutheil, C., Gräwe, U., Hieronymus, M., Neumann, T., Radtke, H., Schimanke, S., Su, J., & Väli, G. (2022). The Baltic Sea Model Intercomparison Project (BMIP) - a platform for model development, evaluation, and uncertainty assessment. *Geoscientific Model Development*, *15*(22), 8613–8638. https://doi.org/10.5194/gmd-15-8613-2022

Gula, J., Molemaker, M. J., & McWilliams, J. C. (2015). Topographic vorticity generation, submesoscale instability and vortex street formation in the Gulf Stream. *Geophysical Research Letters*, *42*(10), 4054–4062. https://doi.org/10.1002/2015GL063731

Gurova, E., & Chubarenko, B. (2012). Remote-sensing observations of coastal sub-mesoscale eddies in the south-eastern Baltic. *Oceanologia*, *54*(4), 631–654. https://doi.org/10.5697/oc.54-4.631

Haine, T. W. N., & Marshall, J. (1998). Gravitational, Symmetric, and Baroclinic Instability of the Ocean Mixed Layer. *Journal of Physical Oceanography*, *28*(4), 634–658. https://doi.org/10.1175/1520-0485(1998)028<0634:GSABIO>2.0.CO;2

Hersbach, H., Bell, B., Berrisford, P., Hirahara, S., Horányi, A., Muñoz-Sabater, J., Nicolas, J., Peubey, C., Radu, R., Schepers, D., Simmons, A., Soci, C., Abdalla, S., Abellan, X., Balsamo, G., Bechtold, P., Biavati, G., Bidlot, J., Bonavita, M., … Thépaut, J. (2020). The ERA5 global reanalysis. *Quarterly Journal of the Royal Meteorological Society*, *146*(730), 1999–2049. https://doi.org/10.1002/qj.3803

Hofmeister, R., Burchard, H., & Beckers, J.-M. (2010). Non-uniform adaptive vertical grids for 3D numerical ocean models. *Ocean Modelling*, *33*(1–2), 70–86. https://doi.org/10.1016/j.ocemod.2009.12.003

Hosegood, P. J., Nightingale, P. D., Rees, A. P., Widdicombe, C. E., Woodward, E. M. S., Clark, D. R., & Torres, R. J. (2017). Nutrient pumping by submesoscale circulations in the mauritanian upwelling system. *Progress in Oceanography*, *159*, 223–236. https://doi.org/10.1016/j.pocean.2017.10.004

Hoskins, B. J. (1974). The role of potential vorticity in symmetric stability and instability. *Quarterly Journal of the Royal Meteorological Society*, *100*(425), 480–482. https://doi.org/10.1002/qj.49710042520

Hoskins, B. J. (1982). The Mathematical Theory of Frontogenesis. *Annual Review of Fluid Mechanics*, *14*(1), 131–151. https://doi.org/10.1146/annurev.fl.14.010182.001023

Hoskins, B. J., & Bretherton, F. P. (1972). Atmospheric Frontogenesis Models: Mathematical Formulation and Solution. *Journal of the Atmospheric Sciences*, *29*(1), 11–37. https://doi.org/10.1175/1520-0469(1972)029<0011:AFMMFA>2.0.CO;2

IOC, SCOR, & IAPSO. (2010). The international thermodynamic equation of seawater – 2010: Calculation and use of thermodynamic properties. *Intergovernmental Oceanographic Commission, Manuals and Guides No. 56*, *Paris: UNESCO*.

Johnson, L., Lee, C. M., D'Asaro, E. A., Thomas, L., & Shcherbina, A. (2020). Restratification at a California Current Upwelling Front. Part I: Observations. *Journal of Physical Oceanography*, *50*(5), 1455–1472. https://doi.org/10.1175/JPO-D-19-0203.1

Johnston, T. M. S., & Rudnick, D. L. (2009). Observations of the Transition Layer. *Journal of Physical Oceanography*, *39*(3), 780–797. https://doi.org/10.1175/2008JPO3824.1

Kikas, V., & Lips, U. (2016). Upwelling characteristics in the Gulf of Finland (Baltic Sea) as revealed by Ferrybox measurements in 2007–2013. *Ocean Science*, *12*(3), 843–859. https://doi.org/10.5194/os-12-843-2016

Klingbeil, K., Lemarié, F., Debreu, L., & Burchard, H. (2018). The numerics of hydrostatic structured-grid coastal ocean models: State of the art and future perspectives. *Ocean Modelling*, *125*, 80–105. https://doi.org/10.1016/j.ocemod.2018.01.007

Kolodziejczyk, N., Testor, P., Lazar, A., Echevin, V., Krahmann, G., Chaigneau, A., Gourcuff, C., Wade, M., Faye, S., Estrade, P., Capet, X., Mortier, L., Brehmer, P., Schütte, F., & Karstensen, J. (2018). Subsurface Fine-Scale Patterns in an Anticyclonic Eddy Off Cap-Vert Peninsula Observed From Glider Measurements. *Journal of Geophysical Research: Oceans*, *123*(9), 6312–6329. https://doi.org/10.1029/2018JC014135

Kondo, J. (1975). Air-sea bulk transfer coefficients in diabatic conditions. *Boundary-Layer Meteorology*, *9*, 91–112. https://doi.org/10.1007/BF00232256

Kubryakov, A., Aleskerova, A., Plotnikov, E., Mizyuk, A., Medvedeva, A., & Stanichny, S. (2023). Accumulation and Cross-Shelf Transport of Coastal Waters by Submesoscale Cyclones in the Black Sea. *Remote Sensing*, *15*(18), 4386. https://doi.org/10.3390/rs15184386

Lehmann, A., & Myrberg, K. (2008). Upwelling in the Baltic Sea — A review. *Journal of Marine Systems*, *74*, S3–S12. https://doi.org/10.1016/j.jmarsys.2008.02.010

Lehmann, A., Myrberg, K., & Höflich, K. (2012). A statistical approach to coastal upwelling in the Baltic Sea based on the analysis of satellite data for 1990–2009. *Oceanologia*, *54*(3), 369–393. https://doi.org/10.5697/oc.54-3.369

Leppäranta, M., & Myrberg, K. (2009). *Physical Oceanography of the Baltic Sea*. Springer.

Lévy, M., Franks, P. J. S., & Smith, K. S. (2018). The role of submesoscale currents in structuring marine ecosystems. *Nature Communications*, *9*(1), 4758. https://doi.org/10.1038/s41467-018-07059-3

Liblik, T., Laanemets, J., Raudsepp, U., Elken, J., & Suhhova, I. (2013). Estuarine circulation reversals and related rapid changes in winter near-bottom oxygen conditions in the Gulf of Finland, Baltic Sea. *Ocean Science*, *9*(5), 917–930. https://doi.org/10.5194/os-9-917-2013

Liblik, T., & Lips, U. (2011). Characteristics and variability of the vertical thermohaline structure in the Gulf of Finland in summer. *Boreal Environment Research*, *16*(suppl. A), 73–83.

Liblik, T., & Lips, U. (2017). Variability of pycnoclines in a three-layer, large estuary: the Gulf of Finland. *Boreal Environment Research* , *22*, 27–47.

Liblik, T., Väli, G., Lips, I., Lilover, M. J., Kikas, V., & Laanemets, J. (2020). The winter stratification phenomenon and its consequences in the Gulf of Finland, Baltic Sea. *Ocean Science*, *16*(6), 1475–1490. https://doi.org/10.5194/os-16-1475-2020

Liblik, T., Väli, G., Salm, K., Laanemets, J., Lilover, M. J., & Lips, U. (2022). Quasi-steady circulation regimes in the Baltic Sea. *Ocean Science*, *18*(3), 857–879. https://doi.org/10.5194/os-18-857-2022

Lilover, M. J., Elken, J., Suhhova, I., & Liblik, T. (2017). Observed flow variability along the thalweg, and on the coastal slopes of the Gulf of Finland, Baltic Sea. *Estuarine, Coastal and Shelf Science*, *195*, 23–33. https://doi.org/10.1016/j.ecss.2016.11.002

Lilover, M. J., Lips, U., Liblik, T., Suhhova, I., & Väli, G. (2025). Variability of stratification and currents at the submesoscale detected from CTD and current profiles in the central Gulf of Finland. *Boreal Environment Research*, *30*, 77–92. https://doi.org/10.60910/ber2025.jtg5-j683

Lindström, G., Pers, C., Rosberg, J., Strömqvist, J., & Arheimer, B. (2010). Development and testing of the HYPE (Hydrological Predictions for the Environment) water quality model for different spatial scales. *Hydrology Research*, *41*(3–4), 295–319. https://doi.org/10.2166/nh.2010.007

Lips, I., & Lips, U. (2010). Phytoplankton dynamics affected by the coastal upwelling events in the Gulf of Finland in July-August 2006. *Journal of Plankton Research*, *32*(9), 1269–1282. https://doi.org/10.1093/plankt/fbq049

Lips, I., Lips, U., & Liblik, T. (2009). Consequences of coastal upwelling events on physical and chemical patterns in the central Gulf of Finland (Baltic Sea). *Continental Shelf Research*, *29*(15), 1836–1847. https://doi.org/10.1016/j.csr.2009.06.010

Lips, I., Rünk, N., Kikas, V., Meerits, A., & Lips, U. (2014). High-resolution dynamics of the spring bloom in the Gulf of Finland of the Baltic Sea. *Journal of Marine Systems*, *129*, 135–149. https://doi.org/10.1016/j.jmarsys.2013.06.002

Lips, U., Kikas, V., Liblik, T., & Lips, I. (2016). Multi-sensor in situ observations to resolve the sub-mesoscale features in the stratified Gulf of Finland, Baltic Sea. *Ocean Science*, *12*(3), 715–732. https://doi.org/10.5194/os-12-715-2016

Lips, U., Laanemets, J., Lips, I., Liblik, T., Suhhova, I., & Suursaar, Ü. (2017). Wind-driven residual circulation and related oxygen and nutrient dynamics in the Gulf of Finland (Baltic Sea) in winter. *Estuarine, Coastal and Shelf Science*, *195*, 4–15. https://doi.org/10.1016/j.ecss.2016.10.006

Lips, U., & Lips, I. (2014). Bimodal distribution patterns of motile phytoplankton in relation to physical processes and stratification (Gulf of Finland, Baltic Sea). *Deep*

Sea Research Part II: Topical Studies in Oceanography, *101*, 107–119. https://doi.org/10.1016/j.dsr2.2013.05.029

Lips, U., Lips, I., Liblik, T., Kikas, V., Altoja, K., Buhhalko, N., & Rünk, N. (2011). Vertical dynamics of summer phytoplankton in a stratified estuary (Gulf of Finland, Baltic Sea). *Ocean Dynamics*, *61*(7), 903–915. https://doi.org/10.1007/s10236-011-0421-8

Lips, U., Lips, I., Liblik, T., & Kuvaldina, N. (2010). Processes responsible for the formation and maintenance of sub-surface chlorophyll maxima in the Gulf of Finland. *Estuarine, Coastal and Shelf Science*, *88*(3), 339–349. https://doi.org/10.1016/j.ecss.2010.04.015

Mahadevan, A. (2016). The Impact of Submesoscale Physics on Primary Productivity of Plankton. *Annual Review of Marine Science*, *8*(1), 161–184. https://doi.org/10.1146/annurev-marine-010814-015912

Mahadevan, A., Pascual, A., Rudnick, D. L., Ruiz, S., Tintoré, J., & D'Asaro, E. (2020). Coherent Pathways for Vertical Transport from the Surface Ocean to Interior. *Bulletin of the American Meteorological Society*, *101*(11), E1996–E2004. https://doi.org/10.1175/BAMS-D-19-0305.1

Mahadevan, A., Tandon, A., & Ferrari, R. (2010). Rapid changes in mixed layer stratification driven by submesoscale instabilities and winds. *Journal of Geophysical Research: Oceans*, *115*(C3). https://doi.org/10.1029/2008JC005203

Maljutenko, I., & Raudsepp, U. (2019). Long-term mean, interannual and seasonal circulation in the Gulf of Finland — The wide salt wedge estuary or gulf type ROFI. *Journal of Marine Systems*, *195*, 1–19. https://doi.org/10.1016/j.jmarsys.2019.03.004

McDougall, T. J., & Barker, P. M. (2011). *Getting started with TEOS-10 and the Gibbs Seawater (GSW) oceanographic toolbox : version 3.0*. SCOR/IAPSO WG127.

McWilliams, J. C. (2016). Submesoscale currents in the ocean. *Proceedings of the Royal Society A: Mathematical, Physical and Engineering Sciences*, *472*(2189), 20160117. https://doi.org/10.1098/rspa.2016.0117

McWilliams, J. C. (2019). A survey of submesoscale currents. *Geoscience Letters*, *6*(1), 3. https://doi.org/10.1186/s40562-019-0133-3

Meng, Q., Xuan, J., Zhang, W., Zhou, F., Hao, Q., Zhao, Q., & Schrum, C. (2020). Impact of Submesoscale Vertical Advection on Primary Productivity in the Southern East China Sea. *Journal of Geophysical Research: Biogeosciences*, *125*(8). https://doi.org/10.1029/2019JG005540

Myrberg, K., & Andrejev, O. (2003). Main upwelling regions in the Baltic Sea – a statistical analysis based on three-dimensional modeling. *Boreal Environment Research*, *8*, 97–112.

Naveira Garabato, A. C., Yu, X., Callies, J., Barkan, R., Polzin, K. L., Frajka-Williams, E. E., Buckingham, C. E., & Griffies, S. M. (2022). Kinetic energy transfers between mesoscale and submesoscale motions in the open ocean's upper layers. *Journal of Physical Oceanography*, *52*(1), 75–97. https://doi.org/10.1175/JPO-D-21-0099.1

Pavelson, J. (2005). *Mesoscale physical processes and the related impact on the summer nutrient fields and phytoplankton blooms in the western Gulf of Finland*. Tallinn University of Technology.

Pedlosky, J. (1996). Vertical Structure: Baroclinic Quasi-Geostrophic Models. In *Ocean Circulation Theory* (1st ed.). Springer.

Pham, H. T., Verma, V., Sarkar, S., Shcherbina, A. Y., & D'Asaro, E. A. (2024). Rapid Downwelling of Tracer Particles Across the Boundary Layer and Into the Pycnocline at Submesoscale Ocean Fronts. *Geophysical Research Letters*, *51*(17). https://doi.org/10.1029/2024GL109674

Ramachandran, S., Tandon, A., Mackinnon, J., Lucas, A. J., Pinkel, R., Waterhouse, A. F., Nash, J., Shroyer, E., Mahadevan, A., Weller, R. A., & Farrar, J. T. (2018). Submesoscale Processes at Shallow Salinity Fronts in the Bay of Bengal: Observations during the Winter Monsoon. *Journal of Physical Oceanography*, *48*(3), 479–509. https://doi.org/10.1175/JPO-D-16-0283.1

Rudnick, D. L., & Cole, S. T. (2011). On sampling the ocean using underwater gliders. *Journal of Geophysical Research*, *116*(C8), C08010. https://doi.org/10.1029/2010JC006849

Shang, X., Shu, Y., Wang, D., Yu, J., Mao, H., Liu, D., Qiu, C., & Tang, H. (2023). Submesoscale Motions Driven by Down-Front Wind Around an Anticyclonic Eddy With a Cold Core. *Journal of Geophysical Research: Oceans*, *128*(8). https://doi.org/10.1029/2022JC019173

Smith, K. S., & Ferrari, R. (2009). The Production and Dissipation of Compensated Thermohaline Variance by Mesoscale Stirring. *Journal of Physical Oceanography*, *39*(10), 2477–2501. https://doi.org/10.1175/2009JPO4103.1

Spall, M. A. (1995). Frontogenesis, subduction, and cross-front exchange at upper ocean fronts. *Journal of Geophysical Research: Oceans*, *100*(C2), 2543–2557. https://doi.org/10.1029/94JC02860

Stipa, T. (2004). Baroclinic adjustment in the Finnish coastal current. *Tellus A: Dynamic Meteorology and Oceanography*, *56*(1), 79. https://doi.org/10.3402/tellusa.v56i1.14391

Stipa, T., Tamminen, T., & Seppälä, J. (1999). On the creation and maintenance of stratification in the Gulf of Riga. *Journal of Marine Systems*, *23*(1–3), 27–49. https://doi.org/10.1016/S0924-7963(99)00049-4

Su, Z., Wang, J., Klein, P., Thompson, A. F., & Menemenlis, D. (2018). Ocean submesoscales as a key component of the global heat budget. *Nature Communications*, *9*(1), 775. https://doi.org/10.1038/s41467-018-02983-w

Suhhova, I., Liblik, T., Lilover, M. J., & Lips, U. (2018). A descriptive analysis of the linkage between the vertical stratification and current oscillations in the Gulf of Finland. *Boreal Environment Research*, *23*, 83–103.

Swart, S., du Plessis, M. D., Nicholson, S.-A., Monteiro, P. M. S., Dove, L. A., Thomalla, S., Thompson, A. F., Biddle, L. C., Edholm, J. M., Giddy, I., Heywood, K. J., Lee, C., Mahadevan, A., Shilling, G., & de Souza, R. B. (2023). The Southern Ocean mixed layer and its boundary fluxes: fine-scale observational progress and future research priorities. *Philosophical Transactions of the Royal Society A: Mathematical, Physical and Engineering Sciences*, *381*(2249). https://doi.org/10.1098/rsta.2022.0058

Tarry, D. R., Ruiz, S., Johnston, T. M. S., Poulain, P., Özgökmen, T., Centurioni, L. R., Berta, M., Esposito, G., Farrar, J. T., Mahadevan, A., & Pascual, A. (2022). Drifter Observations Reveal Intense Vertical Velocity in a Surface Ocean Front. *Geophysical Research Letters*, *49*(18). https://doi.org/10.1029/2022GL098969

Taylor, J. R., & Ferrari, R. (2009). On the equilibration of a symmetrically unstable front via a secondary shear instability. *Journal of Fluid Mechanics*, *622*, 103–113. https://doi.org/10.1017/S0022112008005272

Taylor, J. R., & Ferrari, R. (2010). Buoyancy and Wind-Driven Convection at Mixed Layer Density Fronts. *Journal of Physical Oceanography*, *40*(6), 1222–1242. https://doi.org/10.1175/2010JPO4365.1

Taylor, J. R., & Thompson, A. F. (2023). Submesoscale Dynamics in the Upper Ocean. *Annual Review of Fluid Mechanics*, *55*(1), 103–127. https://doi.org/10.1146/annurev-fluid-031422-095147

Thomas, L. N. (2005). Destruction of Potential Vorticity by Winds. *Journal of Physical Oceanography*, *35*(12), 2457–2466. https://doi.org/10.1175/JPO2830.1

Thomas, L. N., & Ferrari, R. (2008). Friction, Frontogenesis, and the Stratification of the Surface Mixed Layer. *Journal of Physical Oceanography*, *38*(11), 2501–2518. https://doi.org/10.1175/2008JPO3797.1

Thomas, L. N., & Lee, C. M. (2005). Intensification of Ocean Fronts by Down-Front Winds. *Journal of Physical Oceanography*, *35*(6), 1086–1102. https://doi.org/10.1175/JPO2737.1

Thomas, L. N., Tandon, A., & Mahadevan, A. (2008). Submesoscale processes and dynamics. In *Geophysical Monograph Series* (Vol. 177, pp. 17–38). Blackwell Publishing Ltd. https://doi.org/10.1029/177GM04

Thomas, L. N., Taylor, J. R., Ferrari, R., & Joyce, T. M. (2013). Symmetric instability in the Gulf Stream. *Deep Sea Research Part II: Topical Studies in Oceanography*, *91*, 96–110. https://doi.org/10.1016/j.dsr2.2013.02.025

Thompson, A. F., Lazar, A., Buckingham, C., Naveira Garabato, A. C., Damerell, G. M., & Heywood, K. J. (2016). Open-Ocean Submesoscale Motions: A Full Seasonal Cycle of Mixed Layer Instabilities from Gliders. *Journal of Physical Oceanography*, *46*(4), 1285–1307. https://doi.org/10.1175/JPO-D-15-0170.1

Umlauf, L., & Burchard, H. (2005). Second-order turbulence closure models for geophysical boundary layers. A review of recent work. *Continental Shelf Research*, *25*(7–8), 795–827. https://doi.org/10.1016/j.csr.2004.08.004

Väli, G., Meier, H. E. M., & Elken, J. (2013). Simulated halocline variability in the Baltic Sea and its impact on hypoxia during 1961–2007. *Journal of Geophysical Research: Oceans*, *118*(12), 6982–7000. https://doi.org/10.1002/2013JC009192

Väli, G., Meier, H. E. M., Liblik, T., Radtke, H., Klingbeil, K., Gräwe, U., & Lips, U. (2024). Submesoscale processes in the surface layer of the central Baltic Sea: A high-resolution modelling study. *Oceanologia*, *66*(1), 78–90. https://doi.org/10.1016/j.oceano.2023.11.002

Väli, G., Meier, H. E. M., Placke, M., & Dieterich, C. (2019). River runoff forcing for ocean modeling within the Baltic Sea Model Intercomparison Project. *Marine Science Reports*, *113*. https://doi.org/10.12754/msr-2019-0113

Väli, G., Zhurbas, V., Lips, U., & Laanemets, J. (2017). Submesoscale structures related to upwelling events in the Gulf of Finland, Baltic Sea (numerical experiments). *Journal of Marine Systems*, *171*, 31–42. https://doi.org/10.1016/j.jmarsys.2016.06.010

Wenegrat, J. O., & Thomas, L. N. (2020). Centrifugal and Symmetric Instability during Ekman Adjustment of the Bottom Boundary Layer. *Journal of Physical Oceanography*, *50*(6), 1793–1812. https://doi.org/10.1175/JPO-D-20-0027.1

Westerlund, A., Tuomi, L., Alenius, P., Myrberg, K., Miettunen, E., Vankevich, R. E., & Hordoir, R. (2019). Circulation patterns in the Gulf of Finland from daily to seasonal timescales. *Tellus A: Dynamic Meteorology and Oceanography*, *71*(1), 1627149. https://doi.org/10.1080/16000870.2019.1627149

Wong, A., Keeley, R., Carval, T., & Argo Data Management Team. (2019). *Argo Quality Control Manual for CTD and Trajectory Data, Version 3.2*. https://doi.org/10.13155/33951

Yang, Y., McWilliams, J. C., San Liang, X., Zhang, H., Weisberg, R. H., Liu, Y., & Menemenlis, D. (2021). Spatial and Temporal Characteristics of the Submesoscale Energetics in the Gulf of Mexico. *Journal of Physical Oceanography*, *51*(2), 475–489. https://doi.org/10.1175/JPO-D-20-0247.1

Ylöstalo, P., Seppälä, J., Kaitala, S., Maunula, P., & Simis, S. (2016). Loadings of dissolved organic matter and nutrients from the Neva River into the Gulf of Finland – Biogeochemical composition and spatial distribution within the salinity gradient. *Marine Chemistry*, *186*, 58–71. https://doi.org/10.1016/j.marchem.2016.07.004

Yoshikawa, Y., Lee, C. M., & Thomas, L. N. (2012). The Subpolar Front of the Japan/East Sea. Part III: Competing Roles of Frontal Dynamics and Atmospheric Forcing in Driving Ageostrophic Vertical Circulation and Subduction. *Journal of Physical Oceanography*, *42*(6), 991–1011. https://doi.org/10.1175/JPO-D-11-0154.1

Yu, X., Naveira Garabato, A. C., Martin, A. P., Buckingham, C. E., Brannigan, L., & Su, Z. (2019). An Annual Cycle of Submesoscale Vertical Flow and Restratification in the Upper Ocean. *Journal of Physical Oceanography*, *49*(6), 1439–1461. https://doi.org/10.1175/JPO-D-18-0253.1

Zhang, Z., Zhang, X., Qiu, B., Zhao, W., Zhou, C., Huang, X., & Tian, J. (2021). Submesoscale Currents in the Subtropical Upper Ocean Observed by Long-Term High-Resolution Mooring Arrays. *Journal of Physical Oceanography*, *51*(1), 187–206. https://doi.org/10.1175/JPO-D-20-0100.1

Zhu, R., Yang, H., Li, M., Chen, Z., Ma, X., Cai, J., & Wu, L. (2024). Observations reveal vertical transport induced by submesoscale front. *Scientific Reports*, *14*(1), 4407. https://doi.org/10.1038/s41598-024-54940-x

Zhurbas, V., Laanemets, J., & Vahtera, E. (2008). Modeling of the mesoscale structure of coupled upwelling/downwelling events and the related input of nutrients to the upper mixed layer in the Gulf of Finland, Baltic Sea. *Journal of Geophysical Research: Oceans*, *113*(C5). https://doi.org/10.1029/2007JC004280

Zhurbas, V., Väli, G., & Kuzmina, N. (2022). Striped texture of submesoscale fields in the northeastern Baltic Proper: Results of very high-resolution modelling for summer season. *Oceanologia*, *64*(1), 1–21. https://doi.org/10.1016/j.oceano.2021.08.003

Acknowledgements

First, I would like to express my profound gratitude to my supervisor, Urmas Lips, for his invaluable guidance and support throughout my PhD journey. I am also very grateful to Germo Väli and Taavi Liblik for their contributions to the articles that form the basis of this thesis. In addition, I sincerely thank Urmas Raudsepp for reviewing this thesis and providing insightful feedback.

I would also like to thank my colleagues in the Department of Marine Systems at TalTech and the crew of RV Salme for their assistance during the deployment and recovery of the glider.

The numerical model results used in this thesis were produced using computational resources provided by TalTech HPC, which are gratefully acknowledged. I also acknowledge the GETM community, including the Leibniz Institute for Baltic Sea Research Warnemünde (IOW), for maintaining and supporting the development of the GETM model code.

At different stages, this work was supported by the Estonian Research Council grant PRG602 and the institutional research funding IUT-19-6 of the Estonian Ministry of Education and Research. The glider mission in summer 2019 was carried out as part of the LAkHsMI project (Sensors for LArge scale HydrodynaMic Imaging of ocean floor), which received funding from the European Union's Horizon 2020 Research and Innovation Programme under grant agreement No. 635568.

Finally, I would like to give special thanks to my family and friends for their patience and unconditional support.

Abstract

Submesoscale variability in the Baltic Sea: occurrence and role in the redistribution of physical tracers

As a transitional regime between quasi-geostrophic flow and three-dimensional turbulence, submesoscale (SMS) processes mediate horizontal and vertical tracer exchange. Although SMS processes have been studied extensively in the open ocean, their expression and significance in shallow, strongly forced basins such as the Baltic Sea remain comparatively understudied.

SMS motions typically span 200 m–20 km in the ocean but are expected at smaller scales in the Baltic Sea (<10 km) because of its high latitude, shallow depth, and layered structure. Strong horizontal buoyancy gradients, which provide the frontal setting required for SMS activity, are common due to freshwater input and persistent salinity contrasts. Differential warming and cooling between coastal and offshore areas further generate horizontal variability. Circulation is also strongly influenced by wind, and in narrow basins such as the Gulf of Finland, upwelling and downwelling events are frequent.

These characteristics provide favourable conditions for widespread SMS activity, motivating investigation of the conditions under which SMS variability emerges. The central aim of this thesis is to examine the roles of mesoscale dynamics, atmospheric forcing, and stratification in shaping SMS variability, and to assess how SMS processes contribute to tracer redistribution and exchange.

This thesis combines repeated high-resolution glider observations across frontal and stratified regions with a realistic high-resolution simulation. The observations are used to analyse fine-scale thermohaline variability and filamentary tracer intrusions, apply spice as a tracer diagnostic, and characterize the dynamical regime using along-isopycnal temperature spectra. This is complemented by model-derived diagnostics that provide standard dynamical indicators of SMS activity.

The results show that SMS variability in the Gulf of Finland is structured both horizontally and vertically. Larger-scale atmospheric forcing regulates when and where SMS activity emerges by shaping horizontal buoyancy gradients and mesoscale structures. SMS-related tracer redistribution persists under stratified conditions, but its vertical expression changes seasonally with the evolving water-column structure. During the late-summer upwelling event, SMS subduction is interpreted to explain the spatial offset between tracer-based and dynamical indicators, suggesting that along-isopycnal tracer transport can contribute to coastal–offshore exchange. Consistent near-k^{-2} slopes of along-isopycnal temperature spectra in the surface layer and thermocline further support the presence of active SMS dynamics below the surface.

Overall, the thesis identifies SMS processes as pathways that couple lateral and vertical tracer redistribution within evolving mesoscale buoyancy structures. These processes contribute to multiscale coastal circulation and energy transfer in the Baltic Sea, underscoring the need for sub-grid parameterisations of SMS pathways in coarse-resolution ocean and climate models.

Lühikokkuvõte

Submesomastaapi muutlikkus Läänemeres: esinemine ja roll vee füüsikaliste omaduste ümberjaotamises

Submesomastaap kirjeldab vahepealset dünaamilist režiimi kvasi-geostroofilise kahemõõtmelise voolu ja kolmemõõtmelise isotroopse turbulentsi vahel, kus protsessid vahendavad trasserite horisontaalset ja vertikaalset vahetust ning ümberjaotumist. Kuigi submesomastaapseid (SMM) protsesse on avaookeanis palju uuritud, on nende avaldumine ja tähtsus madalates, keeruka vertikaalse struktuuriga basseinides, mida mõjutab oluliselt atmosfääri mõju muutlikkus, endiselt võrdlemisi vähe uuritud.

Võrreldes ookeaniga (200 m–20 km), esinevad SMM protsessid Läänemeres mõnevõrra väiksemas mõõtkavas (<10 km), tulenevalt mere suhteliselt kõrgest laiuskraadist, väikesest sügavusest ning tugevalt kihistunud struktuurist. Tugevad horisontaalsed tihedusgradiendid, mis loovad SMM-aktiivsuseks vajaliku frontaalse keskkonna, on Läänemeres tavalised suure magevee sissevoolu ja püsivate horisontaalsete soolsuskontrastide tõttu. Ranniku- ja avamerealade erinev soojenemine ja jahtumine tekitab täiendavat horisontaalset muutlikkust. Tsirkulatsiooni mõjutab oluliselt ka tuul ning kitsastes basseinides, näiteks Soome lahes, on süvaveekerke ja pealisvee sukeldumise sündmused sagedased.

Need iseärasused loovad soodsad tingimused SMM protsesside arenguks, ajendades uurima, millistel tingimustel SMM-muutlikkus kujuneb. Käesoleva väitekirja keskne eesmärk on selgitada, kuidas mesomastaapne dünaamika, atmosfääri mõju ja kihistumine kujundavad SMM-muutlikkust ning kuidas SMM-protsessid panustavad trasserite ümberjaotumisse ja vahetusse.

Käesolev väitekiri ühendab kõrglahutuslikud glideri mõõdistused frontaalsetes ja kihistunud piirkondades realistliku kõrglahutusliku simulatsiooniga. Vaatluste põhjal analüüsitakse väiksemastaapset termohaliinset muutlikkust ja trasseri käitumist kasutades spice'i ning iseloomustatakse dünaamilist režiimi piki isopükne arvutatud temperatuurispektrite abil. Analüüsi täiendavad mudelipõhised dünaamilised näitajad, mida kasutatakse standardsete indikaatoritena SMM aktiivsuse jaoks.

Tulemused näitavad, et SMM muutlikkus Soome lahes on struktureeritud nii horisontaalselt kui ka vertikaalselt. Suuremõõtmeline atmosfääriline mõju reguleerib, millal ja kus aktiivsus avaldub, kujundades horisontaalseid tihedusgradiente ja mesomastaapseid struktuure. SMM seotud trasserite ümberjaotumine püsib kihistunud tingimustes, kuid selle vertikaalne väljendumine muutub sesoonselt koos veesamba struktuuri arenguga. Hilissuvise süvaveekerke sündmuse ajal tõlgendatakse SMM subduktsiooni trasseripõhiste ja dünaamiliste indikaatorite ruumilise nihke võimaliku seletusena, mis viitab sellele, et piki isopükne toimuv trasseritransport võib panustada ranniku ja avamere vahelisse vahetusse. Piki isopükne arvutatud temperatuurispektrite ligikaudu k^{-2} kalded pinnakihis ja termokliinis toetavad omakorda aktiivse SMM dünaamika olemasolu ka pinnast allpool.

Kokkuvõttes näitab väitekiri, et SMM protsessid seovad trasserite horisontaalset ja vertikaalset ümberjaotumist arenevates mesomastaapsetes struktuurides. Need protsessid panustavad Läänemere rannikumere tsirkulatsiooni ja on olulisel kohal mastaapide vahelises energia ülekandes, rõhutades vajadust arvestada SMM protsessidega madala lahutusega ookeani- ja kliimamudelite parametriseeringutes.

Appendix

Publication I

Salm, K.; Liblik, T.; Lips, U. (2023). Submesoscale Variability in a Mesoscale Front Captured by a Glider Mission in the Gulf of Finland, Baltic Sea. Frontiers in Marine Science, 10. DOI: 10.3389/fmars.2023.984246.

frontiers | Frontiers in Marine Science

TYPE Original Research
PUBLISHED 31 January 2023
DOI 10.3389/fmars.2023.984246

Check for updates

OPEN ACCESS

EDITED BY
Chunyan Li,
Louisiana State University, United States

REVIEWED BY
Renhao Wu,
Sun Yat-sen University, China
Enric Pallàs-Sanz,
Center for Scientific Research and Higher Education in Ensenada (CICESE), Mexico

*CORRESPONDENCE
Kai Salm
Kai.Salm@taltech.ee

SPECIALTY SECTION
This article was submitted to Physical Oceanography, a section of the journal Frontiers in Marine Science

RECEIVED 01 July 2022
ACCEPTED 19 January 2023
PUBLISHED 31 January 2023

CITATION
Salm K, Liblik T and Lips U (2023) Submesoscale variability in a mesoscale front captured by a glider mission in the Gulf of Finland, Baltic Sea. *Front. Mar. Sci.* 10:984246. doi: 10.3389/fmars.2023.984246

COPYRIGHT
© 2023 Salm, Liblik and Lips. This is an open-access article distributed under the terms of the Creative Commons Attribution License (CC BY). The use, distribution or reproduction in other forums is permitted, provided the original author(s) and the copyright owner(s) are credited and that the original publication in this journal is cited, in accordance with accepted academic practice. No use, distribution or reproduction is permitted which does not comply with these terms.

Submesoscale variability in a mesoscale front captured by a glider mission in the Gulf of Finland, Baltic Sea

Kai Salm*, Taavi Liblik and Urmas Lips

Department of Marine Systems, Tallinn University of Technology, Tallinn, Estonia

Modern research methods enable unfolding the structure of the water column with higher resolution than ever, revealing the importance of submesoscale. Submesoscale processes have intermediate space and time scales of <5 km and a few days in the Baltic Sea. A glider mission was conducted in the Gulf of Finland in May 2018. The appearance of a mesoscale front as a response to the persisting NE–E winds was observed. Within the front, smaller scale features at a lateral scale of a km were apparent. The tracer patterns indicated the presence of two adjacent motions – cold (warm) water penetrating upward (downward) on the lighter (denser) side of the front. We suggest they were traces of ageostrophic secondary circulation emerging while the loss of the upwelling-favorable forcing arrested the strengthening of the front. The analysis showed favorable conditions for the baroclinic and wind-driven instability. Such circulations could work to equalize the differences in cross-front direction, affecting the stratification and acting against the persistence of the mesoscale front. The spatial spectra of isopycnal tracer variance revealed the depth-dependence of the spectral slopes at the lateral scales of 1–10 km in the upper part of the water column. The differing of the slopes in the density layers associated with the mesoscale front indicates that frontal dynamics contribute to the energy cascade.

KEYWORDS

glider, horizontal buoyancy gradient, submesoscale, stratification, Baltic Sea

1 Introduction

The growth in the resolution capabilities of ocean observations has unfolded a rich structure on lateral scales of a kilometer (Karimova and Gade, 2016; Lips et al., 2016; Carpenter et al., 2020). This scale, referred to as submesoscale, forms by the interplay between atmospheric forcing and mesoscale motions. Turbulent motions associated with atmospheric forcing mix the surface layer in the vertical and mesoscale horizontal flows advect water masses introducing lateral variability (Ferrari and Boccaletti, 2004). Dynamically ocean's submesoscale is defined with order one Rossby and balanced Richardson number expressed respectively as $Ro = \frac{\zeta}{f}$ and $Ri_b = \frac{f^2 N^2}{b_y^2}$, where ζ is vertical vorticity, f Coriolis frequency, N^2 vertical buoyancy gradient and b_y horizontal buoyancy gradient (Thomas et al., 2008).

Therefore, by definition, submesoscale is active in regions of strong horizontal buoyancy gradients, strong vorticity, and weak vertical stratification. However, observations have shown that energetic submesoscale can be triggered throughout the ocean (Thompson et al., 2016; Yu et al., 2019b).

Comprehending the nature of submesoscale proposes a challenge as the dynamics is neither fully two- nor three-dimensional. Although being constrained by geostrophic and hydrostatic momentum balance to some extent, submesoscale flows can break this balance to show a forward energy cascade (McWilliams, 2016). Fronts are recognized as one of the primary sources of submesoscale motions (Thomas et al., 2013; Garcia-Jove et al., 2022). Fronts are known to be subject to frontogenesis (Lapeyre et al., 2006), frictional forces (Thomas and Ferrari, 2008), baroclinic instability (Boccaletti et al., 2007), and baroclinic submesoscale instability (Fox-Kemper et al., 2008; Thomas et al., 2013). Frontal submesoscale efficiently transfers energy to small-scale diapycnal mixing and dissipation through induced submesoscale flows, resulting in modified stratification. Therefore, the horizontal variations are closely related to the changes in the vertical structure.

Frontogensesis is a process that leads to the local intensification of the horizontal buoyancy gradient, requiring an acceleration of the along-front velocity to hold the geostrophic balance in the cross-front direction. An ageostrophic secondary circulation emerges to compensate for the acceleration. The overturning circulation is directed from the anticyclonic (light) to the cyclonic (dense) side of the front as the relative vorticity near the surface intensifies. Downwelling (upwelling) results from the conservation of potential vorticity that requires the horizontal flow to be convergent (divergent) on the dense (light) side of the front (Spall, 1995). We refer the reader to Figure 3 of Spall (1995). While the up- and downwelling rates are high (Yu et al., 2019a), returning of the water parcels to their original depth away from the fronts takes longer. Meanwhile, the external forcing has a chance to interact with the upper ocean, meaning that, in the real ocean, the horizontal buoyancy gradient is simultaneously subject to frictional forces, which can lead to modifications in the heat fluxes (Thomas, 2005). The wind generates Ekman currents that de- or restratify the water column, depending on the orientation between the wind and the baroclinic geostrophic flow along the front. Downfront (upfront) winds are aligned with (oriented against) the frontal jet, driving denser (lighter) fluid over lighter (denser) (Thomas and Ferrari, 2008). We refer the reader to Figure 1 of Thomas and Ferrari (2008).

Downfront winds reduce the potential vorticity in the Ekman layer but can additionally induce secondary circulations that extract potential vorticity from the pycnocline (Thomas, 2005). The mixed layer deepens as a result. When the potential vorticity turns negative, the flow becomes unstable (Hoskins, 1974) and symmetric instability can develop if the mixed layer is deeper than the Ekman layer (Thomas et al., 2013). Produced slantwise overturning cell at the base of the front (Taylor and Ferrari, 2009) pushes the system toward zero potential vorticity (Thomas et al., 2013). Thus, the stratification is modified by a combination of restratification by frontal circulation and surface forcing induced mixing of the density profile by convection. If the front persists while being marginally stable to symmetric instability, baroclinic instability can restratify the water column through the generation of secondary circulation by releasing potential energy (Boccaletti et al., 2007).

A large part of the insight into the submesoscale processes has been achieved thanks to numerical simulations (Boccaletti et al., 2007; Thomas et al., 2008; Mahadevan et al., 2010), while observations are challenging due to the processes' ephemeral nature (Yu et al., 2019a). However, focusing on the regions where the environment favors the presence of submesoscale flows, recent glider observations have well demonstrated fine-scale water column structure. For instance, Pietri et al. (2013) sampled an upwelling system and discussed a driving mechanism that could explain observed submesoscale variability compatible with cross-frontal cells. Further, Pérez et al. (2022) analyzed submesoscale instabilities in a warm core ring and showed the core to be susceptible to gravitational instability and the periphery to symmetric instability under favorable downfront wind forcing. While in the ocean, the use of gliders is common, only a few studies have been conducted using gliders in the Baltic Sea (Karstensen et al., 2014; Meyer et al., 2018; Carpenter et al., 2020; Liblik et al., 2022). Observations by towed and autonomous devices (e.g., Lips et al., 2016; Carpenter et al., 2020) have indicated the presence of submesoscale activity, but the analysis of their nature is lacking.

Understanding the dynamics of the submesoscale allows for improving numerical models to which a physically complex environment like the Baltic Sea proposes a challenge (e.g., Tuomi et al., 2012). In the Baltic Sea, the water column has a layered structure that forms due to the atmospheric forcing and input of fresh river water and saltier North Sea water. Although, in general, the sea is shallow, the depth varying from a few tens of meters to a hundred meters determines the characteristic structure of the water column. The thermohaline structure can have one, two, or three layers. Halocline is persistent at 50–70 m in most of the deeper areas (e.g., Alenius et al., 2003; Liblik and Lips, 2017), and the seasonal thermocline usually develops above 20 m during spring (e.g., Alenius et al., 1998; Liblik and Lips, 2017). The presence of submesoscale flows and features has been often indicated together with rich mesoscale variability (Kikas and Lips, 2016; Zhurbas et al., 2019). Numerous upwelling and downwelling events, fronts, and eddies are characteristic features of the Baltic Sea (Pavelson et al., 1997; Myrberg and Andrejev, 2003; Lehmann et al., 2012). In this study, we use high-resolution glider observations that reveal multi-scale variability of the water column.

A glider mission was conducted in the Gulf of Finland during the formation of the seasonal thermocline. The hypothesis that energetic submesoscale occurs within the mesoscale lateral density gradient under certain atmospheric forcing was tested. The study provided evidence of the frontal submesoscale processes and enabled their preliminary characterization. To our knowledge, the present investigation is the first attempt to study submesoscale processes in a repeated coastal-offshore transect in the Baltic Sea. The paper is organized as follows: Section 2 introduces the observational data and used methods; Section 3 describes the wind forcing and the observed water column structure concerning both the mesoscale and the submesoscale ranges; Section 4 discusses the observed features and their relation with the wind and the stratification; the last section summarizes the work.

2 Data and methods

2.1 Glider observations

The geographic area and season suggest the potential presence of larger-scale horizontal buoyance gradients. Salinity increases from east to west due to the large river discharge at the eastern end of the gulf (Ylöstalo et al., 2016) and a cross-shore temperature gradient could form due to faster warming in shallow areas (Lips et al., 2014; Lips and Lips, 2017). Furthermore, pycnoclines have varying cross-shore inclination depending on the local wind forcing (Liblik and Lips, 2017).

The data set analyzed in the study was gathered from 9 May to 6 June 2018 using an autonomous underwater vehicle – the Slocum G2 Glider MIA deployed in the Gulf of Finland slope area at 59.57° N–25.05° E, Baltic Sea (Figure 1). The glider collected oceanographic data along the 18 km long transect (S–N direction, sampled 26 times). The Slocum glider can perform YOs without reaching the surface. The mission set-up determined the glider to perform 4 YOs between surfacings (i.e., a cycle). The vehicle started turnaround either 4 m before the surface or 6 m before the seafloor. The glider moved at a horizontal speed of 0.32 ± 0.09 m s^{-1}. The average distance between the profiles near the surface was 287 ± 39 m (it reduces with depth due to the sawtooth-shaped sampling trajectory), and a profile took 7.8 ± 0.5 min to complete at a characteristic depth of 80–90 m. Therefore, the glider completed a cycle approximately in an hour after covering about a km horizontally.

Temperature and conductivity (salinity) profiles were collected with a pumped Seabird conductivity-temperature-depth recorder (CTD; model G-1451). Technical specifications of the sensors set the accuracy for pressure 0.1% of the full range (0–200 m), for temperature 0.002°C, and for conductivity 0.01 mS cm^{-1}. The CTD had a sampling rate of 0.5 Hz, and both descending and ascending profiles were recorded. Altogether over 4000 CTD profiles were gathered and analyzed. The raw data was quality controlled, and the coefficients to account for the response time of the sensors and the thermal lag were defined to minimize differences between two consecutive CTD profiles (Appendix). The typical vertical resolution of the raw CTD data was around 0.2 dbar. The half YOs were bin-averaged to a uniform 0.5 dbar vertical grid and arranged as profiles, meaning an average time and coordinates were attributed to a half YO. While the glider data has time-varying orientation in horizontal direction, for this analysis, each transect was interpolated on a regular grid with a latitudinal step of 0.0018° (if not specified otherwise). The horizontal step, equal to 200 m, was slightly larger than the distance between half YOs generally (median 135 ± 56 m) and thus, the interpolated fields were smoother. Note that this median distance between half YOs corresponds to the horizontal distance between the midpoints of the half YOs.

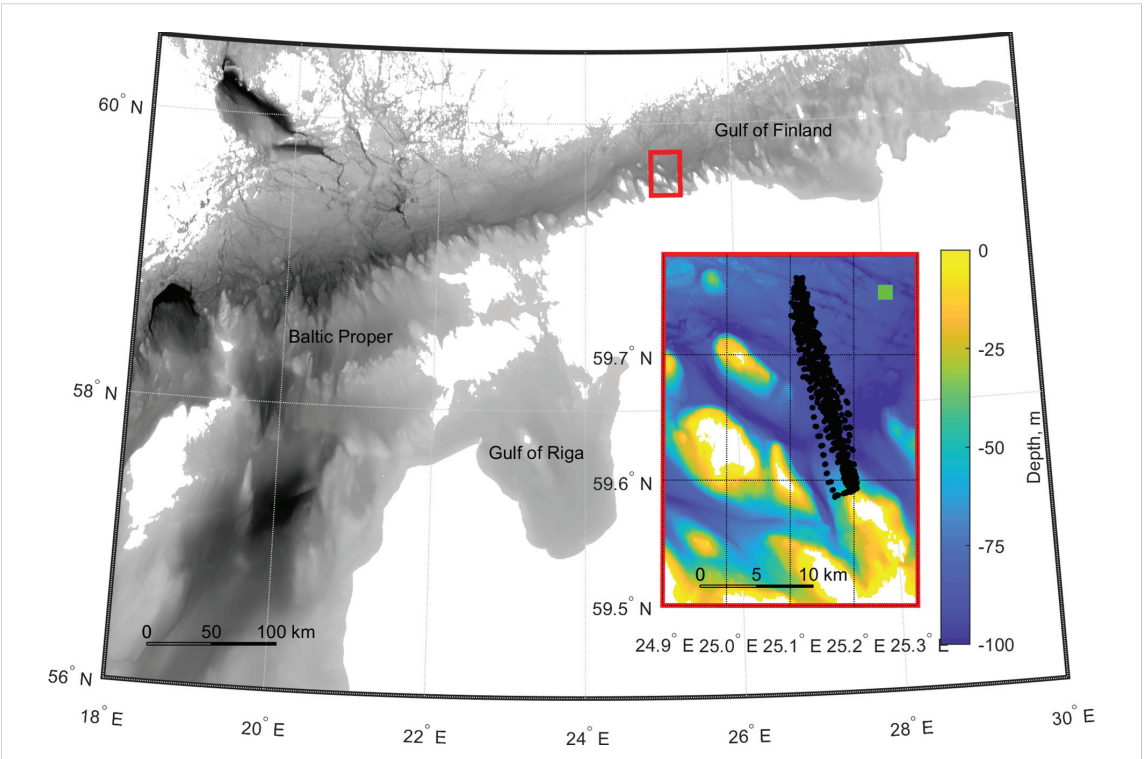


FIGURE 1
Map of the study area in May 2018. The overlaid plot shows the bathymetry (EMODnet digital terrain model) of the deployment area highlighted by a red rectangle. Black dots indicate the glider inflections on the surface. The green square shows the position of the ERA5 grid point used for the wind data.

2.2 Velocity

Velocity calculations from the glider observations are limited. Absolute geostrophic velocity can be produced using the hydrographic data and the additional information from the depth-averaged current, which is estimated over a cycle based on dead reckoning and GPS fixes at the surface. The relative geostrophic velocity components were calculated using the dynamic method based on the geostrophic relationships

$$v_g = -\frac{1}{f}\frac{\partial \phi}{\partial x}$$

$$u_g = -\frac{1}{f}\frac{\partial \phi}{\partial y}$$

where the geopotential, ϕ, is proportional to dynamic height, D, as

$$\phi = gD$$

Coriolis parameter is noted with f and gravitational acceleration with g. Therefore, the horizontal pressure gradient is presented through the geopotential slope of an isobaric surface. The relative geostrophic velocity is evaluated using a dynamic height anomaly relative to a reference pressure. The dynamic height that depends on the density of the seawater was determined from the measured temperature and salinity profiles according to McDougall and Barker (2011) (IOC et al., 2010).

The relative geostrophic velocity component was estimated from the glider CTD data at a lateral scale of 5 km. The choice of reference level (85 dbar) was based on the lowest variability (i.e., standard deviation) of density along isobars, interpreted as the effect of the baroclinic velocity field becoming negligible there. To involve shallower profiles in the geostrophic velocity estimations, the stepped no-motion level method described in Rubio et al. (2009) was used. While the 2D nature of the glider data allows us to estimate only the across-transect component of the geostrophic velocity, the depth-averaged velocity components were rotated to be compatible with cross- and along-transect components. On average, the transect was tilted 14° to the left from the S–N axis. As the glider orientation was relatively stable along the path, the approach of using an average tilt was adopted for simplicity.

2.3 Horizontal and vertical gradients

Buoyancy is expressed as $by = g(1 - \frac{\rho}{\rho_0})$, where ρ_0 is reference density of 1003 kg m^{-3}. Along-transect buoyancy gradients, $b_y = \frac{\partial b}{\partial y}$, with a step of 5 km, were calculated to characterize the observed mesoscale frontal structure. Note that the notation y stands for the along-transect component and notation x for the across-transect component from here on. The stratification of the water column was characterized by the squared Brunt-Väisälä frequency (vertical buoyancy gradient) $N^2 = -\frac{g}{\rho}\frac{\partial \rho}{\partial z}$, where ρ is density and $\frac{\partial \rho}{\partial z}$ its vertical gradient.

2.4 Smaller scale variability

The analysis of smaller scale variability focused on temperature variations on the isopycnal surfaces. At the same density surfaces, water properties act as passive tracers, and the effect of internal waves is assumed negligible (Rudnick and Cole, 2011). The smaller scale signal was defined as the deviations from the smoothed isopycnal temperature field (moving average of 4 km). The length scale was chosen based on the internal Rossby deformation radius, which is typically 2–4 km in the Gulf of Finland (Alenius et al., 2003). The deviations visualize the patterns created by the smaller scale motions, including the submesoscale range.

2.5 Submesoscale analysis

2.5.1 Submesoscale instabilities

Potential vorticity can be used to identify the potential for flow instabilities. Potential vorticity with the opposite sign of the Coriolis parameter indicates the unstable flow (Hoskins, 1974). Glider sampling capabilities limit the calculation of potential vorticity. Following Thompson et al. (2016), the potential vorticity can be expressed as

$$q = (f + \zeta)N^2 - \frac{b_y^2}{f}$$

Vertical vorticity, ζ, is given here by the along-transect gradient of the across-transect velocity. Cross-transect velocities and along-transect density variations make the dominant contribution only if the glider transect is perpendicular to the front, highlighting the main assumption for this estimate of potential vorticity. The buoyancy gradients are underestimated in the glider measurements if the front is crossed at an angle different from the perpendicular orientation (Thompson et al., 2016). Therefore, the poor representation of the submesoscale instabilities because of the observational biases should be considered. In this study, neither the position of the front nor the crossing angle can be estimated.

The instability types are identified by the balanced Richardson angle

$$\phi_{Ri_b} = \tan^{-1}(-Ri_b^{-1})$$

One could expect $-90° < \phi_{Ri_b} < \phi_c$, where $\phi_c = \tan^{-1}(-1 - \frac{\zeta}{f})$ and $0 < Ri_b < 1$ near strong horizontal buoyancy gradients, meaning the dominance of symmetric instability (Thomas et al., 2013). We refer the reader to Figure 1 of Thomas et al. (2013) for further relations of ϕ_{Ri_b} in case of different submesoscale instabilities. Symmetric instability is favored under destabilizing atmospheric forcing. However, the upper mixed layer needs to be deeper than the convective layer for overturning motions to dominate over convective mixing induced by surface forcing (Taylor and Ferrari, 2010).

Without knowing the angle between the wind vector and the geostrophic shear, the ratio of the convective layer depth, h, to the mixed layer depth, H, cannot be estimated. However, Obukhov length, L_o, can be used along with the convective layer to analyze the depth where symmetric instability can be expected. The wind stress dominates the turbulence between the surface and L_o, and the combination of the surface and wind-driven buoyancy fluxes from L_o to the convective layer depth (Taylor and Ferrari, 2010). Thus, L_o. implies the presence of the symmetric instability region if it is small

compared to H. L_o is expressed as

$$L_o = \frac{U_*^3}{\kappa B}$$

where κ is the von Karman constant and U_* friction velocity found from wind stress, τ_w, and reference density as

$$U_* = \sqrt{\frac{\tau_w}{\rho_0}}$$

(Taylor and Ferrari, 2010). Net surface buoyancy flux, B, is expressed as

$$B = \frac{g\alpha Q_s}{\rho_0 C_p} + g\beta(E - P)S_s$$

where C_p the specific heat of seawater, α and β are the thermal expansion and saline contraction coefficients evaluated respectively from the surface temperature and salinity, and S_s is the surface salinity (Buckingham et al., 2019). The net surface heat flux, Q_s, is the sum of the net short-wave and long-wave radiation, and the sensible and latent heat fluxes. The net freshwater flux comes from subtracting precipitation, P, from evaporation, E. Positive values correspond to stabilizing conditions.

The study period was characterized by the formation of seasonal thermal stratification, meaning the upper mixed layer developed near the surface. We defined it as the minimum depth where $\rho_z \geq \rho_1 + 0.25\ kg\ m^{-3}$ was satisfied (ρ_z is the density at depth z and ρ_1 at 1 m). However, this shallow upper mixed layer does not characterize the water layer where the submesoscale circulations associated with the mesoscale front would rise if present. Thus, the upper boundary of the cold intermediate layer (CIL), defined as a water layer of <3°C, was used as H. The CIL boundaries were set as the average density at 3°C and the upper boundary corresponded to 4.4 kg m^{-3}. The depth of the upper mixed layer further helps to estimate the ratio of the convective layer depth to the mixed layer depth because stronger stratification acts to impede the vertical mixing.

2.5.2 Wind-driven and baroclinic instability

Baroclinic submesoscale instability affects potential vorticity by returning it to a neutrally stable state ($q < 0 \rightarrow q = 0$), but horizontal buoyancy gradient may be subject to other physical processes that change the stratification and can also modify potential vorticity to be positive through the processes (Thompson et al., 2016). The relaxation of isopycnals back towards the horizontal occurs over a period of days, providing a reservoir of potential energy (Boccaletti et al., 2007) and potential for surface wind stress to induce overturning circulations through horizontal Ekman flows (Thomas and Ferrari, 2008). Downfront (upfront) winds have a destratifying (restratifying) effect. Secondary circulations generated through the release of potential energy by baroclinic instability act to restratify the water column. The possibility for the emergence of wind-driven and baroclinic instability can be estimated from the related buoyancy fluxes that can be expressed respectively as equivalent heat fluxes

$$Q_{Ek} = -\frac{b_y \tau_x}{f}\frac{C_p}{\alpha g}$$

$$Q_{BCI} = 0.06\frac{b_y^2 H^2}{f}\frac{C_p \rho_0}{\alpha g}$$

The parametrizations are published respectively by Thomas (2005) and Fox-Kemper et al. (2008) but adopted for the glider data by Thompson et al. (2016). Negative Q_{Ek} reduces the stratification and corresponds to downfront wind orientation. However, Q_{BCI} is always a positive quantity. Note that Q_{BCI} relies on the simulation-derived coefficient, which may not be optimal in other regions. Here, the surface values for b_y and α correspond to 3 m depth to exclude the possible contamination from waves and/or surface glider maneuverer. We acknowledge that as only the along-track glider data is used to calculate the equivalent heat fluxes, the angle at which the glider crosses the horizontal buoyancy gradient can bias the results. While Q_{BCI} is mainly underestimated, Q_{Ek} can be affected in both ways. Q_{Ek} is well underestimated if the horizontal buoyancy gradient is captured poorly and a large along-front component present in reality is missed, or well overestimated if the wind is interpreted to have a larger along-front component than it actually has (Thompson et al., 2016).

2.6 Wavenumber spectrum

The dominating contribution to the energy fluxes at the submesoscale range in the transfer of energy from large to dissipative scales has remained debatable. We calculated the power spectrum of isopycnal temperature in the wavenumber domain, composing the data as a function of cumulative distance. Isopycnal temperature fields on a regular grid were constructed due to irregular sampling in both space and time. First, the temperature profiles were averaged in density bins (step 0.1 kg m^{-3}), and then interpolated on a grid with a constant horizontal step of 150 m. Averaging in advance allowed us to reduce the effect of spatial and temporal smoothening due to interpolation, which tends to bias spectra towards steepening (e.g., Wortham and Wunsch, 2014). Before taking Fast Fourier Transform, the linear trend was removed and Hanning window applied. The smoothed power spectrum was obtained using 31 elementary frequency bands for averaging. The number of elementary frequency bands can be equalized with the degrees of freedom to find confidence limits (95%).

The wavenumber spectra of isopycnal temperature were calculated in the density range of 3.6–6.0 kg m^{-3} with a step of 0.1 kg m^{-3} (covered depths from 3–50 m). The spectral slopes were estimated between the spatial scales of 1–10 km. The resolved horizontal length scale was not separated because the short data series limit the resolution of the spectrum and the scales where the transition between distinct dynamics occurs are not known. The glider sampled the 18 km long section repeatedly and thus, the lower wavenumbers than the one corresponding to 10 km were disregarded. The submesoscale in the Baltic Sea can be expected to be active around 1–2 km. The spectrum at <1 km was not analyzed due to greater uncertainties at smaller scales (Nyquist frequency corresponds to the spatial scale of 0.3 km).

2.7 Surface forcing

Atmospheric forcing is presented through wind, net surface heat flux, and freshwater flux. Parameters defining heat exchange between the atmosphere and the sea surface were extracted on the product grid cells that covered the study area (59.50–59.75° N, 25.00–25.25° E) for May–June 2018 from European Centre for Medium-Range Weather Forecasts atmospheric reanalysis data set (ERA5 hourly data on single levels from 1979 to present, horizontal resolution of 0.25°×0.25°, Hersbach et al., 2020; Hersbach et al., 2022). Hourly u- and v-components of wind at 10 m height, mean surface net short-wave and long-wave radiation flux, mean surface latent and sensible heat flux, mean total precipitation rate, and mean evaporation rate were used.

The net freshwater flux is converted to an equivalent heat flux as also used by Giddy et al. (2021)

$$Q_f = \rho_0 C_p \frac{\beta}{\alpha} S_s (E - P)$$

Wind components taken from the nearest cell to the glider section (59.75° N, 25.25° E) were smoothed by a Gaussian low pass filter for 6 h. Wind stress is expressed as

$$\tau = c_d \rho_a |U_a| U_a$$

where c_d is the drag coefficient ($1.2 \cdot 10^{-3}$; Large and Pond, 1981), ρ_a the air density (1.2 kg m^{-3}), and U_a stands for wind speed. The cumulative wind stress (in N m^{-2} h) is the product of wind stress and its duration, demonstrating the impact of the wind during a longer period.

3 Results

3.1 Surface forcing

Winds and buoyancy fluxes drive mixing in the near-surface layers and affect the development of stratification. In general, wind speed during the study period was <4.5 m s^{-1} (Figure 2). At the beginning of the glider mission, E winds prevailed, being relatively strong on 9–12 May and subsiding afterwards (to an average of 2.5 m s^{-1}). On 18–19 May, stronger northerly winds occurred for a short period, while the last third of May was characterized by alternating E and W winds. The W winds were stronger, on average, 5.4 ± 2.0 m s^{-1} compared to E winds of 3.8 ± 0.9 m s^{-1}. The strong W–NW winds started to prevail on 1 June. The cumulative wind stress perpendicular to the glider transect (approximately positive towards E) picks up the three distinct periods during the mission – from the beginning until 19 May, wind forcing was to W, after that until 31 May, forcing varied between E and W, and from 1 June, it was to E (Figure 2).

3.2 Thermohaline structure

The mission was conducted during the formation of the seasonal thermocline. The distributions of temperature, salinity, density, and geostrophic velocity were constructed (Figure 3 shows the composite plots of the upper 25 m from the beginning, middle and end of the mission, 10 days apart). During the mission, the sea surface (0–4 m) temperature increased from 6.7 to 15.2°C, and the salinity decreased from 5.3 to 4.2 g kg^{-1}. The decrease in salinity indicates the advection of fresher water, which possibly originates from the eastern part of the gulf. The temperatures below the developing seasonal thermocline in the CIL were around 2°C, and the thermocline, characterized by the maximum temperature gradient of about 3°C dbar^{-1}, was observed at 10–15 m by the beginning of June.

3.3 Horizontal buoyancy gradient

The mesoscale front was defined as an evident inclination in the density distribution, extending over the sampled transect. The horizontal (across-shore) buoyancy gradient formed as a response to the moderate NE–E winds that dominated for ten days prior to 19 May (Figure 2). The NE–E winds force surface waters to move offshore along the southern coast of the Gulf of Finland. Deep water rises in turn, tilting the pycnocline. Figure 4 shows the structure of the water column during the appearance of the front in the study window (~2.5-day period). The variability of buoyancy over

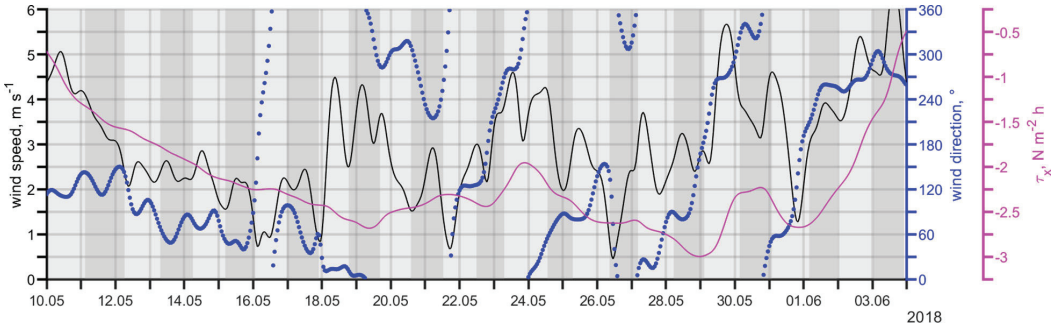


FIGURE 2
Wind forcing during the study period in May–June 2018 based on hourly data extracted from ERA5. Wind speed is shown in black and direction in blue, and cumulative wind stress in magenta. Shadowing indicates the orientation of the glider (light shows movement to N and dark to S).

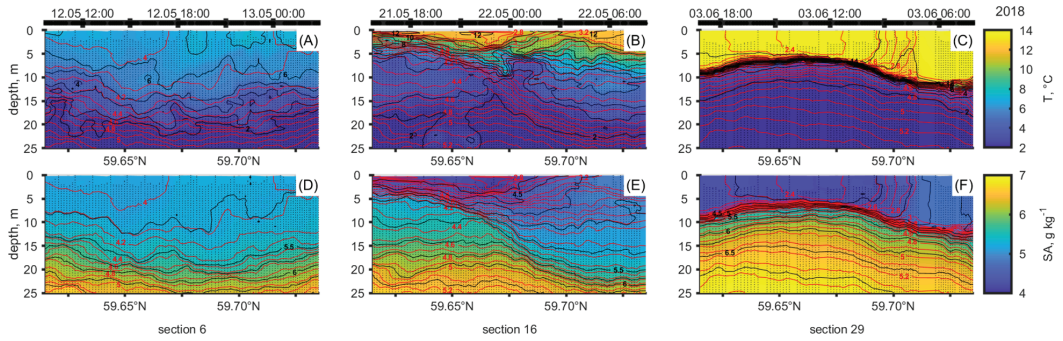


FIGURE 3
Temporal changes in temperature (**A–C**, black contours with a step of 1°C) and salinity (**D–F**, black contours with a step of 0.5 g kg^{-1}) distribution as a function of depth (0–25 m) along three glider sections in May–June 2018 (~10 days apart). The distributions are overlaid with red contours marking potential density anomaly with a step of 0.1 kg m^{-3}. The sampling timeline is at the top of the columns. The left side of a subplot is located closer to the coast and presents the southern part of the section. The area between ticks presenting latitude is about 2.7 km.

the sampled section was small on 20–21 May, apart from the small area at the southern end of the transect, which indicated denser water rising (Figure 4A). However, a westward flow compatible with the geostrophic frontal jet appeared to be developing (Figure 4D). The frontal jet in thermal wind balance flows in the same direction as the wind. The buoyancy increased from south to north at 15 and 25 m depth on 21–23 May, indicating the presence of a horizontal buoyancy gradient (Figures 4B, C). The strong westward flow with velocities over 20 cm s^{-1} spanning over the inclined density distribution suggested the presence of the frontal jet (Figures 4E, F).

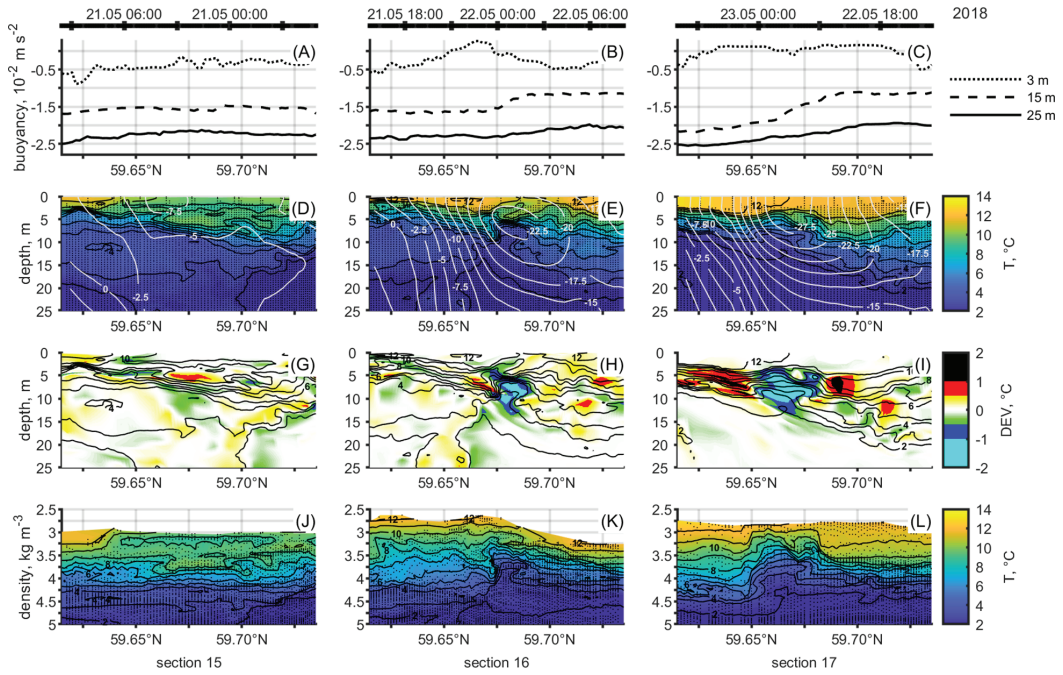


FIGURE 4
(A–C) Buoyancy along the glider transect at 3, 15, and 25 m depth on 20–23 May 2018. **(D–F)** Temperature distributions (black contours with a step of 1° C) as a function of depth (0–25 m) overlaid with white contours marking the relative geostrophic velocity (positive values show eastward movement) with a step of 2.5 cm s^{-1} on 20–23 May 2018. The sampling timeline is at the top of the columns. The left side of a subplot is located closer to the coast and presents the southern part of the section. The area between ticks presenting latitude is about 2.7 km. **(G–I)** Temperature deviations as a function of pressure along the glider section on 20–23 May 2018. Black contours mark potential density anomaly with a step 0.1 kg m^{-3}. **(J–L)** Isopycnal temperature distributions (black contours with a step of 1°C) along the glider section on 20–23 May 2018.

The appearance of the front in the measurement window could be related to the stronger winds from N–NW on 19–20 May, meaning the generation of the front was not captured. The mesoscale front reaching the surface was not observed. Figure 5C shows smaller scale horizontal buoyancy gradients near the surface. They often had the opposite sign (a decrease of buoyancy from south to north) and were probably related to the fresher water advected into the study area. The mesoscale front persisted until June (Figure 5D), despite rather weak upwelling-favorable conditions alternating with the wind from the opposite direction in the last third of May. It is supported by the geostrophic velocities that exhibit persistence of the negative (westward) flow core. All measured temperature and salinity distributions with density distributions and geostrophic velocities are found in Supplement 1.

3.4 Vertical buoyancy gradient

Horizontal variations are closely related to the vertical structure. Figures 5A, B illustrates the change in the vertical stratification in the northern and southern part of the transect, compatible with the lighter and denser side of the front, respectively. The beginning of the mission was characterized by weak haline stratification (N^2 = 0.001 – 0.002 s^{-2}). The near-surface thermal stratification started to develop on 15–16 May. The appearance of the front on 21–22 May promoted the strengthening of the stratification on the denser side of the front because of the interaction between surface heating and vertical motions associated with the mesoscale front. The stratification was significantly stronger on the denser side of the front than on the lighter side, where actually two pycnoclines were observed after the appearance of the front.

The pycnoclines weakened and strengthened daily on both sides of the front. Pycnoclines on the lighter side appeared to be forced to merge episodically, indicating the alternating of the forcing and/or processes in favor and against the persistence of the front. We suggest that the weakening of the upwelling-favorable forcing arrested the strengthening of the front. Instead of collapsing abruptly, the front hosted ageostrophic frontal processes that equalized the differences in the cross-front direction by slowing the development of the stratification on one side of the front and promoting it on the other. The uniform stratification formed by 3 June over the course of a day, coinciding with the vanishing of the mesoscale front in the study area. Compared to the denser side of the front, the stratification remained slightly weaker on the lighter side.

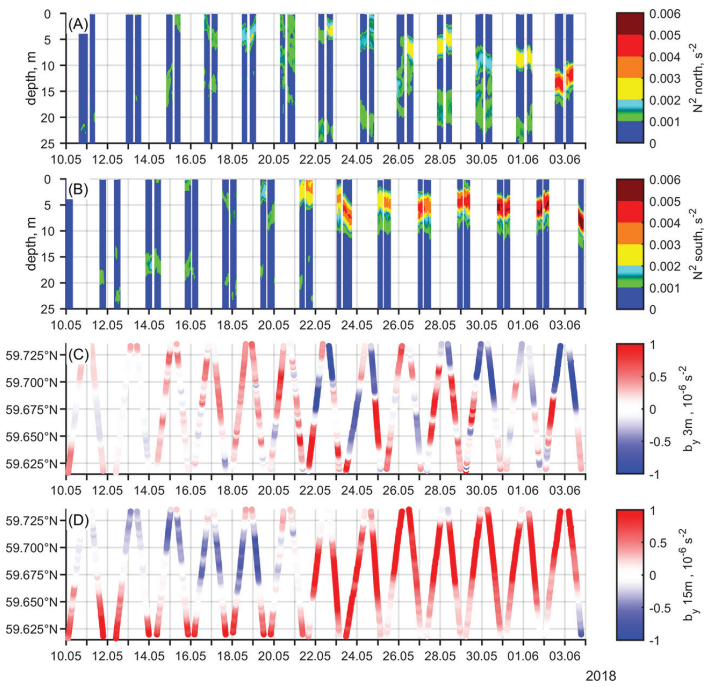


FIGURE 5
(A, B) Temporal changes in N^2 on the lighter and denser side of the mesoscale front in the upper 25 m, respectively. The lighter side is compatible with the position in the northern part of the glider transect (59.7242° N), and denser side with the position in the southern part (59.6252° N). Positions are 11 km apart. Note that one colored bar corresponds to about 1 km horizontal distance around the chosen position. To better illustrate the data, the distance correspondence in time is amplified about 5 times (bar width is increased). On average, the plotted distance was sampled in 1.4 ± 0.3 h. The movement of the glider between the southern and northern position can be deduced from subplots **(B–D)** that show along-transect horizontal buoyancy gradient as a function of time and latitude at 3, and 15 m depth, respectively. Positive gradient shows the increasing buoyancy along the sampled transect from S to N.

3.5 Observed submesoscale pattern

To demonstrate the evolving smaller scale dynamics in the background of the mesoscale front, we analyzed the smaller scale thermohaline variability during the appearance of the horizontal buoyancy gradient. Isopycnal temperature distributions contrast water mass characteristics and/or visualize local diapycnal mixing spots. Figure 4K shows an intrusion manifested as a two-way intersection at 59.675° N – a cold water patch (around 3°C) penetrates through several isopycnal layers from 4.1 to 3.7 kg m^{-3} and a warm water patch (around 8°C) penetrates from 3.3 to 3.7 kg m^{-3}. A similar pattern was observed at 59.65–59.675° N on the following day (Figure 4L), but not the day before (Figure 4J). Therefore, this structure emerged simultaneously with the appearance of the front in the measurement window.

Figures 4G–I demonstrates the smaller scale variations in the temperature by showing the deviations from the surrounding mean (4 km). Two adjacent temperature deviations with opposite signs characterizing the pattern indicated that the observed pattern consisted of two motions in opposite directions. Focusing on the described pattern, the deviations revealed extrema of 1.2°C and -1.4°C at 59.675° N on 21–22 May (Figure 4H). The extrema were larger on the following day (1.3°C and -2.1°C at 59.65–59.675° N, Figure 4I). The sign of the deviation indicated the water to originate from either shallower or deeper layers assuming that higher temperatures had their origin at the sea surface.

3.6 Submesoscale analysis

The last third of May was characterized by the persistence of the mesoscale front as well as the development of seasonal thermal stratification and the upper mixed layer, where the smaller scale horizontal buoyancy gradients formed. The diurnal cycle of net surface heat flux had a maximum of 400–500 W m^{-2} (Figure 6A). The freshwater flux was insignificant compared to it. Previously described tracer patterns, which consisted of warmer water plunging down and colder water penetrating upward, were mapped repeatedly on the background of the mesoscale front. From here on, those intrusions are referred to as a submesoscale pattern.

The structure of the submesoscale patterns suggests that they were traces of cross-front ageostrophic secondary circulation that is known to be generated while a horizontal buoyancy gradient is subject to baroclinic submesoscale, wind-driven and/or baroclinic instability. To identify whether the conditions favored the growth of different instabilities, the potential vorticity, and the equivalent heat fluxes related to restratification processes energized by surface wind forcing or the release of potential energy by baroclinic instability were calculated. Although the heat fluxes demonstrate the impact on the stratification, the elevated values also suggest the potential presence of frontal circulations.

The most pronounced submesoscale patterns captured during 21–23 May could be resulted from different physical processes. The period of the appearance of the mesoscale front in the study window

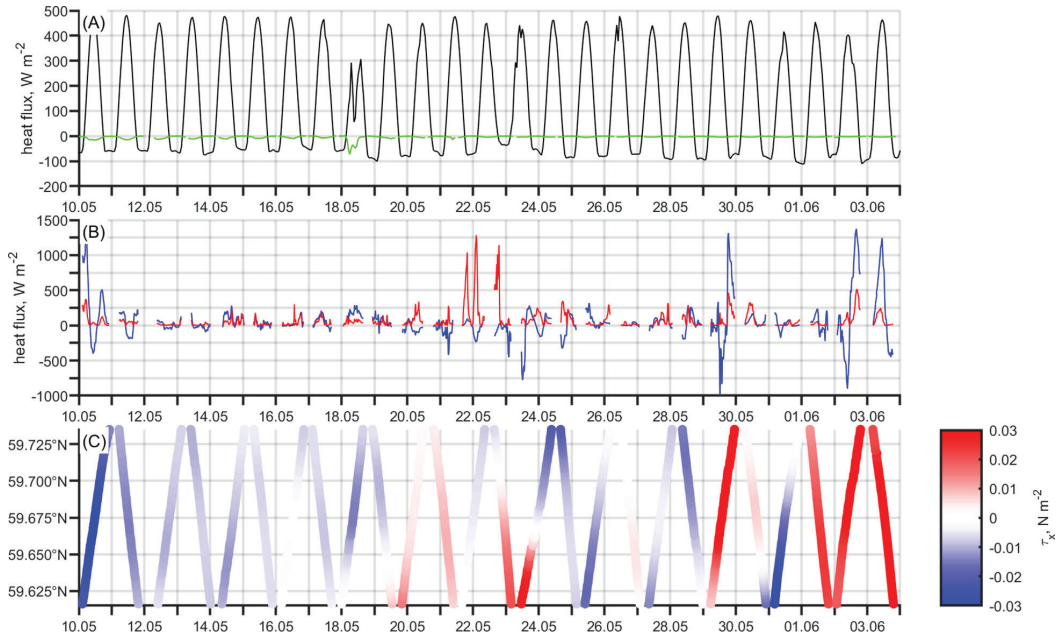


FIGURE 6
Equivalent heat fluxes associated with restratification processes during the study period in May–June 2018: **(A)** surface heat flux (black) and freshwater flux (green), **(B)** submesoscale overturning due to wind-driven processes (blue) and due to mixed layer baroclinic instability (red). **(C)** Component of wind stress perpendicular to the glider section as a function of time and latitude.

coincides with the most significant episode of the equivalent heat flux related to baroclinic instability (Figure 6B), suggesting the pattern in Figure 4H to result from the frontal circulation generated through the release of potential energy by baroclinic instability. The equivalent heat flux related to wind-induced instability episodically also had comparable magnitudes (Figure 6B). However, this estimate is more likely to be more biased than the estimates suggesting baroclinic instability events. The negative equivalent heat flux from the surface wind forcing suggests destabilization of the water column and possible generation of the overturning circulation, extracting potential vorticity from the pycnocline. The water column structure captured on 23–24 May can be found in Supplement 1.

Downfront winds make the flow susceptible to symmetric instability by reducing potential vorticity. Figure 6C shows the component of wind stress perpendicular to the sampled transect, indicating downfront (upfront) orientation if positive (negative). The unstable flow is characterized by negative potential vorticity. Figure 7A demonstrates the dominance of positive potential vorticity that is in agreement with the development of the seasonal thermocline (relatively strong stratification) near the surface, but a stronger negative signal is found in the second half of the mission. Although the variety of instabilities can develop when $q< 0$, the ϕ_{Ri_b} criteria suggested the presence of only symmetric instability (i.e., $0< Ri_b< 1$ and $-90°<\phi_{Ri_b}<\phi_c$). The balanced Richardson number, which was always positive, showed the largest potential for symmetric instability in association with the mesoscale front on 23–24 May (elevated values at 5–10 m, Figures 7B, C). However, the Obukhov length was comparable with the depth of the upper mixed layer and the boundary of the CIL, meaning the criteria $-H< z< -h$ was probably not satisfied. Although potential vorticity was reduced notably in the upper mixed layer in June, the relatively large Obukhov length suggested the convective layer depth to be similar in magnitude to the mixed layer depth, making the generation of symmetric instability still unlikely.

The analysis suggests that the conditions favored the generation of the wind-induced and baroclinic instability, supporting the assumptions for the prevalence of the submesoscale despite the limitations: 1) the calculations relied on the assumption that the glider sampled perpendicular to the horizontal buoyancy gradient; 2) neither the position of the horizontal buoyancy gradients nor the angle at which the glider sampled is known; 3) poorly resolved individual submesoscale features, while sampling at an angle, can go unnoticed due to not satisfying the conditions of the analysis. Further conclusions should be made with caution as several assumptions were made (see section 2.5).

3.7 Wavenumber spectrum

Spatial variability of isopycnal temperature was analyzed in the upper part of the water column. The weakening of spectral energy on deeper isopycnals refers to the decrease in the temperature variability

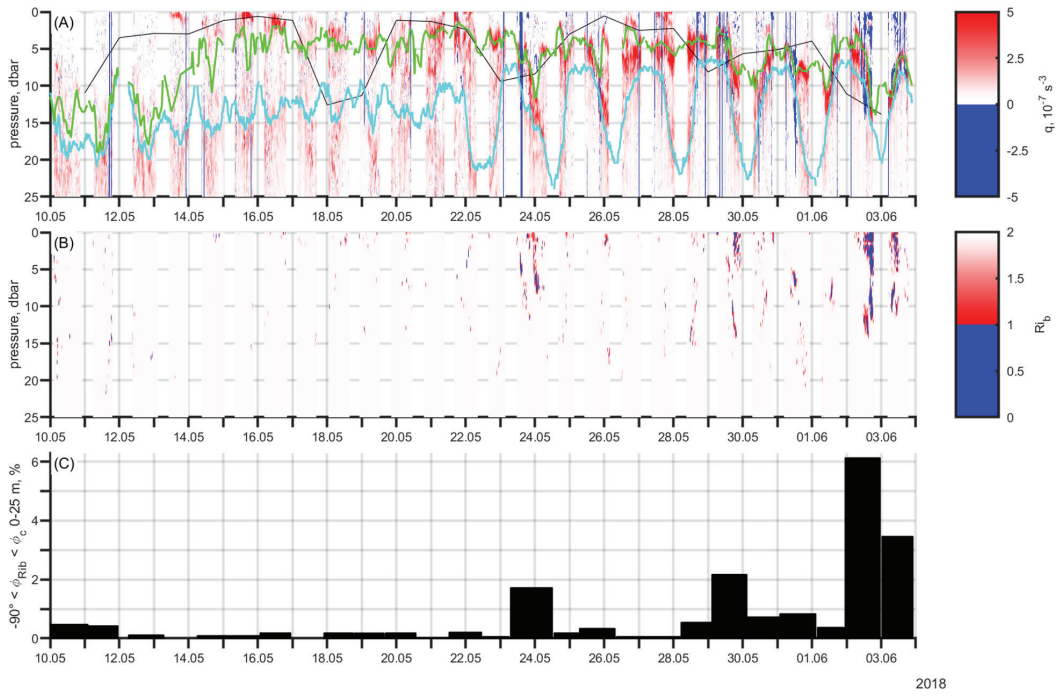


FIGURE 7
(A) Potential vorticity, q, and **(B)** balanced Richardson number, Ri_b, during the study period in May–June 2018. The Obukhov length (black), the depth of the upper mixed layer (green), and the boundary of the CIL (cyan) are shown with potential vorticity. We have emphasized respectively $q< 0$ and $0< Ri_b< 1$ in solid blue. **(C)** The percentage of balanced Richardson angle in the range of −90° to determined critical angle of -45° in the upper 25 m per sampled transect.

with depth (Figure 8). The slopes were estimated for the length scale from 1–10 km, and the individual σ-layers characterized by similar spectral slopes were averaged. The slopes for averaged spectra in the density ranges of 3.6–3.9 (3–10 m), 4.3–4.6 (10–20 m), 4.9–5.2 (15–25 m), and 5.7–6.0 (35–50 m) kg m^{-3} were -2.14, -1.72, -1.84, -1.20, respectively. The slope was the gentlest on the isopycnals positioned in the CIL (5.7–6.0 kg m^{-3}). The slope near -1 suggests the applicability of the interior-quasigeostrophic theory and the domination of large-scale motions. Upper layers exhibit clearly steeper slopes, suggesting depth-dependence. The atmospheric forcing dominates in the uppermost layers, and energetic smaller scales stir the generated variability relatively efficiently. However, the trend of shallower spectral slopes with increasing depth did not express in the layers associated with the mesoscale front. This indicates the activity of frontal processes and their contribution to the energy flux.

Constantly changing stratification affects the spectra but the extent of it is unknown. Additionally, rather short data series limit the spectral analysis. For that reason, the emphasis is more on the dynamics than the certain values of the slopes, which were near k^{-2} in the upper part of the water column though. The observations support the suggestion that the submesoscale flows emerge within the mesoscale front revealed as the enhanced tracer variability in this layer compared to the variability in the layers above or below.

4 Discussion

Modern measuring vehicles such as gliders provide *in situ* data with sufficient spatial and temporal resolution to resolve the submesoscale successfully. The shallow depths in the Baltic Sea enable sampling at high resolution – profiles separated by 150 m on

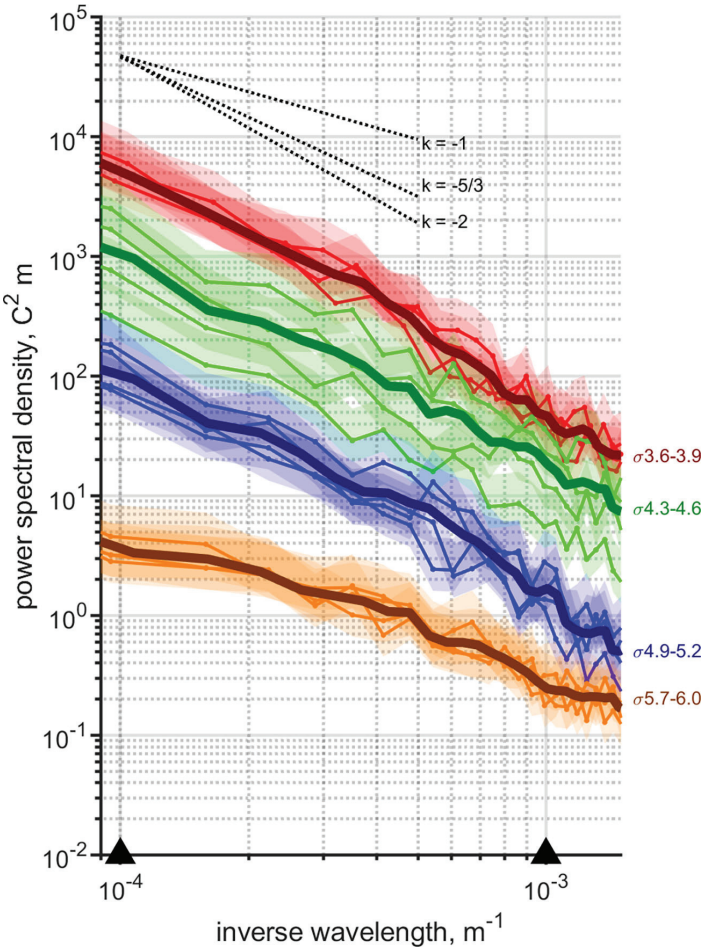


FIGURE 8
The wavenumber spectrum of isopycnal temperature of glider mission in May–June 2018. Thin lines present spectra along individual isopycnal surfaces (with a step of 0.1 kg m^{-3}) in the density ranges of 3.6–3.9 (red), 4.3–4.6 (green), 4.9–5.2 (blue), and 5.7–6.0 (orange) kg m^{-3} with the shadowing showing the 95% confidence limits. Thick lines demonstrate the averages of the individual spectra. Black dotted lines show the slopes of -1, -5/3, and -2. From left to right, the black triangles are located at wavenumbers corresponding to 10 km and 1 km.

average are sampled under 10 min in the characteristic depth of about 100 m. Therefore, spatial scales of 1–10 km around the average Rossby radius (2–4 km; Alenius et al., 2003) are well resolved. In this study, we analyzed a month-long glider mission carried out in May–June 2018 and investigated the structure of the water column during the formation of the seasonal stratification. We elucidate the appearance of the mesoscale front in the study area, show the development of the stratification on both sides of the front, and characterize the associated elevated smaller scale variability. This data set provides a unique opportunity to resolve individual submesoscale features and analyze the potential mechanisms leading to their formation. We aim to demonstrate the occurrence of active submesoscale in the Baltic Sea under certain atmospheric forcing and hydrographic conditions.

4.1 Observed variability and possible drivers

The structure of the frontal submesoscale processes has remained theoretical despite the effort that has been devoted to observing the smaller scale variations. Although recent observational studies well support the presence of the frontal instabilities in the quiescent open-ocean environment, in the Subantarctic region, as well as near boundary currents (e.g., Callies et al., 2015; du Plessis et al., 2017; Yu et al., 2019b), few provide the information on the projection of submesoscale flows in the measurements (Pietri et al., 2013; de Verneil et al., 2019; Pérez et al., 2022). For instance, de Verneil et al. (2019) have demonstrated the orientation of fine-scale phytoplankton patches to be consistent with an ageostrophic secondary circulation generated by frontogenesis, providing, thus, the evidence on submesoscale flows modifying the vertical dynamics of phytoplankton.

According to the dynamical characterization, the coastal sea provides favorable conditions for the submesoscale processes. The transition to the open sea favors the colliding of water masses whether through the meeting of different flow structures or coastal processes like upwelling events, promoting, therefore, the formation of larger and smaller scale horizontal buoyancy gradients. By observing the coastal-offshore area at the end of spring 2018, we captured the appearance of the mesoscale front. The horizontal buoyancy gradient formed due to the wind-induced upwelling forced by the prevailing NE–E winds during the first ten days of the survey.

Simultaneously with the appearance of the mesoscale front, a pronounced submesoscale pattern emerged. The pattern showed upwelling of cold water on the lighter side of the front accompanied by downwelling of warm water on the denser side. The temperatures indicated the origin of the water from deeper or shallower layers, respectively, and, thus, suggested the presence of two adjacent movements in different directions. We suggest the presence of ageostrophic secondary circulation with a width of a couple of km on the profile of the mesoscale front between 5–10 m (Figure 3B). To support this suggestion, we attempt to infer the driving mechanisms that could explain the observed submesoscale activity.

A secondary circulation emerges in the form of an overturning cell as the front is subject to baroclinic, wind-induced, and/or baroclinic submesoscale instability. The submesoscale analysis revealed the large potential role of baroclinic instability on 21–22 May, suggesting that the observed submesoscale features resulted from the secondary circulations generated through the release of potential energy stored in the horizontal buoyancy gradient. The baroclinic instability can act together with surface frontogenesis (Lapeyre et al., 2006) but the surface signature was not observed in the study window. Additionally, the position of the captured feature on top of the mesoscale front is not compatible with frontogenetic secondary circulation that tends to subduct water below the front (Spall, 1995). Baroclinic instability occurs over a period of days (Boccaletti et al., 2007), indicating the possible interaction with the wind-induced instability. The analysis showed the effect of downfront winds that would counteract the restratification on the following days. On 22–23 May, the slope of the isopycnals was relaxed, and a few m deep upper mixed layer had formed (Figure 4F). Destabilizing atmospheric forcing can also favor symmetric instability. However, this is unlikely because the upper mixed layer needs to be deeper than the convective layer for overturning motions to dominate over convective mixing induced by surface forcing (Thomas et al., 2013).

The evolution of smaller scale variability in the background of the mesoscale front suggests the presence of several dynamical processes. Similar tracer patterns with various extent and intensity were mapped repeatedly until the end of the month, but the limitations of the glider observations complicate the interpretations. Fronts are a dynamical phenomenon and the 2D nature of the glider measurements prevents following the evolution of the front. In addition, observational biases should be considered when inferring the dynamical mechanism because of the adoptions for the glider data assuming the sampling perpendicular to the horizontal buoyancy gradient (Thompson et al., 2016). Further, the captured features are subject to soothing due to the effect of time-space aliasing.

4.2 Impact of wind

Horizontal variations are related to atmospheric forcing and to stirring by larger-scale flow fields. In the Baltic Sea, inclined pycnoclines and coastal upwelling events that appear as a response to winds are frequent (Lehmann et al., 2012; Liblik and Lips, 2017). The Gulf of Finland, a sub-basin of the Baltic Sea, is elongated in the W–E direction. The moderate winds blowing along the gulf are common (Keevallik and Soomere, 2014). The NE–E winds favor upwelling events near the southern coast of the gulf. A corresponding development of hydrographic fields was captured as a mesoscale front in the glider measurement window in May 2018. Although E and W winds alternated after 19 May, the mesoscale front persisted until early June.

The wind has a role in allowing the submesoscale flows to arise due to the disturbance of the balance when the external forces reduce and/or change. We have indicated that on 21–22 May, baroclinic instability appeared to develop during the temporary decrease in wind stress. Interpreting the orientation of the wind with respect to the geostrophic shear is challenging, but a rough estimate would be that the front was oriented approximately in the

W–E direction at the sampling site. The sampled section positioned approximately along the S–N axis and the inclination in the density distribution that could be manifested as a front was observable. In accordance with this assumption, the wind changing from E to W direction indicates that mostly the wind had the component either up- or downfront. Thus, this variability of the wind would cause the alignment between the front and the wind direction to be lost or gained episodically (Mahadevan et al., 2010).

4.3 Impact on the stratification

The horizontal buoyancy gradients affect the stratification directly through the submesoscale processes. While the stratification is generated and destroyed through diabatic processes and frictional forces, frontal submesoscale can convert gradients from horizontal to vertical (McWilliams, 2016). Lateral variability introduced by the advection of water masses favors the appearance of horizontal buoyancy gradients and, in turn, suggests the emergence of the submesoscale. The glider observations revealed the complex structure of the water column. Atmospheric forcing acting on the sea surface contributed to the formation of the upper mixed layer and seasonal thermal stratification. The appearance of the mesoscale front created favorable conditions for the stratification to strengthen more rapidly in the southern part of the sampled transect as the mesoscale dynamics raised the isopycnals near the surface. We observed the stratification changing daily and developing differently on the denser and lighter side of the front (compatible with the southern and the northern part of sampled transect, respectively; Figures 5A, B). While the denser side was characterized by the strong stratification near the surface, two pycnoclines were observed on the lighter side.

We propose that the mesoscale front hosted ageostrophic frontal processes as the upwelling-favorable forcing weakened. The submesoscale circulations equalized the differences in the cross-front direction by slowing the development of the stratification on one side of the front and promoting it on the other. The overturning circulation induced by baroclinic instability slides dense water under light, acting to slump the front from the horizontal to vertical (Boccaletti et al., 2007). Thus, the baroclinic instability acted toward restratification on 21–22 May. The wind increased on the following days, suggesting the possible interaction with wind-induced instability. The overturning circulations acting toward restratification appeared to be dominating but the temporary return of the NE–E winds supported the persistence of the front. Two pycnoclines were observed on the lighter side of the front again on 27 May. However, the front appeared to shift toward the open sea (northern part), suggesting that partly the frontal circulations managed to restratify the water column. The presence of the submesoscale flows within the horizontal buoyancy gradient could have contributed to the development of the seasonal stratification. The effect of the submesoscale can be especially important during seasonal warming because stratification events can occur more rapidly than solely surface heating could drive (du Plessis et al., 2019). Enhanced stratification favors primary production (Swart et al., 2015).

4.4 Spectral analysis

While measuring submesoscale flow fields is challenging, the underlying dynamics can be deduced by investigating the variability of tracer fields along the same density surfaces (Callies and Ferrari, 2013; Jaeger et al., 2020). Submesoscale flows can cause substantial heterogeneity in tracer distribution because of their dynamics, which by its nature should connect fully two- and three-dimensional motions (McWilliams, 2016). Submesoscale processes have gained more attention in the Baltic Sea only in recent years, though (Lips et al., 2016; Carpenter et al., 2020). Lips et al. (2016) have presented the spectrum of an active tracer in the sub-surface layers (note that the tracer variance along the isobaric surfaces was evaluated). The spectra showed slopes closing to -2 at 1–10 km during periods of high variability of temperature due to upwellings. The discrepancy from -3 that is predicted by quasigeostrophic theory (Charney, 1971) was interpreted as the contribution of the ageostrophic submesoscale processes to the energy cascade.

The studies from the ocean environment are well presented (e.g., Cole and Rudnick, 2012; Callies and Ferrari, 2013; Kunze et al., 2015; Jaeger et al., 2020). However, the processes setting the spectra have remained obscure. In the open ocean, the -2 slope independent of depth has been reported at the submesoscale range (Cole and Rudnick, 2012; Callies and Ferrari, 2013). The main contribution to the energy at the submesoscale comes possibly from unbalanced flows. The characteristics of the Baltic Sea (e.g., the shallow depth, strong stratification, seasonality, negligible tidal forcing) distinguish the sea from the ocean, forming a dynamically complex environment (Tuomi et al., 2012). There are some studies carried out in the stratified environment. Kunze et al. (2015) found tracer variance spectra sloping with a k^{-2} at the horizontal length scale 0.03–10 km in the seasonal pycnocline at 20–60 m depth. Evident fronts were not observed at every study site, though. On the other hand, Jaeger et al. (2020) showed steep slopes (k^{-3}) at 1–10 km in the stratified upper 75 m. Above 10 km scales the spectral slope was closer to -2. They proposed that ageostrophic dynamics could cascade variance in the pycnocline more rapidly than predicted. We, however, found gentler spectral fall-off in the layers associated with the mesoscale front compared to the layers above. This indicates that frontal submesoscale preserves tracer variability longer than the turbulence in the upper layers. The short data series acts as both an advantage and a disadvantage in this study while allowing us to analyze one specific situation but prevents broader conclusions. We will test this suggestion in a future study by incorporating a wide range of glider data sets from different seasons.

Observational spectra are independent of predictions and, thus, extensive data collections contribute to shaping understanding of the energy cascade. The observations have revealed the discrepancies from the quasigeostrophy, but often the limitations prevent identifying the reasons. We conclude that the contribution of the ageostrophic frontal effects is likely in the upper part of the water column (0–25 m in the Baltic Sea). The depth-dependence may be related to the stratified environment as it was noticed here and by Jaeger et al. (2020). Flatter spectral slopes in the deeper part of the water column coincide with stirring by two-dimensional homogeneous turbulence that leads to a tracer spectrum following k^{-1} (Callies and Ferrari, 2013).

5 Conclusions

Mostly the presence of submesoscale phenomena in the Baltic Sea has been demonstrated using numerical modeling (e.g., Väli et al., 2017), and observational studies are scarce. This is the first study analyzing individual submesoscale features in a coastal-offshore transect of the Baltic Sea. The glider measurements gathered at the end of spring 2018 revealed smaller scale features within the mesoscale front. Submesoscale tracer patterns, characterized by two adjacent motions showing the upwelling on the lighter and downwelling on the denser side of the front, were captured. We proposed they were traces of the frontal submesoscale circulations, as the analysis suggested favorable conditions for the baroclinic and wind-induced instability. The frontal submesoscale acted against the persistence of the front. The constant presence of submesoscale variability in the background of the front indicates active submesoscale flows in the Baltic Sea. In addition, the role of the submesoscale processes appeared to increase under reduced wind stress. This result emphasizes the need for further studies, as the classical expectation is that strong vertical mixing occurs through turbulence when wind speeds are high.

6 Appendix

Minimizing instrumental error is important when the analysis focuses on the small-scale variability. Gliders are known to provide high spatial resolution in the vertical but only in one horizontal direction. Small errors in profile-to-profile measurements modify the data artificially. In this study, all applied corrections rely exclusively on the glider data and assume that compared consecutive profiles correspond to the same water mass. Consecutive profiles refer to the profiles that are the closest to each other in space (the parts of profiles with a "∧" or "∨" shape, Figure 9E) because the largest errors associate with the strong gradients. The Baltic Sea is strongly stratified – the upper (lower) pycnocline coincides with the thermocline (halocline).

First, temperature and conductivity sensors are subject to response time. While transiting through strong vertical

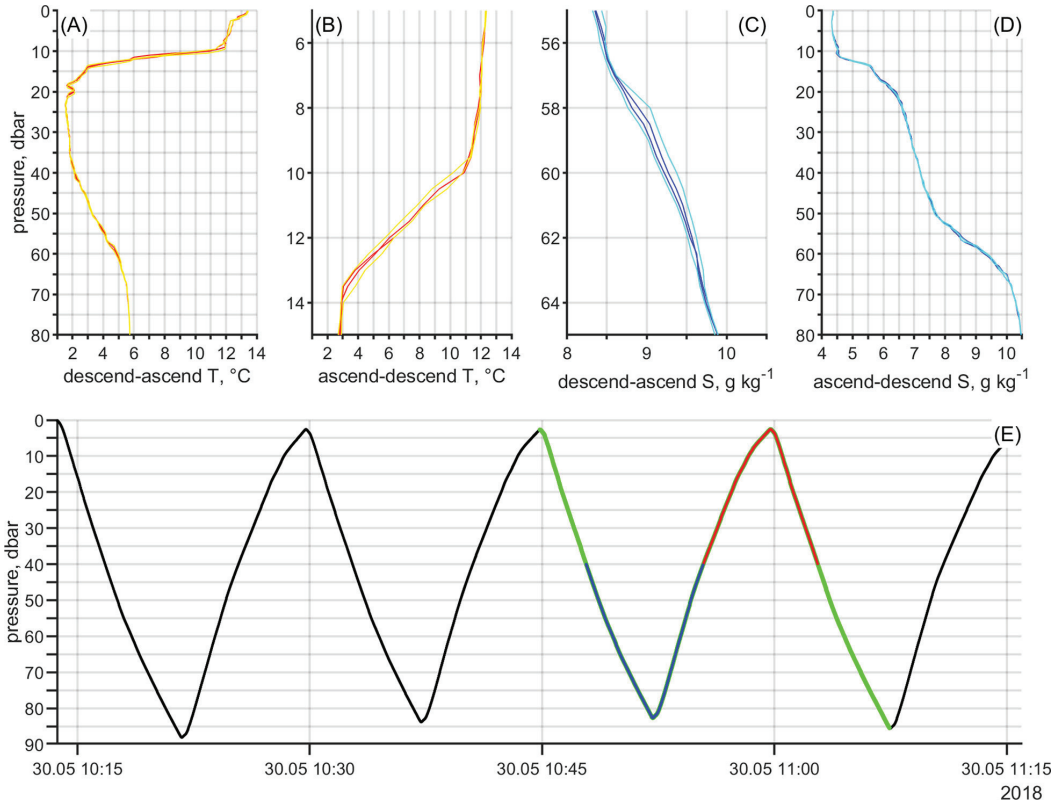


FIGURE 9
(A, B) Examples of raw (yellow) and corrected (response time, red) temperature profiles respectively over the water column and the thermocline depth range in case of descend-ascend (highlighted with blue in **E**) and ascend-descend (highlighted with red in **E**). **(C, D)** Examples of raw (cyan) and corrected (thermal lag, blue) salinity profiles respectively over the halocline depth range and the water column in case of descend-ascend and ascend-descend. **(E)** An example of a cycle shown as a time series of pressure. Green highlights the consecutive profiles. Overlaid blue shows the parts of profiles with a "∨" shape, and red a "∧" shape.

gradients, the water properties can change quicker than the sensor is capable of registering, resulting in the misalignment of the measurement with pressure. The lag is in opposite direction for a descend and an ascend because of the transition direction, for example first from warmer to colder (fresher to saltier) water and then reversely. Next, the conductivity cell's capacity of storing heat causes small errors in inferred salinity. The effect is referred to as thermal lag. Measured temperature corresponds to the ambient temperature of the conductivity cell, but conductivity is measured inside the cell. To obtain accurate salinity estimate, measured temperature is reassessed. The temperature inside the conductivity cell is evaluated by subtracting the correction, T_{tl}, from the temperature readings, T. The correction is found using the relation:

$$T_{tl}(n) = -bT_{tl}(n-1) + a[T(n) - T(n-1)]$$

Coefficients a and b are determined by

$$a = \frac{4f_n\alpha_{tl}\tau_{tl}}{1 + 4f_n\tau_{tl}}$$

$$b = 1 - \frac{2a}{\alpha_{tl}}$$

where f_n is the sampling frequency, α_{tl} amplitude of the temperature error, and τ_{tl} relaxation time constant (Mensah et al., 2009).

A linear time shift was applied to temperature and conductivity according to the estimated data misalignment with pressure. A similar method with varying shifts has been presented by Bishop (2008), and Garau et al. (2010) have shown the concept of minimizing the area between two profiles. The time shifts were varied from 0 s to 3 s by 0.1 s steps. The mean area (trapezoidal method) were calculated between two consecutive profiles at the depth range of 20 m around the depth of the strongest gradient. The median of the area was found for each time shift and the optimal time shift was chosen based on the lowest one under the assumption of lowest discrepancy between profiles. In this study, the temperature was re-aligned by 1.4 s and conductivity by 1.1 s (Figures 10A, B).

We show the quality of the correction based on temperature. Figures 9A, B shows the examples of corrected temperature profile. Full profile is shown for the case descend-ascend (shape "∨"), and the depth range of the upper pycnocline for the case ascend-descend (shape

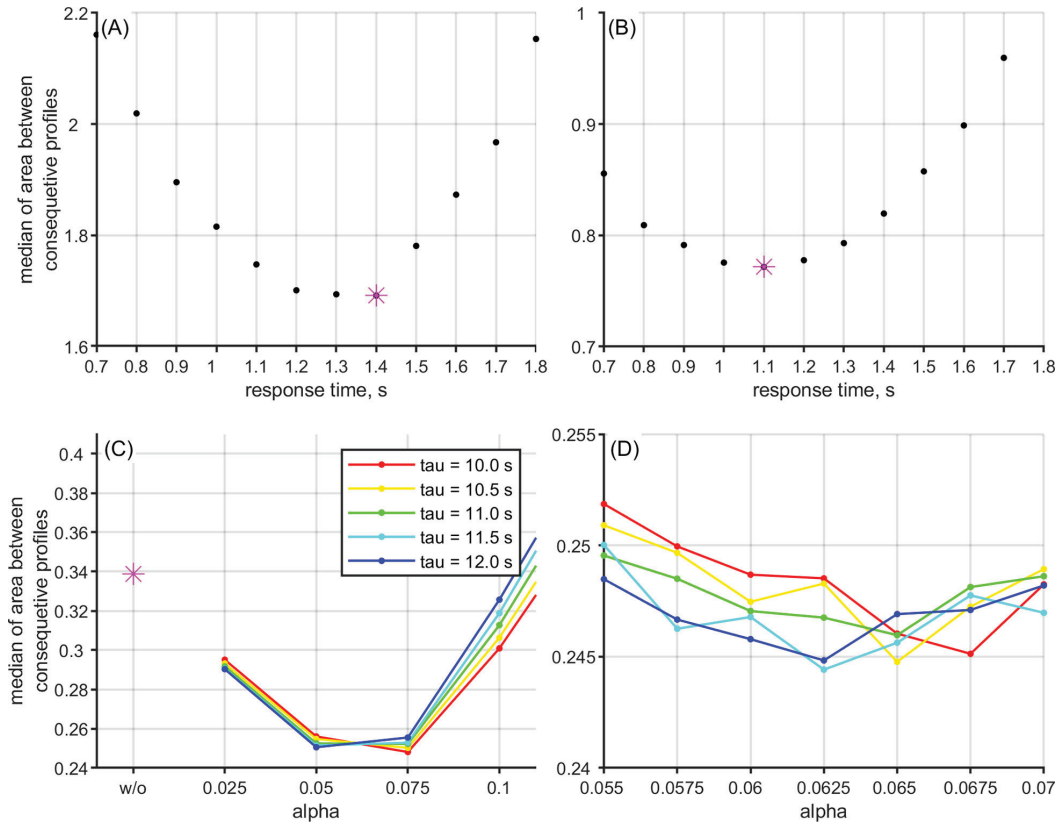


FIGURE 10
(A, B) The change in the median of the mean area between profiles as response time correction was applied respectively for temperature and conductivity. The optimal time shift is shown with magenta star. **(C, D)** The change in the median of the mean area between profiles as thermal lag correction was applied with respect to the one calculated based on the raw data (magenta). The median value decreases at first as α_{tl} increases. Colored lines correspond to τ_{tl} values from 10 to 12 s with 0.5 s step. The optimal combination of α_{tl} and τ_{tl} were chosen near minimal median value **(D)**.

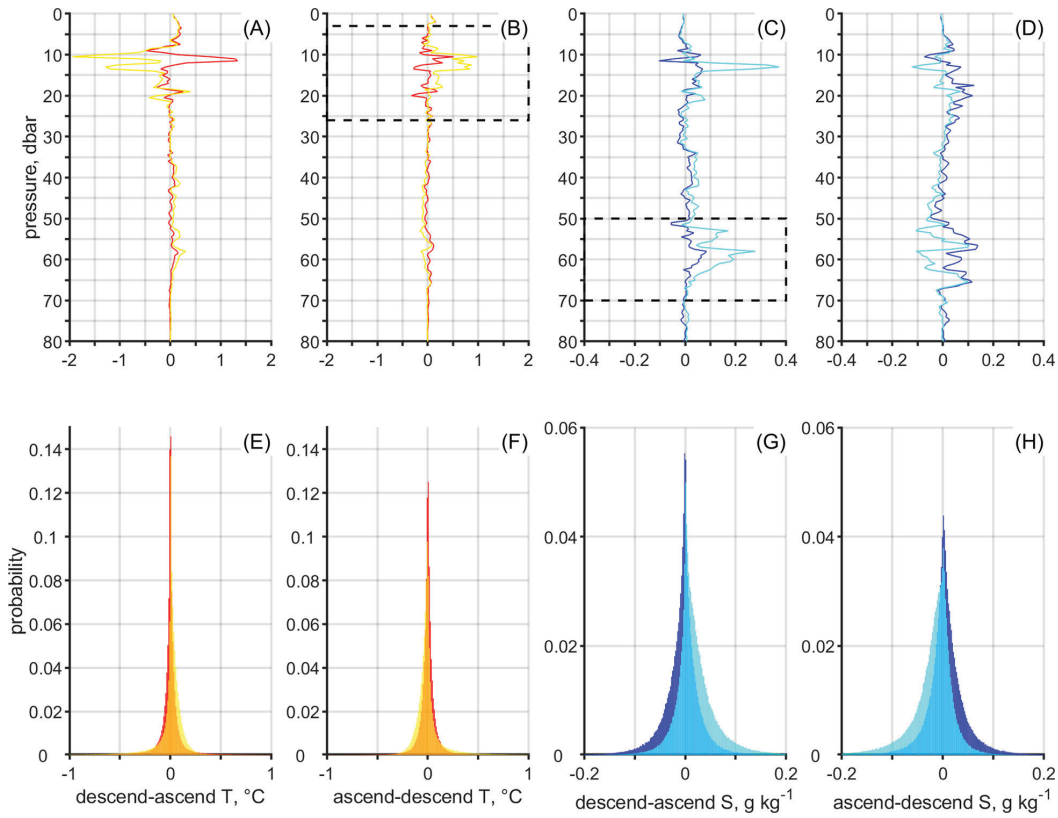


FIGURE 11
(A–D) The discrepancy respectively between two consecutive temperature and salinity profiles as shown in Figures 9A–D). The dashed line in the upper part of the water column highlights the thermocline range **(B)** and in the lower part the halocline range **(C)**. **(E–H)** The histogram of discrepancies respectively for all the compared temperature (raw in yellow and corrected in red) and salinity (raw in cyan and corrected in blue) profiles in case of descend-ascend and ascend-descend.

"∧") to better demonstrate the agreement between the corrected profiles. Figures 11A, B shows the discrepancy between two consecutive profiles shown in Figures 9A, B. The profiles show better agreement in case of ascend-descend because the data in the thermocline range is measured with little time separation. Figures 11E, F shows the histogram of discrepancies for all the compared profiles. The skew present in the discrepancies between raw profiles is removed after shifting despite comparing descend with ascend or the opposite.

To compensate for the thermal lag of the CTD, combinations of α_{tl} (from 0.025 to 0.1 by 0.025) and τ_{tl} (from 9 to 14 s by 0.5 s) were applied to the temperature data to derive salinity. The optimal coefficients were chosen by comparing temperature-salinity diagrams similarly as was done for response time. The median value of the mean area was expected to be smaller than the ones calculated based on the raw data (Figures 10C, D). In this study, the satisfying result was obtained in the case of $\alpha_{tl} = 0.0625$ and $\tau_{tl} = 11.5s$. Figures 9C, D shows examples of corrected salinity profile. Note that now the zoomed plot is the case descend–ascend. Figures 11C, D shows the discrepancy between two consecutive profiles shown in Figures 9C, D. The profiles show better agreement in case of descend-ascend because the data in the halocline range is measured with little time separation. Figures 11G, H shows the histogram of discrepancies for all the compared profiles. The discrepancies between profiles were improved after calculating salinity with reassessed temperature.

Data availability statement

The datasets presented in this study can be found in online repositories. The names of the repository/repositories and accession number(s) can be found below: https://doi.org/10.17882/84802 SEANOE.

Author contributions

KS was responsible for processing and analyzing the glider data and writing the paper. UL contributed to the analysis setup and writing the paper. TL contributed to writing the paper. All authors participated in designing the survey and piloting the glider. All authors contributed to the article and approved the submitted version.

Funding

This work was supported by the Estonian Research Council grant (PRG602) and institutional research funding (IUT-19-6) of the Estonian Ministry of Education and Research.

Acknowledgments

We would like to thank our colleagues and the crew of RV Salme for their assistance during the deployment and recovery of the glider.

Conflict of interest

The authors declare that the research was conducted in the absence of any commercial or financial relationships that could be construed as a potential conflict of interest.

Publisher's note

All claims expressed in this article are solely those of the authors and do not necessarily represent those of their affiliated organizations, or those of the publisher, the editors and the reviewers. Any product that may be evaluated in this article, or claim that may be made by its manufacturer, is not guaranteed or endorsed by the publisher.

Supplementary material

The Supplementary Material for this article can be found online at: https://www.frontiersin.org/articles/10.3389/fmars.2023.984246/full#supplementary-material

References

Alenius, P., Myrberg, K., and Nekrasov, A. (1998). The physical oceanography of the gulf of Finland: a review. *Boreal Environ. Res.* 3, 97–125.

Alenius, P., Nekrasov, A., and Myrberg, K. (2003). Variability of the baroclinic rossby radius in the gulf of Finland. *Continent. Shelf Res.* 23 (6), 563–573. doi: 10.1016/S0278-4343(03)00004-9

Bishop, C. M. (2008). *Sensor dynamics of autonomous underwater gliders (master's thesis)* (Canada: Memorial University of Newfoundland). Available at: http://research.library.mun.ca/id/eprint/9330. Retrieved from Memorial University Research Repository.

Boccaletti, G., Ferrari, R., and Fox-Kemper, B. (2007). Mixed layer instabilities and restratification. *J. Phys. Oceanogr.* 37 (9), 2228–2250. doi: 10.1175/JPO3101.1

Buckingham, C. E., Lucas, N. S., Belcher, S. E., Rippeth, T. P., Grant, A. L. M., Lesommer, J., et al. (2019). The contribution of surface and submesoscale processes to turbulence in the open ocean surface boundary layer. 11 (12), 4066–4094. doi: 10.1029/2019MS001801

Callies, J., and Ferrari, R. (2013). Interpreting energy and tracer spectra of upper-ocean turbulence in the submesoscale range (1–200 km). *J. Phys. Oceanogr.* 43 (11), 2456–2474. doi: 10.1175/JPO-D-13-063.1

Callies, J., Ferrari, R., Klymak, J. M., and Gula, J. (2015). Seasonality in submesoscale turbulence. *Nat. Commun.* 6, 6862. doi: 10.1038/ncomms7862

Carpenter, J. R., Rodrigues, A., Schultze, L. K. P., Merckelbach, L., Suzuki, N., Baschek, B., et al. (2020). Shear instability and turbulence within a submesoscale front following a storm. *Geophys. Res. Lett.* 47 (23), e2020GL090365. doi: 10.1029/2020GL090365

Charney, J. G. (1971). Geostrophic turbulence. *J. Atmos. Sci.* 28 (6), 1087–1095. doi: 10.1175/1520-0469(1971)028<1087:GT>2.0.CO;2

Cole, S., and Rudnick, D. L. (2012). The spatial distribution and annual cycle of upper ocean thermohaline structure. *J. Geophys. Res. Atmos.* 117 (C2), C02027. doi: 10.1029/2011JC007033

de Verneil, A., Franks, P. J. S., and Ohman, M. D. (2019). Frontogenesis and the creation of fine-scale vertical phytoplankton structure. *J. Geophys. Res.: Oceans* 124, 1509–1523. doi: 10.1029/2018JC014645

du Plessis, M., Swart, S., Ansorge, I. J., and Mahadevan, A. (2017). Submesoscale processes accelerate seasonal restratification in the subantarctic ocean. *J. Geophys. Res.: Oceans* 122 (4), 2960–2975. doi: 10.1002/2016JC012494

du Plessis, M., Swart, S., Ansorge, I. J., Mahadevan, A., and Thompson, A. F. (2019). Southern ocean seasonal restratification delayed by submesoscale wind–front interactions. *J. Phys. Oceanogr.* 49 (4), 1035–1053. doi: 10.1175/JPO-D-18-0136.1

Ferrari, R., and Boccaletti, G. (2004). Eddy-mixed layer interactions in the ocean. *Oceanography* 17 (3), 12–21. doi: 10.5670/oceanog.2004.26

Fox-Kemper, B., Ferrari, R., and Hallberg, R. (2008). Parameterization of mixed layer eddies. part I: Theory and diagnosis. *J. Phys. Oceanogr.* 38, 1145–1165. doi: 10.1175/2007JPO3792.1

Garau, B., Ruiz, S., Zhang, W. G., Pascual, A., Heslop, E., Kerfoot, J., et al. (2010). Thermal lag correction on Slocum CTD glider data. *J. Atmos. Ocean. Technol.* 28 (9), 1065–1071. doi: 10.1175/JTECH-D-10-05030.1

Garcia-Jove, M., Mourre, B., Zarokanellos, N. D., Lermusiaux, P. F. J., Rudnick, D. L., and Tintoré, J. (2022). Frontal dynamics in the alboran Sea: 2. processes for vertical velocities development. *J. Geophys. Res.: Oceans* 127, e2021JC017428. doi: 10.1029/2021JC017428

Giddy, I., Swart, S., du Plessis, M., Thompson, A. F., and Nicholson, S.-A. (2021). Stirring of sea-ice meltwater enhances submesoscale fronts in the southern ocean. *J. Geophys. Res.: Oceans* 126, e2020JC016814. doi: 10.1029/2020JC016814

Hersbach, H., Bell, B., Berrisford, P., Biavati, G., Horányi, A., Muñoz Sabater, J., et al. (2022)ERA5 hourly data on single levels from 1979 to present. Copernicus climate change service (C3S) climate data store (CDS) (Accessed JAN-2022).

Hersbach, H., Bell, B., Berrisford, P., Hirahara, S., Horányi, A., Muñoz-Sabater, J., et al. (2020). The ERA5 global reanalysis. *Q. J. R. Meteorol. Soc.* 146, 1999–2049. doi: 10.1002/qj.3803

Hoskins, B. J. (1974). The role of potential vorticity in symmetric stability and instability. *Q. J. R. Meteorol. Soc.* 100, 480–482. doi: 10.1002/qj.49710042520

IOC, SCOR and IAPSO. (2010). The international thermodynamic equation of seawater – 2010: Calculation and use of thermodynamic properties. Intergovernmental Oceanographic Commission, Manuals and Guides No. 56, Paris: UNESCO (English), 196 pp. Available at: https://www.teos-10.org/pubs/TEOS-10_Manual.pdf.

Jaeger, G. S., MacKinnon, J. A., Lucas, A. J., Shroyer, E., Nash, J., Tandon, A., et al. (2020). How spice is stirred in the bay of Bengal. *J. Phys. Oceanogr.* 50 (9), 2669–2688. doi: 10.1175/JPO-D-19-0077.1

Karimova, S., and Gade, M. (2016). Improved statistics of sub-mesoscale eddies in the Baltic Sea retrieved from SAR imagery. *Int. J. Remote Sens.* 37 (10), 2394–2414. doi: 10.1080/01431161.2016.1145367

Karstensen, J., Liblik, T., Fischer, J., Bumke, K., and Krahmann, G. (2014). Summer upwelling at the boknis eck time-series station, (1982 to 2012) – a combined glider and wind data analysis. *Biogeosciences* 11, 3603–3617. doi: 10.5194/bg-11-3603-2014

Keevallik, S., and Soomere, T. (2014). Regime shifts in the surface-level average air flow over the gulf of Finland during 1981-2010. *Proc. Estonian Acad. Sci.* 63 (4), 428–437. doi: 10.3176/proc.2014.4.08

Kikas, V., and Lips, U. (2016). Upwelling characteristics in the gulf of Finland (Baltic Sea) as revealed by ferrybox measurements in 2007–2013. *Ocean Sci.* 12 (6), 2863–2898. doi: 10.5194/osd-12-2863-2015

Kunze, E., Klymak, J. M., Lien, R.-C., Ferrari, R., Lee, C. M., Sundermeyer, M. A., et al. (2015). Submesoscale Water-Mass Spectra in the Sargasso Sea *J. Phys. Oceanogr.* 45 (5), 1325–1338. doi: 10.1175/JPO-D-14-0108.1

Lapeyre, G., Klein, P., and Hua, B. L. (2006). Oceanic restratification forced by surface frontogenesis. *J. Phys. Oceanogr.* 36 (8), 1577–1590. doi: 10.1175/JPO2923.1

Large, W. G., and Pond, S. (1981). Open ocean momentum flux measurements in moderate to strong winds. *J. Phys. Oceanogr.* 11 (3), 324–336. doi: 10.1175/1520-0485(1981)011<0324:OOMFMI>2.0.CO;2

Lehmann, A., Myrberg, K., and Höflich, K. (2012). A statistical approach to coastal upwelling based on the analysis of satellite data for 1990–2009. *Oceanologia* 54 (3), 369–393. doi: 10.5697/oc.54-3.369

Liblik, T., and Lips, U. (2017). Variability of pycnoclines in a three-layer, large estuary: the gulf of Finland. *Boreal Environ. Res.* 22, 27–47.

Liblik, T., Väli, G., Salm, K., Laanemets, J., Lilover, M.-J., and Lips, U. (2022). Quasi-steady circulation regimes in the Baltic Sea. *Ocean Sci.* 18(3), 857–879. doi: 10.5194/os-18-857-2022

Lips, U., Kikas, V., Liblik, T., and Lips, I. (2016). Multi-sensor *in situ* observations to resolve the sub-mesoscale features in the stratified gulf of Finland, Baltic Sea. *Ocean Sci.* 12 (3), 715–732. doi: 10.5194/os-12-715-2016

Lips, I., and Lips, U. (2017). The importance of mesodinium rubrum at post-spring bloom nutrient and phytoplankton dynamics in the vertically stratified Baltic Sea. *Front. Mar. Sci.* 4. doi: 10.3389/fmars.2017.00407

Lips, I., Rünk, N., Kikas, V., Meerits, A., and Lips, U. (2014). High-resolution dynamics of spring bloom in the gulf of Finland, Baltic Sea. *J. Mar. Syst.* 129, 135–149. doi: 10.1016/j.jmarsys.2013.06.002

Mahadevan, A., Tandon, A., and Ferrari, R. (2010). Rapid changes in mixed layer stratification driven by submesoscale instabilities and winds. *J. Geophys. Res. Atmos.* 115 (C3), C03017. doi: 10.1029/2008JC005203

McDougall, T., and Barker, P. M. (2011). Getting started with TEOS-10 and the Gibbs Seawater (GSW) Oceanographic Toolbox, 28pp., SCOR/IAPSO WG127, ISBN 978-0-646-55621-5." Available at: https://www.teos-10.org/software.htm.

McWilliams, J. C. (2016). "Submesoscale currents in the ocean," in . *Proc. R. Soc. A.*, Vol. 472(2189):20160117. doi: 10.1098/rspa.2016.0117

Mensah, V., Menn, M. L., and Morel, Y. (2009). Thermal mass correction for the evaluation of salinity. *J. Atmos. Ocean. Technol.* 26 (3), 665–672. doi: 10.1175/2008JTECHO612.1

Meyer, D., Lips, U., Prien, R. D., Naumann, M., Liblik, T., Schuffenhauer, I., et al. (2018). Quantification of dissolved oxygen dynamics in a semi-enclosed sea - a comparison of observational platforms. *Continent. Shelf Res.* 169, 34–45. doi: 10.1016/j.csr.2018.09.011

Myrberg, K., and Andrejev, O. (2003). Main upwelling regions in the Baltic Sea – a statistical analysis based on three-dimensional modeling. *Boreal Environ. Res.* 8, 97–112.

Pavelson, J., Laanemets, J., Kononen, K., and Nõmman, S. (1997). Quasipermanent density front at the entrance to the gulf of Finland: Response to wind forcing. *Continent. Shelf Res.* 17, 253–265. doi: 10.1016/S0278-4343(96)00028-3

Pérez, J. G. C., Pallàs-Sanz, E., Tenreiro, M., Meunier, T., Jouanno, J., and Ruiz-Angulo, A. (2022). Overturning instabilities across a warm core ring from glider observations. *J. Geophys. Res.: Oceans* 127, e2021JC017527. doi: 10.1029/2021JC017527

Pietri, A., Testor, P., Echevin, V., Chaigneau, A., Mortier, L., Eldin, G., et al. (2013). Finescale vertical structure of the upwelling system off southern Peru as observed from glider data. *J. Phys. Oceanogr.* 43 (3), 631–646. doi: 10.1175/JPO-D-12-035.1

Rubio, A., Bosch, D. G., Jordà, G., and Infantes, M. E. (2009). Estimating geostrophic and total velocities from CTD and ADCP data: intercomparison of different methods. *J. Mar. Syst.* 77 (1), 61–76. doi: 10.1016/j.jmarsys.2008.11.009

Rudnick, D. L., and Cole, S. (2011). On sampling the ocean using underwater gliders. *J. Geophys. Res.* 116 (C8), C08010. doi: 10.1029/2010JC006849

Spall, M. A. (1995). Frontogenesis, subduction, and cross-front exchange at upper ocean fronts. *J. Geophys. Res.* 100 (C2), 2543–2557. doi: 10.1029/94JC02860

Swart, S., Thomalla, S. J., and Monteiro, P. M. S. (2015). The seasonal cycle of mixed layer dynamics and phytoplankton biomass in the Sub-Antarctic zone: A high-resolution glider experiment. *J. Mar. Syst.* 147 (15), 103–115. doi: 10.1016/j.jmarsys.2014.06.002

Taylor, J., and Ferrari, R. (2009). On the equilibration of a symmetrically unstable front *via* a secondary shear instability. *J. Fluid Mech.* 622, 103–113. doi: 10.1017/S0022112008005272

Taylor, J. R., and Ferrari, R. (2010). Buoyancy and wind-driven convection at mixed layer density fronts. *J. Phys. Oceanogr.* 40 (6), 1222–1242. doi: 10.1175/2010JPO4365.1

Thomas, L. N. (2005). Destruction of potential vorticity by winds. *J. Phys. Oceanogr.* 35 (12), 2457–2466. doi: 10.1175/JPO2830.1

Thomas, L., and Ferrari, R. (2008). Friction, frontogenesis, and the stratification of the surface mixed layer. *J. Phys. Oceanogr.* 38 (11), 2501. doi: 10.1175/2008JPO3797.1

Thomas, L., Tandon, A., and Mahadevan, A. (2008). Submesoscale processes and dynamics. *Washington DC Am. Geophys. Union Geophys. Monogr. Ser.* 177, 17–38. doi: 10.1029/177GM04

Thomas, L. N., Taylor, J. R., Ferrari, R., and Joyce, M. T. (2013). Symmetric instability in the gulf stream. *Deep Sea Res. Part II: Topical Stud. Oceanogr.* 91, 96–110. doi: 10.1016/j.dsr2.2013.02.025

Thompson, A. F., Lazar, A., Buckingham, C., Naveira Garabato, A. C., Damerell, G. M., and Heywood, K. J. (2016). Open-ocean submesoscale motions: A full seasonal cycle of mixed layer instabilities from gliders. *J. Phys. Oceanogr.* 46 (4), 1285–1307. doi: 10.1175/JPO-D-15-0170.1

Tuomi, L., Myrberg, K., and Lehmann, A. (2012). The performance of the parameterisations of vertical turbulence in the 3D modelling of hydrodynamics in the Baltic Sea. *Continent. Shelf Res.* 50/51, 64–79. doi: 10.1016/j.csr.2012.08.007

Väli, G., Zhurbas, V., Lips, U., and Laanemets, J. (2017). Submesoscale structures related to upwelling events in the gulf of Finland, Baltic Sea (numerical experiments). *J. Mar. Syst.* 171 (1), 31–42. doi: 10.1016/j.jmarsys.2016.06.010

Wortham, C., and Wunsch, C. (2014). A multidimensional spectral description of ocean variability. *J. Phys. Oceanogr.* 44 (3), 944–966. doi: 10.1175/JPO-D-13-0113.1

Ylöstalo, P., Seppälä, J., Kaitala, S., Maunula, P., and Simis, S. (2016). Loadings of dissolved organic matter and nutrients from the Neva river into the gulf of Finland – biogeochemical composition and spatial distribution within the salinity gradient. *Mar. Chem.* 186, 58–71. doi: 10.1016/j.marchem.2016.07.004

Yu, X., Naveira Garabato, A. C., Martin, A. P., Evans, D. G., and Su, Z. (2019b). Wind-forced symmetric instability at a transient mid-ocean front. *Geophys. Res. Lett.* 46 (11), 281–11, 291. doi: 10.1029/2019GL084309

Yu, X., Naviera Garabato, A. C., Martin, A., Buckingham, C., Brannigan, L., and Su, Z. (2019a). An annual cycle of submesoscale vertical flow and restratification in the upper ocean. *J. Phys. Oceanogr.* 49 (6), 1439–1461. doi: 10.1175/JPO-D-18-0253.1

Zhurbas, V., Väli, G., Kostianoy, A. G., and Lavrova, O. (2019). Hindcast of the mesoscale eddy field in the southeastern Baltic Sea: Model output vs satellite imagery. *Russian J. Earth Sci.* 19 (4), 1–17. doi: 10.2205/2019ES000672

Publication II

Salm, K.; Väli, G.; Liblik, T.; Lips, U. (2025). Forcing-dependent submesoscale variability and subduction in a coastal sea area (Gulf of Finland, Baltic Sea). Ocean Science, 21 (5), 2555–2577. DOI: 10.5194/os-21-2555-202

Ocean Sci., 21, 2555–2577, 2025
https://doi.org/10.5194/os-21-2555-2025
© Author(s) 2025. This work is distributed under
the Creative Commons Attribution 4.0 License.

Ocean Science Open Access EGU

Forcing-dependent submesoscale variability and subduction in a coastal sea area (Gulf of Finland, Baltic Sea)

Kai Salm, Germo Väli, Taavi Liblik, and Urmas Lips

Department of Marine Systems, Tallinn University of Technology, Tallinn, Estonia

Correspondence: Kai Salm (kai.salm@taltech.ee)

Received: 20 December 2024 – Discussion started: 15 January 2025
Revised: 1 July 2025 – Accepted: 1 September 2025 – Published: 22 October 2025

Abstract. Submesoscale (SMS) processes in a stratified coastal environment of the Gulf of Finland (Baltic Sea) were investigated using glider missions and a realistic simulation with a grid spacing of 0.125 nautical miles. The study period covered the transition from developing to established seasonal stratification. SMS variability, defined as small-scale anomalies of temperature and salinity cancelling each other's contribution to density (spice), was concentrated around the base of the upper mixed layer (UML) in spring and within the seasonal thermocline in late summer. We suggest that this shift was caused by the changes in surface heat flux and wind forcing. Both observations and simulations revealed events of high SMS variability, which can be related to background mesoscale dynamics and changes in wind forcing. We examined the event in which elevated spice in the subsurface layer did not coincide with the high Rossby number O(1) in the surface layer but instead appeared offshore of a coastal baroclinic current. Sloping isopycnals and intensified vertical velocities pointed to active SMS subduction. We propose that frontal instabilities, likely related to flow–topography interactions, drive the lateral and downward transport of surface waters, contributing to tracer redistribution below the thermocline.

1 Introduction

Submesoscale (SMS) flows, occupying the intermediate horizontal scale of ~ 1 km (Taylor and Thompson, 2023), are increasingly recognized as critical drivers of vertical exchanges of heat, carbon, and nutrients in the upper ocean, with important implications for stratification, biogeochemical cycling, and ecosystem productivity (e.g., Mahadevan, 2016). These processes bridge the energy transfer between larger, geostrophically balanced motions and microscale turbulence, making them central to upper-ocean dynamics (Capet et al., 2008; Naveira Garabato et al., 2022).

The ocean is a vast dynamic system driven by winds, tides, and density gradients due to temperature and salinity differences. These forces generate motion across a wide range of spatial scales, from large-scale geostrophic currents to small-scale turbulent mixing. Traditionally, upper ocean turbulence has been understood as a combination of mesoscale quasi-geostrophic eddies, internal waves, and microscale three-dimensional turbulence. Mesoscale dynamics, with characteristic horizontal scales of O(10–100) km in the ocean and O(5–20) km in the Baltic Sea, are characterized by small Rossby number ($Ro = \frac{U}{fL}$, $Ro \ll 1$) and large Richardson number ($Ri = \frac{N^2H^2}{U^2}$, $Ri \gg 1$), reflecting dominance of rotational and buoyancy forces (Taylor and Thompson, 2023). Here, U is a characteristic horizontal velocity scale, L and H are horizontal and vertical length scales, f is the Coriolis parameter, and N is the Brunt–Väisälä frequency. In contrast, SMS dynamics are characterized by Ro O(1) and $Ri < 1$, indicating a dynamic regime where rotation, stratification, and inertial forces all play important roles (Thomas et al., 2008). The weaker rotational constraint allows SMS processes to generate strong vertical velocities (e.g., Chrysagi et al., 2021; Tarry et al., 2022).

Recent advances in observational technology, particularly the use autonomous gliders, have significantly improved our ability to detect SMS structures. With their high spatial resolution and adaptive sampling capabilities, gliders are well suited to capturing the smaller-scale variability associated with SMS processes. For example, Jhugroo et al. (2020) identified low-salinity SMS features driven by riverine input

in a New Zealand shelf sea, which could intensify local stratification and displace a well-mixed surface layer up to 100 km offshore before being entrained by regional currents. Similarly, Bosse et al. (2021) used gliders to sample frontal zones in the northwestern Mediterranean Sea, revealing strong vertical motions and subduction events. In the Baltic Sea, studies such as by Carpenter et al. (2020) and Salm et al. (2023) have begun to reveal the role of SMS dynamics in shaping water column structure and vertical exchanges. However, given the region's complex stratification and ecological sensitivity, further glider-based studies are needed to resolve SMS processes and their biogeochemical implications in more detail.

This study focuses on the Gulf of Finland (GoF), an elongated sub-basin of the Baltic Sea – a semi-enclosed, brackish, shallow marginal sea in Northern Europe that stretches from 54 to 66° N. The sea has limited water exchange with the North Sea, and the input of fresh river water is large. The Neva River, the largest freshwater source, discharges at the eastern end of the GoF. Meanwhile, saltier water is transported into the gulf through its western border, creating a pronounced horizontal salinity gradient across the gulf.

The flow field in the GoF, which governs the freshwater transport and shapes both horizontal and vertical salinity gradients, is significantly influenced by the wind (Lilover et al., 2017; Westerlund et al., 2019). Prevailing along-gulf winds can establish a wind-driven circulation pattern, with currents along the wind near the coasts and counter-flows in the central gulf (Lips et al., 2017; Elken et al., 2011). These circulation patterns enhance transverse salinity gradients. Along-gulf winds also promote upwelling and downwelling events along the northern and southern coasts (Kikas and Lips, 2016; Lehmann et al., 2012). The summer upwelling events are typically associated with substantial temperature gradients at the sea surface (Lips et al., 2009; Uiboupin and Laanemets, 2009), and due to the strong horizontal and vertical salinity gradients and the development of jet currents along the upwelling fronts, also lead to pronounced salinity redistribution (Suursaar and Aps, 2007). Frontal structures and hydrographic variability associated with coastal upwelling serve as indicators of enhanced vertical mixing (Lips et al., 2009) and the emergence of SMS features, such as filaments and eddies (Väli et al., 2017).

During spring and summer, a seasonal thermocline typically forms at depths of 10–30 m. Beneath this layer – and throughout the water column during the remainder of the year – vertical stratification is predominantly controlled by salinity. The quasi-permanent halocline lies below 60 m on average (Liblik and Lips, 2017). In winter and early spring, shallow haline stratification can also develop because of freshwater advection (Liblik et al., 2020; Lips et al., 2017). In the GoF, the vertical salinity gradient has an equally important role alongside temperature in shaping the density stratification of the water column, highlighting a key difference from general open ocean conditions.

Building on previous observational evidence of SMS features in the GoF (Salm et al., 2023), this study aims to further investigate the role of SMS processes in this stratified coastal environment using a combination of observational and numerical tools. The appearance of SMS features associated with the development of a mesoscale front and changing wind forcing was documented based on mission data from spring 2018 (Salm et al., 2023). Here, we extend the analysis to all three missions conducted in the same area in spring–summer 2018–2019.

We examine tracer variability, specifically spice, which represents temperature and salinity variations that compensate for each other in density (Rudnick and Cole, 2011). We propose that scale-specific spice at horizontal scales of a few kilometers can be used as an indicator of SMS activity, especially in conditions when temperature and salinity contribute comparably to density stratification. In the GoF, this is applicable in late spring and summer, when both thermal and haline stratification are significant. Although spice can potentially be advected over some distance, the rapidly changing, wind-driven circulation in the GoF (Lilover et al., 2017) limits the transport of SMS features, thereby justifying a localized analysis. Ultimately, spice reveals anomalies and spatial gradients along isopycnals, where SMS processes often act. It serves as a proxy for SMS intensity capturing variability without being masked by vertical excursions of isopycnal surfaces, i.e., internal waves.

We focus on the upper half of the water column, where SMS activity is most prominent and glider data are more densely sampled, allowing more robust analysis. Our study is limited to the spring–summer period, when seasonal stratification develops and becomes well established. This time window allows us to focus on our main objective of understanding SMS generation under stratified conditions.

To complement and expand upon glider observations, we employ a high-resolution numerical model with SMS-permitting horizontal grid spacing (~ 232 m), enabling us to characterize the dynamical background and infer SMS activity beyond the limited scope of *in situ* measurements. For meaningful SMS analysis, model data were averaged over a 10×10 km study window ("time series box"; 59.67–59.76° N, 25.06–25.25° E; see Fig. 1). This averaging accounts for the potential spatial and temporal displacement of SMS features, which are highly sensitive to small changes in initial conditions, model resolution, and parameterized processes. By situating glider observations within a wider model domain, the analysis accommodates these discrepancies and captures how background mesoscale conditions modulate SMS activity, thus enabling more robust interpretations of physical variability.

The following hypotheses are considered in this study. First, we suggest that SMS variability is modulated by both atmospheric forcing, particularly surface heat flux and wind stress, and the background (larger-scale) hydrographic structures, including mesoscale frontal gradients. Second, we pro-

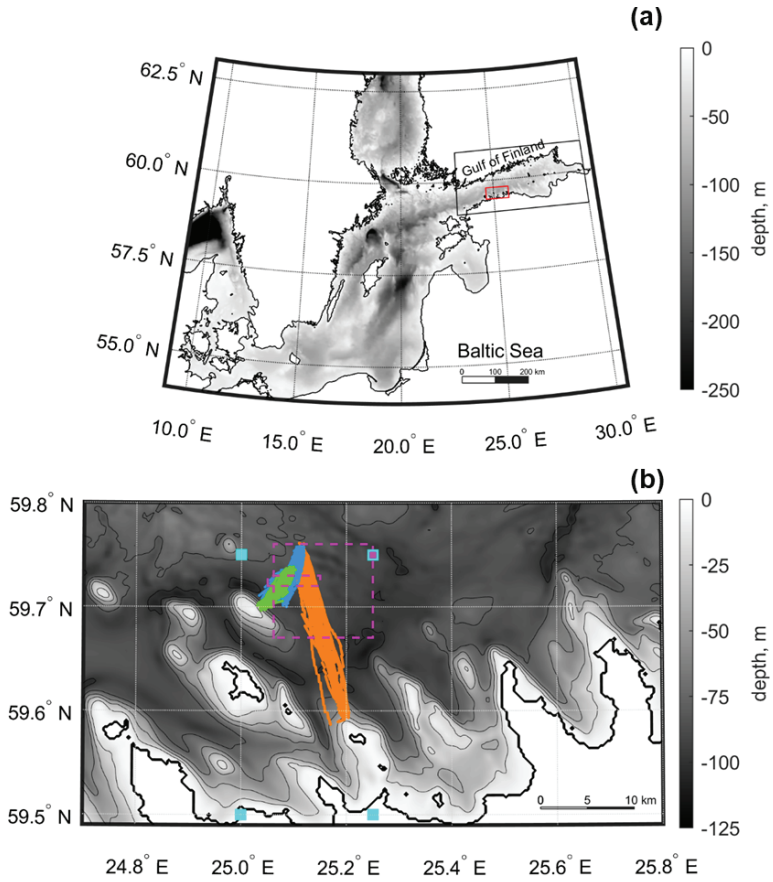


Figure 1. Map of **(a)** the Baltic Sea and **(b)** the study area. The red rectangle in panel **(a)** indicates the location of the study area shown in panel **(b)**. Depth isolines in panel **(b)** are shown with a step of 20 m. Glider missions from May–June 2018, May–June 2019, and July–August 2019 are shown in orange, blue, and green, respectively. The larger magenta box marks the "time series box" chosen for the modelled data, while the smaller magenta box indicates the area common to all missions (59.72–59.73° N 25.05–25.15° E), used for comparing glider and model data. The positions of ERA5 grid points used for extracting radiation data are shown by cyan squares and wind data by the magenta square. The colormap shows the bathymetry used in the model.

pose that topographically or forcing-induced instabilities of baroclinic coastal currents create favourable conditions for SMS subduction, enabling offshore and downward transport of tracers. To test these hypotheses, we use glider data and high-resolution simulations to characterize temporal, vertical and horizontal distributions of SMS features and explore associated dynamical forcing. These complementary approaches allow us to link observed variability at the submesoscale with the underlying physical mechanisms and evaluate the role of SMS processes in stratified coastal environments.

The paper is organized as follows: Sect. 2 introduces the observational datasets, the numerical experiment, and the analysis methods; Sect. 3 presents the results, focusing on the spice variability and the SMS-permitting events; Sect. 4 discusses the implications of our findings for SMS activity in coastal stratified seas; Sect. 5 concludes with a summary of key results and their broader relevance.

2 Data and methods

2.1 Glider observations

Although originally conducted for different research objectives, three glider missions in the GoF, Baltic Sea (Fig. 1), collectively provide a dataset for this study. The field campaigns took place from 9 May to 6 June 2018, from 21 May

to 19 June 2019, and from 21 July to 10 August 2019, during which an autonomous underwater vehicle, the Slocum G2 Glider MIA, collected oceanographic data along predefined transects. In May–June 2018, an 18 km long transect was sampled 26 times, and in 2019, 4.5 and 5.5 km transects were each sampled over 90 times. In total, over 12 000 profiles were gathered. These transects were oriented across the southern coast of the GoF, capturing cross-shore variability. The glider profiled the water column from the surface down to depths of 80–100 m, depending on the position. While under the surface, the glider started to turn around either 4 m before the surface or 5–6 m before the seafloor. Raw data were quality controlled following procedures adapted from Argo quality control protocols (Wong et al., 2025). Corrections for sensor response time and thermal lag were applied to minimize differences between two consecutive CTD profiles, following the approach described by Salm et al. (2023). Up- and downcasts were bin-averaged to a uniform 0.5 dbar vertical grid and arranged as profiles. For the analysis, the data fields were interpolated onto a regular grid with a time step of 10 min, corresponding to an average horizontal distance of 130 m.

2.2 Model setup

We used a three-dimensional nested setup of the General Estuarine Transport Model (GETM; Burchard and Bolding, 2002) to simulate the circulation and the temperature and salinity distributions in the GoF. GETM is a primitive-equation, free-surface, hydrostatic model with built-in vertically adaptive coordinates (Gräwe et al., 2015; Hofmeister et al., 2010; Klingbeil et al., 2018). Such a grid is a generalization of sigma layers with the potential to enhance vertical resolution near boundaries and in layers with strong stratification and shear (Klingbeil et al., 2018). Previous studies have shown that the total variation diminishing (TVD) advection scheme, combined with the superbee limiter, reduces numerical mixing in simulations (Gräwe et al., 2015). Vertical mixing in the GETM was calculated by coupling it with the General Ocean Turbulence Model (GOTM; Umlauf and Burchard, 2005). More precisely, the two-equation k–ε turbulence model (Burchard and Bolding, 2001; Canuto et al., 2001) was used in the simulation.

The entire GoF was the high-resolution model domain, with a uniform horizontal grid spacing of 0.125 nautical miles (approximately 232 m) and 60 adaptive layers in the vertical. Original bathymetry was obtained from the EMODnet database (http://summary.emodnet-hydrography.eu/data-products, last access: 1 June 2025) with a resolution of 1/16 arcmin (approximately 150 m). Bathymetry data were averaged to the model resolution, and missing values were interpolated using the nearest neighbour (NN) technique.

The high-resolution simulation with an open western boundary at the GoF entrance was performed starting on 3 December 2017. The initial temperature and salinity fields and boundary conditions were taken from coarse-resolution simulations covering, respectively, the entire Baltic Sea with a grid step of 1 nautical mile (see Väli et al., 2024 for more details) and the Baltic Proper (including the GoF) with a grid step of 0.5 nautical miles (see Zhurbas et al., 2018 and Liblik et al., 2020, 2022 for more details). As all setups use adaptive coordinates, we first interpolated the profiles from the coarse-resolution model to a fixed 5 m vertical resolution before spatial interpolation to the high-resolution model grid using the NN method. If needed, the profiles were extended to the bottom of the high-resolution grid to compensate for the bathymetric differences. The model run started from a motionless state with zero sea surface height and current components. Previous studies by Krauss and Brügge (1991) and Lips et al. (2016b) have shown that the spin-up time for the Baltic Sea model under atmospheric forcing is less than 10 d. For the boundary conditions, the temperature, salinity, and current profiles, as well as sea surface height, all with a 1 h temporal resolution from the 0.5 nautical mile resolution simulation, were used. The same model setup was used by Siht et al. (2025), where further details and validation results are presented. Some quantitative information on model performance regarding stratification and SMS variability, which are the focus of the present paper, are given in Sect. 3.1.

The atmospheric forcing at the sea surface (the momentum and heat flux) was calculated from the European Centre for Medium-Range Weather Forecasts atmospheric reanalysis dataset (ERA5, Hersbach et al., 2020) by utilizing wind components and other relevant parameters (air temperature, total cloudiness, relative humidity, sea level pressure) for bulk formulae by Kondo (1975). All meteorological parameters were interpolated bi-linearly to the model grid. The riverine freshwater input to the Baltic Sea was taken from the dataset produced for the Baltic Model Intercomparison Project (BMIP; Gröger et al., 2022) based on the E-HYPE (Lindström et al., 2010) hindcast and forecast products by Väli et al. (2019). There were 91 rivers in the dataset, of which 13 were in the GoF.

2.3 Submesoscale analysis

While air-sea fluxes, turbulent mixing, and advection introduce variability in the seawater properties, the dynamical processes act quickly to remove density differences. Spice – the combination of temperature and salinity variations that cancel each other's contribution to density – is the residual signal that remains (Rudnick and Ferrari, 1999). Spice was defined as the sum of the temperature anomalies, ΔT, scaled by the thermal expansion coefficient, α, and the salinity anomalies, ΔS, scaled by the haline contraction coefficient, β, as shown in Eq. (1):

$$\text{spice} = \alpha \Delta T + \beta \Delta S. \quad (1)$$

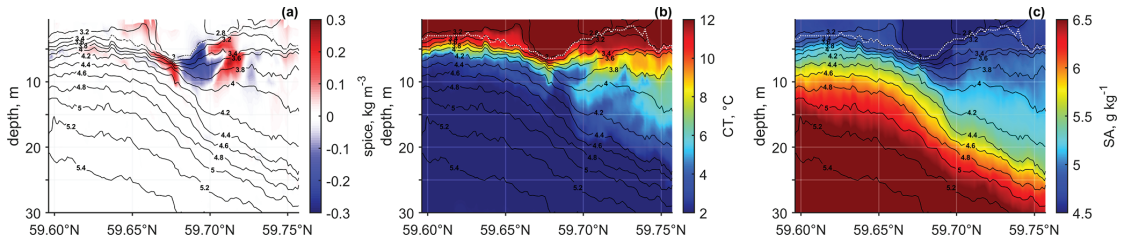


Figure 2. Example sections of **(a)** spice, **(b)** temperature, and **(c)** salinity with overlaid density contours, based on glider data from 24–25 May 2018. The white dashed line indicates the upper mixed layer depth.

The coefficients were calculated according to McDougall and Barker (2011). In this study, anomalies refer to the differences between the measured or modelled Conservative Temperature or Absolute Salinity and their average values along an isopycnal, calculated over a surrounding area of 4 km. For the observations, this was implemented as a moving window along the glider trajectory; for the model, it was computed over a 4×4 km square. The chosen length scale is consistent with the internal Rossby deformation radius in the GoF, which is typically 2–4 km (Alenius et al., 2003). The choice of a 4 km averaging scale offers a practical balance between resolving SMS structures and suppressing high-frequency noise. A smaller averaging scale may exaggerate variability and obscure persistent features, while a larger averaging scale poses a risk of smoothing out key SMS signals. Thus, 4 km averaging preserves the essential gradients and anomalies linked to SMS dynamics without compromising interpretability. Figure 2a shows an example of spice derived from the observations. The patches of positive (negative) spice indicate regions with higher salinities and temperatures (lower salinities and temperatures) compared to the average values in the surrounding 4 km on the same isopycnal surface. Spice effectively highlights smaller-scale (SMS) variability that may be challenging to discern from the vertical sections of temperature and salinity alone (Fig. 2b and c).

The average spice intensity was defined as the root mean square of spice from the sea surface to the depth of minimum temperature. The UML depth was determined as the minimum depth where $\rho_z \geq \rho_3 + 0.25\,\mathrm{kg\,m^{-3}}$ was satisfied (ρ_z is the density at depth z and ρ_3 at 3 m). The strength and position of the pycnocline, primarily associated with the seasonal thermocline, were analysed based on the maximum squared Brunt–Väisälä frequency (N^2) and its corresponding depth. The vertical buoyancy gradient was estimated as $N^2 = b_z$, calculated over 2 m vertical intervals. Buoyancy was defined as Eq. (2):

$$b = -\frac{g}{\rho_0}(\rho - \rho_0), \tag{2}$$

where ρ_0 is the reference density of $1000\,\mathrm{kg\,m^{-3}}$.

Quantities indicative of the SMS regime, such as the Rossby number (Ro), balanced Richardson number (Ri), and horizontal buoyancy gradient, were calculated based on the model data. Ro and Ri were estimated, respectively, as Eq. (3):

$$Ro = \frac{\zeta}{f}, \tag{3}$$

and Eq. (4):

$$Ri = \frac{f^2 N^2}{|\nabla_\mathrm{H} b|^2}. \tag{4}$$

$\zeta = v_x - u_y$ is the vertical component of relative vorticity, f is the Coriolis frequency, and $|\nabla_\mathrm{H} b| = \sqrt{b_x^2 + b_y^2}$ horizontal buoyancy gradient modulus. Centred finite-difference scheme was used to calculate the parameters from the model. Horizontal and vertical steps for estimating gradients were 500 and 2 m, respectively.

Wind data and parameters defining heat exchange between the atmosphere and the sea surface were extracted on the ERA5 product grid cells covering the study area (59.50–59.75° N, 25.00–25.25° E; see Fig. 1). The wind components in the analysis were smoothed by a Gaussian low-pass filter for 6 h to reduce high-frequency noise and highlight relevant forcing scales.

3 Results

3.1 Stratification and spice from observations and model

To present temporal evolutions of stratification and spice in the study area and enable direct comparison, we averaged both model and observational data over the same spatial region. We selected a common area covered in all missions (59.72–59.73° N 25.05–25.15° E, Fig. 1) and averaged the consecutive profiles within this region for each transect. This area corresponds to approximately 1 km of glider track, along which about ten profiles were typically obtained. The model profiles were averaged over a 1×1 km area located within the same overlapping region.

Temporal developments of temperature and salinity distributions, stratification, and spice from the simulation and glider observations are shown in Figs. 3–6. A three-layered structure of the water column, consisting of a warm surface layer (upper mixed layer, UML), a cold intermediate layer (CIL), and a saltier deep layer, was observed and simulated. Observed patterns of variability in temperature and salinity distributions were well simulated by the model (Figs. 3 and 4). In absolute values, salinity was underestimated by $0.4\,\mathrm{g\,kg^{-1}}$, while CIL temperatures were overestimated by approximately 2 °C in 2018 and 1.5 °C in 2019 in the model. In general, the model replicated the characteristic vertical density structure of the water column in the GoF and the development of the seasonal thermocline (Fig. 5). However, when characterizing the vertical structure and stratification of the water column, we point to some discrepancies.

The observed and modelled UML depths were in close agreement during Missions I (7 ± 3.7 and 7 ± 3.1 m) and II (13 ± 4.4 and 13 ± 3.7 m) but diverged more in Mission III, with an observed average depth of 10 ± 4.4 m compared to 6 ± 2.6 m in the model. The depth of the CIL was reasonably well captured by the model in Missions I and III, with average observed and simulated depths of 22 ± 5.0 and 24 ± 5.5 m, and 43 ± 5.2 and 41 ± 6.0 m, respectively – both within the uncertainty of the estimates. However, a significant discrepancy was evident in Mission II, where the model placed the CIL approximately 10 m shallower than observed (29 ± 5.1 m vs. 39 ± 5.5 m).

The observed and simulated depths of the maximum N^2 were, respectively, 10 ± 5.9 and 8 ± 4.0 m during Mission I, 20 ± 7.5 m and $15\,\mathrm{m} \pm 4.1$ m during Mission II and 14 ± 4.8 and 9 ± 3.2 m during Mission III. These differences, ranging from approximately 2 to 5 m, indicate a systematic underestimation of the depth of the strongest stratification in the upper water column by the model. Partly, this could be related to an overall weaker salinity gradient in the model compared to observations. For instance, in the first half of Mission II (spring 2019), the strongest vertical density gradient, as indicated by the maximum N^2, was determined by the vertical salinity distribution, as indicated by the glider data, whereas the model placed it shallower where the seasonal thermocline began to develop. Furthermore, the model did not capture the presence of occasionally observed two local maxima of N^2, e.g., on 21–30 May 2018 and 23–28 July 2019 (Fig. 5). On both occasions, glider observations revealed two distinct stratification peaks: respectively, at 7 ± 2.7 m with the maximum N^2 of $0.0026 \pm 0.0005\,\mathrm{s^{-2}}$ and at 19 ± 4.2 m with $0.0016 \pm 0.0003\,\mathrm{s^{-2}}$, and at 6 ± 2.8 m with $0.0023 \pm 0.0007\,\mathrm{s^{-2}}$ and at 19 ± 2.5 m with $0.0023 \pm 0.0003\,\mathrm{s^{-2}}$. The model showed a single stratification maximum of approximately $0.0017 \pm 0.0003\,\mathrm{s^{-2}}$ at 6 ± 2.6 m on 21–30 May 2018 and $0.0041 \pm 0.0008\,\mathrm{s^{-2}}$ at 5 ± 1.0 m on 23–28 July 2019. These discrepancies suggest that the model underrepresents the vertical complexity of stratification in the upper water column, the point that will be discussed in the Discussion section.

The halocline was generally weaker in the model during all missions (Fig. 5). However, as our focus is on the seasonal thermocline, we do not analyse this further and assume its impact on the upper-layer variability is minimal.

According to both the measurements and the simulation, spice intensity was highest during the summer 2019 mission (Fig. 6a–c), coinciding with the period of strongest vertical gradients in temperature, salinity, and density, and the most intense stratification (Figs. 3–5). The results, specifically the vertical distribution patterns of spice, were generally consistent between the model and observations; however, the model tended to underestimate the maximum spice intensities during spring missions. Nevertheless, both datasets point to a potential relationship between the development of stratification and SMS variability (processes). During the spring missions (May–June 2018 and 2019), spice maxima were located around the base of the UML. They occurred at shallower depths (corresponding to lower densities) than the depth of the maximum vertical density gradient. In contrast, during the summer mission (July–August 2019), the spice peak shifted to greater depths, situated beneath the UML and immediately below the strongest density gradient.

To extend this analysis, we present monthly average stratification parameters and vertical distributions of spice from model output for May through August 2018 and 2019 (Fig. 6d–g). The density range between the UML and the CIL increased from spring to late summer, indicating a deepening and strengthening of the pycnocline. Both the UML depth and the depth of the maximum density gradient shifted toward lower densities over the season, except in July–August 2018, when this trend was less pronounced. In May of both years, the maximum spice was at lower densities than those corresponding to the UML depth and the depth of the maximum density gradient. From June to August, the spice maxima aligned more closely with the density of the maximum vertical density gradient, suggesting a seasonal deepening of spice variability. Elevated spice intensities were spread over a broader density range over the summer months, reflecting the seasonal development of the pycnocline.

Further, in June 2018 and August 2019, a secondary local maximum of spice intensity was detected closer to the sea surface at low densities, indicating enhanced variability in the upper layer during these periods. This suggests that while the primary spice variability deepens with the season, episodic events can still induce significant variability in the upper layers.

Comparing the two years, 2019 exhibited a more pronounced seasonal progression in spice distribution, with a clearer deepening and broadening of the spice-rich layer from May to August. In contrast, 2018 showed a less consistent pattern, particularly in July–August, when the expected shift toward lower densities was not as evident. These interannual differences highlight the influence of varying atmo-

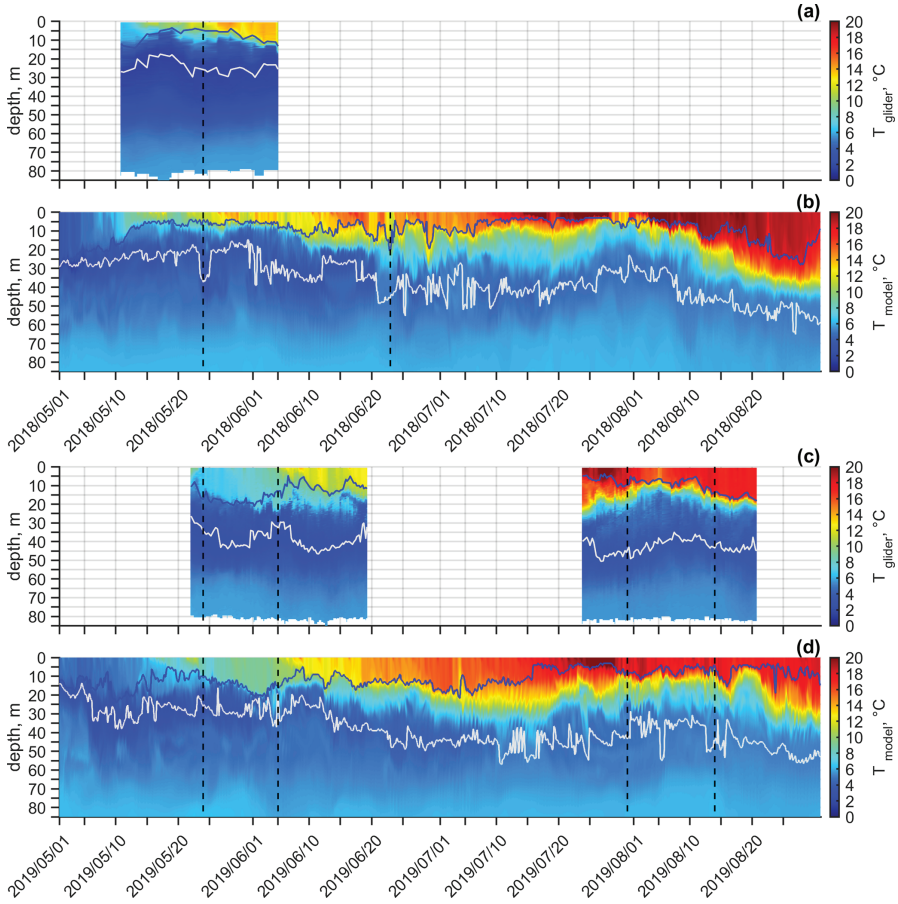


Figure 3. Temperature variability based on glider data **(a, c)** and model data **(b, d)** for May–August 2018 **(a, b)** and 2019 **(c, d)**. The glider data represent average profiles for each section within the selected area, forming a composite temperature field. The model data show average profiles within a 1×1 km window at each model output time. Blue and white lines indicate the depths of the UML and the CIL, respectively. Vertical black lines indicate the dates shown in Fig. 8: 24 May and 23 June 2018 **(a, b)**; 24 May, 5 June, 31 July, and 14 August 2019 **(c, d)**.

spheric and oceanographic conditions on the seasonal development of spice variability.

3.2 Background forcing and large-scale and mesoscale dynamics

Background forcing in the study area in May–August 2018 and 2019 was characterized by mostly positive net surface heat flux (Q) and variable wind conditions (Fig. 7). Short periods of negative Q occurred in early June and July 2018, August 2018, early May and July 2019, and again in late July to early August 2019. Easterly and north-easterly winds, which favour upwelling along the southern coast of the GoF, were prevalent in July 2018 and also notable in May 2018 and May and July 2019 (Fig. 7a, c). Conversely, downwelling-favourable westerly and south-westerly winds dominated in June of both years. August wind patterns were marked by frequent southerly winds, while northerly winds were more common in July 2019. Wind speed rarely exceeded 10 m s^{-1}, except in June 2018, when three episodes of strong westerly winds occurred. These events led to vertical mixing and downwelling in the study area, resulting in deepening of the thermocline and weakened upper layer stratification. N^2 peaked in early June, decreasing from 0.006 s^{-2} on 2 June to 0.002 s^{-2} by 10 June, accompanied by a deepening of its maximum from 5 to 15 m (Fig. 5b). Similarly, downwelling-favourable winds and negative Q at the beginning of July 2019 contributed to reduced vertical stratification. The already weak stratification, characterized by a maximum N^2 of 0.002 s^{-2} at 18 m depth, weakened further be-

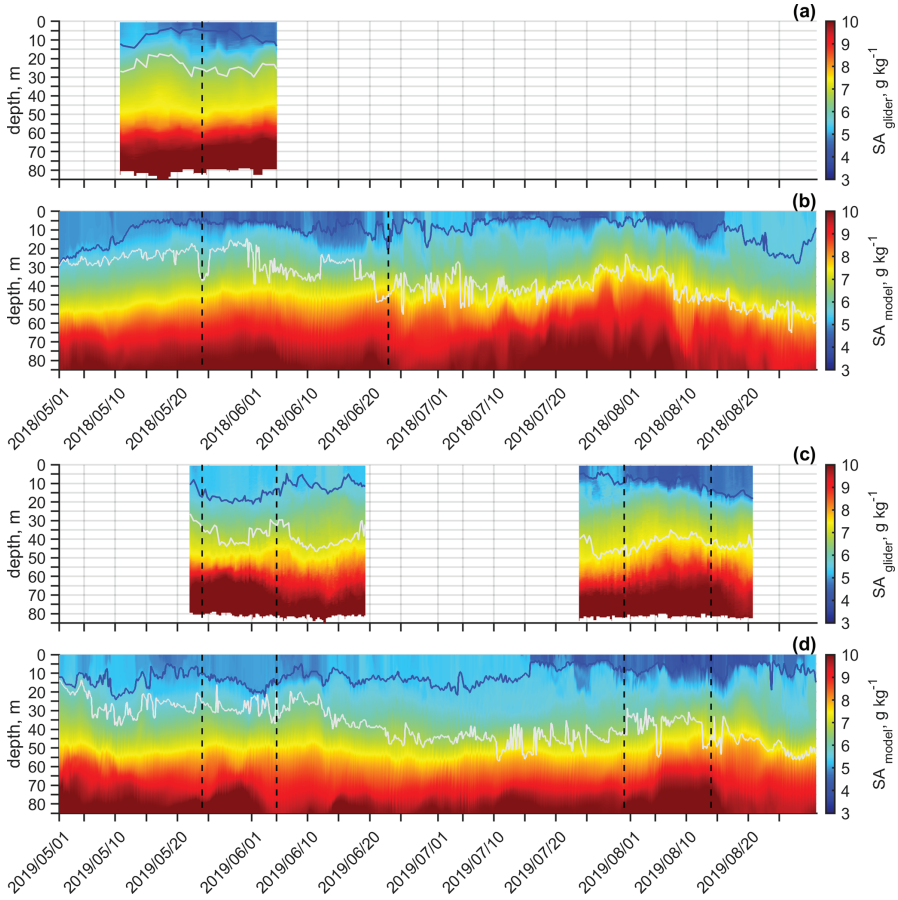


Figure 4. Salinity variability based on glider data **(a, c)** and model data **(b, d)** for May–August 2018 **(a, b)** and 2019 **(c, d)**. The glider data represent average profiles for each section within the selected area, forming a composite salinity field. The model data show average profiles within a 1×1 km window at each model output time. Blue and white lines indicate the depths of the UML and the CIL, respectively. Vertical black lines indicate the dates shown in Fig. 8: 24 May and 23 June 2018 **(a, b)**; 24 May, 5 June, 31 July, and 14 August 2019 **(c, d)**.

tween 1 and 5 July, with the depth of the maximum shifting to 30 m (Fig. 5d). Several calm periods lasting about one to two weeks, namely in May and July of both years, allowed for the development and strengthening of vertical stratification. Substantial stratification strengthening occurred in May and July 2018, with N^2 maxima peaking at 0.006 and 0.01 s^{-2}, respectively (Fig. 5b). In contrast, by the end of July 2019, the N^2 maximum reached only 0.005 s^{-2} (Fig. 5d). In August, SW–W winds dominated in both years, and Q was no longer predominantly positive.

We suggest that wind forcing and surface heat flux played a crucial role in shaping the thermohaline variability in the area, with notable differences between the two years. To better illustrate how atmospheric forcing influenced the development of background hydrographic conditions, we present a series of characteristic events from spring–summer 2018–2019.

In May 2018, NE–E winds (Fig. 7b) triggered upwellings along the southern coast, evident in narrow coastal regions with low temperatures (Fig. 8a). Concurrently, a broader westward flow transported warmer, less salty surface water from the eastern GoF into the study area (Fig. 8a). In June 2018, strong SW–W winds led to downwelling along the southern coast (Fig. 8b), deepening the thermocline and altering the upper-layer structure.

In May 2019, upwelling along the southern coast was more intense than in the previous year, driven by a strong E wind impulse on 22–23 May (Fig. 7d), resulting in pronounced cold water intrusions along the southern coast (Fig. 8c). By June 2019, upwelling subsided as SW–W winds became

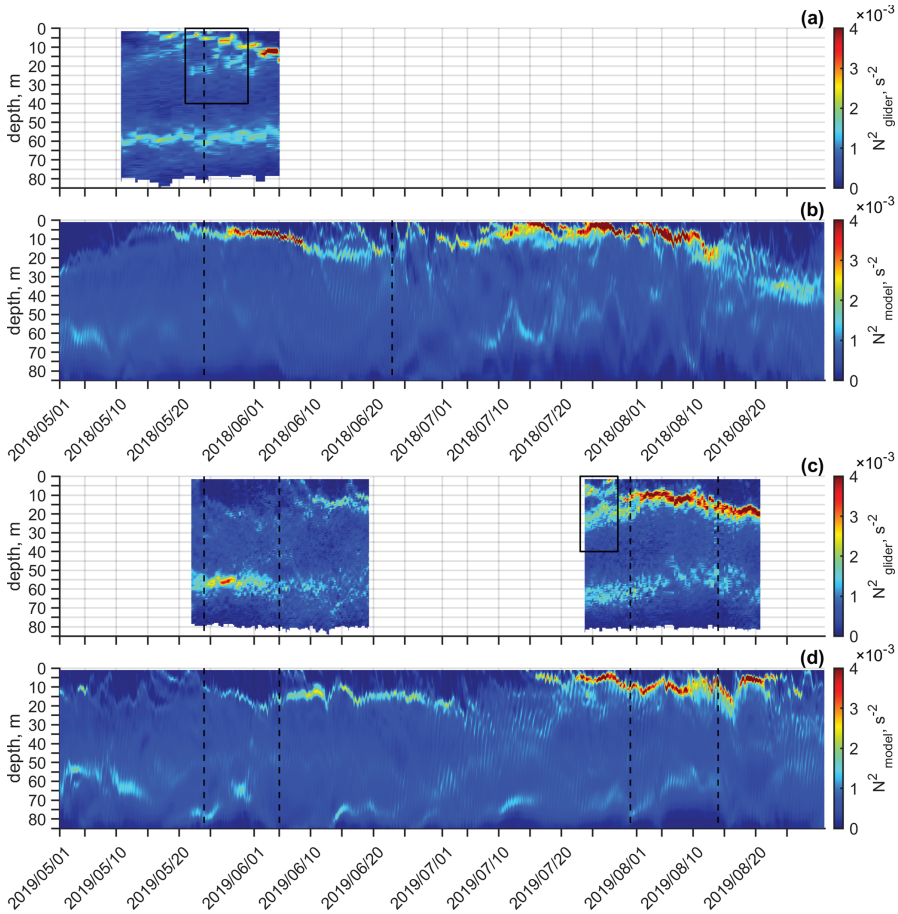


Figure 5. Variability of vertical stratification presented as Brunt–Väisälä frequency squared (N^2) based on glider data **(a, c)** and model data **(b, d)** for May–August 2018 **(a, b)** and 2019 **(c, d)**. The glider data represent average profiles for each section within the selected area, forming a composite salinity field. The model data show average profiles within a 1×1 km window at each model output time. Vertical black lines indicate the dates shown in Fig. 8: 24 May and 23 June 2018 **(a, b)**; 24 May, 5 June, 31 July, and 14 August 2019 **(c, d)**. Black boxes indicate periods of two observed local maxima in N^2: 21–30 May 2018 **(a)** and 23–28 July 2019 **(c)**.

dominant, leading to the formation of mesoscale rotating structures in the central gulf (Fig. 8d). In late July 2019, NE–E winds over several days (Fig. 7d) once again caused upwelling along the southern coast, accompanied by a strong surface-layer outflow from the gulf (Fig. 8e). This outflow weakened in early August as northerly winds and negative Q prevailed (Fig. 7d). However westward advection of fresher water persisted, making the study area a transition zone between distinct water masses (Fig. 8f).

Overall, the dynamical background varied substantially across the study period, reflecting a strong influence of episodic atmospheric forcing. Depending on the prevailing wind conditions, mesoscale features such as upwellings and associated westward flows (Fig. 8a, c and e), downwellings (Fig. 8b), and eddies (Fig. 8d and f) developed. These features coincided with enhanced SMS activity, as evidenced by elevated Ro and intensified horizontal buoyancy gradients in the surface layer, particularly near frontal zones and filaments. In May 2018, May 2019, and July 2019 (Fig. 8a, c, and e), strong lateral gradients and Ro O(1) emerged near the southern coast, aligning with coastal upwelling. Further, the westward intrusion of low-salinity water from the eastern part of the gulf played a notable role in maintaining lateral density gradients across the basin, particularly in August 2019 (Fig. 8f). The SMS-active regions were more pronounced in summer (Fig. 8b, e and f), likely due to sharper

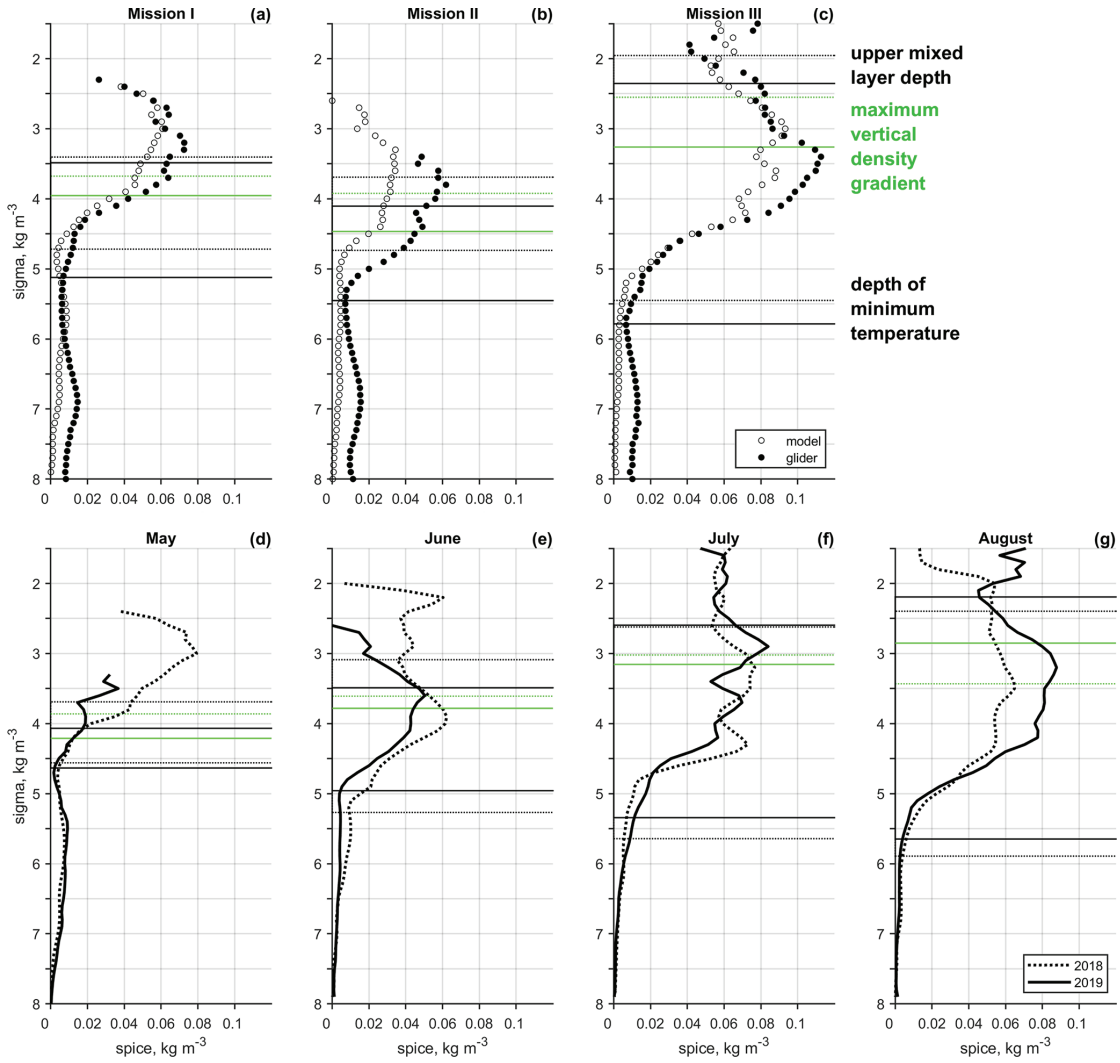


Figure 6. The standard deviation of spice. **(a–c)** First row: measured (black dots) and modelled (white circles) spice variability for each glider mission period. Solid and dashed black lines mark the average UML depth and depth of minimum temperature from measurements and model, respectively. Green lines indicate the average depth of maximum Brunt–Väisälä frequency. **(d–g)** Second row: monthly standard deviation of modelled spice from May to August in 2018 (dashed) and 2019 (solid). Black and green horizontal lines represent the same reference depths as in panels **(a)**–**(c)**. All dashed lines correspond to 2018, and all solid lines to 2019. Model data were averaged over a 1×1 km area (see Fig. 1).

lateral density gradients and a shallower mixed layer, that reduced the local Rossby deformation radius and favoured stronger SMS instabilities by intensifying frontal sharpness and enabling ageostrophic motions at smaller scales. Transient wind events and air–sea fluxes emerge as key drivers of mesoscale and SMS variability in the GoF, generating conditions that favour the development of SMS instabilities. The resulting SMS activity and its spatial distribution are examined in the following section.

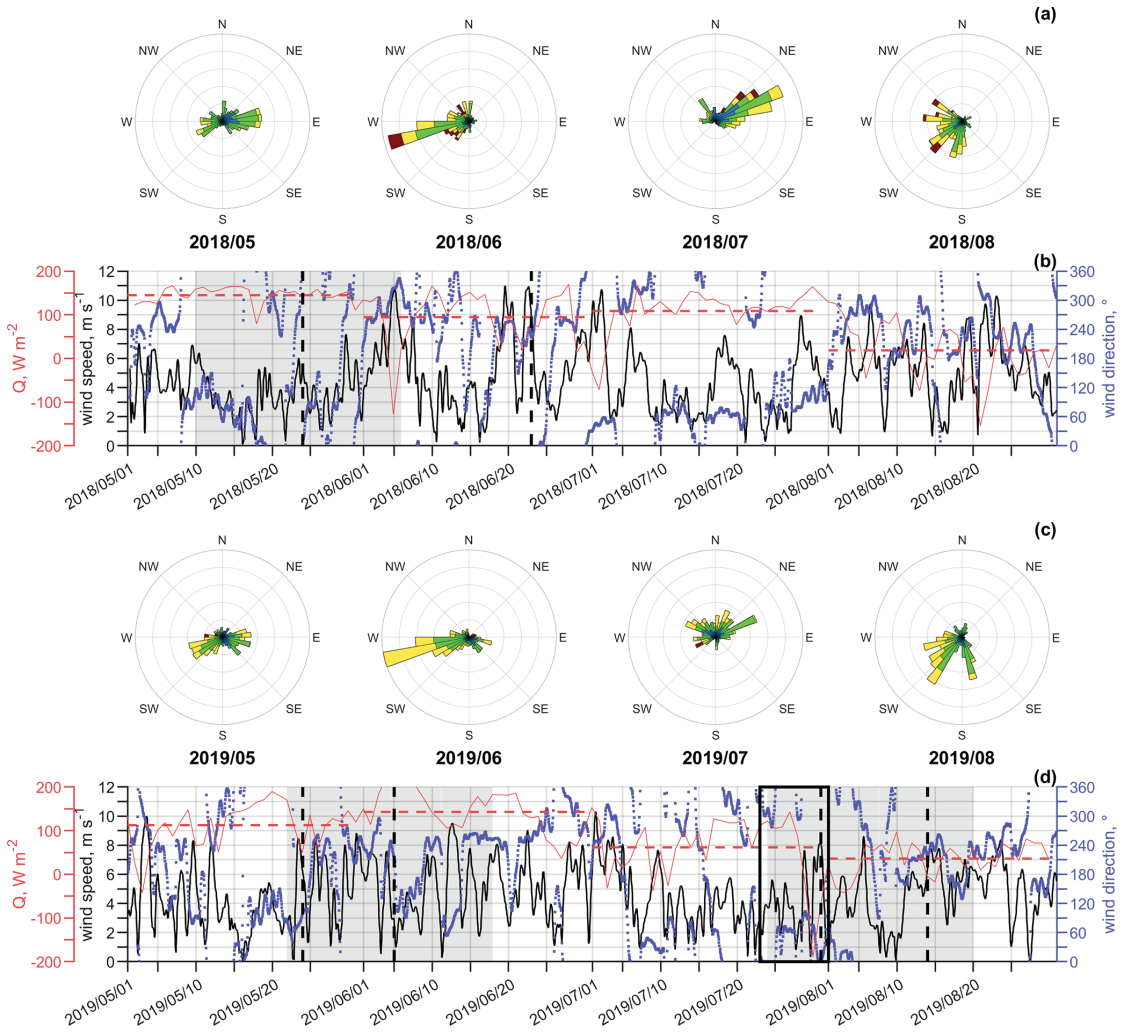


Figure 7. The daily average net surface heat flux, Q, (red, dashed line showing the monthly average), wind speed (black) and direction (blue) in spring–summer 2018–2019 **(b, d)**. Panels **(a)** and **(c)** show the wind roses from May to August for both years, respectively. Vertical black lines indicate the dates shown in Fig. 8: 24 May and 23 June 2018 **(b)**; 24 May, 5 June, 31 July, and 14 August 2019 **(d)**. The black box indicates the period examined in Sect. 3.4: 23–31 July 2019 **(d)**.

3.3 Submesoscale variability from spice in observations and model

The intensity of SMS variability, quantified by the root mean square of spice, displayed multiple peaks throughout the spring–summer periods of 2018 and 2019. Some of these peaks coincided with elevated surface *Ro* variability (indicated by local maxima in the root mean square *Ro*; Fig. 9), such as during 25–27 July and early August 2018 or in August 2019, while others occurred under relatively low *Ro* conditions. Notably, high spice values were observed on 18 June and 11–13 July 2018, as well as between 22 and 30 July 2019, despite moderate to weak *Ro* variability (Fig. 9b and d). This partial decoupling suggests that spice may capture a broader spectrum of SMS variability, including processes less directly linked to elevated relative vorticity.

Spice intensities from glider data and model data show good qualitative agreement, considering that the model values were averaged over the defined time series box (see

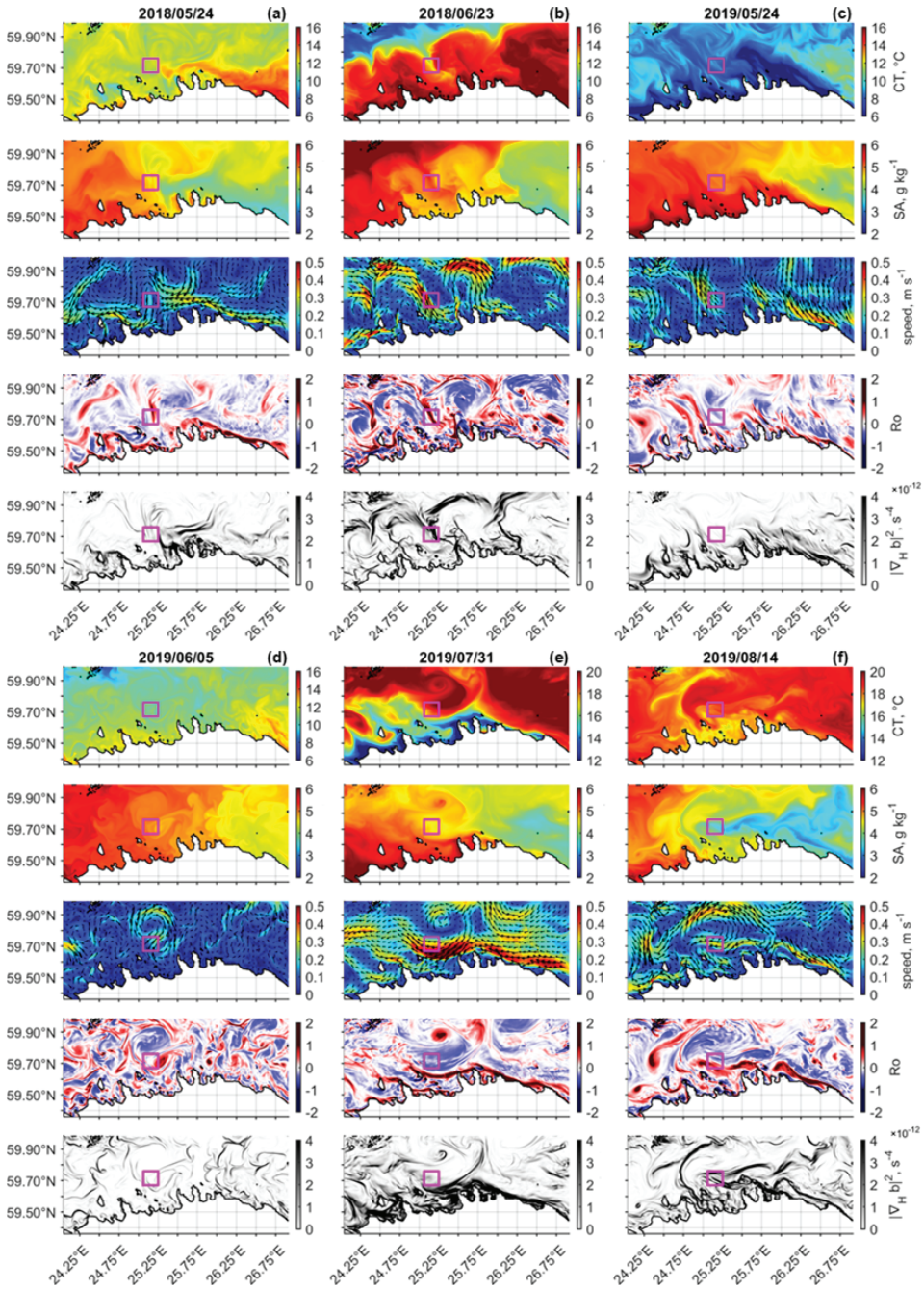


Figure 8. Overview of surface hydrographic and dynamical conditions in the Gulf of Finland during spring–summer 2018–2019, illustrating the variability of SMS-relevant fields. Example dates characterizing the evolving dynamical background are shown in **(a–c)** first row: 24 May 2018, 23 June 2018, and 24 May 2019, and in **(d–f)** second row: 5 June, 31 July, and 14 August 2019. For each date, panels from top to bottom display surface (0–3 m) Conservative Temperature (°C), Absolute Salinity ($g\,kg^{-1}$), velocity ($m\,s^{-1}$), Rossby number, and squared horizontal buoyancy gradient modulus (s^{-4}). The magenta box marks the 10×10 km study window.

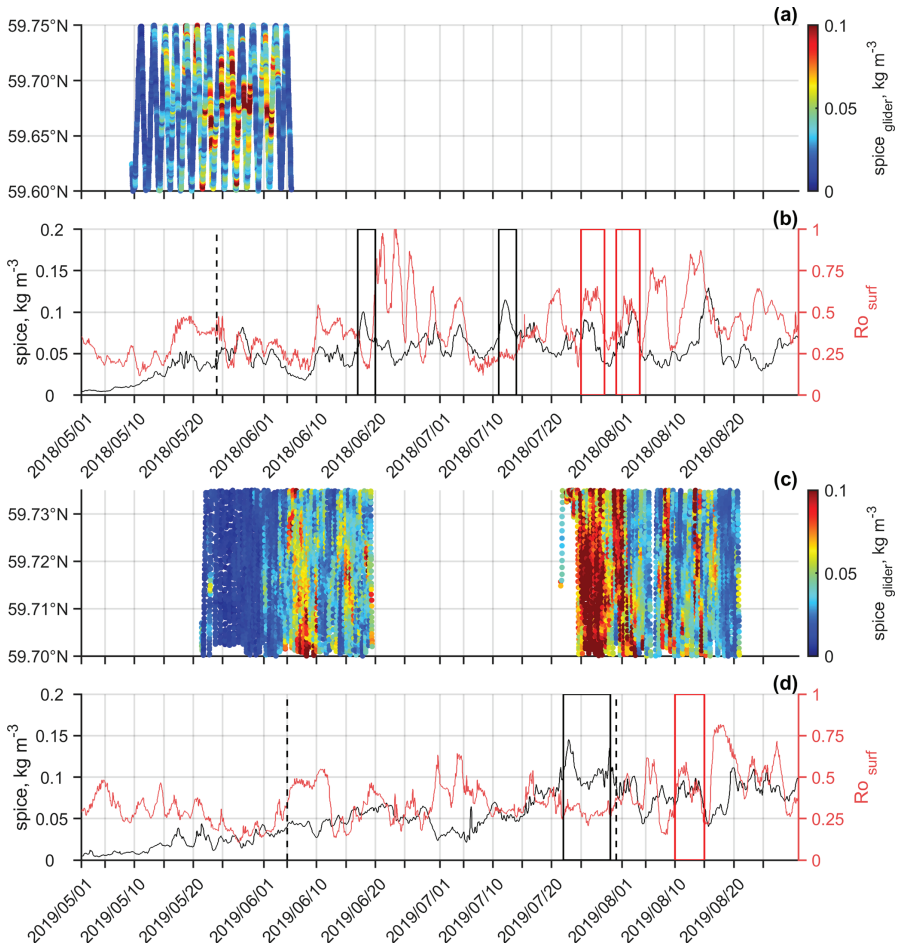


Figure 9. Root mean square spice in the density range from the surface to the depth of minimum temperature in spring–summer 2018–2019. Panels **(a)** and **(c)** show spice intensity along the glider trajectory; panels **(b)** and **(d)** show model results, calculated within a 10×10 km study window. The black line shows spice, and the red line indicates the surface root mean square Rossby number (Ro). Vertical black lines mark the dates shown in Fig. 10, corresponding to periods discussed in Sect. 3.3: 24 May 2018 **(b)**, and 5 June and 31 July 2019 **(d)**. Red boxes highlight example periods of high spice and high Ro, while black boxes indicate periods of high spice and low Ro **(b, d)**.

Fig. 1; compare Fig. 9a and b, and Fig. 9c and d). Both datasets reveal an overall increase in spice intensity from May to August, reflecting the seasonal strengthening of stratification (which is at its maximum in July–August) and the intensification of background temperature and salinity gradients. This seasonal trend is further supported by a concurrent rise in Ro, punctuated by transient peaks driven by episodic strong wind forcing, as in late June 2018 (Fig. 9b).

We selected three periods when both glider and model data were available to demonstrate how the distribution of parameters indicative of SMS instabilities/processes relates to spice. The intensification of spice observed in the second half of May 2018 (Fig. 9a) and simulated by the model (Fig. 9b) coincided with the eastward transport of warmer, less saline water and the formation of horizontal buoyancy gradients (Fig. 8a). During 15–25 May, calm weather prevailed, and Ro, averaged over the time series box, exhibited a sustained increase towards O(1), indicating enhanced SMS activity in the surface layer. The spice intensity concurrently increased, with notable peaks on 18 and 25 May, and reached its maximum on 28 May (Fig. 9b). Figures 8a and 10d demonstrate the presence of elongated SMS structures on 24 May, characterized by Ro O(1), $Ri < 1$, and relatively strong horizontal buoyancy gradients. Elevated spice

intensity was located near these features, indicating enhanced thermohaline variability associated with SMS instabilities (Fig. 10d).

In late May 2019, an intense upwelling occurred along the southern coast (e.g., 24 May; Fig. 8c). However, this did not lead to a notable increase in the spice intensity or *Ro* within the time series box (Fig. 9d). A considerable rise in *Ro* and modest rise in spice intensity occurred at the beginning of June, coinciding with a change from SW winds on 1 June to SE winds on 5 June (Fig. 7d). During this period, a cyclonic eddy ($\sim$ 10 km in diameter) formed in the study area, accompanied by a larger anticyclonic eddy offshore (Fig. 8d). Elevated *Ro* from 5 to 11 June indicated the persistence of this cyclonic feature in the time series box (Fig. 9d). Elevated spice intensity was observed at the periphery of the cyclonic eddy (Fig. 10e), aligned with narrow stripes of relatively high buoyancy gradients and low *Ri* (Figs. 8d and 10b).

High spice intensity observed during the third week of July 2019 (Fig. 9c and d) appeared to be associated with varying wind forcing (Fig. 7d) and the development of a westward current along the southern coast of the GoF (Fig. 8e). Westerly winds at the beginning of July were followed by upwelling-favourable winds on 7–10 July, which evoked the westward coastal current. After that, a period of weaker variable winds followed, and then another stronger pulse of easterly winds occurred, further strengthening the coastal current. Despite the dynamic conditions, *Ro* within the time series box remained relatively low during this period (Fig. 9d). However, Fig. 8e reveals that regions of *Ro* O(1) and strong horizontal buoyancy gradients linked to the coastal current were located just south of the study area. Interestingly, patches of low *Ri* appeared also north of the region with the highest surface current speeds, while areas of high spice intensity were found even farther north (Fig. 10c and f). The observed spatial offsets between *Ro*, *Ri*, and spice intensity suggest that active SMS processes may be vertically and/or laterally displaced from the surface frontal zone. These patterns motivate a closer inspection of the late July period.

3.4 Upwelling-driven submesoscale variability and subduction

The period from 23 to 31 July 2019 was selected for closer analysis due to an observed peak in spice variability (Fig. 9d). For each day within this period, a set of vertical sections, as shown in Fig. 11, was produced (Figs. S1–S9). Prior to the strong easterly wind impulse on 28–29 July, winds varied between NE and NW, averaging 3.5 m s^{-1} (Fig. 7d). After 25 July, the easterly wind component strengthened, and by 26 July 2019, a strong coastal current had emerged, accompanied by high subsurface variability in temperature and salinity across all three selected sections (Figs. S3 and S4). This current intensified by 29 July, coinciding with a clear upwelling event. Surface temperatures dropped from 22 °C, and northward velocities increased sharply in the upper layer (Fig. 11a–d). Isopycnals tilted, with an outcropping of the 3 kg m^{-3} isopycnal (Fig. 11f), reflecting enhanced horizontal buoyancy gradients and frontal sharpening – conditions favourable for SMS instabilities.

Ro reached O(1) near the coastal current zone and topographic features (Fig. 11f) while remaining relatively low in the offshore area (left panel in Fig. 11f and *Ro* curve in Fig. 9d). Vertical velocities increased notably across all transects (Fig. 11e), and horizontal velocity fields indicated intensified shear in the upper 40 m (Fig. 11c and d). These dynamics are consistent with shear-driven instability and frontal subduction.

By 29 July, spice anomalies became more confined to the upper 15 m and showed weaker spatial alignment with elevated *Ro* (Fig. 11g), in contrast to 27–28 July, when enhanced subsurface spice was more closely aligned with regions of *Ro* O(1) (Figs. S5 and S6). Notably, spice extended beyond the core of the coastal current, with elevated values observed near sloping isopycnals and beneath frontal zones (Fig. 11g). These signals, aligned with tilted isopycnals, indicate both vertical and lateral thermohaline displacement.

Horizontal distributions of velocity and spice at the surface and 20 m depth (Fig. 12) highlight the influence of flow–topography interactions on SMS variability. At the surface, the coastal current veered offshore at several locations, particularly downstream of peninsulas and bathymetric irregularities (Fig. 12b). At 20 m, flow patterns differed significantly from the surface, especially near the coast where the flow reversed with depth, indicating strong vertical shear (Fig. 12b and d). Elevated spice intensity near these transitions (Fig. 12f) suggests that such flow structures contribute to the generation and modulation of SMS features. Spice intensity was highest both along the coast and in offshore areas where the coastal current deflected seaward, especially westward (downflow) of coastal and topographic irregularities.

We compared the patterns in the case of upwelling described above with those observed during downwelling conditions in early July 2019. On 3 July, the surface current field was characterized by prevailing shoreward transport and the presence of eddies in the surface layer (Fig. 12a). The flow at 20 m roughly mirrored the surface (Fig. 12c), indicating weaker vertical shear, although localized shear zones were still present near topographic features. High spice intensity was present nearshore and, to a lesser extent, offshore (Fig. 12e), but overall spice intensity was lower than on 29 July.

This contrast is further illustrated by zonal cross-sections (Fig. 13), which provide an alongshore view of the thermohaline and dynamic structure during the two events. While the transects from 3 and 29 July share some structural similarities, they also reveal key dynamic differences. Due to the alongshore orientation and its distance from the coast, signs of upwelling are more difficult to detect directly. However, meridional sections (Figs. S1–S9) confirm the pres-

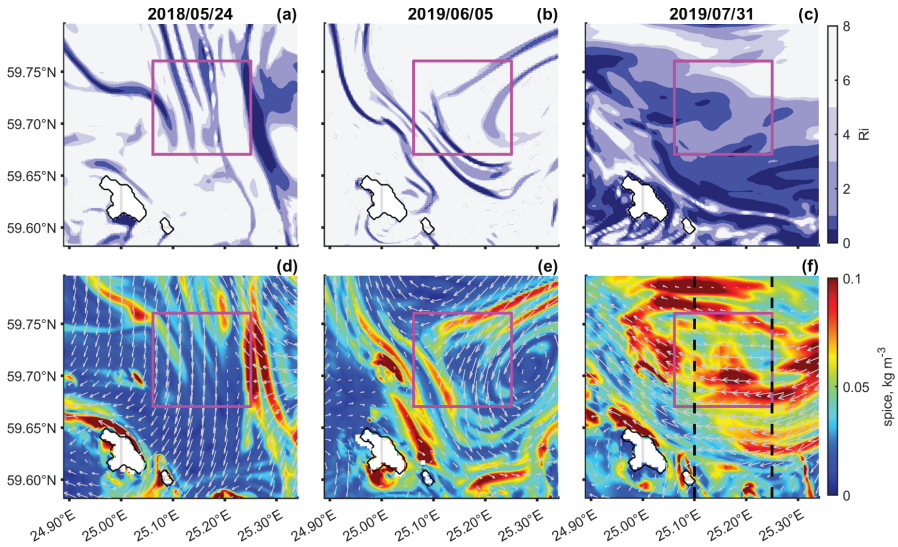


Figure 10. Richardson number **(a–c)** and root mean square spice calculated within the density layer from the surface to the depth of minimum temperature **(d–f)** during spring–summer 2018–2019. Each column shows one example date from a different glider mission period – 24 May 2018, 5 June and 31 July 2019 – corresponding to the dates shown in Fig. 8. The magenta box marks the 10×10 km study window.

ence of upwelled water, indicated by surface temperatures below 20 °C and salinities near 5 g kg^{-1} on the 29 July transect (Fig. 13b and d). In contrast, during downwelling on 3 July, thermohaline gradients were weaker, and the thermocline was deeper, centred around 20 m (Fig. 13a and c). The different flow structure was noticeable. On 29 July, offshore flow was evident in the surface layer, particularly between 24.9 and 25.3° E (Fig. 13f and h). On 3 July, the current exhibited shoreward flow from the surface to 20 m depth, especially between 25.0 and 25.4° E (Fig. 13e and g).

Both dates showed *Ro* O(1) near the topographic feature at ∼ 25.0° E (Fig. 13k and l). The enhancement of spice near this location suggests that coastal topography persistently acts as a hotspot for SMS generation (Fig. 13m and n). However, under upwelling conditions, these features become more dynamic and spatially extensive, amplifying thermohaline variability. Offshore *Ro* values remained generally low on 29 July (Fig. 13l). Interestingly, a frontal zone was beginning to develop in the 25.15–25.25° E region on 3 July (Fig. 13k), highlighting the localized and incipient character of SMS activity under downwelling conditions. Near this structure, vertical velocities were enhanced (Fig. 13i), and a modest increase in spice was seen (Fig. 13m). On 29 July, vertical velocities were more spatially extensive and intensified above sloping topography (Fig. 13j), where enhanced interlayer exchange likely contributed to the observed spice. Spice were more intense and penetrated deeper into the water column on 29 July (Fig. 13n), reflecting both vertical and lateral redistribution of thermohaline properties, consistent with subduction and frontal advection. While meridional sections showed spice becoming more confined to the upper 15 m near the coast (Fig. 11g), the zonal transect revealed broader lateral displacement along the frontal zone.

This comparison of late July upwelling and early July downwelling conditions highlights how wind forcing and topography modulate SMS activity in the GoF. Both periods were governed by stable summer stratification, and recurrent SMS features were observed near topographic structures. However, the upwelling event on 29 July triggered sharper horizontal density gradients, stronger vertical shear, elevated *Ro*, and more extensive vertical velocities. These conditions favoured frontal instabilities, subduction, and lateral advection, resulting in deeper, more structured spice. In contrast, the downwelling regime on 3 July exhibited weaker gradients and more localized, surface-confined SMS signals. Together, vertical sections and horizontal maps reveal how frontal processes and flow–topography interactions jointly control the intensity and extent of SMS variability.

4 Discussion

While satellite imagery has revealed widespread SMS variability at the sea surface in the Baltic Sea (e.g., Lavrova et al., 2018), the vertical structure and dynamics of SMS processes remain underexplored, particularly from observational datasets. In this study, we built upon earlier glider-based observations (Salm et al., 2023), which revealed subsurface

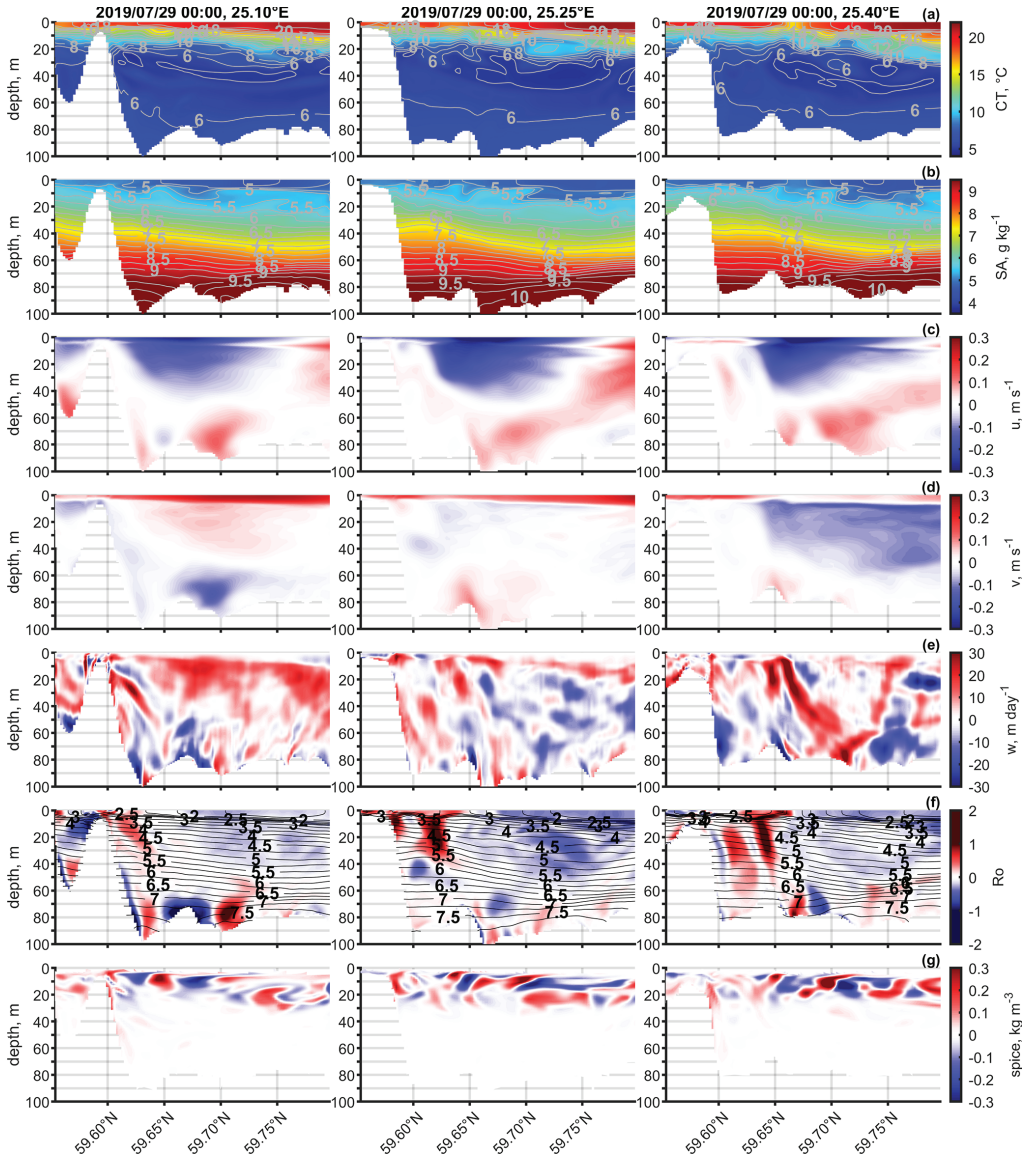


Figure 11. Vertical sections along three meridional transects at 25.10, 25.25, and 25.40° E on 29 July 2019, showing **(a)** Conservative Temperature (°C), **(b)** Absolute Salinity (g kg^{-1}), **(c)** zonal velocity u (m s^{-1}), **(d)** meridional velocity v (m s^{-1}), **(e)** vertical velocity w (m d^{-1}), **(f)** Rossby number (Ro) with overlaid isopycnals (0.25 kg m^{-3} intervals), and **(g)** spice (kg m^{-3}). Transect locations are shown in Fig. 12f.

SMS variability and highlighted the value of high-resolution autonomous measurements. We extend this work by combining observational data with numerical simulations to examine the structure and variability of SMS features more comprehensively. This combined approach provides insight into the three-dimensional nature of SMS processes and enabled us to identify clear spice-based SMS signatures in the subsurface layers, co-located with regions of Ro O(1) and $Ri < 1$ (Figs. 8a, d, e and 10), pointing to active SMS instability and mixing processes. To our knowledge, this is the first study to apply this integrated approach to investigate SMS dynamics in the GoF.

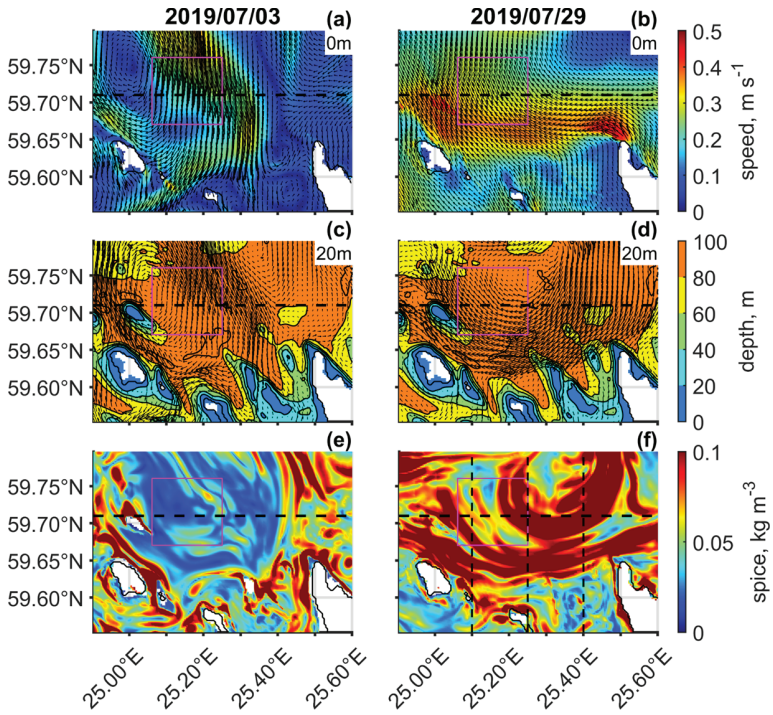


Figure 12. Comparison of surface and subsurface conditions between 3 July **(a, c, e)** and 29 July 2019 **(b, d, f)**. Panels **(a)** and **(b)** show surface horizontal velocity ($m\,s^{-1}$), panels **(c)** and **(d)** velocity vectors at 20 m depth overlaid on bathymetry, and panels **(e)** and **(f)** root mean square of spice anomaly ($kg\,m^{-3}$) in the density range limited from the surface to the depth of minimum temperature. The magenta box marks the 10×10 km study window. The horizontal black lines indicate the zonal transect shown in Fig. 13. The vertical black lines in panel **(f)** indicate the meridional transects shown in Figs. 11 and S1–S9.

The complex physical environment of the Baltic Sea is known to pose a challenge for numerical models, often resulting in biases in the simulated salinity and/or temperature fields, as well as inaccuracies in capturing the pycnoclines correctly (e.g., Gröger et al., 2022; Hordoir et al., 2019; Liblik et al., 2020; Väli et al., 2013). In this study, we showed that the model with the SMS-permitting grid spacing could simulate the development of the vertical structure of the water column and the SMS variability reasonably well. The general patterns of spice variability were consistent between measurements and simulation. The UML depth was also well captured, and the CIL was accurately reproduced during Missions I and III. However, during Mission II, the model underestimated the depth of the CIL by approximately 10 m and systematically underestimated the depth of the maximum N^2, with the largest discrepancy again occurring during Mission II (Fig. 5). Furthermore, the model did not capture the presence of occasionally observed two local maxima of N^2. These discrepancies could be related to difficulties in simulating salinity distributions in this basin (see, e.g., Westerlund et al., 2018). At the beginning of Mission I (spring 2018), the seasonal thermocline was almost absent (Fig. 3), and the salinity gradient defined the vertical density gradient. On the mentioned two occasions of two local N^2 maxima, the deeper one was largely determined by salinity, as detected by the glider. We suggest that the model does not simulate salinity distributions (which are mainly related to the large-scale advection and mixing of freshwater and saltier water) as accurately as temperature distributions (which are mostly defined by local atmospheric forcing).

Despite these limitations, the model successfully captured the key SMS patterns and associated frontal structures, providing a reliable basis for interpreting the observed events and tracer distributions. Note, for instance, the identical vertical location of the highest spice intensity in relation to the UML depth and strongest density gradient in observations and model results (Fig. 6a–c). During spring missions, the spice maximum was situated at the base of the UML, but shallower than the strongest density gradient. During the summer mission, it was located just below the strongest density gradient. Similarly, Chrysagi et al. (2021) showed that

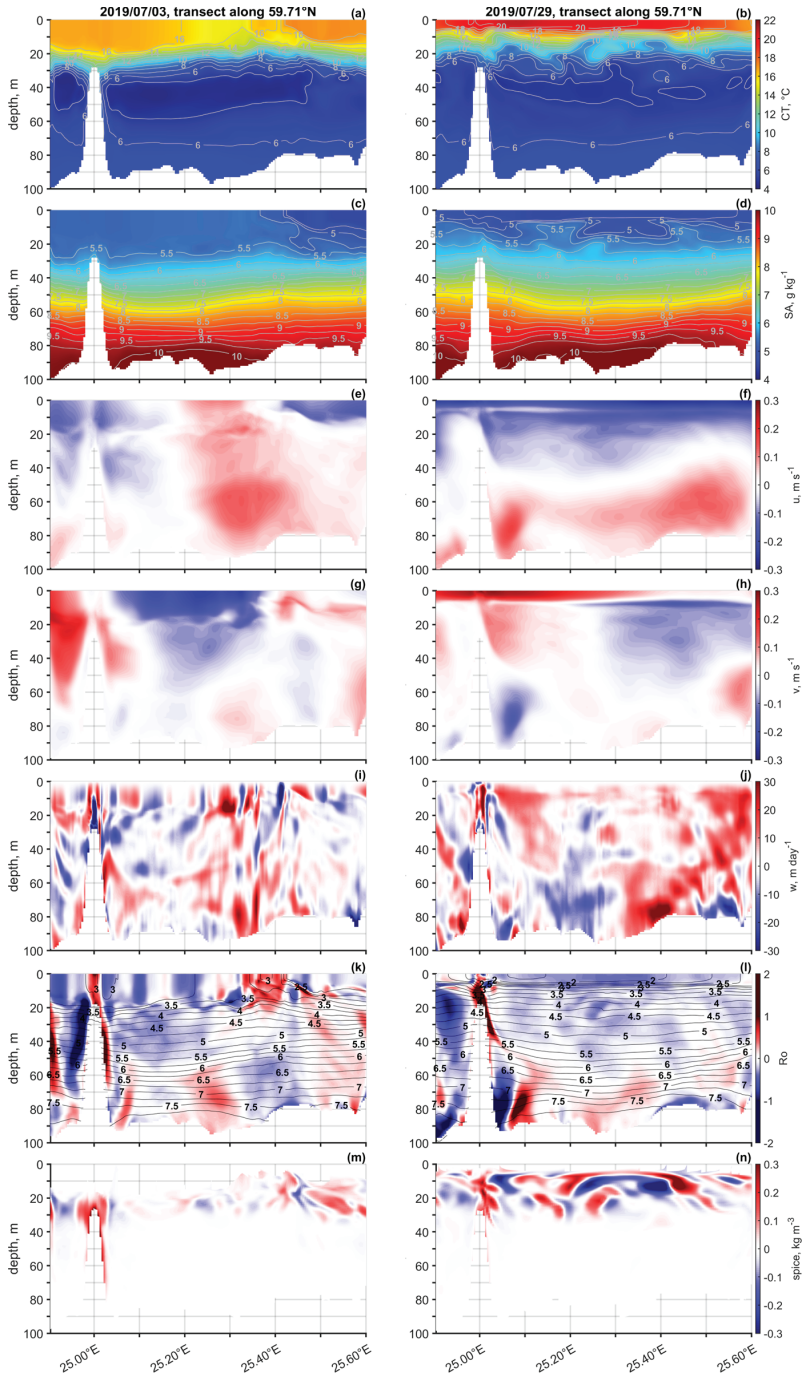


Figure 13. Vertical sections along zonal transects at 59.71° N on 3 July **(a, c, e, g, i, k, m)** and 29 July 2019 **(b, d, f, h, j, l, n)**, showing **(a, b)** Conservative Temperature (°C), **(c, d)** Absolute Salinity ($g\,kg^{-1}$), **(e, f)** zonal velocity u ($m\,s^{-1}$), **(g, h)** meridional velocity v ($m\,s^{-1}$), **(i, j)** vertical velocity w ($m\,d^{-1}$), **(k, l)** Rossby number (Ro) with overlaid isopycnals (0.25 $kg\,m^{-3}$ intervals), and **(m, n)** spice ($kg\,m^{-3}$).

a GETM simulation could replicate the structure of an observed cold SMS filament.

To interpret the SMS structures, we employed spice as a tracer. Spice, which varies from cold and fresh to warm and salty, provides a dynamically passive tracer. We defined spice through along-isopycnal temperature and salinity anomalies with respect to the spatial mean considering typical internal Rossby deformation of 4 km. While some studies compute spice across all spatial scales corresponding to the dataset to examine the spectral properties (e.g., Jaeger et al., 2020; Klymak et al., 2015), our scale-dependent definition emphasizes SMS variability by revealing patchy thermohaline structure near regions of Ro O(1) and elevated vertical velocities (e.g., Fig. 11).

Spice was consistently observed during all glider missions and throughout the modelling periods from May to August 2018 and 2019. Spice intensity tended to increase as the upper layer warmed and the seasonal thermocline developed. We argue that the observed spatial and temporal peaks in spice intensity, against the backdrop of an overall increasing trend, indicate instances with high activity of SMS processes.

Analysis of spice intensity revealed that tracer patches in the vertical structure appear as horizontally elongated features (bottom rows in Figs. 10 and 12), closely matching the estimated dimensions of SMS structures ($\sim$ 10–20 km long, $\sim$ 1 km wide) reported by Zhurbas et al. (2022). That study also suggested a vertical decoupling between SMS processes in the UML and those below. Our findings support this conceptual separation, showing that in summer months, SMS features frequently occurred below the UML (Fig. 6c), often decoupled from elevated surface Ro (Fig. 9).

Furthermore, in early June 2019, the simulation showed a small cyclonic vorticity whose periphery was outlined by elevated spice (Fig. 10b and e), consistent with observations by Yang et al. (2017), who linked such eddy peripheries with intensified mixing. These results indicate the potential of spice to reveal instances of SMS-driven energy transfer toward smaller scales.

Recent studies have shown that surface heating can suppress SMS flows, while surface cooling promotes them. However, favourable wind forcing can still enhance SMS activity under surface heating conditions (Peng et al., 2021; Shang et al., 2023). Changes or reductions in wind forcing can also trigger SMS frontal instabilities that lead to restratification of the UML, as shown by glider measurements and simulations in the Baltic Sea (Carpenter et al., 2020; Chrysagi et al., 2021; Salm et al., 2023). The development of SMS flows depends critically on horizontal buoyancy gradients (e.g., Bosse et al., 2021; Ramachandran et al., 2018;), which in GoF arise from multiple sources (e.g., Lips et al., 2016a). Predominantly positive Q promotes stratification in spring and early summer, although at different rates in coastal and open sea areas (e.g., Lips et al., 2014). Wind forcing influences the inclination of the thermocline (Liblik and Lips, 2017), while upwelling and downwelling events effectively form strong horizontal temperature, salinity and density gradients in spring–summer (e.g., Kikas and Lips, 2016). These lateral buoyancy gradients provide the energy that drives SMS processes (Boccaletti et al., 2007).

We suggest that the SMS spice maxima observed above the maximum vertical density gradient in spring, under conditions of positive Q and weak wind forcing, reflect SMS processes acting to restratify the deeper portion of the UML. The secondary peaks of spice near the sea surface in June 2018 and August 2019 (Fig. 6e and g) could be linked to a characteristic forcing pattern during these months – strong wind mixing events were followed by a period of weaker winds and positive Q. These results suggest that the SMS processes can contribute to restratifcation both near the sea surface (under positive Q) and at the base of the UML, driven by lateral buoyancy gradients, as also noted by Miracca-Lage et al. (2024). Oceanic studies have similarly demonstrated that SMS processes can strongly influence mixed layer depth (e.g., du Plessis et al., 2017), and our findings support this by showing that SMS processes (defined by spice-based signals) play a direct role in shaping the vertical stratification. This highlights the importance of resolving SMS variability in coastal models to improve predictions of stratification evolution and coastal–offshore exchanges.

Conversely, cooling (negative Q) and wind-induced turbulence contribute to the deepening of the UML. However, SMS processes can also emerge below the UML and the maximum vertical density gradient, as observed in July–August 2019, when both wind and Q were more variable. Dove et al. (2021) reported that deepening of the mixed layer in regions of high eddy kinetic energy coincided with increased spice and oxygen concentrations below the mixed layer. In our data, elevated subsurface spice in July–August 2019 did not align with the elevated Ro at the sea surface, but rather with the presence of a baroclinic coastal current. A particular example occurred at the end of July. The situation with Ro O(1) near the topographic features and outcropping isopycnals was characterized by high spice in the offshore subsurface layer (Fig. 11f and g) and intensification of vertical velocities, indicating SMS frontal subduction beneath the upwelling front (Fig. 11e). These signals, aligned with tilted isopycnals, indicate both vertical and lateral thermohaline displacement. The apparent decoupling between spice and Ro patterns likely reflects the downstream advection and transformation of SMS features beyond their generation sites, supporting a scenario of shallow subduction driven by persistent frontal tilting and vertical shear. Similar subduction along the slanted isopycnals associated with the SMS activity at the upwelling front has been described by Hosegood et al. (2017). Capo et al. (2023) further suggested that flow-topography interactions generate vorticities, which are transported offshore in the subsurface layers.

Our results from July 2019 highlight how coastal upwelling and downwelling regimes distinctly modulate SMS variability in the offshore subsurface layer (Figs. 12 and 13).

Winds favourable for upwelling (downwelling) in the southern GoF strengthen (weaken) vertical stratification and move the pycnocline upward (downward) towards the coast (Liblik and Lips, 2017). Coastal downwelling likely favours vertical turbulent mixing by reducing vertical stratification, making SMS features less visible. If SMS subduction occurs under these conditions, tracer patches are likely to be transported shoreward along slanted isopycnals beneath the downwelling-related baroclinic current. It explains a similar localized intensification of spice near the topographic features under upwelling- and downwelling-dominated conditions but with considerably weaker offshore SMS variability in the case of downwelling. This suggests that while topographic features consistently support SMS generation, upwelling enhances frontal subduction and the lateral spread of SMS structures into the basin's interior. Such upwelling-related SMS subduction acts counter to the mesoscale secondary circulation, which typically exhibits offshore surface flow and onshore subsurface return flow.

SMS subduction at fronts may contribute to the dissipation of mesoscale kinetic energy and downward transport of tracers (Archer et al., 2020), including the formation of subsurface chlorophyll maxima (e.g., Hofmann et al., 2024). By transporting phytoplankton-rich surface waters downward along sloping isopycnals, SMS processes can facilitate biomass accumulation below the pycnocline, as observed during summer in connection with anticyclonic circulation cells and SMS intrusions (Lips et al., 2010, 2011; Ruiz et al., 2019). Future analysis of collected glider data from the region, along with a comparison of spice variability with subsurface chlorophyll patchiness, could help to understand better the SMS processes and their biogeochemical impact in the Baltic Sea and similar stratified basins.

5 Conclusions

This study demonstrates that SMS variability in the Gulf of Finland is strongly modulated by both atmospheric forcing – particularly surface heat flux and wind stress – and background hydrographic structures such as mesoscale frontal gradients. Glider observations, supported by high-resolution modelling, revealed consistent spatial patterns of SMS activity, with SMS spice concentrated near the UML base in spring and within the thermocline in late summer, demonstrating the vertical sensitivity of SMS features to seasonal stratification. Wind forcing became dominant to shape the distribution of SMS anomalies when surface buoyancy input was weak. High SMS variability and subduction signatures were consistently found on the offshore side of a baroclinic coastal current, where sloped isopycnals aligned with velocity and SMS spice indicated downward and lateral transport of surface-layer waters. The integration of observations and model output allowed for extrapolation beyond individual glider transects, confirming that SMS processes in this coastal sea are both dynamically active and responsive to variations in external forcing. These results suggest the physical mechanisms that govern SMS variability and subduction in stratified coastal environments. Further studies, including high-resolution observations and modelling, are needed to understand SMS dynamics better and assess their biogeochemical consequences.

Code availability. Scripts to analyse the results are available upon request.

Data availability. The glider datasets analysed for this study can be found in online repository: https://doi.org/10.17882/96561, SEANOE (Salm et al., 2023). Model data is available upon request.

Supplement. The supplement related to this article is available online at https://doi.org/10.5194/os-21-2555-2025-supplement.

Author contributions. KS was responsible for processing the glider data, analysing observational and model data and writing of the paper with contributions from GV, TL, and UL. UL contributed to the analysis setup and supervised the work. UL, TL, and KS participated in designing the surveys and piloting the glider. GV was responsible for the modelling activities.

Competing interests. The contact author has declared that none of the authors has any competing interests.

Disclaimer. Publisher's note: Copernicus Publications remains neutral with regard to jurisdictional claims made in the text, published maps, institutional affiliations, or any other geographical representation in this paper. While Copernicus Publications makes every effort to include appropriate place names, the final responsibility lies with the authors. Also, please note that this paper has not received English language copy-editing. Views expressed in the text are those of the authors and do not necessarily reflect the views of the publisher.

Special issue statement. This article is part of the special issue "Advances in ocean science from underwater gliders". It is a result of the International Underwater Glider Conference 2024, Gothenburg, Sweden, 10–14 June 2024.

Acknowledgements. We would like to thank our colleagues and the crew of RV *Salme* for their assistance during the deployment and recovery of the glider. The computational resources from TalTech HPC are gratefully acknowledged. GETM community in Leibniz Institute for Baltic Sea Research (IOW) is gratefully acknowledged

for maintaining and supporting the model code usage and development.

Financial support. This work was supported by the Estonian Research Council grant (PRG602). The glider mission in the summer of 2019 was carried out as part of LAkHsMI (Sensors for LArge scale HydrodynaMic Imaging of ocean floor) project, which received funding from the European Union's Horizon 2020 Research and Innovation Programme grant no. 635568.

Review statement. This paper was edited by Agnieszka Beszczynska-Möller and reviewed by two anonymous referees.

References

Alenius, P., Nekrasov, A., and Myrberg, K.: Variability of the baroclinic Rossby radius in the Gulf of Finland, Cont. Shelf Res., 23, 563–573, https://doi.org/10.1016/S0278-4343(03)00004-9, 2003.

Archer, M., Schaeffer, A., Keating, S., Roughan, M., Holmes, R., and Siegelman, L.: Observations of submesoscale variability and frontal subduction within the mesoscale eddy field of the Tasman Sea, J. Phys. Oceanogr., 50, 1509–1529, https://doi.org/10.1175/JPO-D-19-0131.1, 2020.

Boccaletti, G., Ferrari, R., and Fox-Kemper, B.: Mixed layer instabilities and restratification, J. Phys. Oceanogr., 37, 2228–2250, https://doi.org/10.1175/JPO3101.1, 2007.

Bosse, A., Testor, P., Damien, P., Estournel, C., Marsaleix, P., Mortier, L., Prieur, L., and Taillandier, V.: Wind-forced submesoscale symmetric instability around deep convection in the Northwestern Mediterranean Sea, Fluids, 6, 123, https://doi.org/10.3390/fluids6030123, 2021.

Burchard, H. and Bolding, K.: Comparative analysis of four second-moment turbulence closure models for the oceanic mixed layer, J. Phys. Oceanogr., 31, 1943–1968, https://doi.org/10.1175/1520-0485(2001)031<1943:CAOFSM>2.0.CO;2, 2001.

Burchard, H. and Bolding, K.: GETM – a general estuarine transport model, Scientific Documentation, Tech. Rep., EUR 20253 EN, Tech. Rep. European Commission, Ispra, Italy, https://op.europa.eu/en/publication-detail/-/publication/5506bf19-e076-4d4b-8648-dedd06efbb38 (last access: 1 October 2025), 2002.

Canuto, V. M., Howard, A., Cheng, Y., and Dubovikov, M. S.: Ocean turbulence. Part I: One-point closure model-momentum and heat vertical diffusivities, J. Phys. Oceanogr., 31, 1413–1426, https://doi.org/10.1175/1520-0485(2001)031<1413:OTPIOP>2.0.CO;2, 2001.

Capet, X., McWilliams, J. C., Molemaker, M. J., and Shchepetkin, A. F.: Mesoscale to submesoscale transition in the California Current system. Part III: Energy balance and flux, J. Phys. Oceanogr., 38, 2256–2269, https://doi.org/10.1175/2008JPO3810.1, 2008.

Capo, E., McWilliams, J. C., and Jagannathan, A.: Flow-topography interaction along the Spanish slope in the Alboran Sea: Vorticity generation and connection to interior fronts, J. Geophys. Res.-Oceans, 128, e2022JC019480, https://doi.org/10.1029/2022JC019480, 2023.

Carpenter, J. R., Rodrigues, A., Schultze, L. K. P., Merckelbach, L. M., Suzuki, N., Baschek, B., and Umlauf, L.: Shear instability and turbulence within a submesoscale front following a storm, Geophys. Res. Lett., 47, https://doi.org/10.1029/2020GL090365, 2020.

Chrysagi, E., Umlauf, L., Holtermann, P., Klingbeil, K., and Burchard, H.: High-resolution simulations of submesoscale processes in the Baltic Sea: The role of storm events, J. Geophys. Res.-Oceans, 126, https://doi.org/10.1029/2020JC016411, 2021.

Dove, L. A., Thompson, A. F., Balwada, D., and Gray, A. R.: Observational evidence of ventilation hotspots in the Southern Ocean, J. Geophys. Res.-Oceans, 126, https://doi.org/10.1029/2021JC017178, 2021.

du Plessis, M., Swart, S., Ansorge, I. J., and Mahadevan, A.: Submesoscale processes promote seasonal restratification in the Subantarctic Ocean, J. Geophys. Res.-Oceans, 122, 2960–2975, https://doi.org/10.1002/2016JC012494, 2017.

Elken, J., Nõmm, M., and Lagemaa, P.: Circulation patterns in the Gulf of Finland derived from the EOF analysis of model results, Boreal Environ. Res., 16, 84–102, 2011.

Gräwe, U., Holtermann, P., Klingbeil, K., and Burchard, H.: Advantages of vertically adaptive coordinates in numerical models of stratified shelf seas, Ocean Model., 92, 56–68, https://doi.org/10.1016/j.ocemod.2015.05.008, 2015.

Gröger, M., Placke, M., Meier, H. E. M., Börgel, F., Brunnabend, S. E., Dutheil, C., Gräwe, U., Hieronymus, M., Neumann, T., Radtke, H., Schimanke, S., Su, J., and Väli, G.: The Baltic Sea Model Intercomparison Project (BMIP) – a platform for model development, evaluation, and uncertainty assessment, Geosci. Model Dev., 15, 8613–8638, https://doi.org/10.5194/gmd-15-8613-2022, 2022.

Hersbach, H., Bell, B., Berrisford, P., Hirahara, S., Horányi, A., Muñoz-Sabater, J., Nicolas, J., Peubey, C., Radu, R., Schepers, D., Simmons, A., Soci, C., Abdalla, S., Abellan, X., Balsamo, G., Bechtold, P., Biavati, G., Bidlot, J., Bonavita, M., De Chiara, G., Dahlgren, P., Dee, D., Diamantakis, M., Dragani, R., Flemming, J., Forbes, R., Fuentes, M., Geer, A., Haimberger, L., Healy, S., Hogan, R. J., Hólm, E., Janisková, M., Keeley, S., Laloyaux, P., Lopez, P., Lupu, C., Radnoti, G., de Rosnay, P., Rozum, I., Vamborg, F., Villaume, S., and Thépaut, J. N.: The ERA5 global reanalysis, Q. J. Roy. Meteorol. Soc., 146, 1999–2049, https://doi.org/10.1002/qj.3803, 2020.

Hofmann, Z., von Appen, W.-J., Kanzow, T., Becker, H., Hagemann, J., Hufnagel, L., and Iversen, M. H.: Stepwise subduction observed at a front in the marginal ice zone in Fram Strait, J. Geophys. Res.-Oceans, 129, e2023JC020641, https://doi.org/10.1029/2023JC020641, 2024.

Hofmeister, R., Burchard, H., and Beckers, J. M.: Non-uniform adaptive vertical grids for 3D numerical ocean models, Ocean Model., 33, 70–86, https://doi.org/10.1016/j.ocemod.2009.12.003, 2010.

Hordoir, R., Axell, L., Höglund, A., Dieterich, C., Fransner, F., Gröger, M., Liu, Y., Pemberton, P., Schimanke, S., Andersson, H., Ljungemyr, P., Nygren, P., Falahat, S., Nord, A., Jönsson, A., Lake, I., Döös, K., Hieronymus, M., Dietze, H., Löptien, U., Kuznetsov, I., Westerlund, A., Tuomi, L., and Haapala, J.: Nemo-Nordic 1.0: a NEMO-based ocean model for the Baltic and North

seas – research and operational applications, Geosci. Model Dev., 12, 363–386, https://doi.org/10.5194/gmd-12-363-2019, 2019.

Hosegood, P. J., Nightingale, P. D., Rees, A. P., Widdicombe, C. E., Woodward, E. M. S., Clark, D. R., and Torres, R. J.: Nutrient pumping by submesoscale circulations in the mauritanian upwelling system, Prog. Oceanogr., 159, 223–236, https://doi.org/10.1016/j.pocean.2017.10.004, 2017.

Jaeger, G. S., Mackinnon, J. A., Lucas, A. J., Shroyer, E., Nash, J., Tandon, A., Farrar, J. T., and Mahadevan, A.: How spice is stirred in the Bay of Bengal, J. Phys. Oceanogr., 50, 2669–2688, https://doi.org/10.1175/JPO-D-19-0077.s1, 2020.

Jhugroo, K., O'Callaghan, J., Stevens, C. L., Macdonald, H. S., Elliott, F., and Hadfield, M. G.: Spatial Structure of Low Salinity Submesoscale Features and Their Interactions With a Coastal Current, Front. Mar. Sci., 7, 557360, https://doi.org/10.3389/fmars.2020.557360, 2020.

Kikas, V. and Lips, U.: Upwelling characteristics in the Gulf of Finland (Baltic Sea) as revealed by Ferrybox measurements in 2007–2013, Ocean Sci., 12, 843–859, https://doi.org/10.5194/os-12-843-2016, 2016.

Klingbeil, K., Lemarié, F., Debreu, L., and Burchard, H.: The numerics of hydrostatic structured-grid coastal ocean models: State of the art and future perspectives, Ocean Model., 125, 80–105, https://doi.org/10.1016/j.ocemod.2018.01.007, 2018.

Klymak, J. M., Crawford, W., Alford, M. H., Mackinnon, J. A., and Pinkel, R.: Along-isopycnal variability of spice in the North Pacific, J. Geophys. Res.-Oceans, 120, 2287–2307, https://doi.org/10.1002/2013JC009421, 2015.

Kondo, J.: Air-sea bulk transfer coefficients in diabatic conditions, Bound.-Lay. Meteorol., 9, 91–112, https://doi.org/10.1007/BF00232256, 1975.

Krauss, W. and Brügge, B.: Wind-produced water exchange between the deep basins of the Baltic Sea, J. Phys. Oceanogr., 21, 373–384, https://doi.org/10.1175/1520-0485(1991)021<0373:WPWEBT>2.0.CO;2, 1991.

Lavrova, O. Y., Krayushkin, E. V., Strochkov, A. Y., and Nazirova, K. R.: Vortex structures in the Southeastern Baltic Sea: satellite observations and concurrent measurements, Proceedings Volume 10784, Remote Sensing of the Ocean, Sea Ice, Coastal Waters, and Large Water Regions, 2018, 1078404, https://doi.org/10.1117/12.2325463, 2018.

Lehmann, A., Myrberg, K., and Höflich, K.: A statistical approach to coastal upwelling in the Baltic Sea based on the analysis of satellite data for 1990–2009, Oceanologia, 54, 369–393, https://doi.org/10.5697/oc.54-3.369, 2012.

Liblik, T. and Lips, U.: Variability of pycnoclines in a three-layer, large estuary: the Gulf of Finland, Boreal Environ. Res., 22, 27–47, 2017.

Liblik, T., Väli, G., Lips, I., Lilover, M. J., Kikas, V., and Laanemets, J.: The winter stratification phenomenon and its consequences in the Gulf of Finland, Baltic Sea, Ocean Sci., 16, 1475–1490, https://doi.org/10.5194/os-16-1475-2020, 2020.

Liblik, T., Väli, G., Salm, K., Laanemets, J., Lilover, M. J., and Lips, U.: Quasi-steady circulation regimes in the Baltic Sea, Ocean Sci., 18, 857–879, https://doi.org/10.5194/os-18-857-2022, 2022.

Lilover, M. J., Elken, J., Suhhova, I., and Liblik, T.: Observed flow variability along the thalweg, and on the coastal slopes of the Gulf of Finland, Baltic Sea, Estuar. Coast. Shelf Sci., 195, 23–33, https://doi.org/10.1016/j.ecss.2016.11.002, 2017.

Lindström, G., Pers, C., Rosberg, J., Strömqvist, J., and Arheimer, B.: Development and testing of the HYPE (Hydrological Predictions for the Environment) water quality model for different spatial scales, Hydrol. Res., 41, 295–319, https://doi.org/10.2166/nh.2010.007, 2010.

Lips, I., Lips, U., and Liblik, T: Consequences of coastal upwelling events on physical and chemical patterns in the central Gulf of Finland (Baltic Sea), Cont. Shelf Res., 29, 1836–1847, https://doi.org/10.1016/j.csr.2009.06.010, 2009.

Lips, I., Rünk, N., Kikas, V., Meerits, A., and Lips, U.: High-resolution dynamics of the spring bloom in the Gulf of Finland of the Baltic Sea, J. Mar. Syst., 129, 135–149, https://doi.org/10.1016/j.jmarsys.2013.06.002, 2014.

Lips, U., Lips, I., Liblik, T., and Kuvaldina, N.: Processes responsible for the formation and maintenance of sub-surface chlorophyll maxima in the Gulf of Finland, Estuar. Coast. Shelf Sci., 88, 339–349, https://doi.org/10.1016/j.ecss.2010.04.015, 2010.

Lips, U., Lips, I., Liblik, T., Kikas, V., Altoja, K., Buhhalko, N., and Rünk, N.: Vertical dynamics of summer phytoplankton in a stratified estuary (Gulf of Finland, Baltic Sea), Ocean Dynam., 61, 903–915, https://doi.org/10.1007/s10236-011-0421-8, 2011.

Lips, U., Kikas, V., Liblik, T., and Lips, I.: Multi-sensor in situ observations to resolve the sub-mesoscale features in the stratified Gulf of Finland, Baltic Sea, Ocean Sci., 12, 715–732, https://doi.org/10.5194/os-12-715-2016, 2016a.

Lips, U., Zhurbas, V., Skudra, M., and Väli, G.: A numerical study of circulation in the Gulf of Riga, Baltic Sea. Part I: Whole-basin gyres and mean currents, Cont. Shelf Res., 112, 1–13, https://doi.org/10.1016/j.csr.2015.11.008, 2016b.

Lips, U., Laanemets, J., Lips, I., Liblik, T., Suhhova, I., and Sonaar, Ü.: Wind-driven residual circulation and related oxygen and nutrient dynamics in the Gulf of Finland (Baltic Sea) in winter, Estuar. Coast. Shelf Sci., 195, 4–15, https://doi.org/10.1016/j.ecss.2016.10.006, 2017.

Mahadevan, A.: The impact of submesoscale physics on primary productivity of plankton, Annu. Rev. Mar. Sci., 8, 161–184, https://doi.org/10.1146/annurev-marine-010814-015912, 2016.

McDougall, T. and Barker, P. M.: Getting started with TEOS-10 and the Gibbs Seawater (GSW) Oceanographic Toolbox, SCOR/IAPSO WG127, 28 pp., ISBN 978-0-646-55621-5, https://www.teos-10.org/software.htm (last access: 1 October 2025), 2011.

Miracca-Lage, M., Becherer, J., Merckelbach, L., Bosse, A., Testor, P., and Carpenter, J. R.: Rapid restratification processes control mixed layer turbulence and phytoplankton growth in a deep convection region, Geophys. Res. Lett., 51, e2023GL107336, https://doi.org/10.1029/2023GL107336, 2024.

Naveira Garabato, A. C., Yu, X., Callies, J., Barkan, R., Polzin, K. L., Frajka-Williams, E. E., Buckingham, C. E., and Griffies, S. M.: Kinetic energy transfers between mesoscale and submesoscale motions in the open ocean's upper layers, J. Phys. Oceanogr., 52, 75–97, https://doi.org/10.1175/JPO-D-21-0099.1, 2022.

Peng, J.-P., Dräger-Dietel, J., North, R. P., and Umlauf, L.: Diurnal variability of frontal dynamics, instability, and turbulence in a submesoscale upwelling filament, J. Phys. Oceanogr., 51, 2825–2843, https://doi.org/10.1175/JPO-D-21-0033.1, 2021.

Ramachandran, S., Tandon, A., Mackinnon, J., Lucas, A. J., Pinkel, R., Waterhouse, A. F., Nash, J., Shroyer, E., Mahadevan, A., Weller, R. A., and Farrar, J. T.: Submesoscale processes at shallow salinity fronts in the Bay of Bengal: Observations during the winter monsoon, J. Phys. Oceanogr., 48, 479–509, https://doi.org/10.1175/JPO-D-16-0283.1, 2018.

Rudnick, D. L. and Cole, S. T.: On sampling the ocean using underwater gliders, J. Geophys. Res.-Oceans, 116, https://doi.org/10.1029/2010JC006849, 2011.

Rudnick, D. L. and Ferrari, R.: Compensation of horizontal temperature and salinity gradients in the ocean mixed layer, Science, 283, 526–529, https://doi.org/10.1126/science.283.5401.526, 1999.

Ruiz, S., Claret, M., Pascual, A., Olita, A., Troupin, C., Capet, A., Tovar-Sánchez, A., Allen, J., Poulain, P.-M., Tintoré, J., and Mahadevan, A.: Effects of oceanic mesoscale and submesoscale frontal processes on the vertical transport of phytoplankton, J. Geophys. Res.-Oceans, 124, 5999–6014, https://doi.org/10.1029/2019JC015034, 2019.

Salm, K., Liblik, T., and Lips, U.: Submesoscale variability in a mesoscale front captured by a glider mission in the Gulf of Finland, Baltic Sea, Front. Mar. Sci., 10, https://doi.org/10.3389/fmars.2023.984246, 2023.

Salm, K., Väli, G., Liblik, T., and Lips, U.: Glider missions in the Gulf of Finland, Baltic Sea 2018–2019 [data set], SEANOE, https://doi.org/10.17882/96561 (last access: 1 October 2025), 2023.

Shang, X., Shu, Y., Wang, D., Yu, J., Mao, H., Liu, D., Qiu, C., and Tang, H.: Submesoscale motions driven by down-front wind around an anticyclonic eddy with a cold core, J. Geophys. Res.-Oceans, 128, https://doi.org/10.1029/2022JC019173, 2023.

Siht, E., Väli, G., Liblik, T., Mishra, A., Buhhalko, N., and Lips, U.: Modeling the pathways of microplastics in the Gulf of Finland, Baltic Sea – sensitivity of parametrizations, Ocean Dynam., 75, 9, https://doi.org/10.1007/s10236-024-01649-0, 2025.

Suursaar, Ü. and Aps, R.: Spatio-temporal variations in hydrophysical and -chemical parameters during a major upwelling event off the southern coast of the Gulf of Finland in summer 2006, Oceanologia, 49, 209–228, 2007.

Tarry, D. R., Ruiz, S., Johnston, T. M. S., Poulain, P.-M., Özgökmen, T., Centurioni, L. R., Berta, M., Esposito, G., Farrar, J. T., Mahadevan, A., and Pascual, A.: Drifter observations reveal intense vertical velocity in a surface ocean front, Geophys. Res. Lett., 49, e2022GL098969, https://doi.org/10.1029/2022GL098969, 2022.

Taylor, J. R. and Thompson, A. F.: Submesoscale dynamics in the upper ocean, Annu. Rev. Fluid Mech., 55, 103–127, https://doi.org/10.1146/annurev-fluid-031422-095147, 2023.

Thomas, L. N., Tandon, A., and Mahadevan, A.: Submesoscale processes and dynamics, Geophys. Monogr. Ser., 177, 17–38, https://doi.org/10.1029/177GM04, 2008.

Uiboupin, R. and Laanemets, J.: Upwelling characteristics derived from satellite sea surface temperature data in the Gulf of Finland, Baltic Sea, Boreal Environ. Res., 14, 297–304, 2009.

Umlauf, L. and Burchard, H.: Second-order turbulence closure models for geophysical boundary layers. A review of recent work, Cont. Shelf Res., 25, 795–827, https://doi.org/10.1016/j.csr.2004.08.004, 2005.

Väli, G., Meier, H. E. M., and Elken, J.: Simulated halocline variability in the baltic sea and its impact on hypoxia during 1961–2007, J. Geophys. Res.-Oceans, 118, 6982–7000, https://doi.org/10.1002/2013JC009192, 2013.

Väli, G., Zhurbas, V., Lips, U., and Laanemets, J.: Submesoscale structures related to upwelling events in the Gulf of Finland, Baltic Sea (numerical experiments), J. Mar. Syst., 171, 31–42, https://doi.org/10.1016/j.jmarsys.2016.06.010, 2017.

Väli, G., Meier, H. E. M., Placke, M., and Dieterich, C.: River runoff forcing for ocean modeling within the Baltic Sea Model Intercomparison Project, Marine Sci. Rep., 113, https://doi.org/10.12754/msr-2019-0113, 2019.

Väli, G., Meier, H. E. M., Liblik, T., Radtke, H., Klingbeil, K., Gräwe, U., and Lips, U.: Submesoscale processes in the surface layer of the central Baltic Sea: A high-resolution modelling study, Oceanologia, 66, 78–90, https://doi.org/10.1016/j.oceano.2023.11.002, 2024.

Westerlund, A., Tuomi, L., Alenius, P., Miettunen, E., and Vankevich, R. E.: Attributing mean circulation patterns to physical phenomena in the Gulf of Finland, Oceanologia, 60, 16–31, https://doi.org/10.1016/j.oceano.2017.05.003, 2018.

Westerlund, A., Tuomi, L., Alenius, P., Myrberg, K., Miettunen, E., Vankevich, R. E., and Hordoir, R.: Circulation patterns in the Gulf of Finland from daily to seasonal timescales, Tellus A, 71, https://doi.org/10.1080/16000870.2019.1627149, 2019.

Wong, A., Keeley, R., Carval, T., and the Argo Data Management Team: Argo Quality Control Manual for CTD and Trajectory Data, ARCHIMER, https://doi.org/10.13155/33951, 2025.

Yang, Q., Zhao, W., Liang, X., Dong, J., and Tian, J.: Elevated mixing in the periphery of mesoscale eddies in the South China Sea, J. Phys. Oceanogr., 47, 895–907, https://doi.org/10.1175/JPO-D-16-0256.1, 2017.

Zhurbas, V., Väli, G., Golenko, M., and Paka, V.: Variability of bottom friction velocity along the inflow water pathway in the Baltic Sea, J. Mar. Syst., 184, 50–58, https://doi.org/10.1016/j.jmarsys.2018.04.008, 2018.

Zhurbas, V., Väli, G., and Kuzmina, N.: Striped texture of submesoscale fields in the northeastern Baltic Proper: Results of very high-resolution modelling for summer season, Oceanologia, 64, 1–21, https://doi.org/10.1016/j.oceano.2021.08.003, 2022.

Publication III

Lips, U.; Salm, K.; Väli, G.; Liblik, T.; Arneborg, L.; Biddle, L. C.; Bulczak, A. I.; Chrysagi, E.; Falarz, M.; Holtermann, P.; Jakacki, J.; Meier, H. E. M.; Mohrmann, M.; Myrberg, K.; Pemberton, P.; Umlauf, L. (2026). Submesoscale dynamics in the Baltic Sea – a review. Progress in Oceanography, 245, #103746. DOI: 10.1016/j.pocean.2026.103746.

Progress in Oceanography 245 (2026) 103746

Contents lists available at ScienceDirect

Progress in Oceanography

journal homepage: www.elsevier.com/locate/pocean

Review

Submesoscale dynamics in the Baltic Sea – a review

Urmas Lips [a,*], Kai Salm [a], Germo Väli [a], Taavi Liblik [a], Lars Arneborg [b], Louise C. Biddle [c], Anna I. Bulczak [d], Evridiki Chrysagi [e,f], Małgorzata Falarz [g], Peter Holtermann [f], Jaromir Jakacki [d], H. E. Markus Meier [f], Martin Mohrmann [c], Kai Myrberg [h], Per Pemberton [b], Lars Umlauf [f]

[a] Department of Marine Systems, Tallinn University of Technology, Akadeemia Rd. 15a, 12618 Tallinn, Estonia
[b] Department of Research and Development, Swedish Meteorological and Hydrological Institute, Göteborgseskaderns Plats 3, 426 71 Västra Frölunda, Sweden
[c] Voice of the Ocean Foundation, Skeppet Árans Väg 19, 426 71 Västra Frölunda, Sweden
[d] Physical Oceanography Department, Institute of Oceanology Polish Academy of Sciences, Sopot, Poland
[e] Institute of Oceanography, University of Hamburg, Bundesstr. 53, 20146 Hamburg, Germany
[f] Department of Physical Oceanography, Leibniz Institute for Baltic Sea Research Warnemünde, Seestrasse 15, 18119 Rostock, Germany
[g] Faculty of Natural Sciences, University of Silesia in Katowice, ul. Bedzinska 60, 41-200 Sosnowiec, Poland
[h] Finnish Environment Institute, Latokartanonkaari 11, 00790 Helsinki, Finland

ARTICLE INFO

Keywords:
Submesoscale
Baltic Sea
Instabilities
Stratification
Mixing
Subduction
Energy transfer

ABSTRACT

The main aim of this work is to provide a comprehensive literature review of the current state of knowledge on submesoscale (SMS) dynamics in the Baltic Sea, with potential implications for other similar coastal and marginal seas. Relevant spatial and temporal scales in the Baltic Sea, as well as idealized quantitative descriptions of SMS instabilities, are presented. The methods for studying SMS processes are described, and the availability of the required research infrastructure and relevant data is discussed. The knowledge on SMS processes and their role in coastal-offshore exchanges, vertical and horizontal mixing, and the development of stratification in the Baltic Sea is reviewed and compared with studies in other regions. Processes at adjacent scales and their links to SMS dynamics, including mesoscale features such as upwelling events, fronts, and baroclinic currents in geostrophic balance, as well as small-scale turbulence, are described. This analysis demonstrates that SMS processes may substantially influence large-scale dynamics of the Baltic Sea, challenging the classical understanding of energy transfer across spatial scales that omits instabilities and feedback loops in the SMS range. The review suggests that SMS processes play a role in the biogeochemical functioning of the Baltic Sea by providing vertical fluxes of substances and redistributing plankton biomass. We emphasize that extensive model validation with high-resolution in-situ data remains an urgent task, and a more accurate description of SMS processes in sub-grid parameterizations within large-scale models is necessary. Gaps in knowledge of SMS dynamics and potential further steps to address them are highlighted.

1. Introduction

Submesoscale (SMS) processes in the ocean occupy spatial scales between geostrophically balanced mesoscale processes and small-scale turbulence, while their temporal scales range from hours to days (Taylor and Thompson, 2023). SMS processes are dynamically characterized by O(1) Rossby (Ro) and balanced Richardson (Ri_b) numbers (Thomas et al., 2008). The former implies that SMS are still influenced but not firmly constrained by the Earth's rotation, indicating that they are associated with large vertical vorticity and thus can enhance fluxes between the surface layer and the ocean interior (Callies et al., 2015). The latter implies that in the presence of horizontal buoyancy gradients, the SMS flows can emerge and restratify the water column (Yu et al., 2019). Submesoscales are therefore particularly prominent in the surface and bottom boundary layers, where horizontal buoyancy gradients are abundant and vertical stratification is weak, contributing significantly to ocean dynamics (Dong et al., 2024) and biogeochemistry (Lévy et al., 2012; Gray et al., 2024). SMS processes provide a pathway for the energy transfer from the mesoscale to smaller scales, ultimately leading to microscale dissipation and diapycnal mixing (McWilliams, 2016;

* Corresponding author.
E-mail address: urmas.lips@taltech.ee (U. Lips).

https://doi.org/10.1016/j.pocean.2026.103746
Received 22 November 2025; Received in revised form 6 April 2026; Accepted 22 April 2026
Available online 30 April 2026
0079-6611/© 2026 The Author(s). Published by Elsevier Ltd. This is an open access article under the CC BY license (http://creativecommons.org/licenses/by/4.0/).

Naveira Garabato et al., 2022). SMS processes may play a role in the global heat budget (Su et al., 2018), and it has been argued that their inaccurate parametrization in coarse-scale ocean (climate) models can cause biases in long-term forecasts (Taylor and Thompson, 2023).

Based on idealized analyses of instabilities, various mechanisms have been suggested that create variability at the submesoscale (Gula et al., 2022; Taylor and Thompson, 2023). SMS baroclinic instability (BI) follows a similar logic to mesoscale instability of large-scale flows (Eady, 1949). Since vertical stratification in the surface mixed layer (SML) is weak, eddies that develop due to BI have smaller spatial scales in the SML than in the ocean pycnocline. Such instability leads to a restratifying buoyancy flux (Boccaletti et al., 2007; Fox-Kemper et al., 2008; Chrysagi et al., 2021), significantly affecting the depth of the mixed layer. Another type of instability – symmetric instability (SI) – develops in stably stratified flows when potential vorticity takes the opposite sign of the Coriolis parameter due to baroclinic effects (Taylor and Ferrari, 2009; Arobone and Sarkar, 2015). SI (Thomas et al., 2013) can be forced, for instance, by surface cooling or downfront winds (directed along the frontal jet). SI and ageostrophic secondary circulation at SMS fronts (McWilliams, 2021) can induce substantial vertical fluxes and subduction of surface waters (Pham et al., 2024).

The main physical forcing components for the Baltic Sea system are atmospheric forcing, including the exchange of heat and freshwater through the sea surface, and the input of freshwater from rivers and saltier water through the Danish Straits (Omstedt et al., 2004). In response to the external forcing, internal dynamics of the system at multiple temporal and spatial scales shape the observed layered structure of the water column, typical lateral gradients of tracers (e.g., salinity), and general circulation of the Baltic Sea (Elken and Matthäus, 2008; Leppäranta and Myrberg, 2009). While the role of mesoscale processes (eddies, fronts, upwelling/downwelling) in the Baltic Sea dynamics is well recognized (Aitsam et al., 1984; Kononen et al., 1996; Vortmeyer-Kley et al., 2016, 2019), the contribution of SMS processes is poorly understood.

An overview of mixing processes in the Baltic Sea by Reissmann et al. (2009) did not explicitly mention SMS processes. However, more recent reviews of physical oceanography (Omstedt et al., 2014), salinity dynamics (Lehmann et al., 2022), and water exchange (Elken and Omstedt, 2025) stress the need for better understanding of small-scale (including SMS) processes and their impact on general, overturning circulation (Döös et al., 2004; Placke et al., 2021). Nevertheless, the variability at the submesoscale and SMS processes in the Baltic Sea have been receiving more attention in recent years, driven by advances in in-situ observations, remote sensing, and numerical modeling (e.g., Lips et al., 2011, 2016a; Liblik and Lips, 2012; Gurova and Chubarenko, 2012; Liblik et al., 2017; Väli et al., 2017, 2024, 2025; Carpenter et al., 2020; Chrysagi et al., 2021, 2022; Salm et al., 2023, 2025; Hariri et al., 2024, 2025; Lilover et al., 2025). A typical example of small-scale inhomogeneities in a cyanobacterial bloom in the Baltic Sea, which can be attributed to the action of SMS processes, is presented in Fig. 1 (ESA Copernicus, Sentinel-2, 8 August 2022; Lilover et al., 2025). We suggest that the synthesis of mixing processes in the Baltic Sea by Reissmann et al. (2009) could be complemented by considering also processes at scales between mesoscale and microscale, their effects, and links to processes and variability at other scales.

SMS processes, with spatial scales from 200 m to 20 km in the ocean (Capet et al., 2008; Taylor and Thompson, 2023), have slightly smaller sizes in the Baltic Sea (Väli et al., 2017) due to its location at relatively high latitudes and shallowness (Fig. 2a), as well as the layered structure of the water column. They are more abundant in the presence of intense mesoscale processes, including mesoscale straining and frontogenesis (Gula et al., 2022; Adams et al., 2017), suggesting their significant role in Baltic Sea dynamics (Lips et al., 2016a). Due to its configuration and stratified water column, local wind forcing generates coastal upwelling and downwelling events characterized by mesoscale baroclinic fronts and currents (Myrberg and Andrejev, 2003; Suursaar and Aps, 2007; Lips et al., 2009; Lehmann et al., 2012). Furthermore, faster warming in shallow areas (Lips et al., 2014), wind-driven cross-shore inclination of pycnoclines (Liblik and Lips, 2017), and riverine water spreading (Stipa et al., 1999; Beszczyńska-Möller, 1999; Lips et al., 2017; Liblik et al., 2020) create horizontal buoyancy gradients that are conducive to SMS development. Thus, the Baltic Sea serves as a natural laboratory for investigating SMS processes due to the ubiquitous lateral density gradients generated by salinity differences and wind-driven upwelling events and fronts. We can test existing SMS concepts here and generate new knowledge that may be relevant elsewhere, especially regarding complex and heterogeneous coastal ocean submesoscales that are difficult to parameterize.

On the other hand, since Baltic Sea conditions are favorable for the development and action of SMS processes, their inclusion is crucial for understanding the dynamics of the Baltic Sea. SMS processes are inherently 3D and contribute to both horizontal and vertical transport and mixing. Acting alongside other processes at a multitude of scales, they alter vertical stratification (Carpenter et al., 2020; Chrysagi et al., 2021), drive exchanges between coastal and offshore regions (Väli et al., 2024) and surface and subsurface layers (Salm et al., 2025), as well as

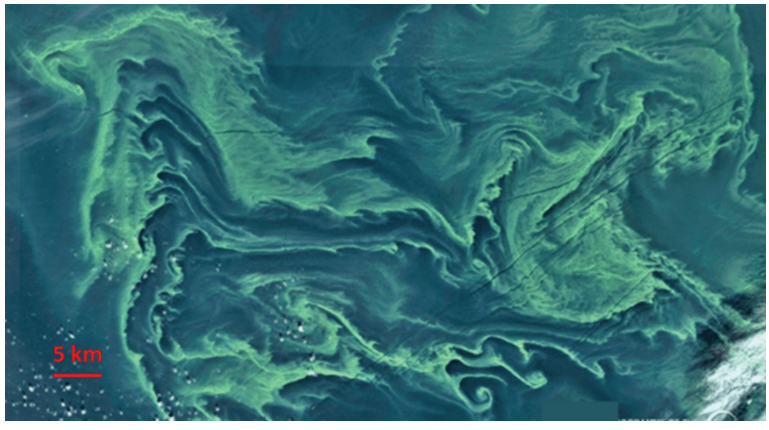


Fig. 1. Satellite image depicts small-scale inhomogeneities in a cyanobacterial bloom in the Baltic Sea (entrance area of the Gulf of Finland, 8 August 2022, European Union, Copernicus Sentinel-2 imagery processed by @DEFIS_Eu). The size of the image is about 90 × 50 km, and its location is shown in Fig. 2b. (from Lilover et al., 2025).

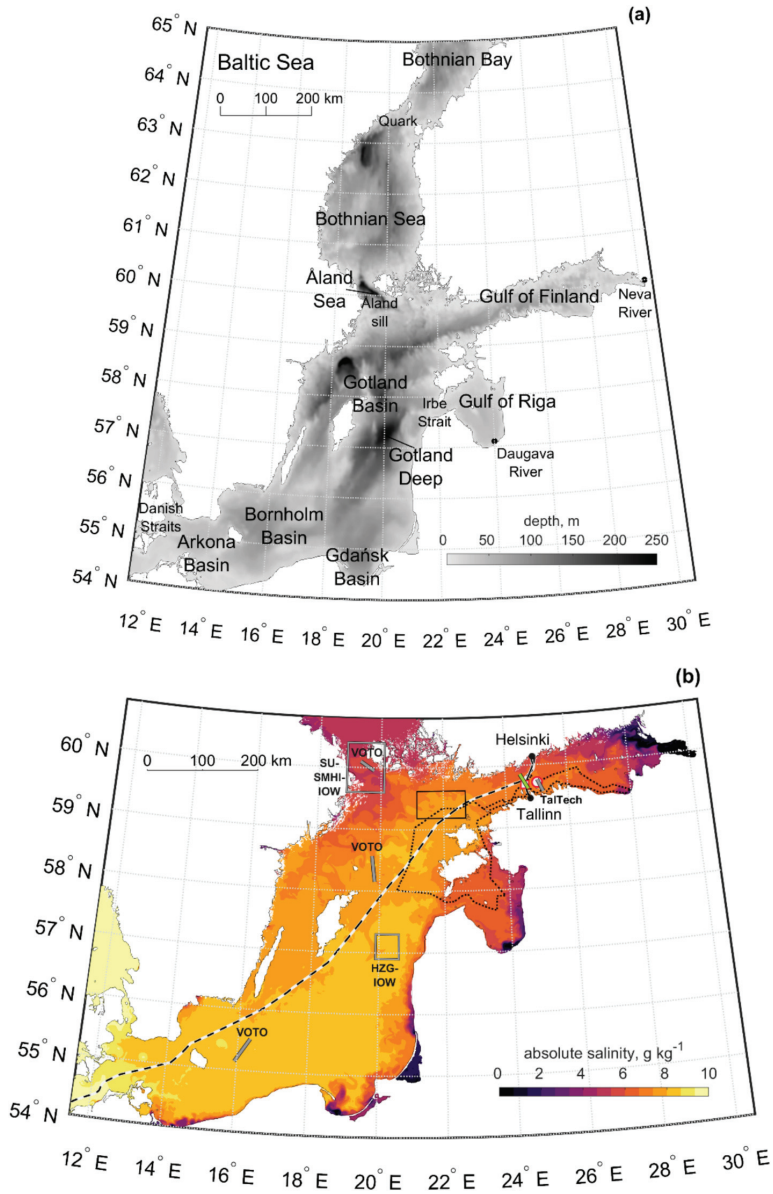


Fig. 2. (a) Baltic Sea bathymetry with sub-basin names and referred sites. (b) Surface salinity distribution in the Baltic Sea (example from a high-resolution, grid step 250 m, simulation by Väli et al. (2024) on 4 April 2017). Black rectangle shows the location of the photo in Fig. 1. Referred study locations and transects are indicated as follows: solid black line – Tallinn-Helsinki, black-white line – Helsinki-Travemünde, dotted line – r/v Salme ferrybox; red circle and square – profilers in the Gulf of Finland; green line – scanfish section; gray lines – glider sections; and gray rectangles – study sites in the Gotland Deep (HZG-IOW) and Aland Sea (SU-SMHI-IOW).

influence larger-scale dynamics (Väli et al., 2025). Intermittent occurrence of SMS processes indicates the conditions under which the coastal-offshore exchange is most intense (Väli et al., 2024) and where the hotspots of estuarine mixing emerge (Henell et al., 2023). Since SMS processes significantly influence the development of seasonal stratification and mixing, they in turn influence productivity (Cahill et al., 2024; Vortmeyer-Kley et al., 2025) and distribution of plankton (Lips et al., 2011; Lips and Lips, 2017), as well as carbon fluxes, as shown in other sea areas (e.g., Omand et al., 2015).

Although SMS phenomena are particularly prominent in SML, they can also emerge in the ocean interior, primarily originating near sloping topography through flow-topography interactions (e.g., Molemaker et al., 2015; Gula et al., 2015; Naveira Garabato et al., 2019). These interior structures can be instrumental for the turbulent boundary mixing and the forward cascade of energy towards the dissipation scales. Near-bottom propagation of dense water and associated entrainment and mixing (Umlauf and Arneborg, 2009a, b) is an important process for the Baltic Sea dynamics. Flows over rough topography can create small-

scale features and turbulence, as shown in the Baltic Sea (Muchowski et al., 2023a, b) and other sea areas (e.g., de Marez et al., 2024). The latter study assigned these small-scale structures to SMS processes. It can be suggested that great similarities exist between the mixing and SMS instabilities in SML, leading to subduction and SMS variability in the sub-thermocline layer (Salm et al., 2025), and the mixing and instabilities in the bottom boundary layer (BBL), leading to interleaving and SMS variability in the sub-halocline layer of the Baltic Sea. Thus, SMS processes may play a significant role in shaping oxygen conditions of deep basins of the Baltic Sea, and advancing related knowledge is crucial for a better understanding of the biogeochemistry of the Baltic Sea and similar stratified coastal sea areas.

Due to their limited spatial and temporal extent, capturing SMS processes requires high-resolution observations and models that can resolve the associated variability. Conventional ship-borne measurements must be complemented by autonomous observational platforms, such as gliders, drifters, and profilers, as well as towed vehicles and flow-through systems (e.g., ferryboxes), which are increasingly employed to resolve the variability associated with SMS dynamics in the ocean (e.g., Rudnick and Cole, 2011; Swart et al., 2023) and the Baltic Sea (Lips et al., 2016a; Carpenter et al., 2020; Salm et al., 2023). Numerical models with SMS-permitting resolutions have revealed high variability and richness of features in the respective wavenumber range (Capet et al., 2008; Väli et al., 2017). Furthermore, finer-resolution models may suggest large-scale circulation patterns that differ from those derived from the coarser-scale simulations (Andrejev et al., 2004; Maljutenko and Raudsepp, 2019; Westerlund et al., 2019). However, the lack of observational data with the required resolution and coverage hinders proper validation of these high-resolution model runs. This observational gap introduces uncertainty into the interpretation of simulation outcomes and complicates the development of accurate subgrid parameterizations for large-scale ocean (climate) models.

While general knowledge of SMS currents and their role in multiscale ocean dynamics has been reviewed by, e.g., McWilliams (2016, 2019) and Taylor and Thompson (2023), comparable syntheses remain lacking for the Baltic Sea. The scope of this review is therefore to summarize the current understanding of SMS processes and their linkages with the dynamics at other scales in the Baltic Sea. Internal waves occupying similar spatial and temporal scales as well as stratified turbulence are not directly within the scope of this review, but the relationship between them and SMS processes is mentioned where relevant.

The paper is organized as follows: SMS domain in space and time and theoretical considerations of SMS development are described in Section 2. Section 3 presents a review of applied methods to study the SMS processes in the Baltic Sea. State-of-the-art knowledge on SMS dynamics and knowledge gaps are presented in Section 4, focusing on horizontal exchanges, development of stratification, subduction, near-bottom flows and mixing, multiscale interactions, and large-scale impacts. A summary and an outlook are compiled in Section 5.

2. SMS domain and processes

2.1. Scales in space and time

The Rossby number ($\boldsymbol{Ro}$), defined as the ratio of inertial and Coriolis forces, can be estimated using relative vertical vorticity ($\boldsymbol{\zeta}$) as

$$\boldsymbol{Ro} = \frac{\zeta}{f}; \zeta = \frac{\partial v}{\partial x} - \frac{\partial u}{\partial y} \tag{1}$$

where $\boldsymbol{f}$ is the Coriolis parameter and $\boldsymbol{u}$ and $\boldsymbol{v}$ are the zonal (along $\boldsymbol{x}$-axis) and the meridional (along $\boldsymbol{y}$-axis) velocities, respectively. According to this formula, $\boldsymbol{Ro}$ can take negative or positive values corresponding respectively to anticyclonic or cyclonic rotation in the Northern Hemisphere.

Assuming a characteristic velocity scale of 0.1 m s^{-1} and Coriolis parameter of 10^{-4} s^{-1} at 50-60°N gives $\boldsymbol{Ro} \approx 1$ at a length scale of 1 km. For $\boldsymbol{Ro} \ll 1$ ($\boldsymbol{L} \geq 10$ km), Earth's rotation dominates, and the flow is close to geostrophic balance, while for $\boldsymbol{Ro} \gg 1$ ($\boldsymbol{L} \leq 100$ m), the Coriolis effect is negligible. The advection timescale ($\boldsymbol{L}/\boldsymbol{U}$) for SMS flows ranges from less than an hour to a few days. Dominating periods of current oscillations in the Baltic Sea, inertial oscillations (14 h) and low-frequency seiches (26–31 h) (e.g., Suhhova et al., 2018; Lilover et al., 2025), fall within the same range.

Vertical stratification in the Baltic Sea is relatively strong compared to the open ocean. A permanent (or quasi-permanent) halocline exists at depths of 40–80 m in deeper basins, and a seasonal thermocline develops at 5–20 m in almost the entire sea area from spring to autumn (Leppäranta and Myrberg, 2009). Vertical stratification is quantified using the Brunt-Väisälä frequency ($\boldsymbol{N}$):

$$\boldsymbol{N} \equiv \sqrt{-\frac{g}{\rho}\frac{\partial \rho}{\partial z}}, \tag{2}$$

where $\boldsymbol{g}$ is gravitational acceleration, $\boldsymbol{\rho}$ is density, and the vertical axis $\boldsymbol{z}$ is directed up. Typical values of $\boldsymbol{N}$ in the seasonal thermocline and halocline are a few times 10^{-2} s^{-1} corresponding to a minimum period of internal waves of a few minutes (e.g. Lass et al., 2003; Alenius et al., 2003; van der Lee and Umlauf, 2011).

The Froude number, defined as the ratio of inertial and gravitational forces, indicates the relative importance of vertical stratification. For $\boldsymbol{Fr} \ll 1$, buoyancy forces dominate, while for $\boldsymbol{Fr} \gg 1$, they are weak. The Froude number separates the domains of stratified turbulence and 3D isotropic turbulence. In the stratified Baltic Sea, conditions relevant to 3D turbulence ($\boldsymbol{Fr} \gg 1$) occur at spatial scales of ≤ 0.1 m.

A widely used parameter indicting a characteristic spatial scale of geostrophically balanced flows (eddies) is the baroclinic Rossby radius ($\boldsymbol{R_d}$) derived as the horizontal scale of the fastest-growing perturbations in conditions of $\boldsymbol{Ro} \ll 1$ (Eady, 1949). It can be roughly estimated as

$$\boldsymbol{R_d} \equiv \frac{c_1}{f} \approx \frac{NH}{f} \tag{3}$$

where $\boldsymbol{c_1}$ is the phase speed of the first baroclinic mode internal waves, $\boldsymbol{H}$ is the sea depth or the water layer thickness, and $\boldsymbol{N}$ is the average buoyancy frequency in the water layer under consideration. In the Baltic Sea, $\boldsymbol{R_d}$ varies between 1.3 km in the shallow Belt Sea and 7 km in the central deep basins (Fennel et al., 1991; Lass et al., 2003; Osiński et al., 2010), is about 4 km in the Gulf of Finland (Alenius et al., 2003) and <3 km in the Gulf of Riga (Lips et al., 2016c). Since the typical baroclinic Rossby radius is 5 km (1–7 km) and strong vertical stratification is a characteristic feature of the Baltic Sea water column, SMS processes and stratified turbulence occupy a broad range of spatial scales between balanced flows and 3D isotropic turbulence (from 5–10 km to 0.1 m).

2.2. SMS instabilities and processes

SMS processes extract energy from the lateral buoyancy gradients (fronts) and larger-scale balanced flows via several proposed instability mechanisms (Thomas et al., 2008; Gula et al., 2022). The horizontal buoyancy gradient is expressed as

$$\boldsymbol{b_s} = -\frac{\partial b}{\partial s}; b = -g\frac{\rho}{\rho_0} \tag{4}$$

where $\boldsymbol{\rho_0}$ is a reference density and the $\boldsymbol{s}$-axis is directed along the maximum horizontal buoyancy gradient (across the front). Under the assumption that background currents are quasi-geostrophic (i.e., there is a balance between the vertically sheared horizontal currents and horizontal buoyancy gradients, the so-called thermal wind balance), the bulk (balanced) Richardson number can be estimated as

$$Ri_b \equiv \frac{N^2H^2}{U^2} = \frac{N^2f^2}{b_s^2} \quad (5)$$

The sheared flow is stable to perturbations when $Ri_b \gg 1$, while SMS instabilities can occur at Ri_b of O(1) or less (except inertial instability, see below), i.e., under conditions of strong horizontal buoyancy gradients and/or weak vertical stratification (Thomas et al., 2008).

Considering $f \approx 10^{-4}$ s^{-1} for the Baltic Sea latitudes, one can derive the relationship between vertical and horizontal buoyancy gradients for O(1) Ri_b. A characteristic pycnocline with $N \approx 10^{-2}$ s^{-1} in the Baltic Sea and a characteristic horizontal density gradient across a mesoscale front (e.g., density difference of 0.5 kg m^{-3} across a front with a width of 5 km at the entrance to the Gulf of Finland observed by Pavelson et al., 1997) with $b_s = 10^{-6}$ s^{-1} result in $Ri_b \sim 1$. For weaker stratification, as in the SML and BBL, the required horizontal buoyancy gradients to achieve O(1) Ri_b can be smaller. For instance, Chrysagi et al. (2021) showed that $Ri_b \sim 1$ and $b_s = 10^{-6} \div 10^{-7}$ s^{-2} are typical in SMS filaments in the surface layer of the central Baltic Sea.

Similar to the baroclinic instability (BI) at the mesoscale with $Ro \ll 1$ (Eady, 1949), BI can develop at smaller scales. For instance, in the SML, where stratification is weak, smaller-scale (SMS) ageostrophic ($Ro \approx 1$) eddies can develop due to BI (Molemaker et al., 2010). This mechanism, also called mixed layer instability (MLI), can restratify the SML by carrying light water up and dense water down (Fox-Kemper et al., 2008; Taylor and Thompson, 2023). Furthermore, it has been shown that the resulting SMS buoyancy fronts can trigger 3D turbulence, providing a route for energy dissipation from the balanced flows via SMS processes (Molemaker et al., 2010).

While MLI draws energy from the horizontal buoyancy gradient (i.e., potential energy), ageostrophic SMS flows can also occur due to gravitational, inertial or shear-induced instabilities. A general condition for such instabilities is formulated by Hoskins (1974), stating that they can develop when potential vorticity (PV) takes the opposite sign of the Coriolis parameter. It can be written as:

$$fq = f(f\hat{k} + \nabla \times \mathbf{u}) \bullet \nabla b < 0 \quad (6)$$

where q is the Ertel potential vorticity, $\hat{k}$ is the unit vector in vertical direction, $\nabla = \left(\frac{\partial}{\partial x}, \frac{\partial}{\partial y}, \frac{\partial}{\partial z}\right)$ is the Del operator, and $\mathbf{u}$ is the velocity vector. Following Thomas et al. (2013) and Gula et al. (2022), the developed instabilities can be divided into different types depending on the energy source. For gravitational instability, energy is provided by the buoyancy flux, e.g., by surface cooling or downfront winds that could lead to unstable vertical stratification ($N^2 < 0$). Inertial instability (II; also called centrifugal instability) develops when $N^2 > 0$ but relative vertical vorticity is negative (in the Northern Hemisphere) with its absolute value exceeding planetary vorticity, i.e., $\zeta_{abs} = f - \frac{\partial u}{\partial y} + \frac{\partial v}{\partial x} < 0$ (Thomas et al., 2013). For II, the energy is extracted from the lateral shear of the flow field, which can be barotropic.

In strongly baroclinic conditions, the flow can become unstable even if $N^2 > 0$ and $\zeta_{abs} > 0$. It is called symmetric instability (SI), which extracts energy from the vertical shear, leading to inertially unstable but gravitationally stable flows (Taylor and Ferrari, 2009; Arobone and Sarkar, 2015). It can be shown that SI occurs when horizontal buoyancy gradient is sufficiently strong to produce a baroclinic (vertically sheared) current. If assumed, as above, that the current is quasi-geostrophic, PV becomes negative when $\left|-\frac{1}{f}b_s^2\right| > f\zeta_{abs}N^2$ (Thomas et al., 2013).

Thomas et al. (2013) showed that the emerging instability type can be related to the value of the balanced Richardson number or so-called Thomas angle (Th; the name introduced by Gula et al., 2022) calculated as

$$Th \equiv tan^{-1}\left(-\frac{1}{Ri_b}\right) \quad (7)$$

When $-180^\circ < Th < -135^\circ$, gravitational instability develops, while for $-135^\circ < Th < -90^\circ$, energy is extracted from both the buoyancy flux and geostrophic shear production, and the instability can be regarded as a hybrid of gravitational and symmetric instabilities. SI develops when $-90^\circ < Th < -45^\circ$ in the case of anticyclonic relative vorticity and when $-90^\circ < Th < Th_c$ in the case of cyclonic relative vorticity, where $Th_c \equiv tan^{-1}\left(-\frac{\zeta_g}{f}\right)$ and ζ_g is the vertical component of the absolute vorticity of the geostrophic flow. Inertial instability (introduced above) can develop in the case of anticyclonic relative vorticity when $-45^\circ < Th < Th_c$.

SI produces symmetric SMS flows predominantly along inclined isopycnals, which do not modify the buoyancy distribution. However, these sheared flows can lead to secondary instabilities that intensify diapycnal turbulent mixing (Taylor and Ferrari, 2010). Furthermore, Wenegrat et al. (2020) demonstrated that a combination of SI-driven along-isopycnal mixing and episodic vertical mixing events (e.g., due to strong winds deepening the SML) can lead to lateral, cross-front, and diapycnal mixing of water properties.

Frontogenesis due to a mesoscale straining flow involves the sharpening of lateral density gradients that can disrupt geostrophic balance in the frontal current and generate an ageostrophic secondary circulation (ASC; McWilliams, 2021). Beyond strain-induced frontogenesis (Hoskins, 1982; Hoskins and Bretherton, 1972), frontogenesis can also occur in SMS fronts and filaments due to a secondary circulation associated with a modified Ekman balance, sometimes referred to as the Turbulent Thermal Wind (TTW) balance (McWilliams et al., 2015; Gula et al., 2014). The TTW balance – which includes not only the Coriolis force and the baroclinic pressure gradient, but also the vertical mixing of momentum due to surface-layer turbulence, provides a good approximation of SML dynamics in the presence of SMS flows, as demonstrated in both open-ocean (e.g., Gula et al., 2014) and Baltic Sea studies (Chrysagi et al., 2021).

Recent studies, focusing mainly on major current systems (e.g., Molemaker et al., 2015; Gula et al., 2015; Naveira Garabato et al., 2019), suggest that SMS processes and instabilities can also emerge near sloping topography through flow-topography interactions. Initial modeling results from the Eastern Gotland Basin suggest that such phenomena can also develop in the Baltic Sea, where pronounced SMS activity was found below the pycnocline, particularly close to sloping topography (for details see Section 4.2). Flow instabilities due to topographic irregularities generate internal waves and SMS eddies, which play a role in the BBL (e.g., Wenegrat et al., 2018). Both these mechanisms can be highly relevant in the Baltic Sea for understanding the pathways, mixing, and transformation of dense saline inflow waters from the North Sea (Meier et al., 2004; Mohrholz et al., 2015; Liblik et al., 2018; Schmidt et al., 2021), especially within the sub-halocline layer (Holtermann et al., 2014; Holtermann et al., 2017). These processes have critical implications for the ventilation of deep basins, the maintenance of oxygen-depleted zones, and the overall biogeochemical cycling in the region.

The above analysis of scales and balances for SMS instabilities under idealized assumptions shows that these instabilities and associated SMS processes are linked to both larger-scale (geostrophic) dynamics and smaller-scale processes (small-scale turbulence). In the Baltic Sea, atmospheric forcing along with basin configuration and topography, can create a variety of background hydrographic conditions favorable for the development of SMS instabilities. From larger to smaller scales, the typical ranges relevant to the SMS in the Baltic Sea are: mesoscales of order 10 km and larger, ageostrophic secondary circulation at fronts and SMS (mixed layer) eddies with scales of order 1 km (the latter depending on the mixed-layer Rossby radius), symmetric and inertial instabilities

with scales from order 1 km to <100 m, stratified turbulence of order 10 to 1 m and small-scale (3D isotropic) turbulence with scales of 0.1 m and less. Understanding these scales guides the selection of observational approaches and determines the resolution of model grids required to permit or resolve SMS processes in the Baltic Sea. If the model grids do not resolve SMS processes, the parametrization of sub-grid processes must account for their impact.

An indication of the role of SMS processes in energy transfer and tracer mixing can be provided by analyzing wavenumber spectra of kinetic and potential energy or tracer variance. Many studies (e.g., Capet et al., 2008) have shown that spectral slopes of kinetic energy tend to converge toward −2 (corresponding to a −2 power law) in the SMS range (see a schematic diagram of typical horizontal wavenumber spectra of kinetic energy in the upper ocean in Fig. 1 of Jing et al., 2021). This is inconsistent with the internal quasi-geostrophic (QG) theory, which predicts a −3 slope (Charney, 1971; Callies and Ferrari, 2013). The surface quasi-geostrophic (SQG) theory (Blumen, 1978) predicts a −5/3 spectral slope in the ocean with constant stratification. Since SQG turbulence is expected to decay rapidly with depth, internal QG should dominate at small scales in the subsurface layers (Callies and Ferrari, 2013), implying that wavenumber spectra would converge toward a −3 slope in the SMS range below the surface.

Another method to reveal the role of SMS processes is to calculate spatial tracer variance spectra along isopycnal surfaces, i.e., along-isopycnal variance of temperature and/or salinity (Ferrari and Rudnick, 2000). A steep spectrum of kinetic energy (i.e., with a slope of −3) could result in a tracer variance spectrum with a slope of −1 (Balwada et al., 2024). However, most of the results indicate slopes close to −2 in both the surface and subsurface layers (Callies and Ferrari, 2013; Cole and Rudnick, 2012; Balwada et al., 2024). It can be interpreted as a result of tracer stirring by local SMS processes (Balwada et al., 2024). Only a few analyses of observational data have been conducted in the Baltic Sea, where shapes of wavenumber spectra are presented to reveal the role of SMS processes in energy transfer and mixing (Lips et al., 2016a; Salm et al., 2023). This topic is discussed further in Section 4.3.

3. Methods

3.1. In-situ observations

Early ship-borne surveys using CTD probes revealed mesoscale eddies in the ocean (MODE Group, 1978) and the Baltic Sea (Aitsam et al., 1984), as well as small-scale structures on vertical profiles that could be assigned to SMS features (Hayes et al., 1975). However, due to relatively long distances between CTD casts, information on the horizontal extent of those small-scale structures was unavailable (except for staircase layering below Mediterranean lenses in the Atlantic, e.g., Lips and Laanemets, 1991). CTD profiling with station spacing shorter than the internal Rossby radius (Sellschopp et al., 2006; Lips et al., 2009; Lips et al., 2010) and from a slow-moving vessel (Kõuts et al., 1990; Piechura et al., 1997; Zhurbas and Paka, 1999; Rak and Wieczorek, 2012) enabled the mapping of, e.g., intra-halocline lenses and subsurface patches of phytoplankton. Although the resolution of these measurements was adequate for studying SMS phenomena, the primary focus of these earlier studies was on mesoscale variability and vertical fine-structure.

Towed undulating vehicles have been used in the Baltic Sea to map mesoscale background and smaller-scale variability in connection with studies of vertical turbulent mixing (Lass et al., 2003), subsurface North Sea water propagation in the Bornholm Basin (Mohrholz et al., 2006), and phytoplankton dynamics (Pavelson et al., 1999; Kononen et al., 2003). Scanfish data provide sufficiently fine horizontal resolution, ranging from 300 m (Lips et al., 2016a) to 1300 m (Meyer et al., 2018), depending on the vessel speed and scanned layer thickness, allowing for the study of variability in the mesoscale-submesoscale domain. Targeted surveys in the Gulf of Finland (see location in Fig. 2b) revealed SMS intrusions, upwelling filaments, and patches of high chlorophyll-a in the water column, along with wavenumber spectra of temperature close to the −2 slope in the seasonal thermocline between the lateral scales from 10 to 1 km (Lips et al., 2016a).

Fixed profilers collect data of very high temporal (~1–6 h, depending on technology and water depth) and vertical resolutions, enabling studies of small-scale variability (Lips et al., 2011; Liblik and Lips, 2012; Prien and Schulz-Bull, 2016; Liblik et al., 2017; Stoicescu et al., 2019). Similar profilers have been used to study SMS variability in other coastal environments. For instance, the Aqualog profiler deployed in 2010 in the Japan Sea was able to register the passage of SMS eddies through the mooring site (Fayman et al., 2019), analogous to SMS patches in central Baltic waters that penetrate into the subsurface layers of the Gulf of Riga (Liblik et al., 2017). Using a set of profilers that measure multiple parameters in a coordinated manner could further improve insight into SMS dynamics (Lilover et al., 2025).

Argo floats were first tested in the Baltic Sea in 2011 (Purokoski et al., 2013). Being part of an international program, they offer high-resolution CTD and biogeochemical data for various applications (Haavisto et al., 2018; Roiha et al., 2018; Siiriä et al., 2018; Walczowski et al., 2020), although the time step between profiles from a single float is usually relatively long (2–7 days) for investigating SMS variability. More recently, Argo floats have been successfully applied in the Baltic Sea in a virtual mooring mode (Merchel et al., 2024) and as anchored systems (Merchel et al., 2025). In principle, these approaches could be suitable for registering SMS variability if the profiling frequency is increased.

Ocean gliders can effectively resolve SMS processes (Rudnick and Cole, 2011; Balwada et al., 2024). This also applies to the relatively shallow Baltic Sea (Alenius et al., 2014), with the horizontal resolution of collected data ranging between 150 and 700 m, depending on the mission design (Meyer et al., 2018; Carpenter et al., 2020; Salm et al., 2023; see locations in Fig. 2b). Regular glider transects have been proven to be an effective approach for studying multi-scale ocean dynamics, offering sufficient coverage and resolution (Rudnick et al., 2017). Similar regular glider observations have been initiated in the Baltic Sea by The Voice of the Ocean Foundation (VOTO; locations are shown in Fig. 2b). These data sets have been used for various applications (Liblik et al., 2022; Mohrmann et al., 2025) and have great potential for advancing knowledge of SMS dynamics.

A combination of long-term and high-resolution measurements enables detection of SMS processes while providing opportunities to analyze seasonal and annual variations across multiple variables, including temperature, salinity, oxygen and bio-optical parameters (chlorophyll-a, phycocyanin, backscatter, turbidity, CDOM, etc.). Furthermore, gliders can be equipped with microstructure shear sensors and an acoustic current profiler, as demonstrated by the glider deployed in the Eastern Gotland Basin in 2016 (Carpenter et al., 2020). The constant presence of gliders helps to catch hardly predictable extreme events, such as storms (Carpenter et al., 2020), subsurface blooms, upwelling events (Karstensen et al., 2014; Salm et al., 2025), Baltic inflows, or industrial accidents (Mohrmann et al., 2025). Glider data collected regularly by the Finnish Meteorological Institute since 2016 (see locations on their dedicated website http://nnodc.fmi.fi/glider/mission_map4.html) have been used to analyze oxygen conditions in the Bothnian Sea (Polyakov et al., 2022), but not yet for studies of SMS variability and processes.

In principle, marine animals can serve as platforms for collecting vertical CTD profiles (McMahon et al., 2021), as demonstrated by Siegelman et al. (2020) in the Antarctic Circumpolar Current. They analyzed data from elephant seals (up to 80 dives per day) to estimate upward heat flux associated with deep SMS fronts. Marine mammals can also be used to collect observations of SMS processes from less accessible environments, such as underneath sea ice (Biddle and Swart, 2020). In the Baltic Sea, ringed seals are tracked using GPS devices (Oksanen et al., 2015); however, wider use of additional sensors has not yet been adopted.

Ferrybox measurements have been proven to be an effective approach for regularly collecting spatially well-resolved data from the surface layer (Rantajärvi, 2003; Lips et al., 2014; Groetsch et al., 2014). Depending on the sampling frequency and vessel speed, the spatial resolution of data is about 150–500 m (Kikas and Lips, 2016). These data sets have been analyzed for various purposes, including cyanobacterial bloom dynamics (Lips and Lips, 2008; Karlson et al., 2022), carbon fluxes (Schneider et al., 2014) and upwellings and their effects on biogeochemistry (Kikas and Lips, 2016; Jacobs et al., 2021).

Baltic Sea ferrybox data are less exploited for studies of SMS variability, although their spatial resolution and regularity make them highly suitable for this purpose (Lips et al., 2016a). They have been used, for example, in SMS studies to validate high-resolution numerical models (Chrysagi et al., 2022), and can be particularly valuable when satellite observations are unavailable. Applying proper statistical methods to data collected along the ship track in the SML could reveal linkages within the multi-scale variability and their regional and seasonal patterns (Ferrari and Rudnick, 2000; Kolodziejczyk et al., 2015). Research vessels are also often equipped with flow-through systems similar to ferryboxes, providing data from the SML with high spatial resolution, e.g., 250 m on board research vessel Salme (Lainela et al., 2024). These data sets have been utilized for various applications (Liblik et al., 2017; Lainela et al., 2024), although not yet extensively in studies focusing on SMS dynamics.

Lagrangian drifters are not systematically used in the Baltic Sea. However, their applications in other regions have shown valuable results regarding SMS dynamics in the surface layer (e.g., d'Asaro et al., 2018; Dräger-Dietel et al., 2018). Delpeche-Ellmann et al. (2021) and Pärt et al. (2023) described surface drift influenced by wind and surface waves in the Gulf of Finland. Kjellsson and Döös (2012) showed that the dispersion of drifters in the sea is much larger than predicted by a coarse-resolution circulation model (with a grid spacing of 2 nm, close to the baroclinic Rossby radius). This data set is not used for comparisons with the results of high-resolution numerical models. In general, Lagrangian drifters can provide in-situ data for validating SMS-permitting and SMS-resolving models.

Standard broadband echo sounders on board research vessels show potential for bridging the gap from SMS to microstructure scales (Muchowski et al., 2022), providing direct evidence of microscale thermal and haline structures in the water column with high (meter-scale) vertical and horizontal resolution. These surveys can be performed at transect speeds large enough to avoid coupling of temporal and spatial variability. Comparison between dissipation rate of turbulent kinetic energy estimates based on microstructure profiles and broadband echo sounder data showed good results for a region with strong turbulence over the southern Quark sill in the northern Åland sill, especially when combined with complementary underway CTD profiles, though the method is sensitive to fish in the water column (Muchowski et al., 2022).

In conclusion, research groups around the Baltic Sea are well-equipped with the necessary infrastructure to study SMS dynamics. It is essential to continue regular observations in the surface layer along the ferry routes and in the water column at fixed stations, as well as to conduct regular glider missions in selected areas and sections. More data with sufficient resolution and coverage are needed to serve emerging data analysis methods (Yao et al., 2025) and validate high-resolution numerical models (Salm et al., 2025). The way forward would be to combine different platforms (Lips et al., 2016a) and organize international measurement campaigns (Liblik et al., 2022) dedicated to SMS processes. Similar efforts were made when mesoscale variability became a major research focus, for example, by arranging the Patchiness Experiment in 1986 in the central Baltic Sea (Kahru et al., 1990). We stress that most of the observational campaigns cited above were not explicitly designed to study SMS processes. Thus, while the research infrastructure with the necessary capabilities is available, focused studies on SMS processes and their impact remain rare and need to be prioritized in the near future.

3.2. Remote sensing

Available satellite techniques for observing mesoscale and SMS structures at the sea surface include synthetic aperture radar (SAR) imagery, true color and infrared (IR) spectroradiometry, and satellite altimetry, specifically the newly available wide-swath altimetry (SWOT). Sea surface height (SSH) from radar altimeters can be used to observe mesoscale eddies but not SMS features in the Baltic Sea (except for SWOT) due to their limited spatio-temporal resolution and long revisit times (10–30 days) between tracks. Sea surface salinity (SSS) can also be retrieved; however, cloud contamination and low data resolution make this method not yet relevant for studying SMS dynamics in the Baltic. Note also that while remote sensing images provide snapshots of large areas simultaneously, the time step between images is relatively long (about a day), and they allow for detecting structures only at the sea surface.

An early study of sea surface temperature (SST) gradients revealed a ubiquity of thermal fronts in the Baltic Sea (Kahru et al., 1995). SST is also used to distinguish cyclones and anticyclones and to detect upwelling events. Upwelling statistics in the Gulf of Finland, as well as the characteristics of filaments stretching towards the open sea from the upwelling areas, were presented by Uiboupin and Laanemets (2009). They detected that the filaments covered the largest offshore area during the strongest upwelling events.

Karimova et al. (2012) used multiple remote sensing datasets to identify SMS eddies in the southern Baltic Sea, whereas Gurova and Chubarenko (2012) employed coastal radar measurements and satellite remote sensing to investigate the development of SMS eddies. Karimova and Gade (2016) detected that the occurrence of SMS eddies on the sea surface depends on wind conditions, and cyclonic eddies are generally smaller than anticyclonic eddies (ASAR images from 2009 to 2011 were used). In a recent study, SMS eddies with spiral structures were detected in the Baltic Sea in 167 of 270 analyzed SAR images with a 20 m spatial resolution (Zi et al., 2024).

Ocean color can be used as a tracer to illustrate the complicated surface structures at the submesoscale. Zhurbas et al. (2019b) compared true color images from Landsat-8 with model results to study coastal SMS dynamics. Marmorino and Chen (2019) demonstrated that using very high-resolution satellite imagery enabled the tracking of the development of a single SMS feature. Cahill et al. (2024) used ocean color observations from Sentinel-3, a coupled bio-optical model and particle tracking techniques to investigate co-occurring marine heatwave and phytoplankton bloom events in the Arkona Basin. They found that these events were primarily associated with eddy-like coherent structures and SMS features.

The launch of the SWOT satellite in December 2022 has enabled direct space-based observations of SMS ocean surface topography (Fu et al., 2024). SWOT offers more than a ten-fold improvement in spatial resolution compared to products derived from all merged altimeters. Validation campaigns have been started in the Baltic Sea (covering the Gotland Basin and Danish Straits), which should be expanded to leverage this data source and enhance our understanding of Baltic Sea dynamics.

3.3. Numerical modeling

Numerical modeling is a widely used tool to study SMS processes and their role in ocean dynamics. Experiments are conducted in idealized conditions (Brannigan et al., 2015) and under realistic forcing (Capet et al., 2008). Realistic simulations in the Baltic Sea have aimed to demonstrate the impact of grid spacing (Gröger et al., 2022), reproduce an observed process or situation (Väli et al., 2017; Chrysagi et al., 2021), extrapolate observational findings over large sea areas (Salm et al., 2025), or characterize temporal and spatial variability in the intensity of

SMS processes (Väli et al., 2024).

To resolve the SMS processes in the Baltic Sea, much finer horizontal (and vertical) grids and a higher temporal resolution are required compared to open-ocean models due to the much smaller Rossby radius of 1–7 km (Fennel et al., 1991). Several recent studies have employed horizontal grid spacings ranging from 250 to 600 m. These simulations were based on either the General Estuarine Transport Model (GETM; Burchard and Bolding, 2002), e.g., Chrysagi et al. (2021) and Väli et al. (2024) or the Princeton Ocean Model (POM; Blumberg and Mellor, 1987), e.g., Väli et al. (2017). Other studies have implemented the Nucleus for European Modelling of Ocean (NEMO; Madec, 2015), e.g., Vankevich et al. (2016) and Westerlund et al. (2019) or the Regional Ocean Modelling System (ROMS; Haidvogel et al., 2000), e.g., Onken et al. (2020).

All these models utilize spherical coordinates on rectangular grids, and sub-grid lateral mixing in most setups is based on the Smagorinsky parameterization (Smagorinsky, 1963). Vertical mixing in numerical experiments is implemented by additional equation(s) for turbulent kinetic energy (and dissipation rate) either from GOTM (General Ocean Turbulence Model; Burchard et al., 1999), directly from K-profile (Large et al., 1994) or Mellor-Yamada turbulence model (Mellor and Yamada, 1982).

The framework for quantifying the numerical mixing of tracers in ocean models was introduced by Burchard and Rennau (2008), revisited for GETM by Klingbeil et al. (2014), and applied to evaluate the physical and numerical mixing in the presence of strong SMS features in the Eastern Gotland Basin (Chrysagi, 2020). Similar or other approaches are used in other numerical models (e.g., Ralston et al., 2017; Broatch and MacCready, 2022; Schlichting et al., 2023). In general, reducing the grid spacing in numerical simulations can reduce numerical diffusion. However, Henell et al. (2023) estimated, by focusing on the Baltic Sea, that numerical mixing could be responsible for about 50% of the total mixing, leading to too deep SML in models (Bulczak et al., 2024). On the other hand, in coarse-resolution circulation model simulations, the SML depth was often underestimated, which over time led to the development of more complex mixing schemes (Meier, 2001). A recent idealized study by Schlichting et al. (2024) suggests that numerical mixing can exceed physical mixing in high-resolution numerical models, especially at fronts due to sharp lateral buoyancy gradients.

Thus, future modeling studies using SMS-resolving grids in the Baltic Sea could also address changes in numerical and physical diffusion through cross-comparison experiments with different resolutions. Diapycnal, numerical mixing due to discrete grids is associated with vertical advection across the model vertical coordinate and with lateral advection in the case of inclined isopycnal surfaces (Fox-Kemper et al., 2019; Gibson et al., 2017). Uncertainties remain regarding the physically most appropriate aspect ratio of vertical and horizontal grid steps, and whether this should differ between coarse-resolution (where sub-grid horizontal mixing can be approximated by QG turbulence) and high-resolution (where sub-grid processes are highly ageostrophic) numerical models. Furthermore, it is unclear whether an uncoupled parameterization of horizontal and vertical mixing can be applied in numerical experiments with SMS-permitting and −resolving grid spacing. We suggest that, in addition to further numerical experiments, extensive validation of model runs with realistic settings is necessary, leveraging the growing data sets of high-resolution observations. Due to the pronounced internal variability, high-resolution data sets need to be available to enable a statistical model-data comparison (Placke et al., 2018).

Using high temporal and spatial grid resolutions in numerical models is computationally expensive. Therefore, most numerical studies in the Baltic Sea, especially those focusing on climate change, typically use coarser-resolution setups in which SMS processes cannot be resolved (Gröger et al., 2022; Meier et al., 2022). Considering that SMS features can significantly alter the depth of the mixed layer (Thompson et al., 2016), parameterizations are needed to reduce biases in the SML, particularly in climate models (Huang et al., 2014; Calvert et al., 2020). For instance, Fox-Kemper et al. (2011) have suggested and implemented a parameterization scheme for restratification by mixed-layer SMS eddies to approximate eddy fluxes of density and other tracers in global ocean models. This parameterization was recently revised by Bodner et al. (2023) to account for frontogenesis arrested by boundary-layer turbulence. Another relevant parametrization that appears to improve stratification and vertical mixing within the SML is that proposed by Bachman et al. (2017) for parameterizing SI. These parameterizations have not yet been tested in Baltic Sea models. One problem is that usually fluxes of turbulent kinetic energy from the atmosphere are insufficiently known (e.g., Meier et al., 2011).

We have different model codes with Baltic Sea settings available to simulate SMS variability, as well as large-scale patterns and long-term changes. The former models (SMS-permitting or SMS-resolving) need to be more extensively validated. Coarser numerical models could benefit from testing sub-grid parameterizations that account for the effects of SMS processes. Furthermore, long-term SMS-resolving model simulations are computationally demanding, and their analysis is partly constrained by data storage limitations. Developing on-the-fly analysis methods will be essential to make full use of future high-resolution simulations.

3.4. Combined approaches

Since all the described approaches have strengths and weaknesses, a combination of multiple methods would be the most beneficial strategy for studying SMS processes and their impacts. For instance, observed SMS features and variability (Carpenter et al., 2020; Salm et al., 2023) can be simulated by numerical models to allow the identification of the mechanisms of their development (Chrysagi et al., 2021) and to extrapolate the observational results over larger areas and longer time periods (Salm et al., 2025).

SMS-resolving simulations used to study the statistical characteristics of SMS processes over large sea areas and time spans (e.g., Väli et al., 2024) need to be accompanied by appropriate in-situ measurements to provide data for validating the results (i.e., the derived statistical characteristics). A large pool of information is available, for instance, from ferrybox measurements in different parts of the Baltic Sea, which have been used to validate the spatial variability in high-resolution simulations, along with direct validations of surface gradients or tracers, such as temperature and salinity (Chrysagi et al., 2022). The value of systematic glider missions, as initiated by VOTO in some Baltic Sea regions, will grow over time, as they can be used for validating SMS-permitting (and SMS-resolving) models, among other applications.

Additionally, remote sensing products can be utilized in conjunction with realistic modeling experiments. A series of images from different dates was qualitatively compared with the model results in the southern Baltic Sea by Zhurbas et al. (2019b). Besides vertical profiles at monitoring stations, Chrysagi et al. (2021) used satellite images from the central Baltic Sea to evaluate how their model reproduces SST variability and spatial structures. Furthermore, remote sensing provides snapshots with good coverage of the sea surface, while in-situ observations and numerical simulations can reveal the dynamics in the subsurface layers, highlighting the need for their simultaneous application. The integration of models, EO observations and in-situ measurements can be used to reconstruct 4D fields of physical and biochemical parameters. This is, for instance, the main objective of the recently started “Baltic Sea Dynamics through 4D Modelling and Integrated Earth Observation” (https://4dbaltdyn.albavalor.es/).

Similar to multi-sensor (e.g., using gliders with a variety of sensors as Carpenter et al., 2020) and multi-platform observational programs (employing research vessel, ferrybox, scanfish and other platforms by Lips et al., 2016a), as well as utilizing an ensemble of models for operational and climate-related applications, combined modeling, in-situ and remote sensing experiments must be arranged for studying SMS

processes in the Baltic Sea. This requires the involvement of several research groups from different Baltic Sea countries, each bringing their expertise and resources to jointly achieve comprehensive coverage of SMS dynamics.

4. State-of-the-art and knowledge gaps

4.1. SMS processes in the surface layer and thermocline

4.1.1. Baltic Sea settings and examples of SMS dynamics

Strong lateral buoyancy gradients – instrumental for the development of submesoscales – are characteristic features of the Baltic Sea due to its estuarine nature, with large freshwater discharge and a general horizontal salinity gradient (Fig. 2b). Because of the relatively narrow basins, frequent upwelling events are generated by variable local wind forcing (e.g. Lehmann et al., 2012; Kikas and Lips, 2016). Strong upwelling events are characterized by strong buoyancy gradients (Lips et al., 2009) and along-coast baroclinic currents (Suursaar and Aps, 2007; Salm et al., 2025). The inclination of pycnoclines (thermocline and halocline) that depends on wind forcing is a common feature across the Gulf of Finland (Liblik and Lips, 2017), even when temperature and salinity gradients at the sea surface are weak. Furthermore, differential warming and cooling of shallow coastal and offshore areas result in horizontal temperature and density gradients in the surface layer (e.g. Lips et al., 2014; Lips et al., 2016a). Thus, large-scale and mesoscale buoyancy gradients in the Baltic Sea create favorable conditions for the generation of SMS processes, which could alter vertical stratification, drive exchanges between coastal and offshore regions and between surface and subsurface layers, as well as influence larger-scale dynamics (Carpenter et al., 2020; Chrysagi et al., 2021; Salm et al., 2023, 2025).

These hydrographic conditions naturally support the SMS activity to emerge across the Baltic Sea. Early indications of SMS features, with distinct patterns at scales below mesoscale, were first illustrated by remote sensing observations (e.g., Karimova, 2012; Karimova and Gade, 2016; McWilliams, 2016; see also Fig. 1). Ferrybox observations in the Gulf of Finland, conducted between Tallinn and Helsinki since 1997 (see location in Fig. 2), have also provided examples of small-scale variability in the surface layer. Kikas and Lips (2016) suggested that, besides events with a single sharp density front, upwelling events, where variability at scales <5 km dominates in the spatial distribution of temperature in the surface layer, often occur. It can be explained by the development of upwelling filaments (Uiboupin and Laanemets, 2009) or SMS instabilities of the upwelling front, especially when the wind forcing that created the upwelling vanishes or varies (Kikas and Lips, 2016). High-resolution numerical simulations in the Eastern Gotland Basin during summer conditions reveal weak SMS activity prior to an upwelling event, followed by the emergence of strong SMS motions after the upwelling episode (Chrysagi et al., 2022).

Beyond surface expressions, early observations also revealed small-scale subsurface variability in the Baltic Sea, although these features were not initially interpreted within an SMS framework. Vertical fine-structure and intrusions/interleaving (Zhurbas and Paka, 1999; Holtermann et al., 2012) were recognized as important for redistributing water mass properties and mixing, but not yet linked to SMS dynamics. Subsurface and deep chlorophyll-a maxima have long been recognized as features of the summer phytoplankton community (Kahru et al., 1982; Pavelson et al., 1999). Lips et al. (2011) suggested that these subsurface patches of high chlorophyll-a could be related to SMS processes. Using vertical profilers, applied since 2009 in the Gulf of Finland, and targeted ship-borne measurements, they revealed subsurface chlorophyll-a maxima, which could contain up to 2.5 million cells l^{-1}, as well as SMS patches of higher temperature in and below the seasonal thermocline. A detailed analysis of data from autonomous profilers by Liblik and Lips (2012) revealed that along-isopycnal SMS intrusions of waters with different temperatures and salinities were the principal thermohaline features in periods of reversed estuarine circulation and its transformation back to the ordinary pattern in the Gulf of Finland.

Lips et al. (2016a) provided a series of examples of SMS occurrences in the surface and subsurface layers of the Gulf of Finland based on data from autonomous and towed instruments. They noted an enhanced presence of SMS salinity intrusions in the seasonal thermocline during upwelling events and their relaxation; however, the generation mechanisms and the role of SMS features in a quantitative form were not analyzed. Scanfish surveys have demonstrated that intrusions of water with different temperatures and salinities (Fig. 3) often occur along inclined pycnoclines (Lips et al., 2016a). Motivated by such observational data collected in the Eastern Gotland Basin (for details see Burchard et al., 2017), Chrysagi et al. (2022) simulated the appearance of salinity inversions (minima) in the thermocline during summer conditions. The inversions were primarily attributed to the interaction between lateral surface salinity gradients and wind-induced differential advection. However, it was suggested that during wind-induced upwelling events, when strong SMS filaments form in the upwelling area, inversions can also be triggered by frontal subduction within these filaments. Such lateral dispersal of waters with different temperatures and salinities near the pycnocline can also be explained by active SMS processes there, as discussed below (section 4.1.4).

To assess whether such mechanisms and SMS structures are robust beyond individual case studies, high-resolution regional modelling has been used to generalize and extend observational evidence. Numerical simulations (grid step 250 m) by Väli et al. (2017) revealed numerous SMS features in the surface layer of the Gulf of Finland. The SMS structures with high Rossby numbers ($\boldsymbol{Ro} > 1$) had the following spatial scales: threads had a characteristic width of 2–3 km and a length of 10–50 km, cyclonic vortices had a characteristic diameter of 3–6 km, and spiral eddies had a characteristic diameter of 10–15 km. Väli et al. (2017) suggested that the high-potential vorticity threads presumably formed during the development phase, while the cyclonic vortices and spiral cyclonic eddies formed during the relaxation phase of upwelling. High Rossby number threads in the surface layer extended to depths of 10 m, while cyclonic vortices with high Rossby number extended to the depths of 20 m.

These model-identified features require validation with high-resolution in-situ observations, particularly those resolving the vertical thermohaline structure such as glider measurements. Glider observations and analyses of SMS dynamics (including relevant instabilities and role) in the surface layer and thermocline have been conducted in the Gotland Basin (Carpenter et al., 2020) and the Gulf of Finland (Salm et al., 2023). When analyzing the intensity of SMS processes, it can be estimated as along-isopycnal spice, i.e., the sum of temperature ($\Delta \boldsymbol{T}$) and salinity ($\Delta \boldsymbol{S}$) fluctuations compensating each other regarding their contribution to density (Salm et al., 2025):

$$\boldsymbol{spice} = \rho(\alpha \Delta \boldsymbol{T} + \beta \Delta \boldsymbol{S}) \tag{8}$$

where $\boldsymbol{\alpha}$ is the thermal expansion coefficient and $\boldsymbol{\beta}$ is the haline contraction coefficient. An example of SMS features at a baroclinic front in the Gulf of Finland, mapped by a glider mission in May 2018, is presented in Fig. 3 (see location in Fig. 2b). Temperature and salinity fluctuations used to calculate spice were defined in relation to average along-isopycnal temperature and salinity values estimated at a base of 4 km along the glider track. Spice highlights SMS variability as patches of positive (negative) anomalies, indicating regions with higher (lower) salinities and temperatures relative to the average values at the isopycnal surfaces. Thus, spice is best visible if large-scale along-isopycnal gradients of temperature and salinity exist and SMS flows act on them.

The baroclinic front presented in Fig. 3 developed in response to prevailing easterly (upwelling-favorable) winds (Salm et al., 2023). However, before this section was mapped, the wind changed (weakened and turned). The appearance of a secondary front (with an opposite inclination of isopycnals) and SMS features indicating upward movement of colder subsurface waters and downward movement of warmer

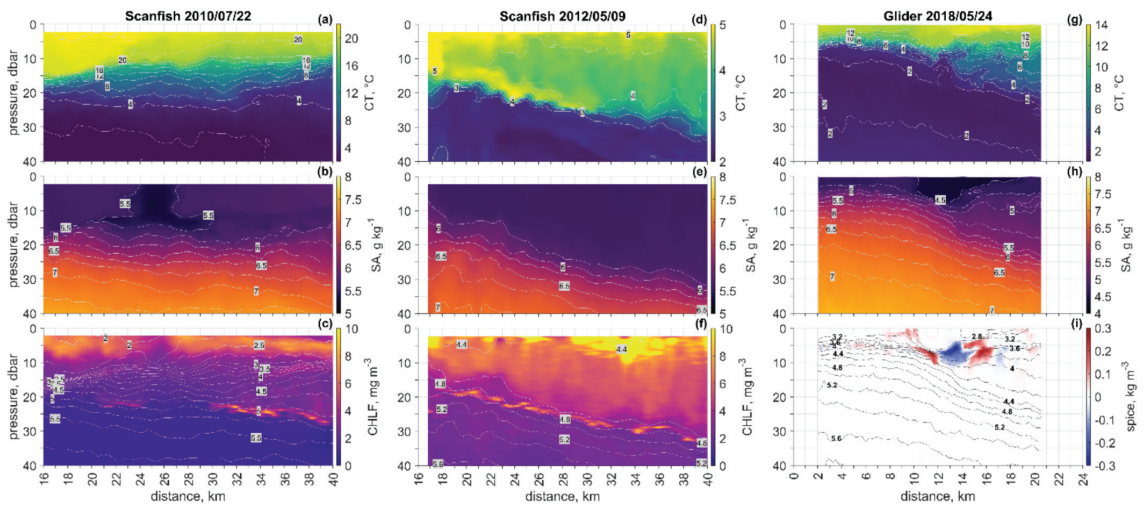


Fig. 3. Vertical sections of temperature, salinity and chlorophyll-a across the Gulf of Finland based on scanfish surveys on 22 July 2010 (a–c) and 9 May 2012 (d–f, see location in Fig. 2; Lips et al., 2016a) and an example of SMS features at a baroclinic front based on a glider mission on 24–25 May 2018 (g–i, see location in Fig. 2). The latter example presents isolines of potential density anomaly with temperature, salinity, and spice distributions (from Salm et al., 2025).

surface waters can be interpreted as a result of instabilities of the baroclinic front under changing wind conditions. SMS features, as noticed in temperature and salinity distributions, are clearly highlighted in the vertical section of spice.

Parts of the Baltic Sea are seasonally ice-covered, but the influence of sea-ice cover on mesoscale and SMS dynamics remains poorly understood in this region. A study in the Arctic Ocean has shown that seasonal sea ice strongly suppresses the propagation of mesoscale eddy activity in the SML, while eddy activity at deeper layers can persist throughout the year (Meneghello et al., 2020). However, the sea-ice edge can also act as a source of eddy formation, as observed by satellite altimetry in the Arctic (Bulczak et al., 2015). Observations using tagged Southern Elephant seal data from the Antarctic seasonal ice zone showed the opposite trend, with increased values for SMS parameters in mid-winter, potentially linked to the presence of leads in sea ice (Biddle and Swart, 2020). In both the Arctic and the Antarctic, the energizing effect of meltwater fronts at the sea-ice edge is important for SMS flows and ocean heat exchange with the atmosphere and sea ice (e.g., Manucharyan and Thompson, 2017; Prend et al., 2025). Due to lower SML salinity in the Baltic Sea, such meltwater-induced buoyancy gradients are presumably weaker, and whether such sea ice meltwater and SMS couplings exist in the Baltic Sea is presently unknown.

4.1.2. *Impact of SMS processes on coastal-offshore exchanges*

River plumes, which transport tracers and nutrients offshore, are affected by variable forcing and may change shape and position drastically over time (Fofonova et al., 2021; Chegini et al., 2020; Hetland and Hsu, 2013). The development of eddies due to the baroclinic instability of the buoyant coastal plume has been shown by Cushman-Roisin et al. (2007) and Kobashi and Hetland (2020). In the Baltic Sea, similar mesoscale eddies have been simulated for the baroclinic coastal current from the Daugava River plume by Lips et al. (2016c). However, SMS eddies associated with river plumes have not yet been captured by observations or simulated by models, probably due to their very small scales in the Baltic Sea. Freshwater discharge from rivers may occupy a relatively thin surface layer under weak winds, e.g., only a few meters as suggested by Soosaar et al. (2016). Thus, the instability scales of such a plume front could be smaller than for the SML elsewhere. Since these scales are small (horizontal scale of ~100 m), strong coupling between SMS dynamics and turbulent mixing can be expected to drive lateral dispersion and vertical fluxes associated with river plumes.

To reveal when and where in the Baltic Sea intense coastal-offshore exchanges can occur, a long-term high-resolution simulation was conducted by Väli et al. (2024). The simulation covered 9 years and had a horizontal grid resolution of ~250 m. In addition to the probability maps of occurrences of high vertical relative vorticity (Fig. 4), indicating active SMS dynamics, we also estimated joint probability density functions (JPDFs) of relative vorticity and strain rate, whereas the latter was calculated as

$$\boldsymbol{Strain} = \sqrt{\left(\frac{\partial \boldsymbol{u}}{\partial \boldsymbol{x}} - \frac{\partial \boldsymbol{v}}{\partial \boldsymbol{y}}\right)^2 + \left(\frac{\partial \boldsymbol{v}}{\partial \boldsymbol{x}} + \frac{\partial \boldsymbol{u}}{\partial \boldsymbol{y}}\right)^2} \tag{9}$$

following an approach by Shcherbina et al. (2013). On the JPDF graphs, presented as 99.9% probability areas (Fig. 5), active SMS regions were identified by Strain $> |\zeta|$ and $|\mathrm{Ro}| > 0.5$, according to Picard et al. (2024).

A relatively inhomogeneous distribution of vorticity (Fig. 4) indicates that SMS processes occur more frequently in narrow straits and several coastal areas of the Baltic Sea (Väli et al., 2024). When comparing five sub-regions of the Baltic Sea using the Strain-Ro graphs (Fig. 5), more frequent occurrences of SMS processes were identified for the Gulf of Finland and the Northern Baltic Proper, while less frequent in the central and southern parts of the Baltic Proper and the Gulf of Riga. Fig. 5 also indicates that intense SMS processes occur more frequently in winter than in summer, consistent with findings elsewhere (Callies et al., 2015; Schubert et al., 2020). Furthermore, $\mathrm{Ro} > 1$ had clearly higher probabilities than $\mathrm{Ro} < -1$ (Fig. 4) and <99.9% probability areas of JPDFs with Strain $> |\zeta|$ and $|\mathrm{Ro}| > 0.5$ were larger on the positive Ro side of Fig. 5, indicating that intense cyclonic vortices are more common than anticyclonic ones. It is in accordance with earlier results (e.g., Shcherbina et al., 2013; Väli et al., 2017) and can be explained by the stable character of strong cyclonic eddies and unstable character of strong anticyclonic eddies with $\boldsymbol{\zeta} < -\boldsymbol{f}$ (Hoskins and Bretherton, 1972).

High probabilities of $|\boldsymbol{Ro}| > 0.5$ in the Gulf of Finland (Figs. 4 and 5) suggest that SMS processes could actively contribute to spreading of coastal waters (including Neva River waters) over this relatively narrow basin. In the Northern Baltic Proper, brackish water is fed into this sea

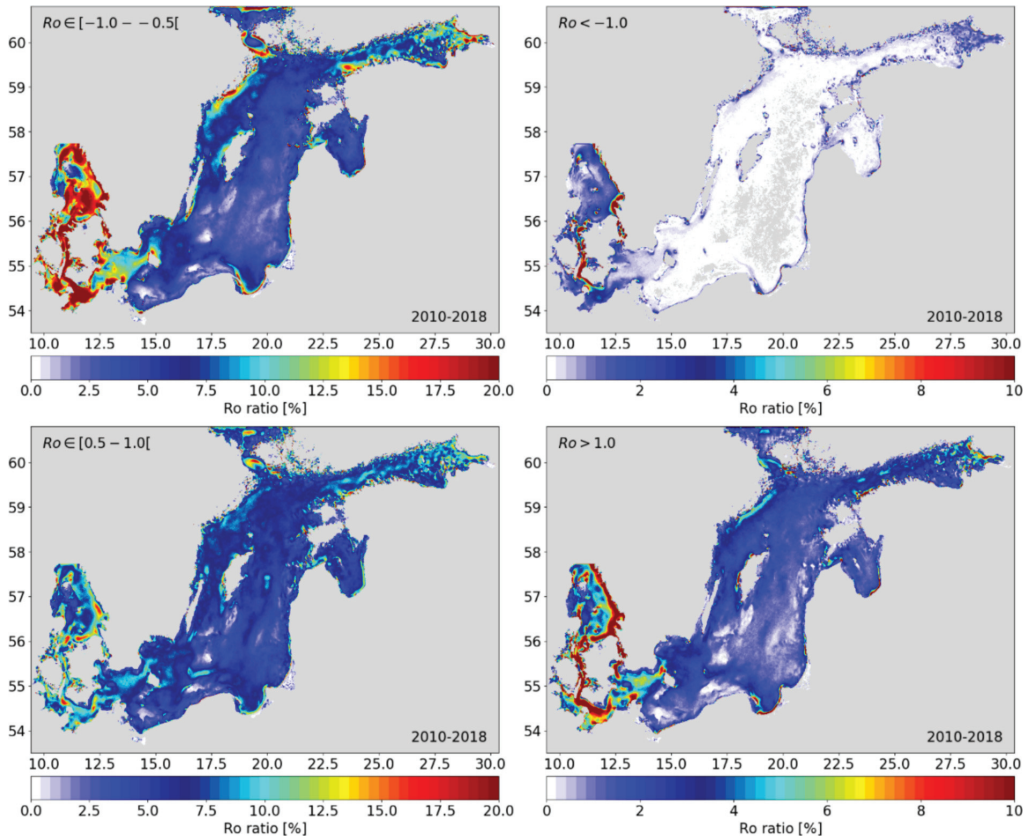


Fig. 4. Spatial distributions of occurrence probabilities of different ranges in Rossby number in the surface layer for the annual mean in 2010–2018 (from Väli et al., 2024).

area from both the Bothnian Sea and the Gulf of Finland, leading to intensive eddy formation due to baroclinic instability, and thus to intense SMS variability (Fig. 4; Väli et al., 2024). Offshore areas of the Central and Southern Baltic Proper generally experience low SMS activity (Fig. 4), while intense SMS features have been suggested to appear in coastal regions (Zhurbas et al., 2019a,b, 2022; Chrysagi et al., 2022). Zhurbas et al. (2019a) demonstrated that cyclonic SMS eddies redistributing the coastal-offshore gradients tend to have higher angular velocities than anticyclonic SMS eddies (implying that cyclonic eddies contribute more actively to vertical exchanges), while anticyclonic vortices could lead to faster lateral transport of particles in the surface layer. Furthermore, Zhurbas et al. (2022) suggested that SMS processes contribute to coastal-offshore exchanges not only in the SML but also in the subsurface layer, influencing exchanges between the slope regions and the basin interior.

The results of the described high-resolution simulation (Väli et al., 2024) were compared with those from the low-resolution simulations, which had horizontal grid resolutions of 926 m (Hariri et al., 2024, 2025) and 1,852 m (Väli et al., 2025), allowing for the analysis of the statistical properties of flow and tracer fields with and without consideration of SMS. These analyses showed that the inclusion of SMS processes hindered rapid transport of coastal waters and tracers toward the basin centers in the SML, but enhanced tracer transport toward the subsurface layer in offshore areas. The results of these studies are reviewed in more detail in subsection 4.4, where large-scale impacts of SMS processes are discussed.

We state that the knowledge and characteristics of coastal-offshore exchanges involving SMS processes need to be advanced. This requires extensive validation of model results using in-situ observations, including focused, regular surveys in selected areas. Additionally, an essential knowledge gap concerns SMS processes associated with river water spreading and their role in coastal-offshore exchange.

4.1.3. SMS processes in the surface layer

Based on data from an ocean glider equipped with a turbulence microstructure package and a high-resolution ADCP, Carpenter et al. (2020) conducted one of the few detailed investigations of SMS fronts during storm conditions that are usually not accessible by ship observations (Fig. 6). Their data from the central Baltic Sea showed that small-scale fronts may impact the SML in contrasting ways: geostrophic adjustment after storm-induced mixing is associated with SML restratification (frontal tilting), which effectively suppresses turbulence by sheltering the deeper parts of the SML from surface forcing. However, they also showed that near-inertial oscillations induced during the adjustment processes may be associated with ageostrophic shear that is sufficient to trigger shear instability. This process was shown to provide an important sink of SMS energy.

Motivated by these glider observations, Chrysagi et al. (2021) used a realistic high-resolution simulation to further investigate the impact of storms on SMS dynamics. Their results revealed pronounced SMS activity in the Eastern Gotland Basin associated with a mesoscale frontal structure. SMS fronts and filaments characterized by sharp lateral

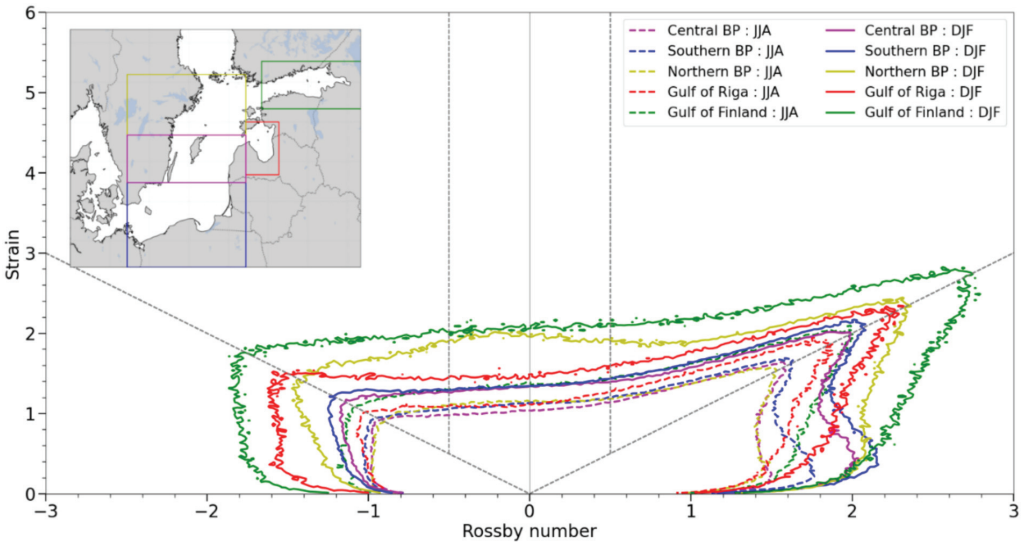


Fig. 5. Joint probability density functions (JPDFs) of relative vorticity and strain rate, showing the areas corresponding to the probability of 99.9% in the five sub-regions of the Baltic Sea in summer (JJA) and winter (DJF). Dashed lines indicate the boundaries of SMS domains identified by Strain > $|\zeta|$ and $|Ro| > 0.5$ (Picard et al., 2024).

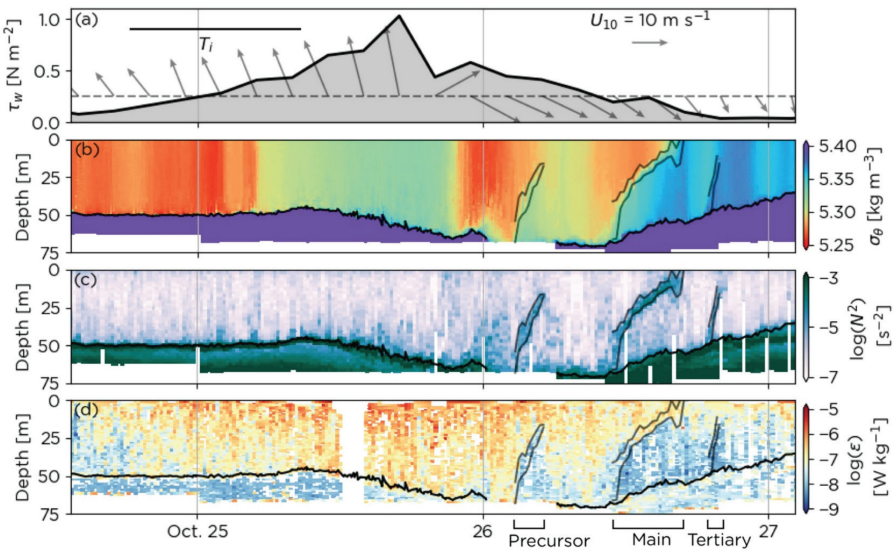


Fig. 6. SML structure during the storm and restratification periods: (a) wind speed and surface stress, (b) potential density (σ_Θ) with a color scale chosen to highlight the SML variability, (c) squared buoyancy frequency, and (d) turbulent dissipation rate. Frontal boundaries are indicated by the dark lines. Sampling times of the three fronts are labeled at the bottom of (d). The base of the SML is indicated by the black line in (b–d). (from Carpenter et al., 2020).

buoyancy gradients, strong surface convergence, and high vertical velocities were widespread in the SML. Inside these features, the mixed layer depth was significantly shallower than in the ambient waters.

The study found that SMS can maintain shallow mixed layers even during storm events and rapidly restratify the SML after each storm episode. This suggests that SMS restratification can counteract the destratifying effects of atmospheric forcing, leading to highly efficient mixing within SMS fronts. On the other hand, both the glider (Carpenter et al., 2020) and the model data (Chrysagi et al., 2021) also revealed an elevated level of microscale turbulent mixing associated with the emerged SMS fronts. While Carpenter et al. (2020) demonstrated that SMS can act both as a source and a sink of turbulence in the SML, Chrysagi et al. (2021) showed, by focusing on a single SMS filament, that the conditions for SI (see section 2.2) were satisfied with the modeled dissipation rates, presenting good agreement with the theoretical estimates.

Note that most of the SMS features in this study were temperature-controlled regarding buoyancy as they emerged from a larger-scale

(upwelling-related) temperature front (Chrysagi et al., 2021). On the other hand, salinity is the main contributor to density variability in the Baltic Sea from late autumn to spring, with temperature contributing at a similar level or exceeding it in summer. There are examples of studies of SMS dynamics in both temperature-stratified and salinity-stratified regions. In the open ocean (temperature-dominated stratification), submesoscales generally induce an upward heat flux (Su et al., 2018), while a downward heat flux similar in magnitude to the net air-sea flux was found in the northern Gulf of Mexico (salinity-dominated stratification; Hilditch et al., 2025). Thus, the Baltic Sea provides suitable conditions to analyze SMS variability regimes and their impacts in seasons (or areas) with temperature- and salinity-dominated stratification.

4.1.4. Role of SMS for the development of seasonal stratification

Numerous examples demonstrate that coarse-scale models are unable to accurately predict mixed layer depths in the ocean (Damerell et al., 2020) and the Baltic Sea (e.g., Tuomi et al., 2012; Bulczak et al., 2024). A general framework for buoyancy fluxes and the development of stratification encompasses air-sea heat flux, evaporation-precipitation, vertical mixing due to winds and currents (such as tides and seiches), and horizontal buoyancy flux resulting from a layered flow structure in the upper ocean. However, simulating the development of seasonal stratification in the surface layer is challenging without an appropriate parameterization of SMS processes and mixing due to the breaking of surface waves and Langmuir circulation. SMS processes can enhance mixing and vertical fluxes under certain conditions and lead to rapid restratification under other conditions (du Plessis et al., 2017), whose impacts are challenging to account for in models (Calvert et al., 2020).

The long-term, high-resolution simulation by Väli et al. (2024) demonstrated that eddy activity exhibits a pronounced seasonal cycle in the Baltic Sea, with higher eddy activity in winter and lower in summer. Thus, SMS processes could influence the development of vertical stratification more in winter, when vertical mixing is at its maximum, than in summer. However, Väli et al. (2024) detected the seasonal minimum in eddy activity in the SML in June, while the seasonal minimum in wind forcing and in kinetic energy was in April (two months earlier). They suggested that this time lag can be explained by the decomposition of larger and stronger eddies into smaller and weaker eddies, which takes longer than the lifetime of individual eddies. It also indicates that lateral buoyancy gradients, resulting from strong vertical mixing in winter and further enhanced by mesoscale eddies, could, in turn, lead to SMS instabilities in the SML during the development phase of seasonal stratification under decreasing wind forcing.

Salm et al. (2025) analyzed SMS variability in the Gulf of Finland surface and subsurface layers (including thermocline) by calculating along-isopycnal spice. They reported that both glider surveys and high-resolution modeling revealed a vertical maximum in SMS variability at the base of the SML under conditions of positive buoyancy flux. The authors suggested that this spice maximum reflects the presence of SMS processes acting to restratify the deeper portion of the SML (Salm et al., 2025). It indicates that SMS processes are active in a lower part of the SML, which is not under direct influence of atmospheric forcing (convection or wind-induced mixing). This agrees with the suggestion that SI can develop under these conditions, particularly in the presence of horizontal buoyancy gradients, such as those caused by slanted isopycnals (Buckingham et al., 2019).

This finding offers an alternative explanation for the development of salinity and temperature inversions near the pycnoclines (as presented in Fig. 3). Besides wind-driven differential advection suggested by Chrysagi et al. (2022) and offshore Ekman transport under significant surface warming (Burchard et. al., 2017), along-isopycnal mixing by SMS flows could create such distributions of temperature (in cases when mostly salinity defines the vertical buoyancy gradient) and salinity (in cases when mostly temperature defines the vertical buoyancy gradient). SMS flows are probably generated by SI near locally enhanced horizontal buoyancy gradients, on the background of a large-scale inclination of the pycnocline. This suggestion aligns with the presentation by Johnston and Rudnick (2009) of the transition layer with the highest SMS spice variance between the SML and the thermocline. Note that, when wind forcing (mixing) reaches the thermocline, the highest SMS variability was found close to or just below the strongest vertical buoyancy gradient (Salm et al., 2025).

These results, together with the example from the previous subsection, highlight the significance of SMS processes in restratifying the SML when negative buoyancy flux vanishes (following a storm), positive buoyancy flux is present and/or wind mixing does not completely arrest the entire SML. In the presence of large horizontal buoyancy gradients in the SML, MLI can occur to restratify the SML. High spice at the base of the SML indicates active SMS flows there, likely due to SI. However, it remains an open question whether such SMS flows are responsible for creating the observed inversions in the vertical distribution of temperature and/or salinity, or whether differential advection is a more dominant driving process.

Further knowledge gaps regarding mixing in the SML and the development of stratification in the Baltic Sea concern the interactions between SMS processes and Langmuir circulation, as well as SMS processes and surface waves. For instance, Hamlington et al. (2014) suggested that Langmuir turbulence counters the restratifying effects of SMS eddies in the SML, indicating a potentially important interplay between these mechanisms that remains poorly understood.

4.1.5. Subduction and vertical fluxes

The most significant vertical mixing of the Baltic Sea water column and vertical fluxes of various substances occur during the autumn–-winter convective and wind-induced mixing period (Reissmann et al., 2009). This is also the period when submesoscales are most abundant, according to a high-resolution simulation in the Baltic Sea by Väli et al. (2024) and several studies focusing on other marine basins (e.g., Brannigan et al., 2015; Mensa et al., 2013). When seasonal thermal stratification has developed, coastal upwelling events are a major process that causes surfacing of sub-thermocline waters, mixing between surface and subsurface waters, and the formation of mesoscale baroclinic fronts and jet currents (Lehmann and Myrberg, 2008), which might be susceptible to SMS instabilities. It has been estimated that the new surface water in the upwelling area contained 85% subsurface water and 15% surface water during the peak of an upwelling event in the Gulf of Finland in August 2006 (Lips et al., 2009). However, except for very simple approximations (Reissmann et al., 2009) and some case studies (Laanemets et al., 2011; Lass et al., 2010), more general estimates of the upwelling contributions to vertical mixing and fluxes are not available for the Baltic Sea or its basins.

Offshore areas of the Baltic Sea are also rich in fronts, which can be detected by SST (Kahru et al., 1995) or salinity differences (e.g., Pavelson et al., 1999; see an overview by Suursaar et al., 2021). Such fronts provide favorable conditions for the development of SMS instabilities and related processes, including SMS subduction and associated vertical fluxes. Enhanced upward heat transport due to existing deep SMS fronts has been proposed by Siegelman et al. (2020). Recently, a further instability mechanism – mixed transitional layer instability (MTI) – which can explain SMS variability below the thermocline in the subtropical ocean, was introduced by Zhang et al. (2025).

Several studies in the Baltic Sea have also indicated that SMS features emerge not only in the SML but also in the thermocline and below (Lips et al., 2016a; Salm et al., 2023). Based on a high-resolution simulation, Zhurbas et al. (2022) found that SMS inhomogeneities or stripes (10–20 km in length and 1 km in width) are common in summer in both the SML and the interior, whereas the interior is not directly exposed to atmospheric forcing. They suggested that SI and strain-induced frontogenesis are probably responsible for the formation of the SMS striped texture. Since conditions for SI were satisfied only in the SML and the near-bottom layer, most probably, SMS stripes in the interior were most

likely generated by strain-induced frontogenesis (Zhurbas et al., 2022). In the presence of large-scale temperature and salinity gradients along isopycnal surfaces, SMS features observed in the temperature and salinity distributions can also form due to the stirring of large-scale gradients by the eddy field.

Further evidence of SMS-driven vertical exchange has been provided by Salm et al. (2025). They compared the occurrence of elevated spice (as a sign of intense SMS variability) with lateral buoyancy gradients and relative vertical vorticity using results of high-resolution, realistic simulations in the Gulf of Finland. They found that high spice can be linked to high vorticity; however, it was not always the case. The highest spice in the thermocline layer (corresponding to a density range selected to represent the thermocline) occurred during a period when ***Ro*** was not elevated in the surface layer of the same sea area. Instead, this situation with high spice in the offshore subsurface layer was characterized by O (1) ***Ro*** near the topographic features and outcropping isopycnals closer to the coast (Fig. 7). Salm et al. (2025) suggested that the spatial decoupling between spice and ***Ro*** patterns likely reflects the downstream advection and transformation of SMS features beyond their generation sites. These results support a mechanism of subduction driven by persistent frontal tilting and vertical shear (see the current fields at the surface and at 20 m depth in Fig. 7), as well as by enhanced vertical velocities. Similar SMS activities at fronts have been described in other regions (e.g., Hosegood et al., 2013).

While downwelling fronts and associated currents could also create favorable conditions for SMS appearance, Salm et al. (2025) did not register a similar enhancement of subsurface SMS variability linked to an analyzed downwelling situation. SMS patterns may have been outside the analyzed area or absent because inclined isopycnals reached the near-bottom layer closer to the coast, where intense microscale mixing could occur. A major difference between upwelling and downwelling situations is the outcropping of isopycnals, which occurs during upwelling but not during downwelling. Thus, a direct impact of wind forcing (turbulent mixing or down-front wind) could lead to SMS instabilities at the front in an upwelling situation and to subduction of surface waters along slanted isopycnals. Furthermore, Salm et al. (2025) suggested that SMS instabilities of the baroclinic current could be induced by the interaction of the current with topographic features. Similar to this result, Capó et al. (2023) suggested that flow-topography interactions generate vertical vorticity, which is advected offshore into the subsurface layers. The effects of topography on SMS variability and processes influencing the dynamics of the SML and the interior have also been demonstrated in several studies in the Southern Ocean (see a review by Swart et al., 2023).

Mixing in the surface water and its subduction along outcropping frontal isopycnal surfaces together with the upwelled water from the pycnocline (that probably occurs over spatially larger regions; Verma et al., 2019), can be a significant mechanism of vertical exchanges in the stratified environment (Thomas et al., 2008; Hosegood et al., 2013; Brannigan et al., 2017; Taylor, 2018). The process of SMS subduction could also explain a fraction of subsurface mixing in estuarine basins, such as the Baltic Sea sub-basins, e.g., the Gulf of Finland. However, no quantitative estimates of the impact of SMS-driven subduction in the Baltic Sea are available.

Furthermore, the dominant sources of instability – whether the interaction of the baroclinic current with topography, SI or other SMS instabilities at fronts (potentially enhanced by variable local forcing), or strain-induced frontogenesis as suggested by Zhurbas et al. (2022) – are not fully understood. These questions may serve as a basis for future studies of SMS dynamics in the Baltic Sea.

4.2. Flow-topography interaction

Although surface SMS have been extensively studied, their counterparts in the oceanic interior are still largely unexplored. However, recent studies focusing mainly on energetic current systems – such as the Gulf Stream (Gula et al., 2015, 2019), the California Undercurrent (Molemaker et al., 2015; Dewar et al., 2015), and the Antarctic

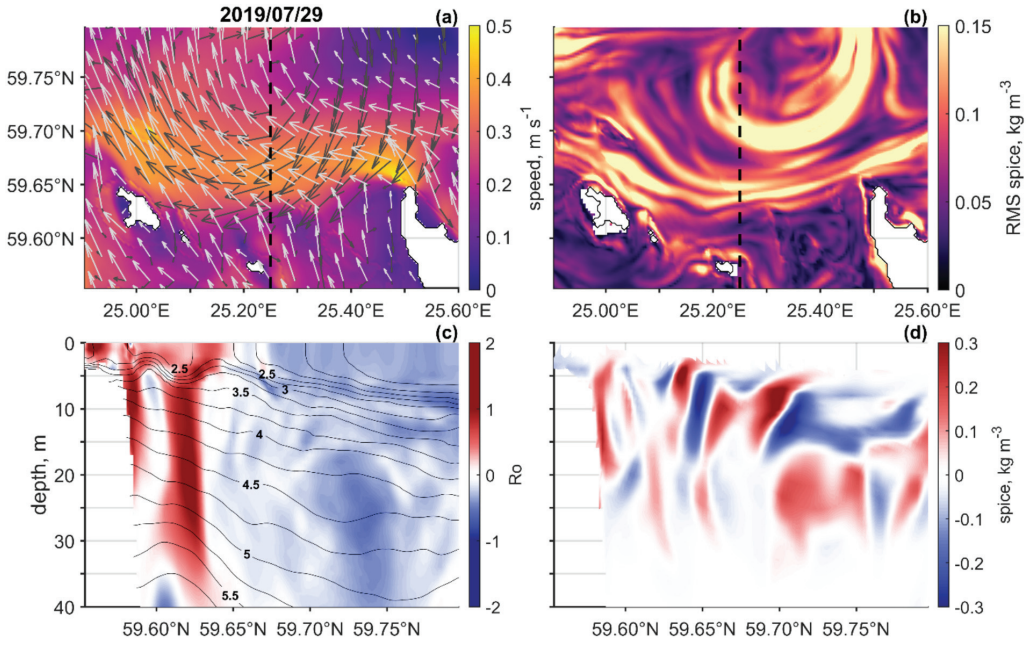


Fig. 7. (a) Current fields at 0 m (light-grey arrows and speed in color) and 20 m (dark-grey arrows) depth, and (b) root mean square of along-isopycnal spice in the density range from the surface until the depth of minimum temperature on 29 July 2019. Vertical sections of Ro and density anomaly (d) and spice (e) along the meridional transect at 25.25° E on 29 July 2019. (from Salm et al., 2025).

Circumpolar Current (Naveira Garabato et al., 2019; Siegelman et al., 2020) – suggest that SMS are widespread in the oceanic interior. These processes primarily arise from flow-topography interactions along sloping bottoms. Strong along-slope currents and steep bathymetric slopes, therefore, appear to promote the development of SMS in the deeper layers of the ocean (Dewar et al., 2015; Wenegrat and Thomas, 2020). Many of the instabilities in the SML described above have their counterparts in the BBL, where bottom friction and mixing generate the lateral buoyancy gradients needed for their development (Gula et al., 2015). An additional process in sloping BBL is the frictional creation of vertical vorticity, which may be exported outside the boundary layer in the case of boundary layer separation, producing cyclonic or anticyclonic eddies depending on the flow direction relative to the bottom (Gula et al., 2015). There are some indications that the latter process may be important for the Baltic Sea deepwater, despite its absence of strong permanent currents or energetic tidal flows.

4.2.1. *Topographic SMS generation*

Preliminary results from a high-resolution, realistic simulation show that filaments, fronts, and spiral-like eddies are widespread in the interior of the Baltic Proper, just below the main pycnocline (located at ~80 m depth, Chrysagi et al., 2021), as can be seen in Fig. 8 for the Eastern Gotland Basin during autumn conditions. These interior structures are characterized by O(1) ***Ro*** dynamics, indicating that they belong to the SMS regime. They largely originate from the lateral boundaries where enhanced Ro results from the vertical vorticity generated by bottom friction of the along-slope current at the sloping bottom shown in Fig. 8b. This is consistent with earlier studies showing that when an interior current moves along sloping topography, bottom friction generates horizontal shear and therefore vertical relative vorticity (enhanced ***Ro*** values). Such regions with enhanced ***Ro*** and small potential vorticity (not shown) may be exported out of the BBL in case of BBL separation. A typical example can be clearly seen in Fig. 8a around 20.4°E and 57.2°N, where the sheared current rolls up and forms an anticyclonic vortex.

To further highlight this process, a passive tracer was released at 80 m depth, exclusively within the BBL (Fig. 8b). The tracer shows distinct structures closely aligned with the Ro anomalies (Fig. 8a), suggesting that ageostrophic features govern lateral dispersion by initially trapping the tracer and then transporting it away from the boundary and into the stratified interior. SMS, therefore, seem to facilitate boundary-interior exchanges, consistent with earlier studies (Naveira Garabato et al., 2019). Such interior-BBL exchange processes mediated by SMS dynamics likely are of special relevance in the Baltic Sea and similar marine and limnic systems, where biogeochemical deep-water properties are largely controlled by benthic fluxes.

A recent observational study Muchowski et al., 2023b) highlights the importance of small-scale topographic corrugations for both isopycnal and diapycnal mixing based on data from the western part of the Åland Sea. This area is characterized by extremely rugged topography at

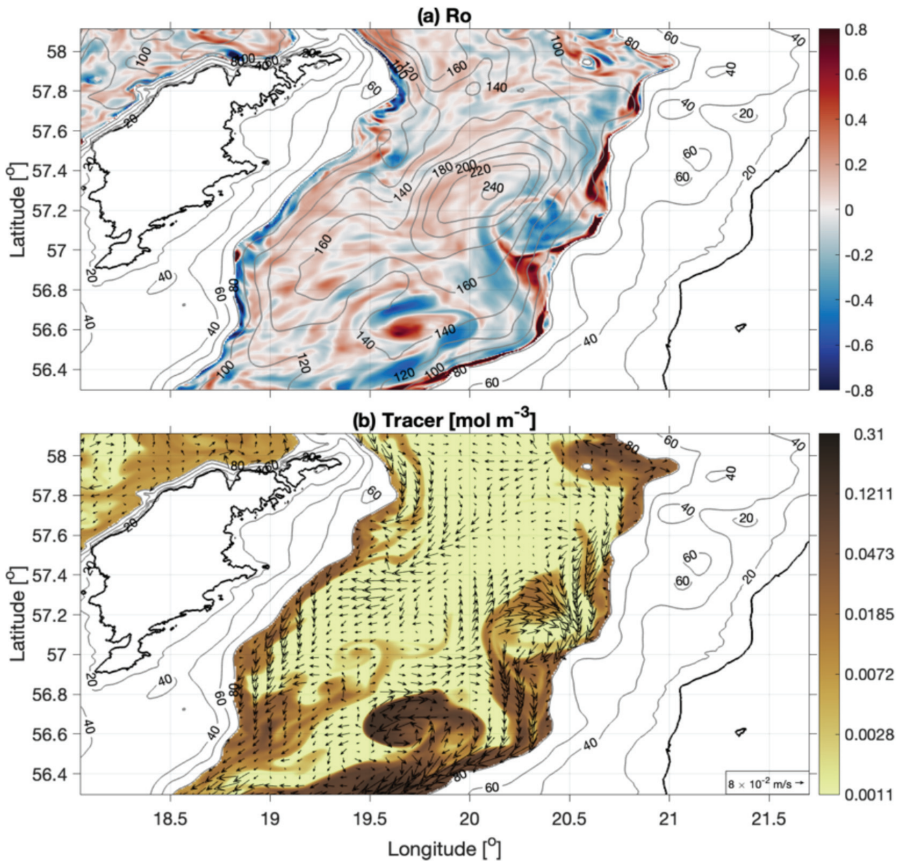


Fig. 8. Spatial distribution of (a) Rossby number and (b) passive tracer concentration with circulation patterns shown as arrows. Gray lines indicate isobaths. Both patterns represent instantaneous fields below the main pycnocline, at 80 m depth, on 23 October 2019 at 09:00 UTC.

horizontal scales of about 100–200 m and vertical topographic variations of about 20 m at depths close to the halocline depth of the Baltic Proper. Such an area with small-scale bathymetric features penetrating the halocline was studied with microstructure and broadband echo sounder transects (Muchowski et al., 2023b), showing highly enhanced dissipation rates of turbulent kinetic energy and diapycnal mixing in the halocline. One of the main hypotheses explaining this strong mixing was the generation of topographic wake eddies by the flow around bathymetric features and boundary layer separation behind them. Another hypothesis was breaking internal lee waves. Both processes transfer energy directly from the large-scale mean flow into the SMS wavenumber regime imposed by the lateral topographic length scales. The rugged bathymetry in large parts of the northern Baltic Sea (e.g., Jakobsson et al., 2019) suggests that similar processes may be broadly important.

Stratified flow over steep topography provides a direct pathway from large-scale barotropic and baroclinic currents into SMS and small-scale features and turbulence, although not all processes strictly qualify as being SMS. Baroclinic flows over the southern Quark sill, a steep sill with vertical and horizontal scales of about 70 m and 500 m in the northern Åland Sea, were studied using microstructure observations, moored ADCPs, and a broadband echo sounder (Muchowski et al., 2022, 2023a; see location in Fig. 2b). The non-tidal flows showed characteristics similar to tidal flows over fjord sills (e.g., Arneborg et al., 2017) with partial blocking of the deepest waters and at times, supercritical overflows with downstream hydraulic jumps, large overturning eddies with vertical length scales of order 100 m, lee waves with lateral length scale similar to the sill (~500 m) breaking in the halocline, and clear Kelvin-Helmholz billows with much smaller horizontal length scale (~50 m) in the halocline. These small-scale dynamics, probably not well represented in any existing models of the Baltic Sea, are important for the exchange of water between the Baltic Proper and the Gulf of Bothnia as well as for modification of the water masses due to mixing (Muchowski et al., 2023b). The 2D interpretation in terms of lee waves and vertically overturning eddies is probably also highly simplified (e.g., Klymak and Gregg, 2001), meaning that there is a 3D continuum of internal waves, jets and eddies, including large vertical vorticity eddies at SMS scales.

4.2.2. Bottom gravity currents and intrusions

Saltwater inflows from the North Sea, including Major Baltic Inflows (MBIs), strongly influence the hydrographic conditions of the deep basins and the overall environmental conditions of the Baltic Sea (e.g., Väli et al., 2013; Eilola et al., 2014; Carstensen et al., 2014; Meier et al., 2018; Mohrholz, 2018; Naumov et al., 2023a, b; Barghorn et al., 2023, 2025). Many studies have focused on the inflows themselves, their occurrence and entrainment of surrounding waters as saltier water is transported towards the central Baltic deep basins (e.g., Meier et al., 2004, 2006; Arneborg et al., 2007; Burchard et al., 2009; Rak, 2016; Bulczak et al., 2016). Building on these earlier studies, recent high-resolution modeling has provided a more quantitative perspective. Based on ensemble simulations with a high-resolution numerical model and a new analysis framework, Henell et al. (2025) quantified water mass transformation during an MBI and estimated the predictability of the MBI pathway and timing during its eastward propagation towards the central Baltic Sea. Complementary observational advances have also emerged. While most observations of MBIs were based on indirect evidence (e.g., changes in water mass properties), recent progress in the development of autonomous sampling systems (Prien and Schulz-Bull, 2016) allowed, for the first time, direct observations of the intruding water masses and mixing parameters during an MBI (Holtermann et al., 2017).

Dense inflows may cause swift bottom gravity currents and set up circulating pools of dense inflow water in downstream basins, both of which may be susceptible to SMS instabilities. However, one of the most detailed studies of dense gravity currents in the Baltic Sea, north of the Kriegers Flak, did not show clear signs of such instabilities (Umlauf et al., 2007; Umlauf and Arneborg, 2009a, b). The study analyzed a dense, narrow (~10 km wide) gravity current with $\boldsymbol{Ro}$ close to 1, flowing into the Arkona Basin, using both observations (Umlauf et al., 2007; Umlauf and Arneborg, 2009a, b) and an idealized model (Umlauf et al., 2010). The study revealed relatively strong transverse density gradients within the gravity current maintained by a transverse circulation moving interfacial fluid towards the shallow side of the geostrophically and frictionally balanced gravity current. It was speculated that the pinching of the interface on the deep side of the current, due to divergent interfacial flow, facilitated the generation of interfacial water and thereby entrainment by decreasing the interfacial gradient Richardson number. Interestingly, no signs of symmetric instabilities were observed despite lateral density gradients of order 10^{-5} s^{-2}, i.e. one to two orders of magnitude larger than the typical cross-front buoyancy gradients found in surface-layer SMS fronts (see above). We attribute this lack of SMS instabilities to the relatively short (compared to the inertial period) passage times of the gravity currents through the topographic constructions, not leaving sufficient time for the growth of SI.

New types of autonomous profiling platforms enabled a detailed investigation of the temporal evolution of deep-water properties in the central Baltic Sea during an MBI (Holtermann et al., 2017) and highlighted the crucial role of frequently occurring small-scale intrusions that import oxic waters at and below the halocline. Later, Holtermann et al. (2020) showed that such intrusions constitute an integrative component of the deep-water dynamics of the Baltic Sea throughout the year, independent of MBI activity. They influence (or even determine) the depth of the redoxcline during stagnation periods, and, contrary to the widespread belief that MBIs provide the most important deep-water oxygen source, were shown to exceed the contribution of MBIs to the deep-water oxygen budget by a factor of 10.

By inducing small-scale temperature inversions in the salinity-stratified deep layers of the Baltic Sea, small-scale lateral intrusions may also create conditions favorable for double diffusion. Based on linear stability analysis, Kuzmina et al. (2005) presented indirect (based on stability parameters) evidence for double diffusion in the central Baltic Sea and suggested that it is a key factor in driving thermohaline interleaving. The first direct observational evidence of double-diffusive staircases in the Baltic Sea was provided by Umlauf et al. (2018) from the Bornholm Basin. Their microstructure data from a glider and an autonomous profiling system revealed rapid formation of sharp (cm-scale) temperature steps of order 1 K at the edges of meter-scale intrusions. Based on their high-resolution temperature data, they computed double-diffusive heat fluxes of order 10–100 W m^{-2}, which are among the largest values ever observed in the ocean. Comparable investigations in other parts of the Baltic Sea are still lacking.

Saline inflows impact Baltic Sea oxygen conditions below the halocline: they improve oxygen conditions in the short term through direct oxygen import, but also strengthen vertical stratification and reduce vertical oxygen fluxes, leading to long-term oxygen deficiency. In the Gulf of Finland, MBIs can initially worsen near-bottom oxygen conditions (Laine et al., 1997; Lessin et al., 2014). The impact of the December 2014 inflow reached the Gulf of Finland nine months later than the Gotland Deep (Liblik et al., 2018). It has been shown that the dense water overflows over the sills separating the Gotland Deep and the north-easterly basins are influenced by prevailing atmospheric forcing (Liblik et al., 2022). Oxygen and nutrient dynamics in the Gulf of Finland have been linked to the conditions in the northern Baltic Proper and wind forcing (Lehtoranta et al., 2017). However, a simple division of the impact of the physical processes on subsurface oxygen dynamics into horizontal advection and vertical mixing (the latter parameterized via local vertical stratification), without considering (SMS) mixing along the inclined isopycnal surfaces, may cause a bias in the estimates of this impact (Stoicescu et al., 2019, 2024).

Similar overflows to those from the Gotland Deep towards the Gulf of Finland and the Åland Sea occur through the Irbe Strait, where, in stratified seasons, waters between the seasonal thermocline and

halocline of the Gotland Deep make their way to the Gulf of Riga (Lilover et al., 1998). The water masses of these inflows are further transported by the basin-wide circulation, which is anti-cyclonic in summer months (Lips et al., 2016b). They experience baroclinic instabilities (Lips et al., 2016c) and can form SMS patches in the subsurface layer (Liblik et al., 2017). These inflows influence the near-bottom oxygen conditions in the Gulf of Riga by bringing more oxygen but strengthening stratification in the deep layer (Stoicescu et al., 2022). The observed short-term variability suggests strong multi-scale control of the dynamics (Liblik et al., 2023), and due to high local consumption, inflow-related improvements are difficult to quantify (Liblik et al., 2023; Stoicescu et al., 2022). High-resolution observations and model runs are therefore needed to disentangle the impacts of riverine inputs, local sedimentation and consumption, and physical processes on near-bottom oxygen dynamics in the Gulf of Riga.

Processes driving vertical mixing in and below the halocline remain poorly quantified (Reissmann et al., 2009), yet evidence suggests that SMS and SMS-scale processes may play a significant role. A tracer release experiment in the Gotland Deep (the BATRE experiment) combined with microstructure measurements showed clearly that diapycnal mixing was primarily happening when the tracer approached the sloping BBL (Holtermann et al., 2012, 2022), as has been shown in other geophysical settings, e.g. the deep ocean, lakes and fjords. The enhanced mixing near the bottom was mainly explained in terms of basin-scale topographic waves, a deep rim current, and near-inertial waves (Holtermann and Umlauf, 2012), but the potential contribution of SMS processes was not investigated.

To advance understanding, combined observational and high-resolution model studies are needed. As emphasized in Sections 3.3 and 3.4, these efforts should (1) verify that SMS processes and other processes of similar length scale over smoothly sloping bottoms as well as rougher topography are correctly represented in high-resolution models, especially regarding water-mass transformation, diapycnal mixing, and water exchange between the benthic boundary layer and the interior; (2) develop parameterizations to include these processes correctly also in coarser models, in order to improve the representation of vertical and lateral mixing in these models as well as the coupling of benthic and interior biogeochemical processes in coupled physical-biogeochemical models.

4.3. Multiscale interactions, energy transfer

Based on ferrybox observations in summers 2009–2012, wavenumber spectra of temperature at 5 m depth had slopes of −2 or flatter for spatial scales ranging from 10 to 0.5 km during periods when relatively high horizontal buoyancy variations at larger scales existed in the area (Fig. 9; Lips et al., 2016a). This suggests the variance is broadly consistent with SQG expectations (spectral slope of −5/3), with eddy generation dominated by baroclinic instabilities in the SML (MLI; Balwada et al., 2024). Based on scanfish observations, wavenumber spectra of temperature at fixed depth also exhibited slopes of about −2 for spatial scales from 10 to 1 km in the surface layer and in the thermocline (Fig. 9; Lips et al., 2016a). Such a slope in the subsurface layers, not only in the SML, is not in accordance with the theory (which would require −5/3 near the surface and −3 in the interior), suggesting that ageostrophic flows play a role at these scales (Callies and Ferrari, 2013). These observations indicate that SMS dynamics are active in the Baltic Sea surface layer and thermocline, modifying the classical energy cascade.

Analysis of wavenumber spectra of temperature and salinity at isopycnal surfaces helps separate SMS-driven stirring from internal-wave signals, as internal waves have a minimal influence on along-isopycnal deviations of temperature and salinity (Ferrari and Rudnick, 2000). Salm et al. (2023) analyzed glider measurements and showed that, in the presence of a mesoscale baroclinic front, wavenumber spectra of isopycnal temperature had slopes close to −2 in the surface layer and the thermocline and were flatter in the layer below the minimum temperature depth (Fig. 9). For interpretation, it is important to recall that a −2 (−1) slope of wavenumber spectra of isopycnal temperature (passive tracer) corresponds to the −2 (−3) slope of wavenumber spectra of kinetic (potential) energy, respectively. This relatively steep slope ($\boldsymbol{k}^{-2}$) of wavenumber spectra is inconsistent with the SQG theory, which predicts flatter tracer variance spectra at these spatial scales in the subsurface layers, e.g., due to the domination of interior QG turbulence or non-local stirring by larger-scale flows (Callies and Ferrari, 2013). Similar −2 slopes of isopycnal temperature variations at the mesoscale-submesoscale transition have been reported by Balwada et al. (2024) based on glider measurements near the Antarctic Circumpolar Current. They concluded that such a spectral shape indicates that SMS variability is primarily driven by local, ageostrophic stirring induced by SMS flows. However, wavenumber spectra of temperature at isopycnal surfaces between 5.7 and 6.0 kg m^{-3} (below the depth of minimum temperature) presented by Salm et al. (2023) exhibited flatter slopes (Fig. 9c), suggesting a reduced influence of SMS and a shift toward interior-dominated dynamics at these depths.

Lilover et al. (2025) analyzed simultaneously measured vertical

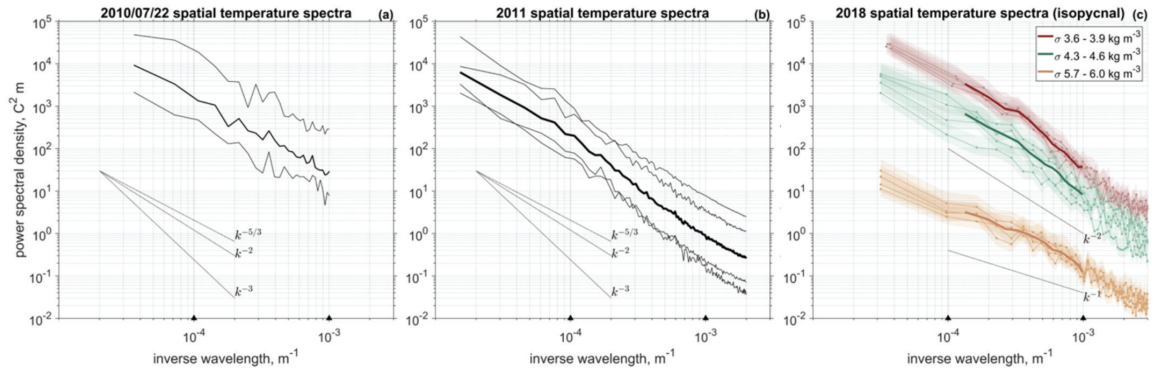


Fig. 9. Examples of wavenumber spectra of temperature variance: (a) in the thermocline based on scanfish data from the Gulf of Finland on 22 July 2010 (thin curves show averages over 10 m layers centered at 15 and 25 dbar, and the thick curve shows the overall average for the 3.5–32 m layer), and (b) in the surface layer based on the Tallinn-Helsinki ferrybox data (thin curves show averages for different periods and the thick line shows the average for the entire analyzed period from 29 June to 31 August 2011) along constant pressure surfaces (from Lips et al., 2016a), as well as (c) in the thermocline and deep layer based on glider data from May–June 2018 along selected isopycnal surfaces (thick curves correspond to the averages over the presented density ranges; from Salm et al., 2023).

profiles of temperature, salinity and currents in the Gulf of Finland (location is marked by red circle in Fig. 2b). They revealed that the temperature spectrum at isopycnal surfaces exhibited a slope of −2, a characteristic sign of active SMS processes. Note that they analyzed the spectra in the frequency domain, which can be compared to spectra in the wavenumber domain if a frozen flow-field approximation is assumed (Balwada et al., 2024). In the thermocline, periods of intensified high-frequency temperature fluctuations coincided with marked changes in the velocity field, suggesting a dynamical link between temperature and flow variability.

They suggested that about 50% of the observed high-frequency temperature variability (in case of intense fluctuations with periods <36 h) could be explained by SMS processes and the remaining 50% by vertical excursions of isopycnals (internal waves). This estimate was obtained by comparing the high-frequency temperature variability at a constant depth with that at the isopycnal surfaces occupying an adjacent depth range during periods of elevated temperature fluctuations. The assumption that temporal variability at isopycnal surfaces can be attributed to SMS processes was tested by calculating the spectral density of isopycnic temperature variations, which did not exhibit peaks at any frequency, including the frequency of inertial oscillations (Lilover et al., 2025). The absence of spectral peaks supports the interpretation that these variations were generated by broadband SMS stirring rather than coherent wave motions.

Their results show that SMS processes, along with the internal waves, could provide a pathway for energy transfer from larger scales to the microscale. However, it is important to note that if the along-isopycnal tracer gradients are weak, SMS signatures may not be detectable via spice or tracer variability at isopycnal surfaces. Thus, it remained unclear whether SMS processes were active when temperature variations at a depth (pressure) level were primarily attributed to internal waves.

In the above analysis, we mostly focused on SMS processes as a pathway of energy transfer from large-scale processes to microscale dissipation. However, they could also transfer energy from small-scale to large-scale motions, thereby influencing the general circulation and the distribution of density (temperature and salinity). For instance, SMS baroclinic instabilities obtain energy from the potential energy associated with horizontal buoyancy gradients in the SML, and this kinetic energy at the submesoscale could cascade upscale and feed larger-scale flows (Taylor and Thompson, 2023). Such multiscale linkages are increasingly recognized as bidirectional rather than purely downscale.

Baltic Sea examples suggest similar connections between processes at different scales. After the relaxation of strong wind forcing, MLI could emerge and convert potential energy (stored in horizontal buoyancy gradients) into kinetic energy (Carpenter et al., 2020; Chrysagi et al., 2021). In addition, generation of SMS flows at the base of the SML, when atmospheric forcing does not reach these depths, could be a reason for high spice (along-isopycnal SMS variability) there (Salm et al., 2025) and for enhanced lateral spreading and dispersion of tracers over large distances (see examples in Fig. 3). Furthermore, SMS subduction has been suggested to provide a direct link between small-scale boundary-layer turbulence and gyre-scale circulation (Wenegrat et al., 2018). By analogy, a similar role of shaping general density (temperature and salinity) distribution and circulation in the Baltic Sea could be assigned to subduction and interleaving originating from the SMS instabilities and mixing in the SML and BBL.

Sketches of interlinkages between processes at different spatial scales, presented in Fig. 10 (with scales shown for the Baltic Sea settings), highlight the differences in concepts with and without SMS processes. If internal gravity waves are assumed to be the primary pathway for energy transfer from the mesoscale to the microscale (Fig. 10a), then turbulent mixing resulting from wave breaking or

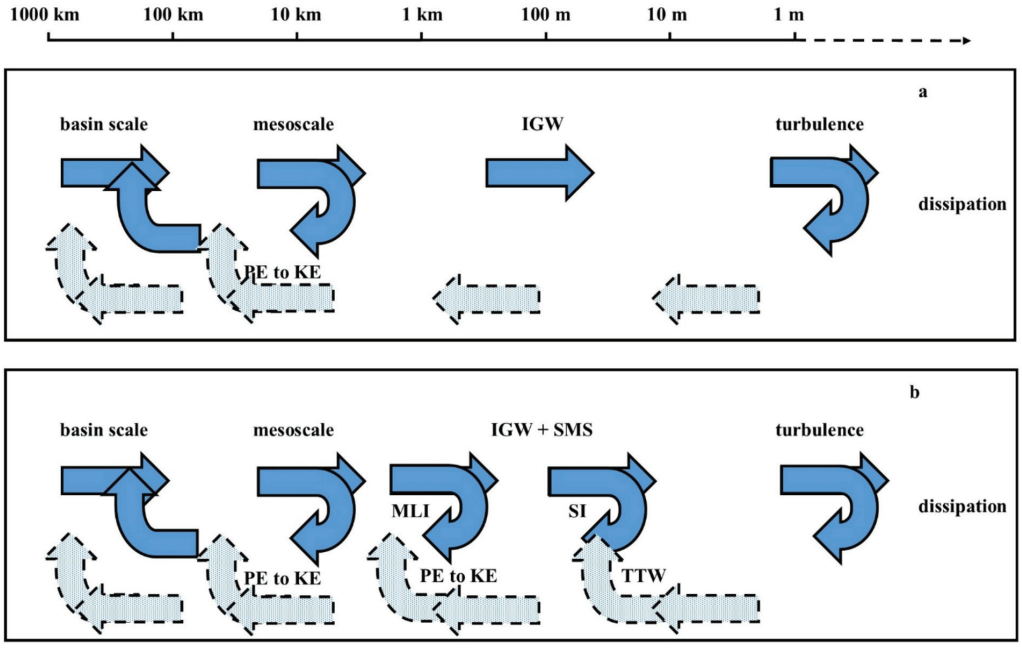


Fig. 10. Simplified sketches of interlinkages between the processes from the basin scale to the microscale, where (a) internal gravity waves (IGW) act as the primary pathway for energy transfer, and (b) SMS processes introduce additional pathways. Energy transfer is shown by filled solid arrows, while dashed arrows indicate the impact of mixing on the distribution of potential energy (PE) and its potential conversion to kinetic energy (KE). In both cases, large-scale energy input is ultimately balanced by microscale mixing and dissipation. However, (a) includes potential feedback at the mesoscale, whereas (b) features additional feedback loops in the SMS range due to MLI and SI/TTW.

boundary-layer processes, along with consequent dissipation, is balanced by the input of energy at larger scales. In contrast, if SMS processes play a role, additional loops for energy transfer between scales exist (Fig. 10b). This introduces a more complex and bidirectional multiscale cascade, where energy transferred from large-scale processes to microscale dissipation is partly utilized along that pathway to create SMS flows through respective instabilities.

For instance, MLI uses potential energy stored in the lateral buoyancy gradient to generate SMS flows and restratify the water column. Similarly, localized mixing (along with down-front wind in the SML) generates SI and subduction along slanted isopycnal surfaces. Thus, part of the available energy is first used to reshape the density structure and redistribute tracers along isopycnal surfaces (which can contribute to interior mixing) before continuing downscale toward dissipation. All these flows may cause secondary mixing. Furthermore, fronts in TTW balance create additional routes to arrive at SI, providing yet another pathway for SMS-driven vertical and lateral exchange.

These additional loops of energy transfer between the scales are in accordance with the flatter slopes of wavenumber spectra of potential energy than expected without SMS processes, since a larger fraction of energy is retained and transformed within the SMS domain. Additionally, this is in accordance with the faster decay of tracer variability in the SMS domain (i.e., steeper slopes of wavenumber spectra of tracers), as active SMS processes redistribute tracers along isopycnal surfaces. Taken together, these arguments and examples above suggest that the balance between energy inputs and dissipation can result in different basin-scale distributions of temperature, salinity, density, and other tracers, depending on the assumed pathways of energy transfer and whether SMS processes are accounted for.

4.4. Large-scale and long-term impacts

A general cyclonic circulation pattern has been suggested for the Baltic Sea (Elken and Matthäus, 2008) and its sub-basins, such as the Gulf of Finland and the Gulf of Riga, based on early measurements (Palmén, 1930) and numerical simulations (Lehmann and Hinrichsen, 2000; Andrejev et al., 2004; Meier, 2007). However, for the Gulf of Finland, this view has been questioned by results from higher-resolution models, especially when different periods and seasons are considered (Westerlund et al., 2019; Maljutenko and Raudsepp, 2019). A discrepancy between modeled and observed surface-layer circulation and salinity distribution has been attributed to stronger vertical mixing near the southern coast than near the northern coast (Maljutenko and Raudsepp, 2019). It remains an open question whether SMS processes play a role (high-resolution simulations should account for their contribution), whether sub-grid parameterization is crucial in defining the residual circulation (since finer grids require adjustments of parameterization), or whether numerical mixing influences the results (as it is still unclear which models simulate the dynamics and circulation more accurately).

The Baltic Sea is a strongly stratified, fjord-like basin, as classified based on the freshwater Froude number and mixing number (Geyer and MacCready, 2014). Lips et al. (2017) suggested that the Gulf of Finland belongs to the stratified estuaries, as expected, except when energetic self-oscillations (seiches) are generated by atmospheric forcing. Burchard (2020) introduced a universal law of estuarine mixing, combining the approaches of salinity coordinates (Walin, 1977), Knudsen relations (Knudsen, 1900), total exchange flow (MacCready, 2011), mixing definition as salinity variance loss (Burchard et al., 2009; Burchard and Rennau, 2008), and the mixing-exchange flow relation (MacCready et al., 2018). This approach to estimating mixing in estuaries is promising, as the classical division into vertical (3D isotropic) and horizontal (QG) mixing is not straightforward at scales and conditions where Ro is O(1).

To fully understand the formation of the general thermohaline structure and circulation of the Baltic Sea, joint modeling and observational studies focusing on small-scale variability are needed (Lehmann et al., 2022). As shown by Henell et al. (2023), the application of the estuarine mixing framework introduced by Burchard (2020) and formulated by Klingbeil and Henell (2023) can identify the mixing hotspots in the Baltic Sea that are essential for the formation of the overturning circulation. The debate continues over the pathways of upward mixing in the ocean meridional overturning circulation (Ferrari et al., 2016) and the Baltic overturning circulation (Henell et al., 2023; Lehmann et al., 2022; Döös et al., 2004; Placke et al., 2021). Using observed temperature and salinity data together with assumed vertical buoyancy fluxes and diffusivity profiles, Hieronymus et al. (2025) showed that the Baltic Sea also supports an overturning circulation characterized by upwelling in the BBL and downwelling in the stratified interior. Additionally, seasonal variability in mixing and SMS intensity must be considered (Väli et al., 2024).

Recent model intercomparisons show that resolution and the representation of SMS processes strongly affect tracer transport and circulation. A comparison of high-resolution and low-resolution simulations revealed that surface-layer transports in the low-resolution models (without SMS processes) are generally larger, moving tracers more rapidly away from the river mouths and the coastal zone than in the high-resolution model, due to higher persistency of surface currents in the low-resolution setup (Väli et al., 2025). This results, for instance, in higher tracer concentrations along the northern coast of the Gulf of Finland and the Gulf of Riga (Väli et al., 2025). However, the calculated patterns are more complex. A higher spatial resolution means, on the one hand, higher horizontal velocities in coastal currents, but, on the other hand, higher vertical velocities, which result in higher diffusivity of tracers and smaller horizontal transports in the surface layer.

Although the methods applied differed (Lagrangian particles vs. Eulerian tracers), Hariri et al. (2024, 2025) found similar results, demonstrating asymmetric particle spread in the Gotland Basin in high- and low-resolution simulations. Hariri et al. (2024) estimated that particle transit times between the coastal zone and the basin center differed by 15–43%, depending on whether SMS processes were included (depending on the applied horizontal resolutions). The range describes transit time differences due to the varying source locations. Hence, large-scale particle spread and connectivity between various coastal areas and between the coastal zone and the offshore area may not be accurately described by state-of-the-art circulation models used for multi-year simulations.

For example, the north-western Gotland Basin is characterized by increased eddy formation due to baroclinic instabilities and associated SMS processes, which contribute to the horizontal and vertical diffusion of particles, especially visible in areas without strong coastal currents (Hariri et al., 2025). This SMS activity is underestimated in coarse-resolution models. Interestingly, greater salinity variability is simulated when SMS processes are taken into account, whereas temperature variability remains largely unchanged, suggesting relatively short time scales for vertical SMS structures (Väli et al., 2025). However, in the sub-basin centers, the differences between simulations with and without SMS processes are small, indicating an overall quasi-steady-state balance in the coastal-offshore exchange.

We do not know whether the investigated high-resolution model accurately describes SMS processes, as systematic validation remains limited due to the lack of high-resolution observational data. Beyond validation, reliable parameterizations of SMS dynamics are also lacking.

4.5. Impact on water column biogeochemistry and fluxes

Without understanding the internal dynamics (i.e., the processes responsible for physical mixing), it is challenging to quantify the role of physical processes in changes in nutrient and oxygen concentrations (Fennel and Testa, 2019; Stoicescu et al., 2019, 2022; Naumov et al., 2023a, b). Since horizontal buoyancy gradients are common in the Baltic Sea, lateral and vertical fluxes associated with SMS processes also shape

the nutriclines, redoxcline, and occurrence of subsurface chlorophyll-a (phytoplankton) maxima (Lips et al., 2016a). In other sea areas, it has been demonstrated that eddy-driven subduction at scales of order 1 to 10 km can lead to episodic injections of water from the SML and a net transport of particulate organic carbon (POC) to depth (Omand et al., 2015). On the other hand, SMS-induced transport and variability are critical in the second half of the summer to maintain the secondary maximum in primary productivity when background nutrient concentrations in the surface layer are negligible (Zeng et al., 2022).

Subsurface maxima of chlorophyll-a and phytoplankton (Fig. 4) are a common feature of summer phytoplankton distribution in the Baltic Sea (Kononen et al., 1998; Lips et al., 2010). Lips et al. (2011) estimated that the dinoflagellate species *Heterocapsa triquetra* (Ehrenberg) Stein, which forms subsurface biomass maxima in the Gulf of Finland, is capable of vertical migration at speeds up to 1.6 m h^{-1}. The potential role of downward nighttime migration, asynchronous upward motions (taking more time), and layered SMS flows in the formation of a bimodal distribution of *H.triquetra* and its biomass growth near the surface has been discussed by Lips and Lips (2014). However, it remains an open question how much this pattern is related to the vertical migration of organisms (Lips et al., 2011; Lips and Lips, 2017) or to physical mesoscale and SMS processes (Berdalet et al., 2014; Lips and Lips, 2014).

Thus, SMS processes likely impact productivity, but the response may vary depending on the organisms (Hernández-Hernández et al., 2020). Furthermore, as demonstrated by a simplified simulation of biogeochemical processes within an eddy-like coherent structure in the southern Baltic Sea, SMS dynamics can promote the growth of specific phytoplankton groups (Vortmeyer-Kley et al., 2025). In general, productivity is believed to increase due to active SMS processes (Lévy et al., 2012). On the other hand, subduction of organic matter-rich upwelled waters at the sharp lateral density gradients of upwelling fronts and filaments has been shown (Nagai et al., 2015). Kessouri et al. (2020) suggested that SMS currents reduce productivity in the productive coastal region while enhancing the upward transport of nutrients and fueling new production in the offshore areas. Data from repeated glider sections, suggesting SMS subduction due to instabilities of the baroclinic current (Salm et al., 2023, 2025), can be used to reveal the development and influence of subsurface chlorophyll-a maxima on phytoplankton dynamics in the Gulf of Finland.

The impact of physical processes on the air-sea exchange of CO_2 (and CH_4) in the Baltic Sea has been studied by Norman et al. (2013), Jacobs et al. (2021) and Lainela et al. (2024). Norman et al. (2013) investigated four upwelling events (two in July, two in October) of the east coast of Gotland in the Baltic Sea, while Jacobs et al. (2021) analyzed ship-of-opportunity (SOOP) data from eight years along the ferry line from Lübeck-Travemünde to Helsinki. Both studies revealed a relationship between pCO_2 (and cCH_4) and SST in the upwelling area. Upwelling events cause the surface water to reverse from a carbon sink to a source, thereby intensifying CH_4 outgassing (Jacobs et al., 2021). There were different regimes with respect to pCO_2-SST correlation in October and July, which are likely due to seasonal differences in thermal stratification and total inorganic carbon in the water column (Norman et al., 2013).

Lainela et al. (2024) associated local maxima of surface layer pCO_2 and cCH_4 in the Gulf of Finland and the Gulf of Riga with river bulges, coastal upwelling events, fronts, and episodes of vertical mixing reaching the seabed in shallow areas. It can be suggested that upwelling events seem to have a major impact on the total Baltic Sea carbon budget. However, the lack of high-resolution observations in the surface layer and simultaneous measurements in the water column, together with high CO_2 variability in the coastal areas, complicates accurate flux estimates. For instance, Lainela et al. (2024) concluded that although seasonal averaging over the CO_2 flux suggests a weak sink for atmospheric CO_2 in the Baltic Sea basins, more data is needed to confirm this. Furthermore, the impact of SMS processes on air-sea fluxes has not yet been studied in the Baltic Sea. At the same time, Resplandy et al. (2009) showed that air-sea flux derived from observed pCO_2 could have an error of 15 to 30% due to undersampling. High variability of CO_2 at submesoscale in the Peruvian upwelling area has been observed by Köhn et al. (2017).

Sea-air fluxes also have an impact on microbiological life in the Baltic Sea (Ploug, 2008). In cyanobacterial layers accumulating in calm weather at the air-sea interface, photosynthesis occurs to a significant extent. Net fluxes of oxygen at the air–water interface are, on average, 2.7 times higher than those at the aggregate–water interface beneath the layers. Photosynthesis ceases in darkness, causing the concentration of oxygen to decline due to its consumption and diffusion away. The pH showed a similar response to light: the microenvironment pH varied between 7.4 and 9.0, depending on the transition from darkness to saturating light.

In summary, studies explicitly addressing the impact of SMS processes on air-sea fluxes are almost absent for the Baltic Sea. However, high-resolution glider and scanfish data sets already exist that allow analyzing statistical properties of along-isopycnal variability of temperature and salinity as passive tracers and chlorophyll-a, which can be influenced by both physical processes and biological behavior of organisms. Such an analysis could enable us to test the assumption that phytoplankton (and ciliates) can take advantage of physical processes at the mesoscale and submesoscale to enhance their growth and distribution.

5. Summary and next steps to advance knowledge

This paper provides an overview of the study results from the last few decades, demonstrating the presence of SMS processes and their interlinkages with processes at adjacent scales in the stratified Baltic Sea. In the surface layer, spatial buoyancy gradients resulting from background freshwater and saltier water inputs, as well as mesoscale stirring and straining, create favorable conditions for SMS instabilities. When atmospheric forcing deepens the SML, large spatial buoyancy gradients may emerge, leading to baroclinic instability and the subsequent reestablishment of vertical stratification. Furthermore, if convective and wind-induced mixing do not occupy the entire depth of the SML, spatial buoyancy gradients in the lower portion of the SML generate SMS flows. Thus, SMS processes play a significant role in the development and maintenance of stratification in the sea surface layer. The development of vertical stratification cannot be approximated as a simple 1D process; instead, SMS processes counteract convective and wind-induced vertical mixing, maintaining stratification strength, which depends not only on atmospheric forcing but also on spatial buoyancy gradients.

Favorable conditions for SMS instabilities to develop in the lower portion of the SML, above the thermocline (or the salinity-maintained pycnocline in winter and early spring), could lead to SMS flows redistributing water mass properties. Such effects are especially evident when either temperature or salinity dominates in their contribution to vertical stratification (salinity in early spring and temperature in summer). It can be assumed that this mechanism also acts even when temperature or salinity inversions are not apparent. The detected spice maximum, located close to the strongest vertical buoyancy gradient at the base of the SML in conditions of positive buoyancy flux from the atmosphere, provides evidence for this process.

Baroclinic fronts and currents in the Baltic Sea, driven by background salinity and temperature gradients, their mesoscale stirring, and coastal upwelling and downwelling events, are conducive to the development of SMS flows and subduction. SMS subduction appears to be a significant contributor to vertical mixing in elongated basins, including their offshore areas. Due to frontal dynamics and upwelling events, subsurface waters are exposed to direct atmospheric forcing and mix with the surface waters. The development of SMS instabilities at fronts leads to the subduction of these mixed waters below the thermocline, particularly when steep isopycnals reach the sea surface or the base of the SML.

This mechanism provides a distinct way for mixing in the subsurface layers, separate from mixing caused by the breaking of internal waves. However, the specific mechanisms leading to SMS instabilities may differ, including instabilities of baroclinic (geostrophic) currents interacting with topography, as well as various types of instabilities, such as SI. SMS flows can emerge due to gravitational (energy provided by buoyancy flux or down-front wind forcing), inertial, or shear-induced instabilities. A similar mechanism of interior mixing could be suggested for near-bottom flows, where mixing occurs near the sloping seabed and over rough topography. The impact is then dispersed by SMS flows across the basin, especially in conditions of slanted isopycnal surfaces.

Thus, SMS processes play a significant role in shaping the spatial distribution of salinity and other substances in estuaries. They hinder the rapid transport of freshwater in the surface layer towards basin centers, but conduct it more effectively towards the subsurface layer in the offshore areas. Such an impact of SMS processes on coastal-offshore exchange has been demonstrated by comparing the outcomes of low-resolution and SMS-resolving (or SMS-permitting) models. However, these high-resolution models still require more extensive validation. Nevertheless, the results indicate that when the SMS processes are explicitly resolved, model outcomes differ markedly from those obtained with low-resolution models that implement QG parametrization of sub-grid horizontal mixing.

The effects of SMS processes on the biogeochemistry of the Baltic Sea remain poorly understood, particularly their impact on the carbon system and associated fluxes. Subsurface SMS patches of phytoplankton are common in summer. Since plankton is not a passive tracer (dinoflagellates and ciliates are capable of vertical migration), the role of SMS flows in generating such patches remains unclear. However, it can be assumed that, similar to zooplankton taking advantage of estuarine circulation, phytoplankton may employ SMS flows for their vertical excursions needed to acquire nutrients at depths and photosynthesize in the euphotic layer. A comparison of statistics regarding passive tracers and along-isopycnal chlorophyll-a variability could shed light on this question.

Thus, the Baltic Sea serves as a unique natural laboratory for SMS studies due to background lateral buoyancy gradients and active mesoscale processes. We conclude that the required expertise and research infrastructure are available in the Baltic Sea basin for SMS analysis. However, high-resolution datasets suitable for it and potential synergies for combining efforts are not yet being used to their full extent. The following list of topics and activities could form a basis for projects and experiments to be implemented in the coming years, collaboratively or by individual research groups or by the whole community targeting SMS processes:

- SMS subduction. Glider missions along coastal-offshore transects and realistic high-resolution simulations shall be conducted to demonstrate and quantify the effects of SMS subduction. The aim is to characterize the subduction process and its relation to background mesoscale dynamics and changes in atmospheric forcing. Microstructure measurements will be conducted to characterize turbulent mixing associated with SMS features.
- Multiscale analysis of spatial variability in the SML. Data collected by ferryboxes, including flow-through systems on board research vessels, will be analyzed to reveal connections between processes at different scales in the SML. Wavenumber spectra of potential energy and spatially binned statistics of tracer variability will be produced and interpreted. Data from SML will be combined with data from the water column (simultaneous glider sections, scanfish tows, and CTD casts) to investigate a potential link between horizontal gradients and vertical stratification. Besides other results, this analysis will characterize thermohaline (SMS) variability regimes in the seasons (or areas) with temperature-dominated stratification (Su et al., 2018) and salinity-dominated stratification (Hilditch et al., 2025). Model experiments should complement this analysis.
- High-resolution mapping and modeling of river plumes to improve the knowledge of mixing and fate of riverine waters in the Baltic Sea system. Immediate mixing near the sources of freshwater can potentially make a significant contribution to the total budget of mixing between marine and terrestrial waters. The recently emerging micro AUVs are promising platforms for conducting in-situ experiments in river mouths, which, when combined with numerical models using unstructured grids, can advance knowledge in these systems with strong gradients. This knowledge is crucial for understanding the Baltic Sea system and estuarine systems in general.
- Near-bottom layer and interior mixing – the role of SMS processes. There is a growing amount of glider data from repeated glider transects at various locations in the Baltic Sea (e.g., VOTO observatories, Fig. 2b). These can be examined for SMS structures in the interior water mass, as well as near sloping topography and near rough topography. At positions of high SMS activity, combined microstructure observations and high-resolution model studies should be performed to quantify the role of SMS processes in diapycnal and isopycnal mixing, as well as in connecting benthic fluxes to the interior water masses.
- Model experiments. Only one multi-year, high-resolution model simulation with a horizontal grid step of 250 m is available for the Baltic Sea. This run was not calibrated. Using available observations, an evaluation and recalibration are needed. Tracer experiments with different horizontal resolutions can illustrate the impact of SMS on particle dispersion, connectivity, and residence times, among other factors.
- SMS processes and subsurface chlorophyll-a patches. Analysis of variability of passive tracers and chlorophyll-a along isopycnal surfaces from repeated glider sections. Differences in spatial variability could reveal how much of the subsurface patchy distribution of chlorophyll-a can be attributed to physical processes, including SMS subduction.
- SMS processes and sea ice. Initiate high-resolution observations in the surface layer throughout the ice season to detect potential effects of ice edge on SMS dynamics in the SML and formation of meltwater-induced buoyancy gradients, as well as estimate whether resulting SMS flows play a role in the Baltic Sea by altering the heat exchange with the atmosphere.

CRediT authorship contribution statement

Urmas Lips: Writing – review & editing, Writing – original draft, Visualization, Conceptualization. **Kai Salm:** Writing – review & editing, Writing – original draft, Visualization. **Germo Väli:** Writing – review & editing, Writing – original draft, Visualization. **Taavi Liblik:** Writing – review & editing. **Lars Arneborg:** Writing – review & editing, Writing – original draft. **Louise C. Biddle:** Writing – review & editing. **Anna I. Bulczak:** Writing – review & editing, Writing – original draft. **Evridiki Chrysagi:** Writing – review & editing, Writing – original draft, Visualization. **Małgorzata Falarz:** Writing – review & editing. **Peter Holtermann:** Writing – review & editing. **Jaromir Jakacki:** Writing – review & editing. **H. E. Markus Meier:** Writing – review & editing, Writing – original draft. **Martin Mohrmann:** Writing – review & editing. **Kai Myrberg:** Writing – review & editing, Writing – original draft. **Per Pemberton:** Writing – review & editing. **Lars Umlauf:** Writing – review & editing, Writing – original draft.

Funding

The authors were supported as follows: Urmas Lips, Kai Salm, Germo Väli, and Taavi Liblik by the Estonian Research Council (grant no PRG602), Anna I. Bulzcak by ESA grant no. 4000143924/24/I-DT; Evridiki Chrysagi by the German Research Foundation (DFG), project

number 274762653 (Collaborative Research Centre TRR 181 Energy Transfers in Atmosphere and Ocean, subproject T2); Jaromir Jakacki by the Argo-Poland project, funded by the Polish Minister of Education and Science (grant no. 2022/WK/04).

Declaration of competing interest

The authors declare that they have no known competing financial interests or personal relationships that could have appeared to influence the work reported in this paper.

Acknowledgments

The research presented in this study is part of the Baltic Earth programme (Earth System Science for the Baltic Sea region, see http://www.baltic.earth). We thank the members of the Working Group on Small-Scale Processes of Baltic Earth for their valuable discussions on the topic of this review paper.

Data availability

It is a review paper. Data availability depends on the authors of original papers.

References

Adams, K.A., Hosegood, P., Taylor, J.R., Sallée, J., Bachman, S., Torres, R., Stamper, M., 2017. Frontal circulation and submesoscale variability during the formation of a Southern Ocean mesoscale eddy. J. Phys. Oceanogr. 47 (7), 1737–1753. https://doi.org/10.1175/JPO-D-16-0266.1.

Aitsam, A., Hansen, H.P., Elken, J., Kahru, M., Laanemets, J., Pajuste, M., Pavelson, J., Talpsepp, L., 1984. Physical and chemical variability of the Baltic Sea: a joint experiment in the Getland Basin. Cont. Shelf Res. 3, 291–310. https://doi.org/10.1016/0278-4343(84)90013-X.

Alenius, P., Nekrasov, A., Myrberg, K., 2003. Variability of the baroclinic Rossby radius in the Gulf of Finland. Cont. Shelf Res. 23, 563–573.

Alenius, P., Tikka, K., Barrera, C., 2014. Gliders for studies of multi-scale variability in the Baltic Sea," 2014 IEEE/OES Baltic International Symposium (BALTIC), Tallinn, Estonia, 1-6, doi: 10.1109/BALTIC.2014.6887868.

Andrejev, O., Myrberg, K., Alenius, P., Lundberg, P.A., 2004. Mean circulation and water exchange in the Gulf of Finland e a study based on three-dimensional modelling. Boreal Environ. Res. 9, 1–16.

Arneborg, L., Fiekas, V., Umlauf, L., Burchard, H., 2007. Gravity current dynamics and entrainment—a process study based on observations in the Arkona Basin. J. Phys. Oceanogr. 37 (8), 2094–2113. https://doi.org/10.1175/JPO3110.1.

Arneborg, L., Jansson, P., Staalstrøm, A., Broström, G., 2017. Tidal energy loss, internal tide radiation, and local dissipation for two-layer tidal flow over a sill. J. Phys. Oceanogr. 47 (7), 1521–1538.

Arobone, E., Sarkar, S., 2015. Effects of three-dimensionality on instability and turbulence in a frontal zone. J. Fluid Mech. 784, 252–273. https://doi.org/10.1017/jfm.2015.564.

Bachman, S.D., Fox-Kemper, B., Taylor, J.R., Thomas, L.N., 2017. Parameterization of frontal symmetric instabilities. I: Theory for resolved fronts. Ocean Model. 109, 72–95. https://doi.org/10.1016/j.ocemod.2016.12.003.

Balwada, D., Gray, A.R., Dove, L.A., Thompson, A.F., 2024. Tracer stirring and variability in the antarctic circumpolar current near the southwest Indian ridge. J. Geophys. Res. Oceans 129, e2023JC019811. https://doi.org/10.1029/2023JC019811.

Barghorn, L., Meier, H.E.M., Radtke, H., 2023. Changes in seasonality of saltwater inflows into the Baltic Sea. Geophys. Res. Lett. 50/12, e2023GL103853. https://doi.org/10.1029/2023GL103853.

Barghorn, L., Meier, H.E.M., Radtke, H., Neumann, T., Naumov, L., 2025. Warm saltwater inflows strengthen oxygen depletion in the western Baltic Sea. Clim. Dyn. 63, 29. https://doi.org/10.1007/s00382-024-07501-x.

Beszczyńska-Möller, A., 1999. Transport of the Odra river waters and circulation patterns in the Pomeranian Bay. Oceanologia 41 (3), 279–308.

Berdalet, E., McManus, M.A., Ross, O.N., Burchard, H., Chavez, F.P., Jaffe, J.S., Jenkinson, I.R., Kudela, R., Lips, I., Lips, U., Lucas, A., Rivas, D., Ruiz-de la Torre, M. C., Ryan, J., Sullivan, J.M., Yamazaki, H., 2014. Understanding harmful algae in stratified systems: review of progress and future directions. Deep Sea Res. Part II: Top. Stud. Oceanogr. 101, 4–20. https://doi.org/10.1016/j.dsr2.2013.09.042.

Biddle, L.C., Swart, S., 2020. The observed seasonal cycle of submesoscale processes in the Antarctic marginal ice zone. J. Geophys. Res. Oceans 125, e2019JC015587. https://doi.org/10.1029/2019JC015587.

Blumberg, A.F., Mellor, G.L., 1987. A Description of a Three-Dimensional Coastal Ocean Circulation Model. In Three-Dimensional Coastal Ocean Models, N.S. Heaps (Ed.). https://doi.org/10.1029/CO004p0001.

Blumen, W., 1978. Uniform potential vorticity flow: part I. Theory of wave interactions and two-dimensional turbulence. J. Atmos. Sci. 35, 774–783.

Boccaletti, G., Ferrari, R., Fox-Kemper, B., 2007. Mixed layer instabilities and restratification. J. Phys. Oceanogr. 37 (9), 2228–2250. https://doi.org/10.1175/JPO3101.1.

Bodner, A.S., Fox-Kemper, B., Johnson, L., Van Roekel, L.P., McWilliams, J.C., Sullivan, P.P., Hall, P.S., Dong, J., 2023. Modifying the mixed layer eddy parameterization to include frontogenesis arrest by boundary layer turbulence. J. Phys. Oceanogr. 53, 323–339. https://doi.org/10.1175/JPO-D-21-0297.1.

Brannigan, L., Marshall, D.P., Naveira Garabato, A.C., Nurser, A.J.G., 2015. The seasonal cycle of submesoscale flows. Ocean Model. 92, 69–84. https://doi.org/10.1016/j.ocemod.2015.05.002.

Brannigan, L., Marshall, D.P., Naveira Garabato, A.C., Nurser, A.J.G., Kaiser, J., 2017. Submesoscale instabilities in mesoscale eddies. J. Phys. Oceanogr. 47, 3061–3085. https://doi.org/10.1175/JPO-D-16-0178.1.

Broatch, E.M., MacCready, P., 2022. Mixing in a salinity variance budget of the salish sea is controlled by river flow. J. Phys. Oceanogr. 52, 2305–2323. https://doi.org/10.1175/JPO-D-21-0227.1.

Buckingham, C.E., Lucas, N.S., Belcher, S.E., Rippeth, T.P., Grant, A.L.M., Le Sommer, J., Ajayi, A.O., Naveira Garabato, A.C., 2019. The contribution of surface and submesoscale processes to turbulence in the open ocean surface boundary layer. J. Adv. Model. Earth Syst. 11, 4066. https://doi.org/10.1029/2019MS001801.

Bulczak, A.I., Bacon, S., Naveira Garabato, A.C., Ridout, A., Sonnewald, M.J.P., Laxon, S. W., 2015. Seasonal variability of sea surface height in the coastal waters and deep basins of the Nordic Seas. Geophys. Res. Lett. 42, 113–120. https://doi.org/10.1002/2014GL061796.

Bulczak, A.I., Nowak, K., Jakacki, J., Muzyka, M., Rak, D., Walczowski, W., 2024. Seasonal variability and long-term winter shoaling of the upper mixed layer in the southern Baltic Sea. Cont. Shelf Res. 276, 105232. https://doi.org/10.1016/j.csr.2024.105232.

Bulczak, A.I., Rak, D., Schmidt, B., Beldowski, J., 2016. Observations of near-bottom currents in Bornholm basin, Slupsk furrow and Gdansk deep. Deep Sea Res. Part II Top. Stud. Oceanogr. 128, 96–113. https://doi.org/10.1016/J.DSR2.2015.02.021.

Burchard, H., 2020. A universal law of estuarine mixing. J. Phys. Oceanogr. 50, 81–93.

Burchard, H., Basdurak, N.B., Gräwe, U., Knoll, M., Mohrholz, V., Müller, S., 2017. Salinity inversions in the thermocline under upwelling favorable winds. Geophys. Res. Lett. 44, 1422–1428. https://doi.org/10.1002/2016GL072101.

Burchard, H., Bolding, K., 2002. GETM – A general estuarine transport model. Scientific documentation. Tech. Rep. EUR 20253 EN, European Commission, 157 pp.

Burchard, H., Bolding K., Villarreal, M.R., 1999. GOTM – a General Ocean Turbulence Model. Theory, implementation and test cases, Tech. Rep. EUR 18745 EN, European Commission.

Burchard, H., Janssen, F., Bolding, K., Umlauf, L., Rennau, H., 2009. Model simulations of dense bottom currents in the Western Baltic Sea. Cont. Shelf Res. 29, 205–220. https://doi.org/10.1016/j.csr.2007.09.010.

Burchard, H., Rennau, H., 2008. Comparative quantification of physically and numerically induced mixing in ocean models. Ocean Model. 20, 293–311.

Cahill, B., Chrysagi, E., Vortmeyer-Kley, R., Gräwe, U., 2024. Deconstructing co-occurring marine heatwave and phytoplankton bloom events in the Arkona Sea in 2018. Front. Mar. Sci. 11, 1323271. https://doi.org/10.3389/fmars.2024.1323271.

Callies, J., Ferrari, R., 2013. Interpreting energy and tracer spectra of upper-ocean turbulence in the submesoscale range (1–200 km). J. Phys. Oceanogr. 43 (11), 2456–2474. https://doi.org/10.1175/JPO-D-13-063.1.

Callies, J., Ferrari, R., Klymak, J.M., Gula, J., 2015. Seasonality in submesoscale turbulence. Nat. Commun. 6. https://doi.org/10.1038/ncomms7862.

Calvert, D., Nurser, G., Bell, M.J., Fox-Kemper, B., 2020. The impact of a parameterisation of submesoscale mixed layer eddies on mixed layer depths in the NEMO ocean model. Ocean Model. 154, 101678. https://doi.org/10.1016/j.ocemod.2020.101678.

Capet, X., McWilliams, J.C., Molemaker, M.J., Shchepetkin, A.F., 2008. Mesoscale to submesoscale transition in the California current system. Part III: Energy balance and flux. J. Phys. Oceanogr. 38 (10), 2256–2269. https://doi.org/10.1175/2008JPO3810.1.

Capó, E., McWilliams, J.C., Jagannathan, A., 2023. Flow-topography interaction along the Spanish slope in the Alboran Sea: vorticity generation and connection to interior fronts. J. Geophys. Res. Oceans 128, e2022JC019480. https://doi.org/10.1029/2022JC019480.

Carpenter, J.R., Rodrigues, A., Schultze, L.K.P., Merckelbach, L.M., Suzuki, N., Baschek, B., Umlauf, L., 2020. Shear instability and turbulence within a submesoscale front following a storm. Geophys. Res. Lett. 47, e2020GL090365. https://doi.org/10.1029/2020GL090365.

Carstensen, J., Conley, D.J., Bonsdorff, E., Gustafsson, B.G., Hietanen, S., Janas, U., Jilbert, T., Maximov, A., Norkko, A., Norkko, J., Reed, D.C., Slomp, C.P., Timmermann, K., Voss, M., 2014. Hypoxia in the Baltic Sea: biogeochemical cycles, benthic fauna, and management. Ambio 43 (1), 26–36. https://doi.org/10.1007/s13280-013-0474-7.

Charney, J.G., 1971. Geostrophic turbulence. J. Atmos. Sci. 28, 1087–1095. https://doi.org/10.1175/1520-0469(1971)028<1087:GT>2.0.CO;2.

Chegini, F., Holtermann, P., Kerimoglu, O., Becker, M., Kreus, M., Klingbeil, K., Gräwe, U., Winter, C., Burchard, H., 2020. Processes of stratification and destratification during an extreme river discharge event in the German Bight ROFI. J. Geophys. Res. Oceans 125, e2019JC015987. https://doi.org/10.1029/2019JC015987.

Chrysagi, E., 2020. Submesoscale processes in the Baltic Sea. University of Rostock. https://doi.org/10.18453/rosdok_id00002961.

Chrysagi, E., Basdurak, N.B., Umlauf, L., Gräwe, U., Burchard, H., 2022. Thermocline salinity minima due to wind-driven differential advection. J. Geophys. Res. Oceans 127, e2022JC018904. https://doi.org/10.1029/2022JC018904.

Chrysagi, E., Umlauf, L., Holtermann, P., Klingbeil, K., Burchard, H., 2021. High-resolution simulations of submesoscale processes in the Baltic Sea: the role of storm events. J. Geophys. Res. Oceans 126, e2020JC016411. https://doi.org/10.1029/2020JC016411.

Cole, S.T., Rudnick, D.L., 2012. The spatial distribution and annual cycle of upper ocean thermohaline structure. J. Geophys. Res. 117 (C2), C02027. https://doi.org/10.1029/2011jc007033.

Cushman-Roisin, B., Korotenko, K.A., Galos, C.E., Dietrich, D.E., 2007. Simulation and characterization of the Adriatic Sea mesoscale variability. J. Geophys. Res. Ocean. 112 (C3). https://doi.org/10.1029/2006JC003515.

Damerell, G.M., Heywood, K.J., Calvert, D., Grant, A.L.M., Bell, M.J., Belcher, S.E., 2020. A comparison of five surface mixed layer models with a year of observations in the North Atlantic. Prog. Oceanogr. 187, 102316.

d'Asaro, E.A., Shcherbina, A.Y., Klymak, J.M., Molemaker, J., Novelli, G., Guigand, C.M., Haza, A.C., Haus, B.K., Ryan, E.H., Jacobs, G.A., Huntley, H.S., Laxague, N.J.M., Chen, S., Judt, F., McWilliams, J.C., Barkan, R., Kirwan, A.D., Poje, A.C., Özgökmen, T.M., 2018. Ocean convergence and the dispersion of flotsam. PNAS 115 (6), 1162–1167. https://doi.org/10.1073/pnas.1718453115.

de Marez, C., Ruiz-Angulo, A., Le Corre, M., 2024. Structure of the bottom boundary current south of Iceland and spreading of deep waters by submesoscale processes. Geophys. Res. Lett. 51, e2023GL107508. https://doi.org/10.1029/2023GL107508.

Delpeche-Ellmann, N., Giudici, A., Rätsep, M., Soomere, T., 2021. Observations of surface drift and effects induced by wind and surface waves in the Baltic Sea for the period 2011-2018. Estuar. Coast. Shelf Sci. 249 (5 February), 107071. https://doi.org/10.1016/j.ecss.2020.107071.

Dewar, W.K., McWilliams, J.C., Molemaker, M.J., 2015. Centrifugal instability and mixing in the California undercurrent. J. Phys. Oceanogr. 45, 1224–1241. https://doi.org/10.1175/JPO-D-13-0269.1.

Dong, J., Fox-Kemper, B., Wenegrat, J.O., Bodner, A.S., Yu, X., Belcher, S., Dong, C., 2024. Submesoscales are a significant turbulence source in global ocean surface boundary layer. Nat. Commun. 15 (1), 9566. https://doi.org/10.1038/s41467-024-53959-y.

Döös, K., Meier, H.E.M., Döscher, R., 2004. The Baltic haline conveyor belt or the overturning circulation and mixing in the Baltic. Ambio 33 (4–5), 261–266.

Dräger-Dietel, J., Jochumsen, K., Griesel, A., Badin, G., 2018. Relative dispersion of surface drifters in the benguela upwelling region. J. Phys. Oceanogr. 48, 2325–2341. https://doi.org/10.1175/JPO-D-18-0027.1.

du Plessis, M., Swart, S., Ansorge, I.J., Mahadevan, A., 2017. Submesoscale processes promote seasonal restratification in the Subantarctic Ocean. J. Geophys. Res.-Oceans 122, 2960–2975. https://doi.org/10.1002/2016JC012494.

Eady, E.T., 1949. Long waves and cyclone waves. Tellus 1 (3), 33–52.

Eilola, K., Almroth-Rosell, E., Meier, H.E.M., 2014. Impact of saltwater inflows on phosphorus cycling and eutrophication in the Baltic Sea. a 3D model study. Tellus A 66, 23985.

Elken, J., Matthäus, W., 2008. "Baltic Sea oceanography," in Regional climate studies, assessment of climate change for the Baltic Sea basin annex A. Editors H.-J. Bolle, M. Meneti, and I. Rasool (Berlin: Springer), 379–385.

Elken, J., Omstedt, A., 2025. Water exchange in the Baltic Sea: a historical view of research approaches from basin scales to submesoscale. Front. Earth Sci. 13, 1598983. https://doi.org/10.3389/feart.2025.1598983.

Fayman, P., Ostrovskii, A., Lobanov, V., Park, J.-H., Park, Y.-G., Sergeev, A., 2019. Submesoscale eddies in Peter the Great Bay of the Japan/East Sea in winter. Ocean Dyn. 69, 443–462. https://doi.org/10.1007/s10236-019-01252-8.

Fennel, K., Testa, J.M., 2019. Biogeochemical controls on coastal hypoxia. Annu. Rev. Mar. Sci. 11, 105–130. https://doi.org/10.1146/annurev-marine-010318-095138.

Fennel, W., Seifert, T., Kayser, B., 1991. Rossby radii and phase speeds in the Baltic Sea. Cont. Shelf Res. 11, 23–36. https://doi.org/10.1016/0278-4343(91)90032-2.

Ferrari, R., Rudnick, D.L., 2000. Thermohaline variability in the upper ocean. J. Geophys. Res. Oceans 105 (C7), 16857–16883.

Ferrari, R., Mashayek, A., McDougall, T.J., Nikurashin, M., Campin, J., 2016. Turning ocean mixing upside down. J. Phys. Oceanogr. 46, 2239–2261. https://doi.org/10.1175/JPO-D-15-0244.1.

Fofonova, V., Kärnä, T., Klingbeil, K., Androsov, A., Kuznetsov, I., Sidorenko, D., Danilov, S., Burchard, H., Wiltshire, K.H., 2021. Plume spreading test case for coastal ocean models. Geosci. Model Dev. 14, 6945–6975. https://doi.org/10.5194/gmd-14-6945-2021.

Fox-Kemper, B., Ferrari, R., Hallberg, R., 2008. Parameterization of mixed layer eddies. Part I: theory and diagnoosis. J. Phys. Oceanogr. 38, 1145–1165. https://doi.org/10.1175/2007JPO3792.1.

Fox-Kemper, B., Danabasoglu, G., Ferrari, R., Griffies, S.M., Hallberg, R.W., Holland, M. M., Maltrud, M.E., Peacock, S., Samuels, B.L., 2011. Parameterization of mixed layer eddies. III: implementation and impact in global ocean climate simulations. Ocean Model. 39, 61–78. https://doi.org/10.1016/j.ocemod.2010.09.002.

Fox-Kemper, B., Adcroft, A., Böning, C.W., Chassignet, E.P., Curchitser, E., Danabasoglu, G., Eden, C., England, M.H., Gerdes, R., Greatbatch, R.J., Griffies, S.M., Hallberg, R.W., Hanert, E., Heimbach, P., Hewitt, H.T., Hill, C.N., Komuro, Y., Legg, S., Le Sommer, J., Masina, S., Marsland, S.J., Penny, S.G., Qiao, F., Ringler, T. D., Treguier, A.M., Tsujino, H., Uotila, P., Yeager, S.G., 2019. Challenges and prospects in ocean circulation models. Front. Mar. Sci. 6, 65. https://doi.org/10.3389/fmars.2019.00065.

Fu, L.-L., Pavelsky, T., Cretaux, J.-F., Morrow, R., Farrar, J.T., Vaze, P., Sengenes, P., Vinogradova-Shiffer, N., Sylvestre-Baron, A., Picot, N., Dibarboure, G., 2024. The surface water and ocean topography mission: a breakthrough in radar remote sensing of the ocean and land surface water. Geophys. Res. Lett. 51, e2023GL107652. https://doi.org/10.1029/2023GL107652.

Geyer, W.R., MacCready, P., 2014. The estuarine circulation. Annu. Rev. Fluid Mech. 46, 175–197.

Gibson, A.H., Hogg, A.M., Kiss, A.E., Shakespeare, C.J., Adcroft, A., 2017. Attribution of horizontal and vertical contributions to spurious mixing in an Arbitrary Lagrangian–Eulerian ocean model. Ocean Model. 119, 45–56. https://doi.org/10.1016/j.ocemod.2017.09.008.

Gray, P.C., Savelyev, I., Cassar, N., Lévy, M., Boss, E., Lehahn, Y., Bourdin, G., Thompson, K.A., Windle, A., Gronniger, J., Floge, S., Hunt, D.E., Silsbe, G., Johnson, Z.I., Johnston, D.W., 2024. Evidence for kilometer-scale biophysical features at the Gulf Stream front. J. Geophys. Res. Oceans 129, e2023JC020526. https://doi.org/10.1029/2023JC020526.

Groetsch, P.M., Simis, S.G., Eleveld, M.A., Peters, S.W., 2014. Cyanobacterial bloom detection based on coherence between ferrybox observations. J. Marine Syst. 140 (A), 50–58. https://doi.org/10.1016/j.jmarsys.2014.05.015.

Gröger, M., Placke, M., Meier, H.E.M., Börgel, F., Brunnabend, S.-E., Dutheil, C., Gräwe, U., Hieronymus, M., Neumann, T., Radtke, H., Schimanke, S., Su, J., Väli, G., 2022. The Baltic Sea model inter-comparison project BMIP – a platform for model development, evaluation, and uncertainty assessment. Geosci. Model Dev. 15, 8613–8638. https://doi.org/10.5194/gmd-15-8613-2022.

Gula, J., Blacic, T.M., Todd, R.E., 2019. Submesoscale coherent vortices in the Gulf Stream. Geophys. Res. Lett. 46.

Gula, J., Molemaker, M.J., McWilliams, J.C., 2014. Submesoscale cold filaments in the Gulf Stream. J. Phys. Oceanogr. 44, 2617–2643.

Gula, J., Molemaker, M.J., McWilliams, J.C., 2015. Topographic vorticity generation, submesoscale instability and vortex street formation in the Gulf Stream. Geophys. Res. Lett. 42, 4054–4062.

Gula, J., Taylor, J., Shcherbina, A., Mahadevan, A., 2022. Chapter 8 - Submesoscale processes and mixing. In: Ocean mixing (Meredith, M., Naveira Garabato, A.C., Eds), Elsevier, 181–214, doi:10.1016/B978-0-12-821512-8.00015-3.

Gurova, E., Chubarenko, B., 2012. Remote-sensing observations of coastal sub-mesoscale eddies in the south-eastern Baltic. Oceanologia 54 (4), 631–654. https://doi.org/10.5697/oc.54-4.631.

Haavisto, N., Tuomi, L., Roiha, P., Siiriä, S.-M., Alenius, P., Purokoski, T., 2018. Argo floats as a novel part of the monitoring the hydrography of the Bothnian Sea. Front. Mar. Sci. 5, 324. https://doi.org/10.3389/fmars.2018.00324.

Haidvogel, D.B., Arango, H.G., Hedstrom, K., Beckmann, A., Malanotte-Rizzoli, P., Shchepetkin, A.F., 2000. Model evaluation experiments in the North Atlantic Basin: simulations in nonlinear terrain-following coordinates. Dyn. Atmos. Oceans 32, 239–281. https://doi.org/10.1016/S0377-0265(00)00049-X.

Hamlington, P.E., Van Roekel, L.P., Fox-Kemper, B., Julien, K., Chini, G.P., 2014. Langmuir–submesoscale interactions: descriptive analysis of multiscale frontal spindown simulations. J. Phys. Oceanogr. 44 (9), 2249–2272. https://doi.org/10.1175/JPO-D-13-0139.1.

Hariri, S., Meier, H.E.M., Väli, G., 2024. Investigating the influence of sub-mesoscale current structures on Baltic Sea connectivity through a Lagrangian analysis. Front. Mar. Sci. 11. https://doi.org/10.3389/fmars.2024.1340291.

Hariri, S., Väli, G., Meier, H.E.M., 2025. Impact of coastal currents and eddies on particle dispersion in the Baltic Sea: a Lagrangian approach to marine ecosystems. Front. Mar. Sci. 12, 1–12. https://doi.org/10.3389/fmars.2025.1545035.

Hayes, S.P., Joyce, T.M., Millard Jr., R.D., 1975. Measurements of vertical fine structure in the Sargasso Sea. J. Geophys. Res. Ocean. 80 (3), 314–319. https://doi.org/10.1029/JC080i003p00314.

Henell, E., Burchard, H., Gräwe, U., Klingbeil, K., 2023. Spatial composition of the diahaline overturning circulation in a fjord–type, non–tidal estuarine system. J. Geophys. Res. Ocean. 128 (12), e2023JC019862. https://doi.org/10.1029/2023JC019862.

Henell, E., Burchard, H., Gräwe, U., Holtermann, P., Naumann, M., Umlauf, L., Klingbeil, K., 2025. Exploring the variability of a non-tidal marginal sea with a single-model ensemble. Ocean Model. 102615.

Hernández-Hernández, N., Arístegui, J., Montero, M.F., Velasco-Senovilla, E., Baltar, F., Marrero-Díaz, Á., Martínez-Marrero, A., Rodríguez-Santana, Á., 2020. Drivers of Plankton distribution across mesoscale eddies at submesoscale range. Front. Mar. Sci. 7, 667. https://doi.org/10.3389/fmars.2020.00667.

Hetland, R.D., Hsu, T.J., 2013. Freshwater and sediment dispersal in large river plumes. In: Bianchi, T.S., Allison, M.A., Cai, W.-.-J. (Eds.), Biogeochemical Dynamics at Major River-Coastal Interfaces: Linkages with Global Change. Cambridge University Press, Cambridge, pp. 55–85.

Hieronymus, M., Pemberton, P., Hordoir, R., Mulder, M., 2025. Hypsographic control on the diapycnal flow in the eastern gotland basin of the Baltic Sea. J. Phys. Oceanogr. 55, 361–375. https://doi.org/10.1175/JPO-D-24-0120.1.

Hilditch, J.P., Bergentz, K., Northcott, D., Luko, C.D., Cohanim, K., Schlichting, D., Sanchez-Rios, A., Weiss, K., Hetland, R., MacKinnon, J., Nash, J., Shearman, R.K., Thomas, L.N., 2025. Observations of subduction, downward heat flux and dense filament collapse in the northern Gulf of Mexico. J. Geophys. Res. Oceans 130, e2025JC022570. https://doi.org/10.1029/2025JC022570.

Holtermann, P., Umlauf, L., 2012. The Baltic sea tracer release experiment. 2. Mixing processes. J. Geophys. Res. Oceans 117, C01022. https://doi.org/10.1029/2011JC007445.

Holtermann, P.L., Umlauf, L., Tanhua, T., Schmale, O., Rehder, G., Waniek, J.J., 2012. The Baltic sea tracer release experiment: 1. Mixing rates. J. Geophys. Res. Oceans 117, C01021. https://doi.org/10.1029/2011JC007439.

Holtermann, P., Burchard, H., Gräwe, U., Klingbeil, K., Umlauf, L., 2014. Deep-water dynamics and boundary mixing in a non-tidal stratified basin. A modeling study of Baltic Sea. J. Geophys. Res. 119, 1465–1487. https://doi.org/10.1002/2013JC009483.

Holtermann, P.L., Prien, R., Naumann, M., Mohrholz, V., Umlauf, L., 2017. Deepwater dynamics and mixing processes during a major inflow event in the central Baltic Sea. J. Geophys. Res. Oceans 122, 6648–6667. https://doi.org/10.1002/2017JC013050.
Holtermann, P., Prien, R., Naumann, M., Umlauf, L., 2020. Interleaving of oxygenized intrusions into the Baltic Sea redoxcline. Limnol. Oceanogr. 65, 482–503. https://doi.org/10.1002/lno.11317.
Holtermann, P., Pinner, O., Schwefel, R., Umlauf, L., 2022. The role of boundary mixing for diapycnal oxygen fluxes in a stratified marine system. Geophys. Res. Lett. 49, e2022GL098917. https://doi.org/10.1029/2022GL098917.
Hosegood, P.J., Gregg, M.C., Alford, M.H., 2013. Wind-driven submesoscale subduction at the north Pacific subtropical front. J. Geophys. Res. Oceans 118, 5333–5352. https://doi.org/10.1002/jgrc.20385.
Hoskins, B., 1974. The role of potential vorticity in symmetric stability and instability. Q. J. R. Meteorol. Soc. 100 (425), 480–482.
Hoskins, B.J., 1982. The mathematical theory of frontogenesis. Annu. Rev. Fluid Mech. 14, 131–151. https://doi.org/10.1146/annurev.fl.14.010182.001023.
Hoskins, B.J., Bretherton, F.P., 1972. Atmospheric frontogenesis models: mathematical formulation and solution. J. Atmos. Sci. 29 (1), 11–37. https://doi.org/10.1175/1520-0469(1972)029%E8;0011:afmmfa%E9;2.0.co;2.
Huang, C.J., Qiao, F., Dai, D., 2014. Evaluating CMIP5 simulations of mixed layer depth during summer. J. Geophys. Res. Oceans 119, 2568–2582. https://doi.org/10.1002/2013JC009535.
Jacobs, E., Bittig, H.C., Gräwe, U., Graves, C.A., Glockzin, M., Müller, J., Schneider, B., Rehder, G., 2021. Upwelling-induced trace gas dynamics in the Baltic Sea inferred from 8 years of autonomous measurements on a ship of opportunity. Biogeosciences 18, 2679–2709. https://doi.org/10.5194/bg-18-2679-2021.
Jakobsson, M., Stranne, C., O'Regan, M., Greenwood, S.L., Gustafsson, B., Humborg, C., Weidner, E., 2019. Bathymet ric properties of the Baltic Sea. Ocean Sci. 15, 905–992. https://doi.org/10.5194/os-15-905-2019.
Jing, Z., Fox-Kemper, B., Cao, H., Zheng, R., Du, Y., 2021. Submesoscale fronts and their dynamical processes associated with symmetric instability in the northwest pacific subtropical ocean. J. Phys. Oceanogr. 51, 83–100. https://doi.org/10.1175/JPO-D-20-0076.1.
Johnston, T.M.S., Rudnick, D.L., 2009. Observations of the transition layer. J. Phys. Oceanogr. 39, 780–797. https://doi.org/10.1175/2008JPO3824.1.
Kahru, M., Aitsam, A., Elken, J., 1982. Spatio-temporal dynamics of chlorophyll in the open Baltic Sea. J. Plankton Res. 4 (4), 779–790. https://doi.org/10.1093/plankt/4.4.779.
Kahru, M., Leppänen, J.-M., Nõmmann, S., Passow, U., Postel, L., Schulz, S., 1990. Spatio-temporal mosaic of the phytoplankton spring bloom in the open Baltic Sea in 1986. Mar. Ecol. Prog. Ser. 66 (3), 301–309. http://www.jstor.org/stable/24844566.
Kahru, M., Håkansson, B., Rud, O., 1995. Distributions of the sea-surface temperature fronts in the Baltic Sea as derived from satellite imagery. Cont. Shelf Res. 15, 663–679. https://doi.org/10.1016/0278-4343(94)E0030-P.
Karimova, S., 2012. Spiral eddies in the Baltic, Black and Caspian seas as seen by satellite radar data. Adv. Space Res. 50, 1107–1124. https://doi.org/10.1016/j.asr.2011.10.027.
Karimova, S., Gade, M., 2016. Improved statistics of sub-mesoscale eddies in the Baltic Sea retrieved from SAR imagery. Int. J. Remote Sens. 37 (10), 2394–2414. https://doi.org/10.1080/01431161.2016.1145367.
Karimova, S.S., Lavrova, O.Y., Solovev, D.M., 2012. Observation of eddy structures in the Baltic Sea with the use of radiolocation and radiometric satellite data. Izv. Atmos. Ocean. Phys. 48, 1006–1013. https://doi.org/10.1134/S0001433812090071.
Karlson, B., Arneborg, L., Johansson, J., Linders, J., Liu, Y., Olofsson, M., 2022. A suggested climate service for cyanobacteria blooms in the Baltic Sea – comparing three monitoring methods. Harmful Algae 118, 102291. https://doi.org/10.1016/j.hal.2022.102291.
Karstensen, J., Liblik, T., Fischer, J., Bumke, K., Krahmann, G., 2014. Summer upwelling at the boknis eck time-series station, (1982 to 2012) – a combined glider and wind data analysis. Biogeosciences 11, 3603–3617. https://doi.org/10.5194/bg-11-3603-2014.
Kessouri, F., Bianchi, D., Renault, L., McWilliams, J.C., Frenzel, H., Deutsch, C.A., 2020. Submesoscale currents modulate the seasonal cycle of nutrients and productivity in the California Current System. Global Biogeochem. Cycles 34, e2020GB006578. https://doi.org/10.1029/2020GB006578.
Kikas, V., Lips, U., 2016. Upwelling characteristics in the Gulf of Finland (Baltic Sea) as revealed by Ferrybox measurements in 2007-2013. Ocean Sci. 12, 843–859. https://doi.org/10.5194/os-12-843-2016.
Kjellsson, J., Döös, K., 2012. Surface drifters and model trajectories in the Baltic Sea. Boreal Environ. Res. 17 (6), 447–459.
Klingbeil, K., Henell, E., 2023. A Rigorous derivation of the water mass transformation framework, the relation between mixing and diasurface exchange flow, and links to recent theories in estuarine research. J. Phys. Oceanogr. https://doi.org/10.1175/JPO-D-23-0130.1.
Klingbeil, K., Mohammadi-Aragh, M., Gräwe, U., Burchard, H., 2014. Quantification of spurious dissipation and mixing – discrete variance decay in a finite-volume framework. Ocean Model. 81, 49–64. https://doi.org/10.1016/j.ocemod.2014.06.001.
Klymak, J.M., Gregg, M.C., 2001. Three-dimensional nature of flow near a sill. J. Geophys. Res. Oceans 106 (C10), 22295–22311.
Knudsen, M., 1900. Ein hydrographischer Lehrsatz. Ann. Hydrogr. Marit. Meteor. 28 (7), 316–320.
Kobashi, D., Hetland, R., 2020. Reproducibility and variability of submesoscale frontal eddies on a broad, low-energy shelf of freshwater influence. Ocean Dyn. 70, 1377–1395. https://doi.org/10.1007/s10236-020-01401-4.
Köhn, E.E., Thomsen, S., Arévalo-Martínez, D.L., Kanzow, T., 2017. Submesoscale CO_2 variability across an upwelling front off Peru. Ocean Sci. 13, 1017–1033. https://doi.org/10.5194/os-13-1017-2017.
Kolodziejczyk, N., Reverdin, G., Boutin, J., Hernandez, O., 2015. Observation of the surface horizontal thermohaline variability at mesoscale to submesoscale in the north-eastern subtropical Atlantic Ocean. J. Geophys. Res. Oceans 120 (2588–2600), 2015.
Kononen, K., Kuparinen, J., Mäkela, K., Laanemets, J., Pavelson, J., Nõmmann, S., 1996. Initiation of cyanobacterial blooms in a frontal region at the entrance of the Gulf of Finland, Baltic Sea. Limnol. Oceanogr. 41, 98–112.
Kononen, K., Hällfors, S., Kokkonen, M., Kuosa, H., Laanemets, J., Pavelson, J., Autio, R., 1998. Development of a subsurface chlorophyll maximum at the entrance to the Gulf of Finland, Baltic Sea. Limnol. Oceanogr. 43, 1089–1106.
Kononen, K., Huttunen, M., Hällfors, S., Gentien, P., Lunven, M., Huttula, T., Laanemets, J., Lilover, M.-J., Pavelson, J., Stips, A., 2003. Development of a deep chlorophyll maximum of Heterocapsa triquetra Ehrenb. at the entrance to the Gulf of Finland. Limnol. Oceanogr. 48, 594–607.
Kõuts, T., Elken, J., Lips, U., 1990. Late autumn intensification of deep thermohaline anomalies and formation of lenses in the Gotland Deep, in Proc. 17th Conf. Baltic Oceanogr., Norrköping, 280–293.
Kuzmina, N., Rudels, B., Stipa, T., Zhurbas, V., 2005. The structure and driving mechanisms of the Baltic intrusions. J. Phys. Oceanogr. 35 (6), 1120–1137.
Laine, A.O., Sandler, H., Andersin, A.-B., Stigzelius, J., 1997. Long-term changes of macrozoobenthos in the Eastern Gotland Basin and the Gulf of Finland (Baltic Sea) in relation to the hydrographical regime. J. Sea Res. 38 (1), 135–159. https://doi.org/10.1016/S1385-1101(97)00034-8.
Lainela, S., Jacobs, E., Stoicescu, S.-T., Rehder, G., Lips, U., 2024. Seasonal dynamics and regional distribution patterns of CO2 and CH4 in the north-eastern Baltic Sea. Biogeosciences 21 (20), 4495–4519. https://doi.org/10.5194/egusphere-2024-598.
Laanemets, J., Väli, G., Zhurbas, V., Elken, J., Lips, I., Lips, U., 2011. Simulation of mesoscale structures and nutrient transport during summer upwelling events in the Gulf of Finland in 2006. Boreal Environ. Res. 16A, 15–26.
Large, W.G., McWilliams, J.C., Doney, S.C., 1994. Oceanic vertical mixing: a review and a model with a nonlocal boundary layer parameterization. Rev. Geophys. 32 (4), 363–403. https://doi.org/10.1029/94RG01872.
Lass, H.U., Mohrholz, V., Nausch, G., Siegel, H., 2010. On phosphate pumping into the surface layer of the eastern Gotland Basin by upwelling. J. Mar. Syst. 80, 71–89. https://doi.org/10.1016/j.jmarsys.2009.10.002.
Lass, H.U., Prandke, H., Liljebladh, B., 2003. Dissipation in the Baltic proper during winter stratification. J. Geophys. Res. Oceans 108. https://doi.org/10.1029/2002JC001401.
Lehmann, A., Hinrichsen, H.H., 2000. On the wind driven and thermohaline circulation of the Baltic Sea. Phys. Chem. Earth, Part B Hydrology, Oceans Atmos. 25, 183–189. https://doi.org/10.1016/s1464-1909(99)00140-9.
Lehmann, A., Myrberg, K., 2008. Upwelling in the Baltic Sea – a review. J. Mar. Syst. 74, S3–S12. https://doi.org/10.1016/j.jmarsys.2008.02.010.
Lehmann, A., Myrberg, K., Höflich, K., 2012. A statistical approach to coastal upwelling in the Baltic Sea based on the analysis of satellite data for 1990–2009. Oceanologia 54, 369–393.
Lehmann, A., Myrberg, K., Post, P., Chubarenko, I., Dailidiene, I., Hinrichsen, H.-H., Hüssy, K., Liblik, T., Meier, H.E.M., Lips, U., Bukanova, T., 2022. Salinity dynamics of the Baltic Sea. Earth Syst. Dyn. 13 (1), 373–392. https://doi.org/10.5194/esd-13-373-2022.
Lehtoranta, J., Savchuk, O.P., Elken, J., Kim, D., Kuosa, H., Raateoja, M., Kauppila, P., Räike, A., Pitkänen, H., 2017. Atmospheric forcing controlling inter-annual nutrient dynamics in the open Gulf of Finland. J. Mar. Syst. 171, 4–20.
Leppäranta, M., Myrberg, K., 2009. Physical Oceanography of the Baltic Sea. Springer-Verlag, Berlin-Heidelberg.
Lessin, G., Raudsepp, U., Stips, A., 2014. Modelling the Influence of Major Baltic Inflows on Near-Bottom Conditions at the Entrance of the Gulf of Finland. PLoS One 9 (11), e112881. https://doi.org/10.1371/journal.pone.0112881.
Lévy, M., Ferrari, R., Franks, P.J.S., Martin, A.P., Rivière, P., 2012. Bringing physics to life at the submesoscale. Geophys. Res. Lett. 39 (14). https://doi.org/10.1029/2012GL052756.
Liblik, T., Lips, U., 2012. Variability of synoptic-scale quasi-stationary thermohaline stratification patterns in the Gulf of Finland in summer 2009. Ocean Sci. 8, 603–614. https://doi.org/10.5194/os-8-603-2012.
Liblik, T., Lips, U., 2017. Variability of pycnoclines in a three-layer, large estuary: the Gulf of Finland. Boreal Environ. Res. 22, 27–47.
Liblik, T., Naumann, M., Alenius, P., Hansson, M., Lips, U., Nausch, G., Tuomi, L., Wesslander, K., Laanemets, J., Viktorsson, L., 2018. Propagation of impact of the recent Major Baltic Inflows from the Eastern Gotland Basin to the Gulf of Finland. Front. Mar. Sci. 5 (222), 1–23. https://doi.org/10.3389/fmars.2018.00222.
Liblik, T., Skudra, M., Lips, U., 2017. On the buoyant sub-surface salinity maxima in the Gulf of Riga. Oceanologia 59 (2), 113–128. https://doi.org/10.1016/j.oceano.2016.10.001.
Liblik, T., Stoicescu, S.-T., Buschmann, F., Lilover, M.-J., Lips, U., 2023. High-resolution characterization of the development and decay of seasonal hypoxia in the Gulf of Riga, Baltic Sea. Front. Mar. Sci. 10, 1–8. https://doi.org/10.3389/fmars.2023.1119515.
Liblik, T., Väli, G., Lips, I., Lilover, M.-J., Kikas, V., Laanemets, J., 2020. The winter stratification phenomenon and its consequences in the Gulf of Finland, Baltic Sea. Ocean Sci. 16, 1475–1490. https://doi.org/10.5194/os-16-1475-2020.
Liblik, T., Väli, G., Salm, K., Laanemets, J., Lilover, M.-J., Lips, U., 2022. Quasi-steady circulation regimes in the Baltic Sea. Ocean Sci. 18, 857–879. https://doi.org/10.5194/os-18-857-2022.

Lilover, M.-J., Lips, U., Laanearu, J., Liljebladh, B., 1998. Flow regime in the Irbe Strait. Aquat. Sci. 60, 253–265. https://doi.org/10.1007/s000270050040.
Lilover, M.-J., Lips, U., Liblik, T., Suhhova, I., Väli, G., 2025. Variability of stratification and currents at the submesoscale detected from CTD and current profiles in the central Gulf of Finland. Boreal Environ. Res. 30, 77–92. https://doi.org/10.60910/ber2025.jtg5-j683.
Lips, I., Lips, U., 2008. Abiotic factors influencing cyanobacterial bloom development in the Gulf of Finland (Baltic Sea). Hydrobiologia 614 (1), 133–140.
Lips, I., Lips, U., 2017. The importance of mesodinium rubrum at post-spring bloom nutrient and phytoplankton dynamics in the vertically stratified Baltic Sea. Front. Mar. Sci. 4. https://doi.org/10.3389/fmars.2017.00407.
Lips, I., Lips, U., Liblik, T., 2009. Consequences of coastal upwelling events on physical and chemical patterns in the central Gulf of Finland (Baltic Sea). Cont. Shelf Res. 29 (15), 1836–1847. https://doi.org/10.1016/j.csr.2009.06.010.
Lips, I., Rünk, N., Kikas, V., Meerits, A., Lips, U., 2014. High-resolution dynamics of the spring bloom in the Gulf of Finland of the Baltic Sea. J. Mar. Syst. 129, 135–149. https://doi.org/10.1016/j.jmarsys.2013.06.002.
Lips, U., Kikas, V., Liblik, T., Lips, I., 2016a. Multi-sensor in situ observations to resolve the sub-mesoscale features in the stratified Gulf of Finland, Baltic Sea. Ocean Sci. 12 (3), 715–732. https://doi.org/10.5194/os-12-715-2016.
Lips, U., Laanemets, J., 1991. On the staircase layering of thermohaline fields beneath a layer of Mediterranean water in the Canary basin. Oceanology 31 (4), 407–411.
Lips, U., Laanemets, J., Lips, I., Liblik, T., Suhhova, I., Suursaar, Ü., 2017. Wind-driven residual circulation and related oxygen and nutrient dynamics in the Gulf of Finland (Baltic Sea) in winter. Estuar. Coast. Shelf Sci. 195, 4–15. https://doi.org/10.1016/j.ecss.2016.10.006.
Lips, U., Lips, I., 2014. Bimodal distribution patterns of motile phytoplankton in relation to physical processes and stratification (Gulf of Finland, Baltic Sea). Deep Sea Res. Part II 101, 107–119.
Lips, U., Lips, I., Liblik, T., Kikas, V., Altoja, K., Buhhalko, N., Rünk, N., 2011. Vertical dynamics of summer phytoplankton in a stratified estuary (Gulf of Finland, Baltic Sea). Ocean Dyn. 61, 903–915. https://doi.org/10.1007/s10236-011-0421-8.
Lips, U., Lips, I., Liblik, T., Kuvaldina, N., 2010. Processes responsible for the formation and maintenance of sub-surface chlorophyll maxima in the Gulf of Finland. Estuar. Coast. Shelf Sci. 88, 339–349. https://doi.org/10.1016/j.ecss.2010.04.015.
Lips, U., Zhurbas, V., Skudra, M., Väli, G., 2016b. A numerical study of circulation in the Gulf of Riga, Baltic Sea. Part I: whole-basin gyres and mean currents. Cont. Shelf Res. 112, 1–13. https://doi.org/10.1016/j.csr.2015.11.008.
Lips, U., Zhurbas, V., Skudra, M., Väli, G., 2016c. A numerical study of circulation in the Gulf of Riga, Baltic Sea. Part II: mesoscale features and freshwater transport pathways. Cont. Shelf Res. 115, 44–52. https://doi.org/10.1016/j.csr.2015.12.018.
MacCready, P., 2011. Calculating estuarine exchange flow using isohaline coordinates. J. Phys. Oceanogr. 41 (6), 1116–1124. https://doi.org/10.1175/2011JPO4517.1.
MacCready, P., Geyer, W.R., Burchard, H., 2018. Estuarine exchange flow is related to mixing through the salinity variance budget. J. Phys. Oceanogr. 48 (6), 1375–1384. https://doi.org/10.1175/JPO-D-17-0266.1.
Madec, G., and the NEMO System Team. (2015). NEMO ocean engine. Note du Pôle de modélisation de l'Institut Pierre-Simon Laplace, No 27, November 2015, version 3.6 stable.
Maljutenko, I., Raudsepp, U., 2019. Long-term mean, interannual and seasonal circulation in the Gulf of Finland – the wide salt wedge estuary or gulf type ROFI. J. Marine Syst. 195, 1–19. https://doi.org/10.1016/j.jmarsys.2019.03.004.
Manucharyan, G.E., Thompson, A.F., 2017. Submesoscale sea ice-ocean interactions in marginal ice zones. J. Geophys. Res. Oceans 122, 9455–9475. https://doi.org/10.1002/2017JC012895.
Marmorino, G., Chen, W., 2019. Use of WorldView-2 along-track stereo imagery to probe a baltic sea algal spiral. Remote Sens. (Basel) 11 (7), 865. https://doi.org/10.3390/rs11070865.
McMahon, C.R., Roquet, F., Baudel, S., Belbeoch, M., Bestley, S., Blight, C., Boehme, L., Carse, F., Costa, D.P., Fedak, M.A., Guinet, C., Harcourt, R., Heslop, E., Hindell, M. A., Hoenner, X., Holland, K., Holland, M., Jaine, F.R.A., Jeanniard du Dot, T., Jonsen, I., Keates, T.R., Kovacs, K.M., Labrousse, S., Lovell, P., Lydersen, C., March, D., Mazloff, M., McKinzie, M.K., Muelbert, M.M.C., O'Brien, K., Phillips, L., Portela, E., Pye, J., Rintoul, S., Sato, K., Sequeira, A.M.M., Simmons, S.E., Tsontos, V. M., Turpin, V., van Wijk, E., Vo, D., Wege, M., Whoriskey, F.G., Wilson, K., Woodward, B., 2021. Animal borne ocean sensors – AniBOS – an essential component of the global ocean observing system. Front. Mar. Sci. 8, 751840. https://doi.org/10.3389/fmars.2021.751840.
McWilliams, J.C., 2016. Submesoscale currents in the ocean. Proc. R. Soc. A 472, 20160117. https://doi.org/10.1098/rspa.2016.0117.
McWilliams, J.C., 2019. A survey of submesoscale currents. Geosci. Lett. 6, 3. https://doi.org/10.1186/s40562-019-0133-3.
McWilliams, J.C., 2021. Oceanic frontogenesis. Ann. Rev. Mar. Sci. 13 (1), 227–253. https://doi.org/10.1146/annurev-marine-032320-120725.
McWilliams, J.C., Gula, J., Molemaker, M.J., Renault, L., Shchepetkin, A.F., 2015. Filament frontogenesis by boundary layer turbulence. J. Phys. Oceanogr. 45, 1988–2005. https://doi.org/10.1175/JPO-D-14-0211.1.
Meier, H.E.M., 2001. On the parameterization of mixing in three-dimensional Baltic Sea models. J. Geophys. Res. 106, 30,997–31,016.
Meier, H.E.M., 2007. Modeling the pathways and ages of inflowing salt- and freshwater in the Baltic Sea. Estuar. Coast. Shelf Sci. 74 (4), 717–734. https://doi.org/10.1016/j.ecss.2007.05.019.
Meier, H.E.M., Dieterich, C., Gröger, M., Dutheil, C., Börgel, F., Safonova, K., Christensen, O.B., Kjellström, E., 2022. Oceanographic regional climate projections for the Baltic Sea until 2100. Earth Syst. Dyn. 13, 159–199. https://doi.org/10.5194/esd-13-159-2022.
Meier, H.E.M., Döscher, R., Broman, B., Piechura, J., 2004. The major Baltic inflow in January 2003 and preconditioning by smaller inflows in summer/autumn 2002: a model study. Oceanologia 46 (4), 557–579.
Meier, H.E.M., Feistel, R., Piechura, J., Arneborg, L., Burchard, H., Fiekas, V., Golenko, N., Kuzmina, N., Mohrholz, V., Nohr, C., Paka, V.T., Sellschopp, J., Stips, A., Zhurbas, V., 2006. Ventilation of the Baltic Sea deep water: a brief review of present knowledge from observations and models. Oceanologia 48, 133–164.
Meier, H.E.M., Höglund, A., Döscher, R., Andersson, H., Löptien, U., Kjellström, E., 2011. Quality assessment of atmospheric surface fields over the Baltic Sea of an ensemble of regional climate model simulations with respect to ocean dynamics. Oceanologia 53, 193–227.
Meier, H.E.M., Väli, G., Naumann, M., Eilola, K., Frauen, C., 2018. Recently accelerated oxygen consumption rates amplify deoxygenation in the Baltic Sea. J. Geophys. Res. 123, 3227–3240. https://doi.org/10.1029/2017JC013686.
Mellor, G.L., Yamada, T., 1982. Development of a turbulence closure model for geophysical fluid problems. Rev. Geophys. 20 (4), 851–875. https://doi.org/10.1029/RG020i004p00851.
Meneghello, G., Doddridge, E., Marshall, J., Scott, J., Campin, J.-M., 2020. Exploring the role of the "ice-ocean governor" and mesoscale eddies in the equilibration of the Beaufort Gyre: lessons from observations. J. Phys. Oceanogr. 50 (1), 269–277. https://doi.org/10.1175/jpo-d-18-0223.1.
Mensa, J.A., Garraffo, Z., Griffa, A., Özgökmen, T.M., Haza, A., Veneziani, M., 2013. Seasonality of the submesoscale dynamics in the Gulf Stream region. Ocean Dyn. 63 (8), 923–941. https://doi.org/10.1007/s10236-013-0633-1.
Merchel, M., Walczowski, W., Rak, D., Wieczorek, P., 2024. The use of Argo floats as virtual moorings for monitoring the South Baltic Sea. Oceanologia 66, 99–110. https://doi.org/10.1016/j.oceano.2024.01.002.
Merchel, M., Walczowski, W., Wieczorek, P., 2025. Anchored Argo profiling float experiments in the southern Baltic Sea: Puck Bay and Hel Peninsula. Front. Mar. Sci. 12, 1569261. https://doi.org/10.3389/fmars.2025.1569261.
Meyer, D., Lips, U., Prien, R.D., Naumann, M., Liblik, T., Schuffenhauer, I., Schulz-Bull, D.E., 2018. Quantification of dissolved oxygen dynamics in a semi-enclosed sea - a comparison of observational platforms. Cont. Shelf Res. 169, 34–45. https://doi.org/10.1016/j.csr.2018.09.011.
Mode Group, 1978. The mid-ocean dynamics experiment. Deep Sea Res. 25, 859–910.
Mohrholz, V., 2018. Major baltic inflow statistics – revised. Front. Mar. Sci. 5, 384. https://doi.org/10.3389/fmars.2018.00384.
Mohrholz, V., Dutz, J., Kraus, G., 2006. The impact of exceptionally warmp summer inflow events on the environmental conditions in the Bornholm Basin. J. Mar. Syst. 60, 285–301. https://doi.org/10.1016/j.jmarsys.2005.10.002.
Mohrholz, V., Naumann, M., Nausch, G., Krüger, S., Gräwe, U., 2015. Fresh oxygen for the Baltic Sea - an exceptional saline inflow after a decade of stagnation. J. Mar. Syst. 148, 152–166. https://doi.org/10.1016/j.jmarsys.2015.03.005.
Mohrmann, M., Biddle, C.L., Rehder, G., Bittig, H.C., Queste, B.Y., 2025. Nord Stream methane leaks spread across 14% of Baltic waters. Nat. Commun. 16, 281. https://doi.org/10.1038/s41467-024-53779-0.
Molemaker, M.J., McWilliams, M.J., Capet, X., 2010. Balanced and unbalanced routes to dissipation in an equilibrated Eady flow. J. Fluid Mech. 654, 35–63.
Molemaker, M.J., McWilliams, J.C., Dewar, W.K., 2015. Submesoscale instability and generation of mesoscale anticyclones near a separation of the california undercurrent. J. Phys. Oceanogr. 45, 613–629. https://doi.org/10.1175/JPO-D-13-0225.1.
Muchowski, J., Arneborg, L., Umlauf, L., Holtermann, P., Eisbrenner, E., Humborg, C., Jakobsson, M., Stranne, C., 2023a. Diapycnal mixing induced by rough small-scale bathymetry. Geophys. Res. Lett. 50, e2023GL103514. https://doi.org/10.1029/2023GL103514.
Muchowski, J., Jakobsson, M., Umlauf, L., Arneborg, L., Gustafsson, B., Holtermann, P., Humborg, C., Stranne, C., 2023b. Observations of strong turbulence and mixing impacting water exchange between two basins in the Baltic Sea. Ocean Sci. 19 (6), 1809–1825.
Muchowski, J., Umlauf, L., Arneborg, L., Holtermann, P., Weidner, E., Humborg, C., Stranne, C., 2022. Potential and limitations of a commercial broadband echo sounder for remote observations of turbulent mixing. J. Atmos. Oceanic Tech. 39 (12), 1985–2003.
Myrberg, K., Andrejev, O., 2003. Main upwelling regions in the Baltic Sea – a statistical analysis based on three-dimensional modeling. Boreal Environ. Res. 8, 97–112.
Nagai, T., Gruber, N., Frenzel, H., Lachkar, Z., McWilliams, J.C., Plattner, G.-K., 2015. Dominant role of eddies and filaments in the offshore transport of carbon and nutrients in the California Current System. J. Geophys. Res. Ocean. 120 (8), 5318–5341. https://doi.org/10.1002/2015JC010889.
Naumov, L., Neumann, T., Radtke, H., Meier, H.E.M., 2023a. Limited ventilation of the central Baltic Sea due to elevated oxygen consumption. Front. Mar. Sci. 10, 1175643. https://doi.org/10.3389/fmars.2023.1175643.
Naumov, L., Meier, H.E.M., Neumann, T., 2023b. Dynamics of oxygen sources and sinks in the Baltic Sea under different nutrient inputs. Front. Mar. Sci. 10, 1233324. https://doi.org/10.3389/fmars.2023.1233324.
Naveira Garabato, A.C., Frajka-Williams, E.E., Spingys, C.P., Legg, S., Polzin, K.L., Forryan, A., Abrahamsen, E.P., Buckingham, C.E., Griffies, S.M., McPhail, S.D., Nicholls, K.W., Thomas, L.N., Meredith, M.P., 2019. Rapid mixing and exchange of deep-ocean waters in an abyssal boundary current. Proc. Natl. Acad. Sci. U.S.A. 116 (27), 13233–13238. https://doi.org/10.1073/pnas.1904087116.
Naveira Garabato, A.C., Yu, X., Callies, J., Barkan, R., Polzin, K.L., Frajka-Williams, E.E., Buckingham, C.E., Griffies, S.M., 2022. Kinetic energy transfers between mesoscale and submesoscale motions in the open ocean's upper layers. J. Phys. Oceanogr. 52 (1), 75–97. https://doi.org/10.1175/JPO-D-21-0099.1.

Norman, M., Parampil, S.R., Rutgersson, A., Sahlée, E., 2013. Influence of coastal upwelling on the air–sea gas exchange of CO_2 in a Baltic Sea Basin. Tellus B: Chem. Phys. Meteorol. 65 (1). https://doi.org/10.3402/tellusb.v65i0.21831.
Oksanen, S.M., Niemi, M., Ahola, M.P., Kunnasranta, M., 2015. Identifying foraging habitats of Baltic ringed seals using movement data. Mov. Ecol. 3, 33. https://doi.org/10.1186/s40462-015-0058-1.
Omand, M.M., D'Asaro, E.A., Lee, C.M., Perry, M.J., Briggs, N., Cetinić, I., Mahadevan, A., 2015. Eddy-driven subduction exports particulate organic carbon from the spring bloom. Science 348, 222–225. https://doi.org/10.1126/science.1260062.
Omstedt, A., Elken, J., Lehmann, A., Piechura, J., 2004. Knowledge of the Baltic Sea physics gained during the BALTEX and related programmes. Prog. Oceanogr. 63 (1), 1–28. https://doi.org/10.1016/j.pocean.2004.09.001.
Omstedt, A., Elken, J., Lehmann, A., Leppäranta, M., Meier, H.E.M., Myrberg, K., Rutgersson, A., 2014. Progress in physical oceanography of the Baltic Sea during the 2003–2014 period. Prog. Oceanogr. 128, 139–171. https://doi.org/10.1016/j.pocean.2014.08.010.
Onken, R., Baschek, B., Angel-Benavides, I.M., 2020. Very high-resolution modelling of submesoscale turbulent patterns and processes in the Baltic Sea. Ocean Sci. 16, 657–684. https://doi.org/10.5194/os-16-657-2020.
Osiński, R., Rak, D., Walczowski, W., Piechura, J., 2010. Baroclinic Rossby radius of deformation in the southern Baltic Sea. Oceanologia 52 (3), 417–429. https://doi.org/10.5697/oc.52-3.417.
Palmén, E., 1930. Untersuchungen über die Strömungen in den Finnland umgebenden Meeren. Comment. physico-mathematicae/Soc. Sci. Fenn. 12.
Pärt, S., Björkqvist, J.-V., Alari, V., Maljutenko, I., Uiboupin, R., 2023. An ocean–wave–trajectory forecasting system for the eastern Baltic Sea: validation against drifting buoys and implementation for oil spill modeling. Mar. Pollut. Bull. 195, #115497. https://doi.org/10.1016/j.marpolbul.2023.115497.
Pavelson, J., Kononen, K., Laanemets, J., 1999. Chlorophyll distribution patchiness caused by hydrodynamical processes: a case study in the Baltic Sea. ICES J. Mar. Sci. 56 (Supplement), 87–99.
Pavelson, J., Laanemets, J., Kononen, K., Nõmmann, S., 1997. Quasi-permanent density front at the entrance to the Gulf of Finland: response to wind forcing. Cont. Shelf Res. 17, 253–265.
Pham, H.T., Verma, V., Sarkar, S., Shcherbina, A.Y., D'Asaro, E.A., 2024. Rapid downwelling of tracer particles across the boundary layer and into the pycnocline at submesoscale ocean fronts. Geophys. Res. Lett. 51, e2024GL109674. https://doi.org/10.1029/2024GL109674.
Picard, T., Gula, J., Vic, C., Mémery, L., 2024. Seasonal tracer subduction in the subpolar North Atlantic driven by submesoscale fronts. J. Geophys. Res. Oceans 129, e2023JC020782. https://doi.org/10.1029/2023JC020782.
Piechura, J., Walczowski, W., Beszczyńska-Möller, A., 1997. On the structure and dynamics of the water in the Słupsk Furrow. Oceanologia 39 (1), 35–54.
Placke, M., Meier, H.E.M., Gräwe, U., Neumann, T., Frauen, C., Liu, Y., 2018. Long-term mean circulation of the Baltic Sea as represented by various ocean circulation models. Front. Mar. Sci. 5, 287. https://doi.org/10.3389/fmars.2018.00287.
Placke, M., Meier, H.E.M., Neumann, T., 2021. Sensitivity of the Baltic Sea overturning circulation to long-term atmospheric and hydrological changes. J. Geophys. Res. Oceans 126, e2020JC016079.
Ploug, H., 2008. Cyanobacterial surface blooms formed by *Aphanizomenon* sp. and *Nodularia spumigena* in the Baltic Sea: small-scale fluxes, pH, and oxygen microenvironments. Limnol. Oceanogr. 53. https://doi.org/10.4319/lo.2008.53.3.0914.
Polyakov, I.V., Tikka, K., Haapala, J., Alkire, M.B., Alenius, P., Kuosa, H., 2022. Depletion of oxygen in the Bothnian Sea since the Mid-1950s. Front. Mar. Sci. 9, 2022. https://doi.org/10.3389/fmars.2022.917879.
Prend, C.J., Swart, S., Stewart, A.L., du Plessis, M.D., Manucharyan, G.E., Thompson, A.F., 2025. Observed regimes of submesoscale dynamics in the Southern Ocean seasonal ice zone. Nat. Commun. 16, 8344. https://doi.org/10.1038/s41467-025-63775-7.
Prien, R.D., Schulz-Bull, D.E., 2016. Technical note: GODESS – a profiling mooring in the Gotland Basin. Ocean Sci. 12, 899–907. https://doi.org/10.5194/os-12-899-2016.
Purokoski, T., Aro, E., Nummelin, A., 2013. First long-term deployment of Argo float in Baltic Sea. Sea Technol. 54, 41–44.
Rak, D., 2016. The inflow in the Baltic proper as recorded in January–February 2015. Oceanologia 58 (3), 241–247. https://doi.org/10.1016/j.oceano.2016.04.001.
Rak, D., Wieczorek, P., 2012. Variability of temperature and salinity over the last decade in selected regions of the southern Baltic Sea. Oceanologia 54 (3), 339–354. https://doi.org/10.5697/oc.54-3.339.
Ralston, D.K., Cowles, G.W., Geyer, W.R., Holleman, R.C., 2017. Turbulent and numerical mixing in a salt wedge estuary: dependence on grid resolution, bottom roughness, and turbulence closure. J. Geophys. Res. Oceans 122, 692–712. https://doi.org/10.1002/2016JC011738.
Rantajärvi, E., (Ed.). (2003). Alg@line in 2003: 10 years of innovative plankton monitoring and research and operational information service in the Baltic Sea, MERI – Report Series of the Finnish Institute of Marine Research, No. 48, 1–36, 2003.
Reissmann, J.H., Burchard, H., Feistel, R., Hagen, E., Lass, H.U., Mohrholz, V., Nausch, G., Umlauf, L., Wieczorek, G., 2009. Vertical mixing in the Baltic Sea and consequences for eutrophication a review. Prog. Oceanogr. 82, 47–80. https://doi.org/10.1016/j.pocean.2007.10.004.
Resplandy, L., Lévy, M., d'Ovidio, F., Merlivat, L., 2009. Impact of submesoscale variability in estimating the air-sea CO_2 exchange: results from a model study of the POMME experiment. Global Biogeochem. Cycles 2009 (23), 1017. https://doi.org/10.1029/2008GB003239.
Roiha, P., Siiriä, S.-M., Haavisto, N., Alenius, P., Westerlund, A., Purokoski, T., 2018. Estimating currents from Argo trajectories in the Bothnian Sea, Baltic Sea. Front. Mar. Sci. 5. https://doi.org/10.3389/fmars.2018.00308.
Rudnick, D.L., Cole, S.T., 2011. On sampling the ocean using underwater gliders. J. Geophys. Res. Oceans 116 (8). https://doi.org/10.1029/2010JC006849.
Rudnick, D.L., Zaba, K.D., Todd, R.E., Davis, R.E., 2017. A climatology of the California current system from a network of underwater gliders. Prog. Oceanogr. 154, 64–106. https://doi.org/10.1016/j.pocean.2017.03.002.
Salm, K., Liblik, T., Lips, U., 2023. Submesoscale variability in a mesoscale front captured by a glider mission in the Gulf of Finland, Baltic Sea. Front. Mar. Sci. 10. https://doi.org/10.3389/fmars.2023.984246.
Salm, K., Väli, G., Liblik, T., Lips, U., 2025. Forcing-dependent submesoscale variability and subduction in a coastal sea area (Gulf of Finland, Baltic Sea). Ocean Sci. 21, 2555–2577. https://doi.org/10.5194/os-21-2555-2025.
Schlichting, D., Qu, L., Kobashi, D., Hetland, R., 2023. Quantification of physical and numerical mixing in a coastal ocean model using salinity variance budgets. J. Adv. Model. Earth Syst. 15, e2022MS003380. https://doi.org/10.1029/2022MS003380.
Schlichting, D., Hetland, R., Jones, C.S., 2024. Numerical mixing suppresses submesoscale baroclinic instabilities over sloping bathymetry. J. Adv. Model. Earth Syst. 16, e2024MS004321. https://doi.org/10.1029/2024MS004321.
Schmidt, B., Wodzinowski, T., Bulczak, A.I., 2021. Long-term variability of near-bottom oxygen, temperature and slinity in the southern Baltic. J. Mar. Syst. 213, 103462. https://doi.org/10.1016/j.jmarsys.2020.103462.
Schneider, B., Gülzow, W., Sadkowiak, B., Rehder, G., 2014. Detecting sinks and sources of CO_2 and CH_4 by ferrybox-based measurements in the Baltic Sea: three case studies. J. Mar. Syst. 140, 13–25. https://doi.org/10.1016/j.jmarsys.2014.03.014.
Schubert, R., Gula, J., Greatbatch, R.J., Baschek, B., Biastoch, A., 2020. The submesoscale kinetic energy cascade: Mesoscale absorption of submesoscale mixed layer eddies and frontal downscale fluxes. J. Phys. Oceanogr. 50, 2573–2589. https://doi.org/10.1175/JPO-D-19-0311.1.
Sellschopp, J., Arneborg, L., Knoll, M., Fiekas, V., Gerdes, F., Burchard, H., Lass, H.U., Mohrholz, V., Umlauf, L., 2006. Direct observations of a medium-intensity inflow into the Baltic Sea. Cont. Shelf Res. 26, 2393–2414.
Shcherbina, A.Y., D'Asaro, E.A., Lee, C.M., Klymak, J.M., Molemaker, M.J., McWilliams, J.C., 2013. Statistics of vertical vorticity, divergence, and strain in a developed submesoscale turbulence field. Geophys. Res. Lett. 40 (17), 4706–4711. https://doi.org/10.1002/grl.50919.
Siegelman, L., Klein, P., Rivière, P., Thompson, A.F., Torres, H.S., Torres, H.S., Flexas, M., Menemenlis, D., 2020. Enhanced upward heat transport at deep submesoscale ocean fronts. Nat. Geosci. 13, 50–55.
Siiriä, S., Roiha, P., Tuomi, L., Purokoski, T., Haavisto, N., Alenius, P., 2018. Applying area-locked, shallow water Argo floats in Baltic Sea monitoring. J. Operat Oceanogr. 12 (1), 58–72. https://doi.org/10.1080/1755876X.2018.1544783.
Smagorinsky, J., 1963. General circulation experiments with the primitive equations. Mon. Wea. Rev. 91, 99–164. https://doi.org/10.1175/1520-0493(1963)091<0099:GCEWTP>2.3.CO;2.
Soosaar, E., Maljutenko, I., Uiboupin, R., Skudra, M., Raudsepp, U., 2016. River bulge evolution and dynamics in a non-tidal sea Daugava River plume in the Gulf of Riga, Baltic Sea. Ocean Sci. 12, 417–432. https://doi.org/10.5194/os-12-417-2016.
Stipa, T., Tamminen, T., Seppälä, J., 1999. On the creation and maintenance of stratification in the Gulf of Riga. J. Mar. Syst. 23 (27–49), 1999.
Stoicescu, S.-T., Lips, U., Liblik, T., 2019. Assessment of eutrophication status based on sub-surface oxygen conditions in the Gulf of Finland (Baltic Sea). Front. Mar. Sci. 6. https://doi.org/10.3389/fmars.2019.00054.
Stoicescu, S.-T., Laanemets, J., Liblik, T., Skudra, M., Samlas, O., Lips, I., Lips, U., 2022. Causes of the extensive hypoxia in the Gulf of Riga in 2018. Biogeosciences 19 (11), 2903–2920. https://doi.org/10.5194/bg-19-2903-2022.
Stoicescu, S.-T., Hoikkala, L., Fleming, V., Lips, U., 2024. Continuing long-term expansion of low-oxygen conditions in the Eastern Gulf of Finland. Oceanologia 66 (1), 139–152. https://doi.org/10.1016/j.oceano.2024.02.002.
Su, Z., Wang, J., Klein, P., Thompson, A.F., Menemenlis, D., 2018. Ocean submesoscales as a key component of the global heat budget. Nat. Commun. 9 (1), 775. https://doi.org/10.1038/s41467-018-02983-w.
Suhhova, I., Liblik, T., Lilover, M.-J., Lips, U., 2018. A descriptive analysis of the linkage between the vertical stratification and current oscillations in the Gulf of Finland. Boreal Environ. Res. 23, 83–103.
Suursaar, Ü., Aps, R., 2007. Spatio-temporal variations in hydro-physical and -chemical parameters during a major upwelling event off the southern coast of the Gulf of Finland in summer 2006. Oceanologia 49, 209–228.
Suursaar, Ü., Elken, J., Belkin, I.M., 2021. Fronts in the Baltic Sea: a review with a focus on its north-eastern part. Chem. Oceanogr Frontal Zones 143–181. https://doi.org/10.1007/698_2021_813.
Swart, S., du Plessis, M.D., Nicholson, S.-A., Monteiro, P.M.S., Dove, L.A., Thomalla, S., Thompson, A.F., Biddle, L.C., Edholm, J.M., Giddy, I., Heywood, K.J., Lee, C., Mahadevan, A., Shilling, G., de Souza, R.B., 2023. The Southern Ocean mixed layer and its boundary fluxes: fine-scale observational progress and future research priorities. Philos. Trans. R. Soc. A 381, 20220058. https://doi.org/10.1098/rsta.2022.0058.
Taylor, J.R., 2018. Accumulation and subduction of buoyant material at submesoscale fronts. J. Phys. Oceanogr. 48, 1233–1241. https://doi.org/10.1175/JPO-D-17-0269.1.
Taylor, J.R., Ferrari, R., 2009. On the equilibration of a symmetrically unstable front via a secondary shear instability. J. Fluid Mech. 622, 103–113. https://doi.org/10.1017/S0022112008005272.

Taylor, J.R., Ferrari, R., 2010. Buoyancy and wind-driven convection at mixed layer density fronts. J. Phys. Oceanogr. 40 (6), 1222–1242. https://doi.org/10.1175/2010JPO4365.1.
Taylor, J.R., Thompson, A.F., 2023. Submesoscale dynamics in the upper ocean. Annu. Rev. Fluid Mech. 55, 103–127. https://doi.org/10.1146/annurev-fluid-031422.
Thomas, L.N., Tandon, A., Mahadevan, A., 2008. Submesoscale processes and Dynamics, Ocean Modeling in an Eddying Regime, 177, 17–38.
Thomas, L.N., Taylor, J.R., Ferrari, R., Joyce, M.T., 2013. Symmetric instability in the gulf stream. Deep Sea Res. Part II: Topp. Stud. Oceanogr. 91, 96–110. https://doi.org/10.1016/j.dsr2.2013.02.025.
Thompson, A.F., Lazar, A., Buckingham, C., Naveira Garabato, A.C., Damerell, G.M., Heywood, K.J., 2016. Open-ocean submesoscale motions: a full seasonal cycle of mixed layer instabilities from gliders. J. Phys. Ocean. 46 (4), 1285–1307.
Tuomi, L., Myrberg, K., Lehmann, A., 2012. The performance of the parameterisations of vertical turbulence in the 3D modelling of hydrodynamics in the Baltic Sea. Cont. Shelf Res. 50–51, 64–79. https://doi.org/10.1016/j.csr.2012.08.007.
Uiboupin, R., Laanemets, J., 2009. Upwelling characteristics derived from satellite sea surface temperature data in the Gulf of Finland, Baltic Sea. Boreal Environ. Res. 14 (2), 297–304.
Umlauf, L., Arneborg, L., Burchard, H., Fiekas, V., Lass, H.U., Mohrholz, V., Prandke, H., 2007. Transverse structure of turbulence in a rotating gravity current. Geophys. Res. Lett. 34 (8).
Umlauf, L., Arneborg, L., 2009a. Dynamics of rotating shallow gravity currents passing through a channel. Part I: observation of transverse structure. J. Phys. Oceanogr. 39 (10), 2385–2401.
Umlauf, L., Arneborg, L., 2009b. Dynamics of rotating shallow gravity currents passing through a channel. Part II: analysis. J. Phys. Oceanogr. 39 (10), 2402–2416.
Umlauf, L., Arneborg, L., Hofmeister, R., Burchard, H., 2010. Entrainment in shallow rotating gravity currents: a modeling study. J. Phys. Oceanogr. 40 (8), 1819–1834.
Umlauf, L., Holtermann, P., Gillner, C.A., Prien, R., Merckelbach, L., Carpenter, J.R., 2018. Diffusive convection under rapidly varying conditions. J. Phys. Oceanogr. 48 (1731–1747), 2018. https://doi.org/10.1175/JPO-D-18-0018.1.
Väli, G., Meier, H.E.M., Elken, J., J., 2013. Simulated halocline variability in the Baltic Sea and its impact on hypoxia during 1961-2007. J. Geophys. Res. 118, 6982–7000. https://doi.org/10.1002/2013JC009192.
Väli, G., Meier, H.E.M., Liblik, T., Radtke, H., Klingbeil, K., Gräwe, U., Lips, U., 2024. Submesoscale processes in the surface layer of the central Baltic Sea: a high-resolution modelling study. Oceanologia 66 (1), 78–90. https://doi.org/10.1016/j.oceano.2023.11.002.
Väli, G., Meier, H.E.M., Radtke, R., Liblik, T., Hariri, S., Lips, U., 2025. Role of small-scale processes in the coastal offshore exchange in the Baltic Sea: results from a multi-year high-resolution modelling study, Front. Earth Sci. (in review).
Väli, G., Zhurbas, V., Lips, U., Laanemets, J., 2017. Submesoscale structures related to upwelling events in the Gulf of Finland, Baltic Sea (numerical experiments). J. Mar. Syst. 171, 31–42. https://doi.org/10.1016/j.jmarsys.2016.06.010.
van der Lee, E.M., Umlauf, L., 2011. Internal wave mixing in the Baltic Sea: near-inertial waves in the absence of tides. J. Geophys. Res. Oceans 116 (C10). https://doi.org/10.1029/2011JC007072.
Vankevich, R.E., Sofina, E.V., Eremina, T.E., Ryabchenko, V.A., Molchanov, M.S., Isaev, A.V., 2016. Effects of lateral processes on the seasonal water stratification of the Gulf of Finland: 3-D NEMO-based model study. Ocean Sci. 12, 987–1001. https://doi.org/10.5194/os-12-987-2016.
Verma, V., Pham, H.T., Sarkar, S., 2019. The submesoscale, the finescale and their interaction at a mixed layer front. Ocean Model. 140, 101400.
Vortmeyer-Kley, R., Berthold, M., Cahill, B., Gräwe, U., Feudel, U., 2025. Unraveling the influence of short-lived, three-dimensional, eddy-like, coherent,m oceanic structures on phytoplankton dynamics and nutrient transport. J. Geophys. Res. Biogeo. 130, e2025JG009107. https://doi.org/10.1029/2025JG009107.
Vortmeyer-Kley, R., Gräwe, U., Feudel, U., 2016. Detecting and tracking eddies in oceanic flow fields: a Lagrangian descriptor based on the modulus of vorticity. Nonlinear Process. Geophys. 23, 159–173. https://doi.org/10.5194/npg-23-159-2016.
Vortmeyer-Kley, R., Lünsmann, B., Berthold, M., Gräwe, U., Feudel, U., 2019. Eddies: fluid dynamical niches or transporters? – a case study in the Western Baltic sea. Front. Mar. Sci. 6, 118. https://doi.org/10.3389/fmars.2019.00118.
Walczowski, W., Merchel, M., Rak, D., Wieczorek, P., Goszczko, I., 2020. Argo floats in the southern Baltic Sea. Oceanologia 62 (4A), 478–488. https://doi.org/10.1016/j.oceano.2020.07.001.
Walin, G., 1977. A theoretical framework for the description of estuaries. Tellus 29, 128–136.
Wenegrat, J.O., Thomas, L.N., 2020. Centrifugal and symmetric instability during ekman adjustment of the bottom boundary layer. J. Phys. Oceanogr. 50, 1793–1812. https://doi.org/10.1175/JPO-D-20-0027.1.
Wenegrat, J.O., Thomas, L.N., Gula, J., McWilliams, J.C., 2018. Effects of the submesoscale on the potential vorticity budget of ocean mode waters. J. Phys. Oceanogr. 48 (9), 2419–2427. https://doi.org/10.1175/JPO-D-17-0219.1.
Wenegrat, J.O., Thomas, L.N., Sundermeyer, M.A., Taylor, J.R., D'Asaro, E.A., Klymak, J. M., Shearman, R.K., Lee, C.M., 2020. Enhanced mixing across the gyre boundary at the Gulf Stream front. PNAS 117 (30), 17607–17614. https://doi.org/10.1073/pnas.2005558117.
Westerlund, A., Tuomi, L., Alenius, P., Myrberg, K., Miettunen, E., Vankevich, R.E., Hordoir, R., 2019. Circulation patterns in the Gulf of Finland from daily to seasonal timescales. Tellus Ser. A Dyn. Meteorol. Oceanogr. 71 (1). https://doi.org/10.1080/16000870.2019.1627149.
Yao, L., Taylor, J.R., Jones, D.C., Bachman, S.D., 2025. Identifying ocean submesoscale activity from vertical density profiles using machine learning. Earth Space Sci. 12, e2022EA002618. https://doi.org/10.1029/2022EA002618.
Yu, X., Naveira Garabato, A.C., Martin, A.P., Buckingham, C.E., Brannigan, L., Su, Z., 2019. An annual cycle of submesoscale vertical flow and restratification in the upper ocean. J. Phys. Oceanogr. 49 (6), 1439–1461. https://doi.org/10.1175/JPO-D-18-0253.1.
Zeng, X., Bracco, A., Tagklis, F., 2022. Dynamical impact of the Mekong River plume in the South China Sea. J. Geophys. Res. Oceans 127, e2021JC017572. https://doi.org/10.1029/2021JC017572.
Zhang, Z., Chang, J., Zhang, X., Zhang, W., 2025. Mixed transitional layer instability: a mechanism for deep-penetrating submesoscale processes in the subtropical upper ocean. J. Phys. Oceanogr. 55 (12), 2269–2283. https://doi.org/10.1175/JPO-D-25-0009.1.
Zhurbas, V.M., Paka, V.T., 1999. What drives thermohaline intrusions in the Baltic Sea? J. Mar. Syst. 21 (1–4), 229–241. https://doi.org/10.1016/S0924-7963(99)00016-0.
Zhurbas, V., Väli, G., Kuzmina, N., 2019a. Rotation of floating particles in submesoscale cyclonic and anticyclonic eddies: a model study for the southeastern Baltic Sea. Ocean Sci. 15, 1691–1705. https://doi.org/10.5194/os-15-1691-2019.
Zhurbas, V., Väli, G., Kostianoy, A., Lavrova, O., 2019b. Hindcast of the mesoscale eddy field in the Southeastern Baltic Sea: model output vs satellite imagery. Russ. J. Earth Sci. 19 (4), 1–17. https://doi.org/10.2205/2019ES000672.
Zhurbas, V., Väli, G., Kuzmina, N., 2022. Striped texture of submesoscale fields in the northeastern Baltic proper: results of very high-resolution modelling for summer season. Oceanologia 64 (1), 1–21. https://doi.org/10.1016/j.oceano.2021.08.003.
Zi, N., Li, X.-M., Gade, M., Fu, H., Min, S., 2024. Ocean eddy detection based on YOLO deep learning algorithm by synthetic aperture radar data. Remote Sens. Environ. 307, 114139. https://doi.org/10.1016/j.rse.2024.114139.

Curriculum vitae

Personal data

Name:	Kai Salm
Date of birth:	17.03.1995
Place of birth:	Estonia
Citizenship:	Estonian

Contact data

E-mail:	kai.salm@taltech.ee

Education

2019–2026	Tallinn University of Technology, School of Science, Physical Sciences, Oceanography and Meteorology, PhD
2017–2019	Tallinn University of Technology, School of Science, Earth Sciences and Geotechnology (Oceanography and Meteorology), MSC
2014–2017	Tallinn University of Technology, School of Science, Earth Sciences, BSC
2011–2014	Paide Co-educational Gymnasium, High school

Language competence

English	Fluent

Professional employment

2019–present	Tallinn University of Technology, School of Science, Department of Marine Systems, Junior Research Fellow
2018–2019	Tallinn University of Technology, School of Science, Department of Marine Systems, Technician

Academic degrees

- Kai Salm, Master's Degree, 2019, (sup) Urmas Lips, Submesomastaapne muutlikkus termokliini kujunemise perioodil (allveeliuguri andmete põhjal Soome lahe nõlva piirkonnas) (Submesoscale variability in the period of thermocline development (using glider data from the Gulf of Finland slope area)), Tallinn University of Technology, School of Science, Department of Marine Systems.

- Kai Salm, PhD student, (sup) Urmas Lips, Submesoscale variability in the Baltic Sea: occurrence and role in the redistribution of physical tracers, Tallinn University of Technology, School of Science, Department of Marine Systems.

Scientific work

Publications according to ETIS

1.1 Lips, U.; Salm, K.; Väli, G.; Liblik, T.; Arneborg, L.; Biddle, L. C.; Bulczak, A. I.; Chrysagi, E.; Falarz, M.; Holtermann, P.; Jakacki, J.; Meier, H. E. M.; Mohrmann, M.; Myrberg, K.; Pemberton, P.; Umlauf, L. (2026). Submesoscale dynamics in the Baltic Sea – a review. Progress in Oceanography, 245, #103746. DOI: 10.1016/j.pocean.2026.103746.

1.1 Liblik, T.; Siht, E.; Buschmann, F.; Kaljumae, M.; Kikas, V.; Lips, U.; Luik, S.-T.; Maslova, D.; Part, K.; Salm, K.; Samlas, O.; Siiria, S.-M.; Sildever, S.; Skudra, M.; Tikka, K.; Tuomi, L. (2025). Recent stagnation period and unprecedented deoxygenation in the Baltic Sea: causes and consequences. Frontiers in Earth Science, 13, #1638978. DOI: 10.3389/feart.2025.1638978.

1.1 Salm, K.; Väli, G.; Liblik, T.; Lips, U. (2025). Forcing-dependent submesoscale variability and subduction in a coastal sea area (Gulf of Finland, Baltic Sea). Ocean Science, 21 (5), 2555−2577. DOI: 10.5194/os-21-2555-2025.

1.1 Salm, K.; Liblik, T.; Lips, U. (2023). Submesoscale Variability in a Mesoscale Front Captured by a Glider Mission in the Gulf of Finland, Baltic Sea. Frontiers in Marine Science, 10. DOI: 10.3389/fmars.2023.984246.

1.1 Liblik, T.; Väli, G.; Salm, K.; Laanemets, J.; Lilover, M.-J.; Lips, U. (2022). Quasi-steady circulation regimes in the Baltic Sea. Ocean Science, 18 (3), 857−879. DOI: 10.5194/os-18-857-2022.

Elulookirjeldus

Isikuandmed

Nimi:	Kai Salm
Sünniaeg:	17.03.1995
Sünnikoht:	Eesti
Kodakondsus:	Eesti

Kontaktandmed

E-post:	kai.salm@taltech.ee

Hariduskäik

2019–2026	Tallinna Tehnikaülikool, Loodusteaduskond, Füüsikalised loodusteadused, Okeanograafia ja meteoroloogia, PhD
2017–2019	Tallinna Tehnikaülikool, Loodusteaduskond, Maa-teadused ja geotehnoloogia (okeanograafia ja meteoroloogia), MSC
2014–2017	Tallinna Tehnikaülikool, Loodusteaduskond, Maa-teadused, BSC
2011–2014	Paide Ühisgümnaasium, keskharidus

Keelteoskus

Inglise keel	kõrgtase

Teenistuskäik

2019–praegu	Tallinna Tehnikaülikool, Loodusteaduskond, Meresüsteemide instituut, doktorant-nooremteadur
2018–2019	Tallinna Tehnikaülikool, Loodusteaduskond, Meresüsteemide instituut, tehnik

Kaitstud lõputööd

- Kai Salm, magistrikraad, 2019, (juh) Urmas Lips, Submesomastaapne muutlikkus termokliini kujunemise perioodil (allveeliuguri andmete põhjal Soome lahe nõlva piirkonnas), Tallinna Tehnikaülikool, Loodusteaduskond, Meresüsteemide instituut.
- Kai Salm, doktorant, (juh) Urmas Lips, Submesoscale variability in the Baltic Sea: occurrence and role in the redistribution of physical tracers (Submesomastaapi muutlikkus Läänemeres: esinemine ja roll vee füüsikaliste omaduste ümberjaotamises), Tallinna Tehnikaülikool, Loodusteaduskond, Meresüsteemide instituut.

Teadustegevus

Publikatsioonid Eesti Teadusinfosüsteemi klassifikaatori järgi

1.1 Lips, U.; Salm, K.; Väli, G.; Liblik, T.; Arneborg, L.; Biddle, L. C.; Bulczak, A. I.; Chrysagi, E.; Falarz, M.; Holtermann, P.; Jakacki, J.; Meier, H. E. M.; Mohrmann, M.; Myrberg, K.; Pemberton, P.; Umlauf, L. (2026). Submesoscale dynamics in the Baltic Sea – a review. Progress in Oceanography, 245, #103746. DOI: 10.1016/j.pocean.2026.103746.

1.1 Liblik, T.; Siht, E.; Buschmann, F.; Kaljumae, M.; Kikas, V.; Lips, U.; Luik, S.-T.; Maslova, D.; Part, K.; Salm, K.; Samlas, O.; Siiria, S.-M.; Sildever, S.; Skudra, M.;

Tikka, K.; Tuomi, L. (2025). Recent stagnation period and unprecedented deoxygenation in the Baltic Sea: causes and consequences. Frontiers in Earth Science, 13, #1638978. DOI: 10.3389/feart.2025.1638978.

1.1 Salm, K.; Väli, G.; Liblik, T.; Lips, U. (2025). Forcing-dependent submesoscale variability and subduction in a coastal sea area (Gulf of Finland, Baltic Sea). Ocean Science, 21 (5), 2555–2577. DOI: 10.5194/os-21-2555-2025.

1.1 Salm, K.; Liblik, T.; Lips, U. (2023). Submesoscale Variability in a Mesoscale Front Captured by a Glider Mission in the Gulf of Finland, Baltic Sea. Frontiers in Marine Science, 10. DOI: 10.3389/fmars.2023.984246.

1.1 Liblik, T.; Väli, G.; Salm, K.; Laanemets, J.; Lilover, M.-J.; Lips, U. (2022). Quasi-steady circulation regimes in the Baltic Sea. Ocean Science, 18 (3), 857–879. DOI: 10.5194/os-18-857-2022.

ISSN 2585-6901
ISBN 978-9916-80-578-7